Reduced Striatal Mn-accumulation in Huntington's Disease Mouse Model Causes Reversible Alterations in Mn-dependent Enzyme Pathways

By

Terry Jo Vetters Bichell

Dissertation
Submitted to the Faculty of the
Graduate School of Vanderbilt University
in partial fulfillment of the requirements
for the degree of

DOCTOR OF PHILOSOPHY
in
NEUROSCIENCE

December, 2016
Nashville, Tennessee

Approved:

Roger Colbran, PhD
Michael Aschner, PhD
Kaylon Bruner-Tran, PhD
Aaron Bowman, PhD

To the department of "no". Give it up. There is always a way.

To menopause.

To the 10,000th hour.

To the young people. This is it. It doesn't get any better.

To Art Beaudet, who believes in cures.

To moms everywhere.

To multi-tasking.

To my family, who puts it all in perspective.

To the other door that opens when the first one closes.

To democrats and gun control and an increase in NIH funding.

To a good $5 bet.

To the Quakers.

To late-bloomers.

To coffee.

To cocktails.

To kindness.

ACKNOWLEDGEMENTS

A huge heartfelt, tear-jerked, humble thank you to all of the following, in order:

My husband, Dr. David Phillip Vetters Bichell, who provides the perfect example of grit. And because, for decades, he has not hesitated to add livestock to the herd and one more potato to the pot. He has been with me through thick and thin for 36 years (that includes financial times, waistlines and headedness). May we grow wise together.

My parents, Mr. and Mrs. Kenneth J. Vetters, who thankfully married young, so they could appreciate their late-blooming children's middle ages. Especially my mother, Frances Gilliland Vetters, who has always loved school and getting the answers right.

My son, Lou Blackburn Vetters Bichell, who is very slowly, and carefully, teaching me how to listen. My daughters, Dr. Beth Rachel Hochman, Rae Ellen Vetters Bichell, Lena Marie Vetters Bichell and Rosa Lee Vetters Bichell, whose wit and curiosity and generosity of spirit give me faith in all millennials. My sons-in-law, Dr. Frank E. Curtis and Dr. Alessandro Franchin, the PhDs, because if they could do it, I could do it.

My brother Dr. Ralph Gilliland Vetters, and the rest of my big diverse family, the Vetters, the Simmons, the Bichells, the Goulds, the Coutinhos and the Hochmans, who have filled in, or tipped a glass, wherever and whenever it was needed.

My Principal Investigator, Dr. Aaron Bowman, who may sometimes have regretted taking me in as a scientific refugee five years ago, but who pushed and guided and led me all the way to the light at the end of the tunnel. He asks the most surprising questions and I wish him all the best.

Dr. Kevin Haas, who is such a nice person, I could never be mad at him.

Dr. Roger Colbran, who I wanted to strangle at times, but he really paid attention, dug through the details, turned out to be right, and has ensured that no one will ever say I didn't deserve my degree. I have immense respect and admiration for him.

The rest of my patient and long-suffering committee: Dr. David Hachey (retired!), Dr. Michael Aschner, Dr. Kaylon Bruner-Tran. Thank you so much for your time and attention.

The kind young scientific mensches who taught me, and tutored me and showed me how this stuff is supposed to be done: Dr. Gunnar Kwakye, Dr. Michal Wegrzynowicz, Chris Jetter, Bryan Cawthon, Dr. Mark Grier, Dr. Shu-Qun Shi, Dr. A.J. Baucum, Dr. Andrew Tidball, Dr. Rob Carson, Dr. Ben Jorge, Dr. Ben Dean, Dr. Brad Kraemer, Dr. Peter Hamilton, Mike Litt, Dr. Trisha Thornton-Wells, and Dr. Sudipta Chakraborty.

The amazing, brilliant, hard-working, sweetheart undergraduates I've had the privilege of having on my Dream Team. You all taught me the latest organic chemistry, the newest lingo, and the best apps. I'm so proud of you all, what you have done, what you are doing and what you will do: Dr. Brooke Huffsmithe, Jinsu Sohn, Dr. Lisa Herrington, Jack Feist, Andrew Stubbs, Michael Uhouse, Preethi Umashanker, Emma Bradley, Tim Halbesma
and especially K. Grace Tipps

Dr. Asad Al-Aboud for always using cynicism and sarcasm in the face of adversity.

Dr. Kevin Kumar, Dr. Diana Neely, Dr. Bingying Han, Miles Bryan, Kyle Horning, Rachana Nitin and Piyush Joshi for caring about manganese, and for sharing benches and reagents and protocols and beers. Your ability to stay awake through powerpoint data presentations will go down in legend.

Drs. Kevin Ess, Marshall Summars, Chaz Hong, Scott Baldwin, Bruce Carter, Doug McMahon, Mary Barger, Eugene Declerq, Lynne Bird, Mark Nespeca and Elisabeth Dykens who are role models and/or mentors and who have believed in me, even when I wasn't so sure myself.

Drs. Carl Johnson, Cary Fu, and Jingqiong "Katty" Kang for continuing the Angelman research, and doing what I wanted to do, but could not.

The women who have kept me scientifically and psychologically sane, Alice Berry Clark, Ellen Lysell Summa, Andrea Baldwin, Dr. Lee Anne O'Brien, Dr. Mara Sanders, Dr. Dana Walrath, the Cedar Lane Chatters, Dr. Juliane Krueger, Dr. Suzanne Avery, Dr. Eva Sawyer, and soon to be doctor, Barbara O'Brien.

Rosalind Johnson

Those therapists and caregivers, Donna Bowins, Karina and Irakli Guergenizde, Anne and Aaron Velthouse, Carmen Rabbitt Davis, Lydia Garrisi, Charles Kay, Erin Jamieson, Fae Lumauag and Natalee McCarthney, who made it possible for me to not feel guilty when I was away from my son because I knew he was learning and growing and safe.

My other kids, not by birthright but connected by choice, and how cool is that!?!
Zoe Ghigo, Nuraini Wulan, Jakob Kubitza, Dr. Nishan Bingham, Graham Bichell, Emily Siner.

The families of people with Huntington's disease, some of whom I have had the privilege to meet, and who have begun to teach me what it means to live with HD.

The other Angelman moms (and occasional dads), who are struggling with the same daily chores and red-eyed nights, and somehow manage to juggle their careers, enjoy the moments, feed their families, raise the siblings, and still work for a cure.
#iwillnotgiveup
#cureangelman

FURTHER ACKNOWLEDGEMENTS

This work would not have been possible without financial support. Work on the data presented in Chapter II was supported by NIH grant ES016931, NICHD grant P30HD15052 to ABB and grant number ES007062 to TRG. Additional support was provided by the Vanderbilt Kennedy Center NIH/NICHD P30HD15052. Most of the remainder of the work presented in this manuscript was supported by NIH/NIEHS RO1 ES016931 to ABB. TJB was supported by the Training Program in Environmental Toxicology NIEHS T32 ES007028. AMT was supported by NINDS F31 NS077632.

The Vanderbilt core facilities and personnel provided essential assistance with many experiments. Rotarod and open field experiments were performed through the use of the Murine Neurobehavior Core lab at the Vanderbilt University Medical Center. We thank Dr. John Allison for the training on using rotarod apparatus and activity chambers and for help with behavioral data collection. We thank Dr. M. Wade Calcutt from the Mass Spectrometry Core for training on the LC-MS system, and Dr. Anthony Tharp and the VBI Core Facility for equipment and technical support. Leptin and cytokine assays were performed in the Vanderbilt Hormone Assay and Analytical Service Core. QRT-PCR experiments were performed through the Molecular Genetics Core and LC-MS through the MSRC Mass Spectrometry Core at the Vanderbilt University Medical Center.

External collaborators also assisted.
We thank Dr. Elena Uribe Perez for providing ALP antibody (data not shown).
We thank Drs. William Caldwell and Ruth Caldwell for Arg1 and Arg2 knockout tissue.

TABLE OF CONTENTS

Page

PUBLICATIONS ACKNOWLEDGED

Much of this document was, or will be, published as part of the following manuscripts:

Bichell TJ. Gene-Environment Interactions in Huntington's Disease. *Vanderbilt Reviews Neuroscience* 2012; 4(2012): 9.

Tidball AM, Bichell TJ, Bowman AB. Manganese and Huntington's Disease. In: Costa L, Aschner M, eds. Manganese in Health and Disease: Royal Society of Chemistry; 2014.

Bichell TJ, Uhouse M, Bradley E, Bowman AB. Gene-Environment Interactions in Huntington's Disease. In: Aschner M, Costa LG, eds. Environmental Factors in Neurodevelopmental and Neurodegenerative Disorders. London: Elsevier, Inc.; 2015: 451.

Wegrzynowicz M, Bichell TJ, Soares BD, Loth MK, McGlothan JS, Mori S, Alikhan FS, Hua K, Coughlin JM, Holt HK, Jetter CS, Pomper MG, Osmand AP, Guilarte TR, Bowman AB. Novel BAC Mouse Model of Huntington's Disease with 225 CAG Repeats Exhibits an Early Widespread and Stable Degenerative Phenotype. *J Huntingtons Dis* 2015; 4(1): 17-36.

Bichell TJ, Halbesma T, Tipps KG, Bowman AB. Metal Biology Associated with Huntington's Disease. In: White A, Aschner M, Costa L, Bush A, eds. Biometals in Neurodegenerative Diseases: Mechanisms and Therapeutics. In Press: Elsevier; 2016.

Bichell TJV, Wegrzynowicz M, Tipps KG, Bradley EM, Uhouse MA, Bryan M, Horning K, Fisher N, Dudek K, Halbesma T, Umashanker P., Stubbs AD, Holt H, Kwakye G, Tidball AM, Colbran RJ, Aschner M, Neely MD, Di Pardo A, Maglione V, Osmand A, Bowman ABB. Reduced bioavailable manganese causes striatal urea cycle pathology in Huntington's disease mouse model. *Submitted and Under Review*.

GENE AND PROTEIN ABREVIATIONS USED

Human genes are capitalized and italicized, for example the human gene Huntingtin is ***HTT.***

Mouse genes are italicized but only the initial letter is capitalized, for example the mouse gene Huntingtin is ***Htt.***

Proteins in either human or mouse will be capitalized and not italicized, for example the protein Huntingtin is **HTT.**

The disorder of Huntington's disease is capitalized and not italicized, for example **HD.**

LIST OF TABLES

LIST OF FIGURES

Chapter I

Chapter II

Chapter III

Chapter IV

Chapter V

Chapter VI

Chapter I

Gene-Environment Interactions in Huntington's Disease

Note: Portions of this chapter have been derived from the following publications:

Bichell TJ. Gene-Environment Interactions in Huntington's Disease. *Vanderbilt Reviews Neuroscience* 2012; 4(2012): 9.

Tidball AM, Bichell TJ, Bowman AB. Manganese and Huntington's Disease. In: Costa L, Aschner M, eds. Manganese in Health and Disease: Royal Society of Chemistry; 2014.

Bichell TJ, Uhouse M, Bradley E, Bowman AB. Gene-Environment Interactions in Huntington's Disease. In: Aschner M, Costa LG, eds. Environmental Factors in Neurodevelopmental and Neurodegenerative Disorders. London: Elsevier, Inc.; 2015: 451.

Bichell TJ, Halbesma T, Tipps KG, Bowman AB. Metal Biology Associated with Huntington's Disease. In: White A, Aschner M, Costa L, Bush A, eds. Biometals in Neurodegenerative Diseases: Mechanisms and Therapeutics. In Press: Elsevier; 2016.

Huntington's disease

Huntington's disease (HD) is a severe autosomal dominant neurodegenerative disorder with a diverse, but devastating pathological course, and a median age of onset at 39.[1] In the mid-1990's, researchers studying an isolated community in Venezuela with a very high incidence of HD pinpointed the genetic cause. The causative mutation is an expanded CAG repeat in the first exon of the Huntingtin gene (*HTT*), which results in an extended polyglutamine sequence in the huntingtin protein (HTT). This excess of CAG repeats leads to an expansion in the polyglutamine (polyQ) tract in the HTT protein.[2]

Including Huntington's disease, there are currently at least nine known neurodegenerative diseases that derive from excess CAG repeats, including spinal muscular atrophy, dentatorubral-pallidoluysian atrophy, and the spinocerebellar ataxias type 1, 2, 3, 6, 7 and 17.[3] These CAG repeat expansion diseases are characterized by severe chromosomal instability, specifically when inheritance is paternal, as expansions are frequent in the male

germline.[4] The neuronal loss of each of these diseases is restricted to specific brain regions with similar intracellular manifestations such as modified metal processing, inclusions, aggregates, and protein misfolding.[5] These molecular findings are also present in non-CAG repeat neurodegenerative diseases such as Alzheimer's Disease and Parkinson's Disease, both of which have a greater environmental over genetic attribution.[6] In each of these neurodegenerative diseases, environmental enrichment, exercise, diet, and xenobiotic exposures have been shown to either exacerbate or alleviate disease.[7,8]

Genetics of Huntington's disease

The *HTT* gene is highly conserved through evolution, but there is wide diversity between species in the number of CAG repeats.[9-11] In humans, between 9 and 34 CAG repeats is thought to be normal, but there are cases of symptomatic HD developing within the range of 27-34 CAG repeats,[1,12,13] and yet it appears that 35-39 CAG repeats is not fully penetrant.[14] A recent study found that 1 in 400 elderly individuals from cohorts in the UK and the US had alleles between 35-39 without HD symptoms,[14] suggesting that the penetrance of disease with CAG repeats under 40 is not predictable, and may reflect the combined impact of CAG repeat length and environmental exposures.

HD is a rare disease. The approximate worldwide prevalence of HD is 2.71 cases per 100,000 population.[15] However, prevalence of HD around the globe ranges from 5.7 in the British Isles to only 0.40 per 100,000 in Asia[15]. While HD affects both men and women in equal numbers,[16] gender appears to play a role in disease progression and HD brain metabolism,[17] as females tend to experience more severe motor and functional symptoms along with a faster rate of disease progression.[18]

Though it has been two decades since the identification of the HD-associated mutation, the detailed mechanisms leading from expression of the mutant gene to neurodegeneration are still unknown, and no successful treatment that would slow disease progression has been described as yet. It remains unclear whether HD pathology is caused by loss of function of the normal HTT protein, or toxic gain of function from the mutant HTT protein, or a combination of both.[19-21] Transgenic mouse models with one mutant allele as well as two functioning wild-type alleles still develop symptoms of HD, suggesting that toxicity of the mutation is the root cause of pathology.[22] Conditional mouse models expressing lower levels of mutant HTT in the cortex and striatum show no behavioral deficits, and neurodegeneration of these brain regions is ameliorated.[23] Yet, over-expression of mutant HTT, as well as knockdown of wild-type HTT, alters vesicular transport, mitochondrial function, and macroautophagy in neurons, both *in vitro* and *in vivo,*[24-28] making both the loss of wild-type function and the toxic gain of mutant function important to HD pathology related to neuronal metal homeostasis. However, a careful study of homozygous human patients, controlled for CAG repeat number on both alleles, demonstrated worsened disease progression compared to heterozygotes.[29] The results from this study suggest that loss of function of normal HTT alone, as well as abnormal function caused by the mutant allele, may still play a role in disease pathology.

Htt knockout mouse models cannot survive past embryonic day 7,[21,30] but the essential role for HTT in embryological development remains unclear. Two recent papers uncovered rare loss of function mutations in the *HTT* gene outside of the HD critical area that cause a Rett's syndrome-like phenotypes, suggesting that loss of wild-type HTT during development could also disrupt neurological function.[31,32]

Symptoms of Huntington's disease

The hallmark symptom of HD is chorea (uncontrolled movements),[16] though psychological and cognitive changes are also common and can be equally as detrimental to quality of life.[33] HD is described as having three phases, both in humans and mouse models:[34]

(i) Pre-manifest, in which the gene mutation has been identified but there are no signs and symptoms;

(ii) Prodromal, during which there are cognitive and emotional signs, but no loss of function;

(iii) Manifest, in which motor symptoms become obvious and there is sharp functional decline.

The prodromal phase is marked by family reports of increased apathy, anxiety, and depression.[35,36] During the prodromal phase, the first losses are of cortical mass followed by degeneration of striatal γ-aminobutyric acid transmitting (GABAergic) medium spiny neurons (MSNs), which suggests that disease processes in cortical neurons may lead to the subsequent excitotoxic post-synaptic deterioration of MSN's.[37-39] In fact, decortication in an HD mouse model has been reported to ameliorate HD symptomology.[37] Additionally, several peripheral tissues have been suggested to contribute to HD pathogenesis.[40]

A clinical diagnosis of adult-onset HD generally relies on the observance of chorea,[41] but as the disease progresses, dystonia and rigidity occur. Overall, symptoms of HD and the disease progression are remarkably heterogeneous across patient populations.

The first symptoms of HD begin, on average, between the ages of 35 and 40,[12] with the age of onset inversely correlated to the number of polyglutamine repeats, though timing varies even among patients with identical CAG number. Sibling and twin studies reveal that modifier genes explain an additional 13% of the variability in age of onset in the studied patient populations, with the remainder attributed to environmental factors.[42-44] This variability in age of onset suggests the possibility that metal toxicity or deficiency could be a factor. After the onset of motor symptoms, patients with HD typically live for 20 additional years, with aspiration pneumonia the most common cause of death, due to dysphagia.[45,46]

The juvenile form of the disease, related to longer CAG repeat length (usually above ~50 repeats, but invariably above 60 repeats) manifests with widespread neurodegeneration and involves different symptoms compared to adult-onset HD.[47,48] Epilepsy, motor rigidity, cognitive issues and behavior issues are common, and are not seen in adult onset HD.[49]

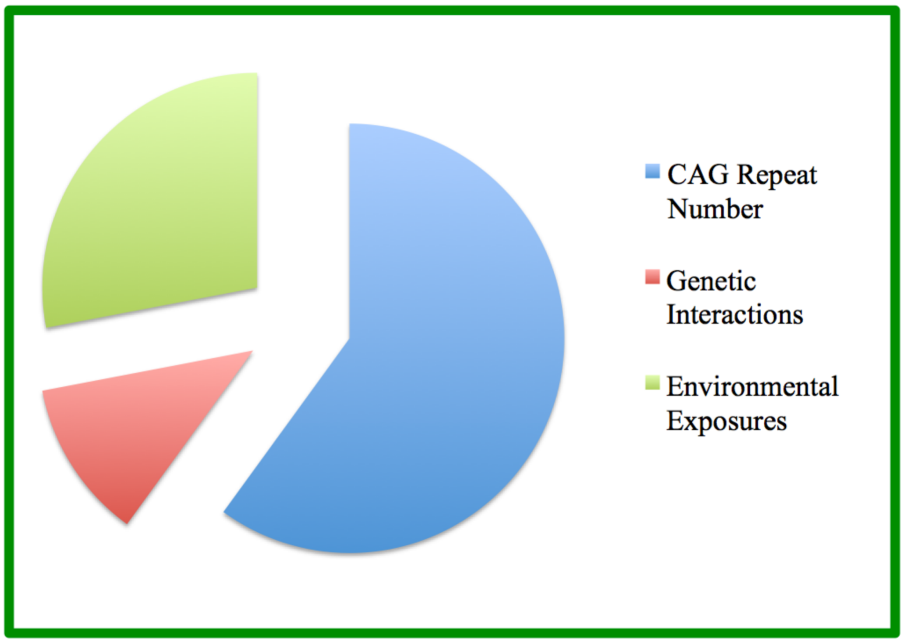

Figure 1-1: Proportion of Variability in Huntington's Disease Age of Onset

Environmental factors such as environmental enrichment (EE), exercise, diet, and exposures to xenobiotics have been reported to worsen or ameliorate disease processes in all polyglutamine expansion diseases.[50]

Neuropathology of HD

Each of the nine neurodegenerative diseases caused by excess CAG repeats have neuronal loss restricted to specific brain regions[5], though they all exhibit similar abnormal metal processing, protein misfolding resulting in inclusions and aggregates.[6] These molecular manifestations are also present in non-CAG repeat neurodegenerative diseases, such as Alzheimer's Disease (AD), and Parkinson's Disease (PD).[6]

The function of the wild-type HTT protein is still not fully explained, but wild-type HTT is part of essential cellular pathways which involve metals as co-factors, for ionic gradients, and for protein stability. These include biological processes such as axonal transport,[51] nuclear export,[52] transcriptional regulation,[52-54] apoptosis,[55,56] autophagy,[57] endocytosis,[58] and the scaffolding of protein interactions.[59,60]

The HTT protein is huge (over 348kDa) and ubiquitously expressed, with more than 300 binding partners identified to date.[19,61,62,63] The expanded polyQ tract takes on a labile conformation (helix, coil, loop) that enables it to function as a regulator of multiple protein interactions.[64,65] The protein is modified post-translationally, primarily in the same N-terminal region as the polyQ expansion, which is also the region linked to the formation of aggregates and to mitochondrial dysfunction, which are molecular hallmarks of HD pathology.[66,67] Post-translational HTT modifications include phosphorylation,[65] sumoylation,[68] ubiquitination,[69] acetylation,[70,71] palmitoylation[72] and myristoylated.[73] The HTT protein is also is cleaved in several different ways by caspases and calpain.[74,75]

HTT is expressed ubiquitously across various cell types and tissues,[19] yet degeneration occurs in restricted brain regions, where it is especially marked in the striatal MSNs in the later phases of the disease. The MSNs make up 90% of the neurons in the striatum.[76] Like the striatum, subtypes of cortical neurons are differentially affected by HD. Large pyramidal neurons originating in cortical layers III, V, and VI, and projecting directly to the striatum, primarily contribute to the loss of cortical volume in HD.[77,78] Other brain regions, such as the hippocampus, thalamus and globus pallidus also degenerate in HD, but not to the extent seen in the striatum,[79] so most studies focus on the neurons of the cortex and striatum.

The striatal MSNs are subcategorized by dopamine receptor expression and projection targets. Those that project to the substantia nigra and the external segment of the globus pallidus and contain D2 dopamine receptors and met-enkephalin, form the indirect pathway, which is the pathway most affected in HD.[80] MSNs projecting to the internal segment of the globus pallidus, expressing D1 receptors and substance P, make up the direct pathway, which is spared from neurodegeneration until later in the disease course. Generally, the D1 containing neurons are thought to be involved with reward processing, while the D2 neurons mediate aversion, but these networks are mixed in some striatal regions[81]. The sequential loss of striatal MSN subtypes is partially related to metal uptake and deposition, and appears to correlate with onset of patient symptoms.[82]

Biological function of wild-type and pathogenic HTT proteins

The crystal structure of HTT has not been entirely elucidated, perhaps because the protein can take on many different structures.[64] The polyQ tract, which is altered by the number of CAG repeats in exon 1, forms a flexible domain that regulates intramolecular proximity and substrate specificity.[83]

Wild-type HTT is located primarily in the cytoplasm,[84,85] but plays a role in protein trafficking between nucleus and cytoplasm through transcriptional regulation of the nuclear pore protein.[52] N-terminal HTT fragments interact with the protein's translocated promoter region, and excessive polyQ expansion decreases this interaction.[52] HTT is modified post-translationally by acetylation, phosphorylation, ubiquitination, palmitoylation and sumoylation, with each modification having effects on function and activity.[68,86,87] With the HD mutation, the HTT protein becomes much less soluble leading to misfolding of the extended polyQ sequences which then form a β-sheet structure, leading to abnormal post-translational modifications.[12,88,89]

Short fragments of mutant HTT form aggregates in the nucleus and cytoplasm, which may be the source of further pathology, but may also be a cellular defense process to sequester the toxic misfolded mutant HTT protein.[90] Cu interacts with the polyQ fragment of HTT and increases aggregation,[76] and Cu ions bind to HTT aggregates and induce oxidation, which increases neuronal oxidative stress,[91] potentially leading to cell death and degeneration. These aggregates can be cleared either by autophagy or by the proteasome system. A recent study indicates that macroautophagy may be more crucial to the clearance of HTT aggregates than the proteasomal process,[92] and autophagy is known to be affected by metal homeostasis.

HTT in vesicular transport

HTT has been associated with both endocytic and microtubule-mediated vesicle transport, mechanisms which transport both the crucial cell survival signal, Brain Derived Neurotrophic Factor (BDNF), as well as various metals into cells and organelles. HTT is closely associated with vesicles and endosomes,[84,93-95] microtubules,[95,96] and directly with the plasma membrane.[97] HTT interacts via HAP1 with an integral member of the microtubule transport system, the dynactin subunit p150Glued,[98,99] and co-fractionates with the transferrin receptor

(TfR).[100,101] Knockdown of HTT expression in zebrafish causes increased transferrin receptor 1 transcription in the presence of hypochromic blood. Interestingly, this phenotype is reversed upon administration of bioavailable iron, demonstrating a functional role of normal HTT to make endocytosed iron accessible.[102] The authors theorize that the function of normal HTT must be related to the release of iron from endocytic vesicles.

HTT is found proximal to vesicles and endosomes[94,96,97] and to microtubules[96,99] and is directly associated with the plasma membrane.[100] HTT is known to interact with a promotor of dynein-driven microtubule transport, dynactin subunit p150Glued, via primary interactions with HAP-1.[71,99,103] Through this protein complex, the HTT protein has been associated with both endocytic and microtubule-mediated vesicle transport, transporting substances such as BDNF and metals into cells and organelles.[27] Overall, mutant HTT impairs vesicular transport of numerous cellular goods, including BDNF.[26]

Models of HD

Animal and cell models replicate many of the pathologies associated with HD, and include mouse, sheep, rat, zebrafish, *Drosophila* (fruit fly), *C. elegans* (worm) and *Saccharomyces cerevisiae* (yeast) models.[104,105] Animal models lack the severe neurodegeneration that is seen in humans,[106] which maybe due to the fact that there is a hominid-specific isoform with a phosphorylation site that does not exist in rodents.[107]

Simple model organisms can be important tools in identifying disease-modifying genes and investigating Huntington's disease mechanisms. For example, *Drosophila* models of polyglutamate expansion diseases display the same cell death and aggregation phenomenon that humans do.[108-111] *D. melanogaster* models of Huntington's disease utilize the UAS-GAL4 system to express N-terminal fragments of mutant *HTT* in targeted cells.[112] Fly models exhibit

progressive degeneration, motor abnormalities and reduced survival[112]. *D. melanogaster* models have been constructed to express human Huntingtin cDNA encoding both pathogenic proteins that result in progressive motor deterioration and decreased survival rates, and nonpathogenic proteins that have no perceptible effect on behavior.[113] Such fly models have become useful in demonstrating the kinetics of protein aggregation in axonal transport disruption and in testing therapeutic approaches such as histone deacetylation inhibitors (HDAC) and protein abundance modulators such as NUB1.[113-115] In testing environmental exposures, the simpler organisms provide an efficient way to study toxicities and mechanistic results of gene-environment interections because they retain molecular pathways that recapitulate those of higher mammals.

A transgenic *C. elegans* model of HD expresses amino terminal fragments of Huntingtin in target neurons.[116,117] The translucent body of *C. elegans* allows *in vivo* visualization of neuronal processes, particularly useful in the study of gene-environment interactions on the effects of metal on neurodegeneration.[118] Even though *C. elegans* lacks an *HTT* orthologue, transgenic expression of mutant *HTT* yields age-dependent mechanosensory defects, neurodegeneration and neuronal dysfunction.[116,117] Via insertion of a polyglutamine repeat of 40 CAG repeats in length, researchers have used *C. elegans* models to examine the effect of diverse genetic backgrounds on HD pathology, as well as preclinical investigations of potential therapeutic targets such as the copper chelating drug, hydroxyquinolone (PBT2).[119,120] A human clinical trial of PBT2 as a treatment for Huntington's disease has shown that the drug is safe and tolerated well, but a study of its effectiveness in ameliorating symptoms was halted due to insufficient improvement.[121,122]

Large animal models such as primates and sheep are particularly useful for studies in which it is vital to replicate the clinical phenotypes of human Huntington's disease as closely as

possible. A transgenic primate model has been developed, but has not been well-studied, and at present, there is only one living transgenic HD rhesus monkey. This animal expresses exon 1 of human *HTT* with only 29 CAG repeats, which should be in the normal range, but it displays dystonia, chorea, decreased hippocampal and striatal volume, and behavioral changes such as difficulty with cognitive abilities, impulsivity and spatial recognition.[123] None of these symptoms developed until later ages, a progression that mirrors human Huntington's disease motor degeneration.[123] Other primate models have been produced by lesioning the striatal region,[124] or by exposing the animals to medications which degenerate the striatal neurons such as 3-nitropropionic acid (3NP).[125] Such non-human primate models have already become relevant in the study of Huntington's disease gene x environment effects in a study that shows increases in spontaneous locomotor activity of both calorically restricted and supplemented primates, as well as increased spatial memory abilities of calorically supplemented animals.[126] Additionally, after chronic manganese exposure, non-human wildtype primate models have demonstrated damaged visuospatial associative learning, neurodegenerative aggregation activity, increases in microglia, and general neurodegeneration characteristic of disorders such as HD.[127] These longterm studies of primates demonstrate that mutant human *HTT* may be unique in its mechanisms and ability to cause neurodegeneration, and that environmental exposures alone may be sufficient to cause an HD-like phenotype, even without the presence of the Huntington's disease mutation.

Researchers have also utilized sheep in the investigation of environmental effects such as sleep disruption on disease onset and progression of HD. Specifically, even young HD-model sheep that express juvenile expanded full-length transgenic human *HTT* display circadian abnormalities in behavior before any other HD-like changes appear, but environment is a crucial

element in this finding; the mutant sheep who were housed with other mutants exhibited aberrant behaviors, but those who were housed with wildtype sheep did not.[128] All of these animal models of Huntington's disease reveal the overlap between gene and environment in the cause and treatment of the disorder, but the molecular link between the Huntingtin protein and the environmental agents that affect symptoms has yet to be elucidated.

A variety of rodent HD models have been developed, of which transgenic and knock-in mice appear to be the most relevant to human pathology (reviewed in [22,105,129]). These mouse models can be divided into three groups: transgenic mice expressing the CAG-expanded N-terminal fragment of human *HTT* (R6/1, R6/2, N171-82Q), transgenic mice expressing full-length mutant *HTT* of human origin (YAC128, BACHD) and knock-in mice in which the CAG mutation was introduced into the endogenous mouse *Htt* gene (HdhQ72, HdhQ94, HdhQ111, HdhQ140).[130] All these models differ from each other significantly with regard to spectrum of phenotype, severity alterations and progression of abnormalities, but the general observation is that knock-in mice display very mild symptoms over their whole life span, comparable with the presymptomatic stage of human HD.

As opposed to mice with a full *HTT* gene knock-in, transgenic mice expressing the human N-terminal *HTT* fragment are characterized by an aggressive phenotype, resulting in rapid death at a young age. The R6/1 and R6/2 transgenic mice carry a fragment of exon 1 from the 5' end of human *HTT* with 113 and 144 CAG repeats, respectively.[67] The R6/2 mouse has a pronounced HD phenotype, developing weight loss, aggregates, brain atrophy, and motor symptoms by 12 weeks.

The YAC128 mouse has a transgene expressing the full-length human *HTT* gene with 128 repeats.[131] Though it lives a normal lifespan and has early increased weight[132] (with later

weight loss), it develops motor abnormalities and has increased n-methyl-D-aspartate (NMDA), AMPA, and metabotropic glutamate receptor (mGluR) binding, and reduced striatal and cortical volume. This YAC128 model appears to replicate human pathology more accurately than other models, with specific striatal and cortical neurodegeneration, and late, progressive motor impairment (reviewed by Crook and Housman[129]). Increased expression of wild-type human *HTT*, even without an expanded CAG repeat, has also been shown to increase body weight.[133]

In order to measure the effects of reductions of wild-type *Htt* versus the effects of the added toxicity of mutant *HTT*, our lab maintains a line with varying numbers of wild-type *Htt* alleles (0,1 or 2 alleles), along with the transgenic human *HTT*, on a C57B6/J background (**Figure 1-2**). Baseline weights of these mice are taken just before exposure protocols, demonstrating that the toxicity of the human *HTT* transgene mutation causes a stronger effect on body weight than the loss of wild-type *Htt* alleles (**Figures 1-3, 1-4, 1-5**). Interestingly, the expanded CAG repeat in the BAC225 mouse generated by our lab (discussed in Chapter II), does not increase weight at this age. Over time, the BAC225 model experiences decreased weight compared to wild-type (**Figure 2-5**) as is seen in juvenile HD,[134] but at this 12 week age-point, the weight decrease is not yet apparent. Our weight data is consistent with the literature that links human *HTT w*ith increased body weight, and may indicate the disease stage in the BAC225 (as weight loss is not severe in human adult-onset HD until the manifest stage[135]), or may indicate the different effect of human *HTT* vs. mouse *Htt* on this phenotype. Interestingly, weight loss is correlated with CAG repeat number in human patients.[136]

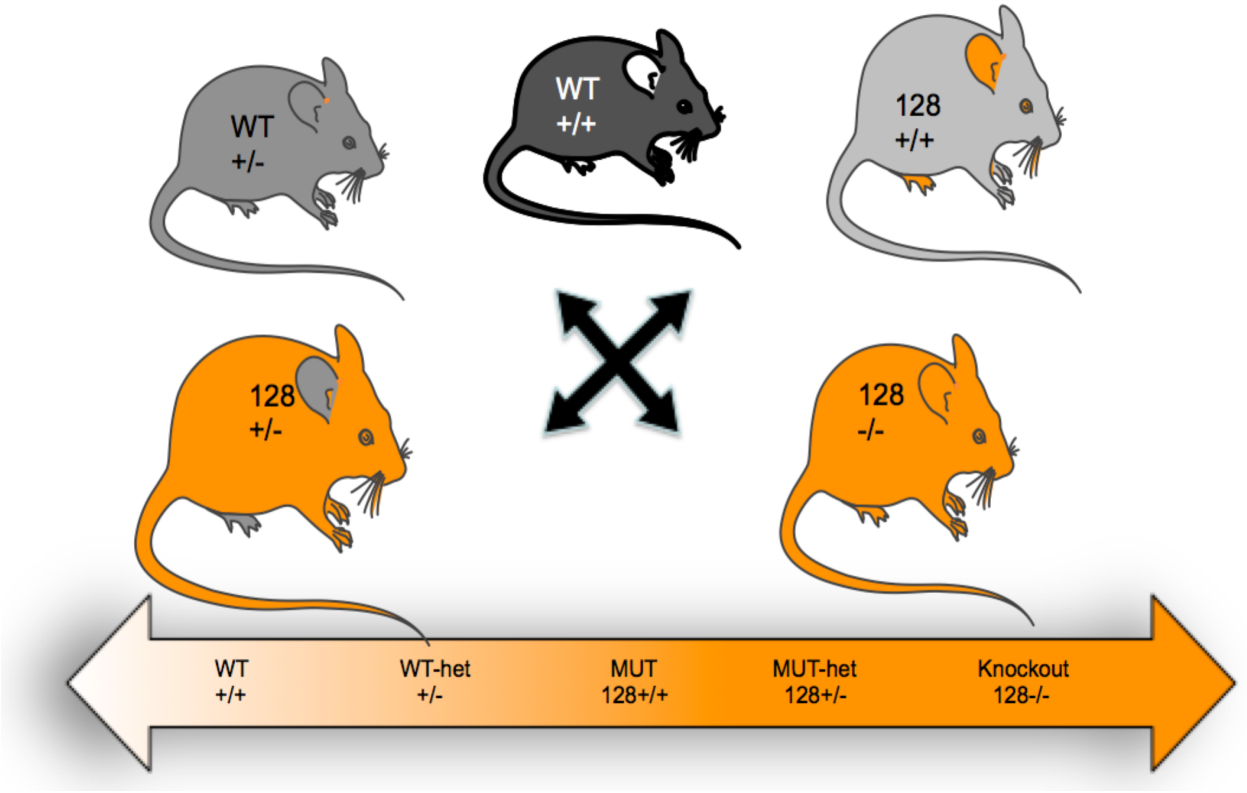

Figure 1-2 Schematic representation of breeding strategy to generate differing numbers of wild-type *Htt* alleles with or without the YAC128 transgene.

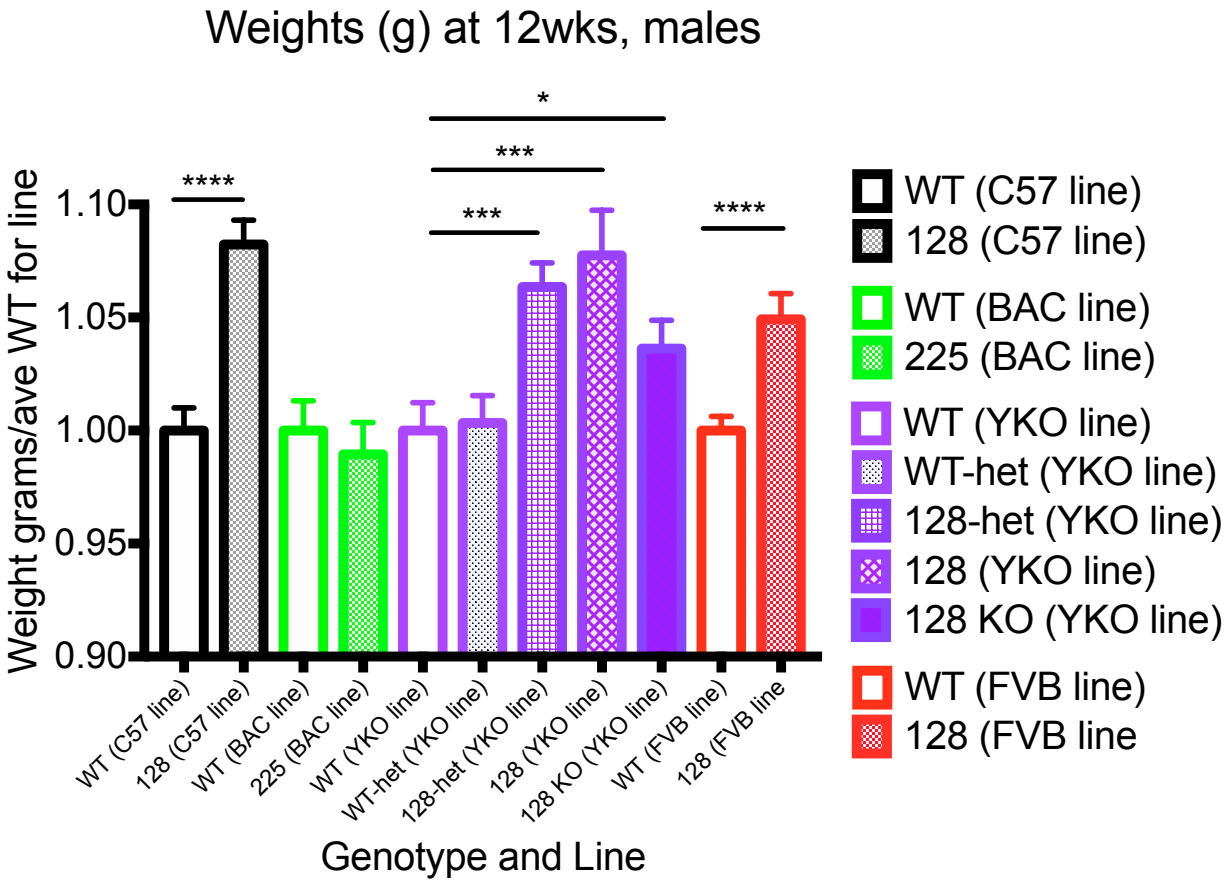

Figure 1-3. The presence of mutant human HTT (YAC128) causes significant increase in weight, regardless of number of WT alleles, though expanded mouse Htt (BAC225) does not. (WT-C57 n=68, 128-C57 n=46, WT-BAC n=49, 225-BAC n=48, WT-YKO n=45, WT-het-YKO n=63, 128-het-YKO n=70, 128-YKO n=27, 128-KO-YKO n=52, WT-FVB n=156, 128-FVB n=102). Difference between mutants is not significant. Data are presented as means ±sem of weights in grams normalized to mean WT Veh from each line, t-tests *p< .05, ***p< .002, ****p< .0001, *post-hoc* binary comparisons by t-test following a significant (p=<.05) ANOVA.

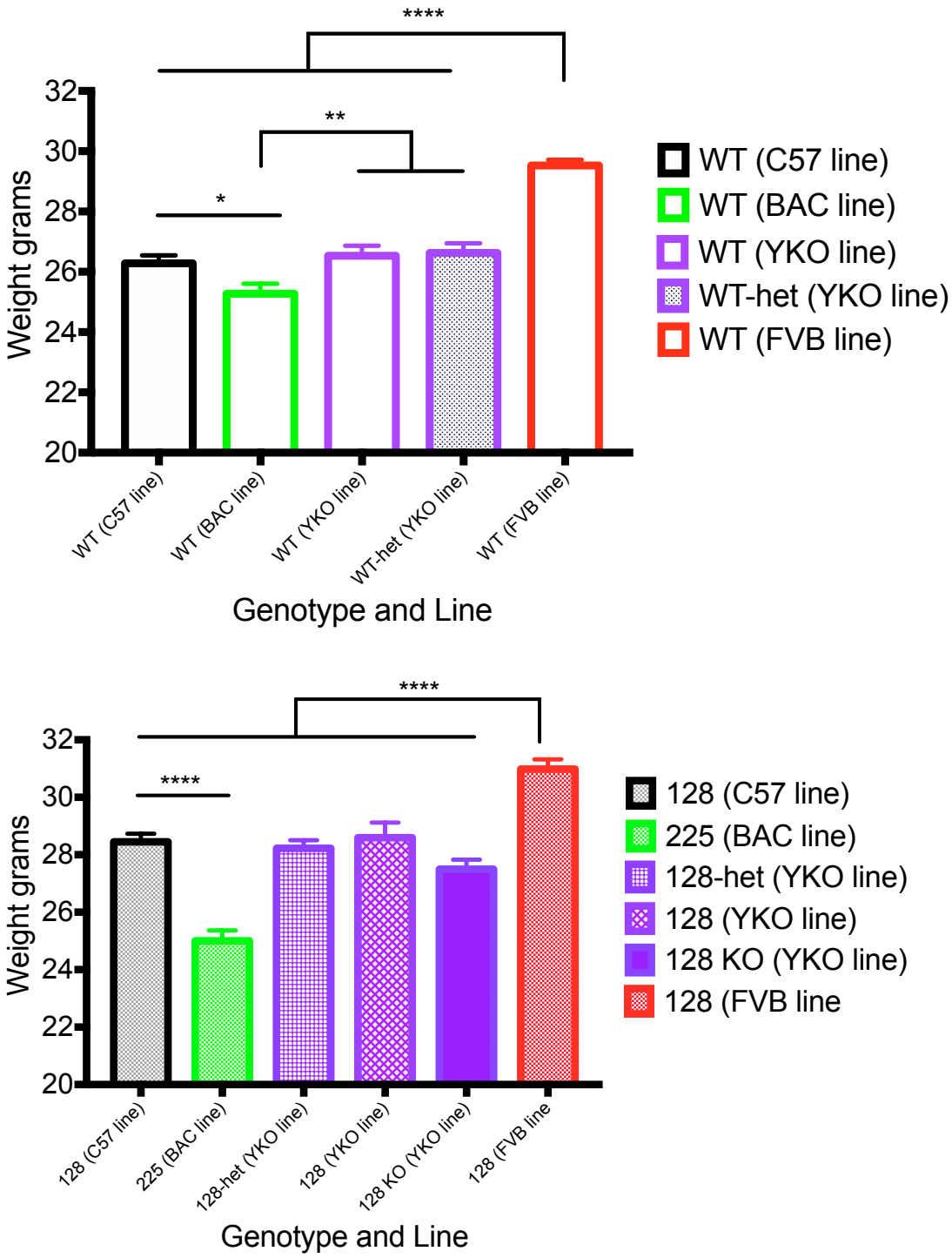

Figure 1-4. Weights in grams, same data as Fig. 1-3, not normalized, 12 week old mice in all lines. Un-normalized difference between WTs not sig (except for BAC line to other C57 lines p=.0178) and all C57 lines to FVB line, diff between all muts and WTs highly significant (p=<.00001). Data are presented as means ±sem, t-tests *p<.02, **p<.0085, ****p<.0001, *post-hoc* binary comparisons by t-test following a significant (p=<.05) ANOVA.

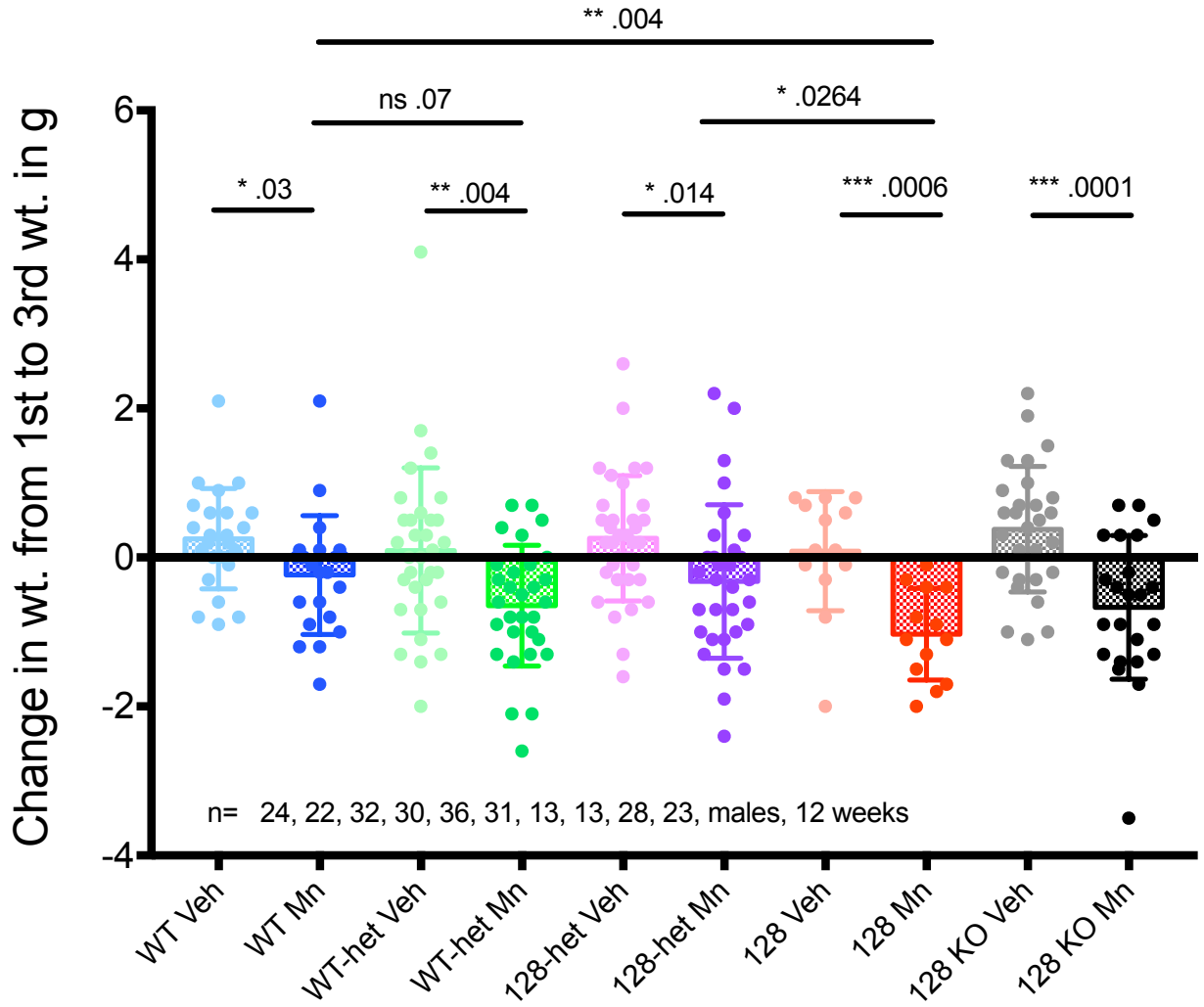

Figure 1-5 Change in weight from pre-exposure to 3 days after the second injections for each animal. Data are presented as means ±sd, t-tests as indicated, *post-hoc* binary comparisons by t-test following a significant (p=<.05) ANOVA. See Appendix D for ANOVA comparisons.

The BACHD transgenic mouse also expresses the full-length *HTT* gene and develops inclusions and brain atrophy, but demonstrates fewer motor abnormalities than the YAC128[137]. Other models with knock-in polyQ sequences inserted into the mouse *htt* gene do not develop a robust phenotype,[138,139] but do show some neuronal defects and motor abnormalities.

None of these models, however, display phenotypes that mimic all of the prominent observable abnormalities associated with HD. Moreover, many symptoms observed in one model are absent in another. A diverse spectrum of available transgenic / knock-in animal models differing in number of CAG repeats, transgene length, transgene locus and polyglutamine (polyQ) / wild-type (WT) *Htt* ratio may therefore be fundamental for successful studies of specific HD pathological mechanisms and to evaluate the efficacy of interventional strategies.

To that end, we generated a transgenic Bacterial Artificial Chromosome (BAC) mouse, expressing full-length mouse *Htt* with ~225 CAG repeats under the control of the mouse *Htt* promoter (**Chapter 2**). This model, displays phenotypes that mimic several of the symptoms that are consistent with juvenile HD: motor abnormalities at a young age, early and widespread brain atrophy, and progressive loss of body weight. Additionally, general symptoms of both juvenile and adult-onset HD are present in these mice, including down-regulation of dopamine receptors in striatum and disturbances in plasma levels of metabolites related to energy metabolism and systemic inflammation.

Environmental influences on HD

Environmental influences have not been demonstrated to accelerate the pace of HD, though exposures that cause oxidative stress are assumed to worsen neuronal health. However, many factors described below (including enriched environments, exercise and diets) have been shown to delay disease progression. Most of these beneficial influences have been demonstrated to increase endogenous brain derived neurotrophic factor (BDNF) levels, with a concomitant delay in disease progression. The pace of neurodegeneration may be due to several

mechanisms, including diminished neurotrophic support and deranged essential metal ion homeostasis *in vivo* **(Figure 1-6).**

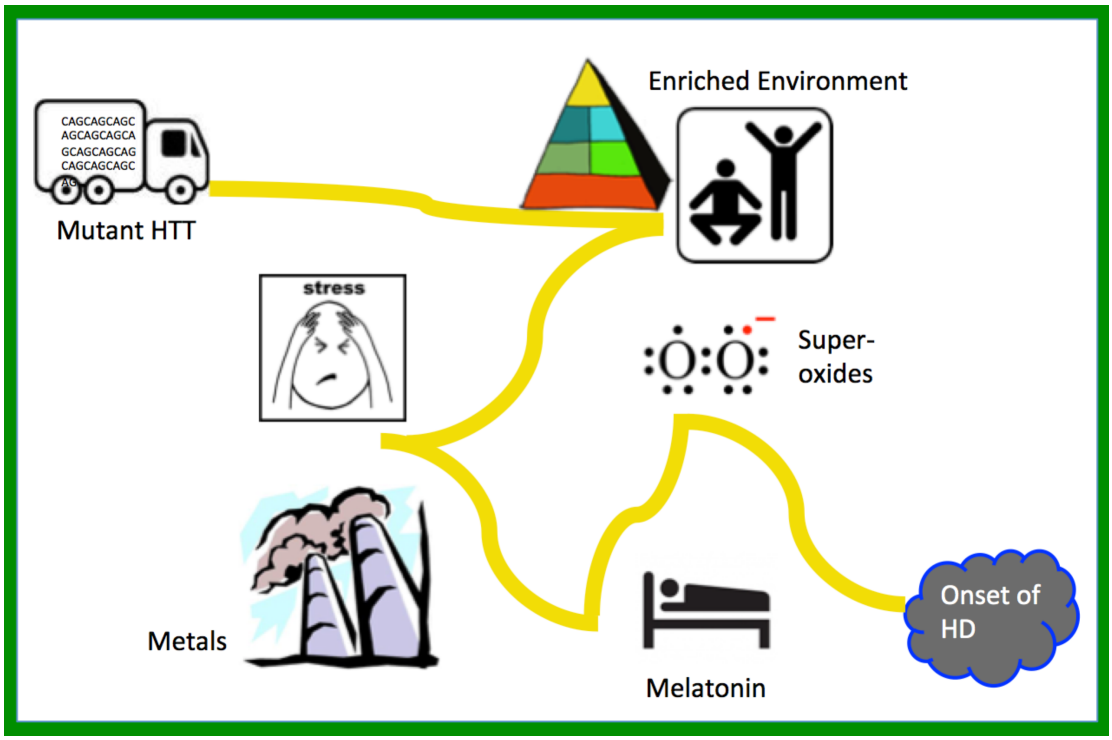

Figure 1-6: Examples of environmental influences which may delay or hasten trajectory to HD onset.

Lifestyle effects

Environmental exposures with an influence on the age of onset of HD include cognitive stimulation, exercise, nutrition, stress, toxic exposures, pollution and metals. Some of these effects may be beneficial and some detrimental. Those most studied will be discussed below.

Exercise and environmental enrichment

Research mice are usually kept in small boxes with bedding, food and water. Under these standardized conditions, mice expressing full length or fragments of the mutant HTT protein develop motor and cognitive disease.[67] However, when allowed access to exercise wheels, stimulating toys and novel objects, their healthy phase is prolonged.[140-142] Exercise

alone prolongs the premanifest phase, as does environmental enrichment alone.[141-145]

Like cognitive enrichment, exercise increases BDNF levels.[146] The general function of BDNF is to promote neurogenesis and neuronal survival[147,148] through binding to the tyrosine kinase B receptor (TrkB), thereby phosphorylating and activating neuroprotective pathways.[147,149] Striatal neurons express TrkB to receive BDNF transported from the cortex or substantia nigra,[27] but have substantially less BDNF when compared to other brain regions.[148] TrkB levels are increased with exercise along with BDNF.[150,151] This addition to the reserve pool of healthy neurons may explain the protective effects observed in neurodegenerative diseases in general.[145] However, BDNF protein levels are increased via EE even in the HD murine model[152]. In HD, BDNF protein levels are reduced in serum and brain tissue,[152,153] as is BDNF gene transcription,[154] with higher levels of BDNF linked to slowing of neurodegeneration.[155]

The striatum relies on BDNF transported from the cortical neurons which produce it, but the vesicular transport system is negatively impacted by mutant HTT. The vesicular transport system depends upon an interaction between the HTT protein and Huntingtin-associated protein 1 (HAP1),[156] with HTT acting as a scaffold, bringing together the transport machinery, and enhancing vesicle travel speed and direction.[157] This will be further discussed below.

In addition HTT also regulates transcription of BDNF through interaction with its promoter and inhibits the neuron restrictive silencer element (NRSE), which inhibits BDNF transcription.[158] Mutant HTT loses this inhibitory capability and thereby decreases BDNF transcription.[158] Increasing BDNF through gene overexpression in mouse models[159] or indirectly through exercise or enrichment[145] protects MSNs and delays degeneration. Links between BDNF and metal in HD will be discussed below.

Emerging evidence has shown that increasing BDNF protein levels protects post-synaptic MSN's even in the presence of mutant *HTT*.[160] Furthermore, overexpression of cortical BDNF transcription ameliorates symptoms in HD model mice[57] and protects mitochondria.[159] Increasing BDNF in the brain, either directly or indirectly, has been suggested to improve the symptoms observed in HD, AD, PD and Amylotrophic Lateral Sclerosis (ALS).

Diet

There is also a role for diet in delaying the inevitable genetic destiny of HD. Glucose metabolism is altered in HD, with early weight gain followed by hyperglycemia and severe weight loss.[161] [162,163] Leptin levels are normal in premanifest human patients,[164] but levels do not increase appropriately with body mass index (BMI)[136,163] and leptin is high in murine models compared to wildtype.[165,166] The R6/2 mouse develops metabolic and motor symptoms similar to what is observed in HD human patients.[167] Treating these mice with dietary supplements of essential fatty acids (linoleic and a-linoleic acids) reduced motor signs such as foot clasping and locomotor deficits, but did not correct weight loss or reduction in dopamine receptors.[168] A randomized placebo-controlled double-blind study of fatty acid supplementation in humans with HD also showed a significant improvement compared to placebo.[169] Interestingly, restriction of a-linoleic acid reduces BDNF in a striatal specific manner in wildtype mice.[170] Other dietary manipulations such as dietary restriction (DR) (fasting on alternate days), have been shown to be neuroprotective in wildtype animals,[171] delaying locomotor dysfunction, reducing oxidative stress, restoring BDNF levels and glucose metabolism, and increasing lifespan in mice.[166] The DR model has also been shown to increase longevity in *C. elegans.*[172,173] Ironically, both DR and fatty acid supplementation increases BDNF, which may be the protective mechanism of dietary manipulation in HD.

Oxidative stress

In addition to the factors that prolong the premanifest phase, oxidative stress and mitochondrial insults[174] from either genetic and/or environmental factors may hasten HD pathology. HD post-mortem tissue exhibits severe reductions in mitochondrial complexes II – IV in the striatum with no effect in the blood.[175] Furthermore, PET studies have revealed abnormalities in energy metabolism prior to striatal loss.[176] Systemic treatment with the complex II inhibitor, 3-nitropropionic acid (3NP), causes HD-like abnormal motor behavior,[177] striatal-specific neurodegeneration[178] and reduced phosphorylation of DARPP-32[179] (a protein encoded by a modifier gene reported to affect HD onset). Interestingly, pre-treatment with BDNF protects neurons from the effects of 3NP.[159]

Mitochondria are abnormal in HD with alterations in enzymatic complexes[180] and calcium (Ca^{2+}) kinetics in HD models.[176] In the YAC128 mouse, mutant HTT interacts with the NR2B subunit of the NMDA receptor, enhancing Ca^{2+} influx and increasing excitotoxicity in striatal MSN's, which carry the NR2B subunit longer in adulthood than most other neurons.[180] Mitochondria are both a source and target of reactive oxygen species,[181] and oxidative stress further hastens pathology, increasing apoptosis and aggregation in cultured cells expressing mutant *HTT*.[182] Overexpression of the mitochondrial enzyme, superoxide dismutase 1 (SOD1), which binds Cu/Zn, reverses oxidative stress in cultured murine cells.[182] Systemic supplementation with mitochondrial components, such as creatine and ubiquinone, also known as coenzymeQ10 (CoQ10), improved HD symptomology in both HD animal models and human clinical trials.[183,184] Perhaps diets highly enriched with creatine and CoQ10 may contribute to delay in onset of HD, while exposure to toxins that target or accumulate in mitochondria may hasten onset.

Metals

Pollutants and heavy metals, such as copper (Cu), iron (Fe), and manganese (Mn), have been suggested to influence the pathology of many neurodegenerative diseases, via alterations in vesicular transport, mitochondrial dysfunction, protein aggregation, and induction of oxidative stress.Though it is well established that metal homeostasis is altered in neurodegenerative diseases, the regional metal deposition profile differs for each disorder. In Huntington's disease (HD), abnormalities have been found in the tissue or cellular deposition or handling of copper (Cu), iron (Fe), calcium (Ca) and manganese (Mn) and in their neuronal functions which are either the result of disease processes, or the cause of pathology.

In general, it is the toxicity of over-exposure, or excess accumulation of metals, that is associated with pathology, such as is seen with Mn or Fe intoxication in parkinsonian conditions.[185] Recently it has been shown that deficiency or maldistribution of metals may be just as pathological as the toxicity of over-exposure. In amyotrophic lateral sclerosis, there is a reduction of Cu and zinc (Zn), while lead exposure is surprisingly protective.[186] In Alzheimer's disease (AD), a deficiency of Cu has been found in AD models, but the Cu content of post-mortem AD brain tissue did not differ from healthy controls, though the Cu stores were abnormally labile, or responsive to chelation.[187] Cell and animal models of HD have shown a surprising resistance to Mn accumulation and uptake, with down-stream reductions in Mn-dependent enzyme activity and metabolism, which will be described below. In the case of HD, a sub-regional or sub-cellular maldistribution of metals may best describe the pathogenic contribution of metallostasis to HD neuropathology.

The influence of metals on HD

Links between pollutants and heavy metals (especially Cu, Fe, and Mn), and neurodegenerative diseases have long been described,[180,188-190] but the role of metal exposure in the progression and symptomology of HD is not yet well understood. Because transition (or related) metals Cu, Fe, Zn, Ca and Mn, are essential to neurobiology, alterations in metallostasis can affect their roles as catalysts in reduction-oxidation reactions, cofactors for enzymes, and metabolism, all of which are important for neurological function.[188] Toxic exposure to these metals has been linked to induction of oxidative stress, mitochondrial dysfunction, protein aggregation, and alterations in vesicular transport[173,191,192] all of which play a part in neurodegenerative diseases. The brain appears to be more vulnerable to the toxic effects of metals than other organs, and the striatum appears to be especially vulnerable to mitochondrial toxins.[180] The presence of mutant HTT on mitochondrial membranes causes mitochondria to be even less resilient to excitotoxic insults than other tissues.

Each of the transition metals plays a part in the pathology of HD, yet the role of Mn is surprisingly reversed. A screen of metals [Mn^{2+}, Fe^{2+}, Cu^{2+}, Zn^{2+}, lead (Pb^{2+}), cadmium (Cd^{2+}), cobalt (Co^{2+}), and nickel (Ni^{2+})] on a striatal cell model of HD with cell survival as the outcome measure revealed a surprising interaction between mutant HTT and Mn.[193] The HD cells took up less Mn than normal controls, and HD cells were protected from Mn^{2+} exposure. This *in vitro* finding was recapitulated *in vivo*, i.e. mouse models of HD accumulated less striatal Mn than wild-type after subcutaneous exposure.[193,194]

Location of metal deposition in brain

Regional accumulation of metals in brain differs by ion and by concentration and duration of exposures, suggesting that different transporters are invoked by acute and or chronic exposures.

Excess exposure

Following excess exposure in wild type rats, Fe accumulates in the globus pallidus, Cu in the striatum and thalamus, and Mn in the thalamus and substantia nigra.[195]

Metal deposition in HD

Emerging studies have demonstrated accumulation of Cu^{2+} and Fe^{2+} in HD[196] and decreased serum ferritin in the striatum of HD.[197] While Mn is surprisingly decreased in HD models, an increase of Fe and Cu is found in the affected brain regions (**Figure 1-7**) (described in each section below). Interestingly, increased striatal Zn concentrations have also been noted in post-mortem HD patient brain.[198]

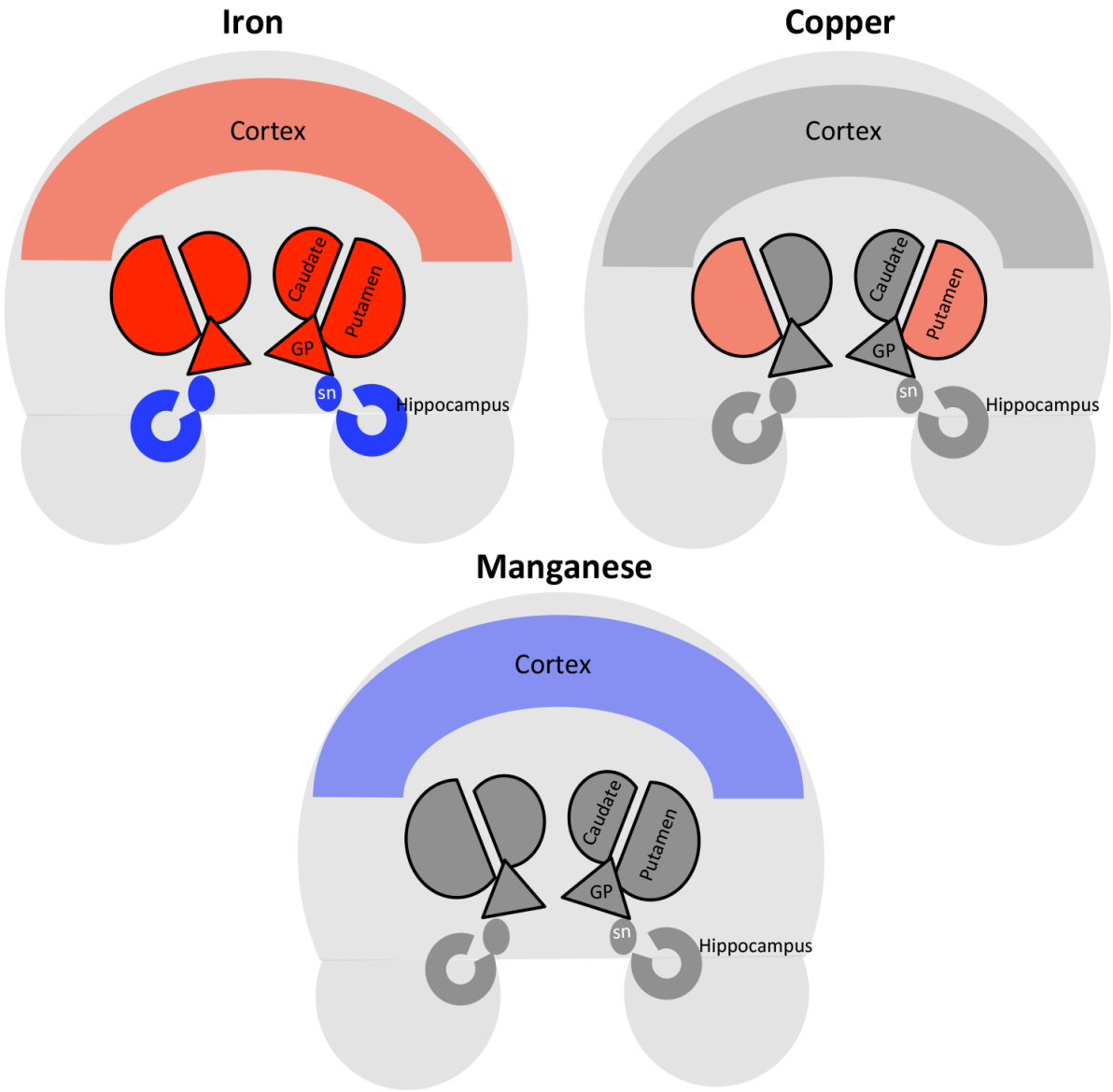

Figure 1-7. Schematic representation of regional metal accumulation in HD. Very few studies have investigated the localization of metal deposits in HD patients. Copper: Post-mortem increases in putamen in one study,[199] no increase in another.[198] Iron: Post-mortem studies show increased Fe in caudate, putamen and globus pallidus.[198-201] Correlations between imaging signal and atomic absorption assay of metal content[200], and correlation of MRI phase evolution of susceptibility signals with ICPMS (FM/ICPMS)[202] suggested increased Fe in caudate nucleus, putamen and globus pallidus, and also found decreased Fe in hippocampus and substantia nigra. Manganese: Post-mortem, no differences between HD and controls.[198,199] as well as FM/ICPMS suggested reductions in cortical subregions.[198] Red indicates excess deposition compared to normal, blue indicates a deficit, dark grey indicates evidence of no change in regional accumulation, light gray indicates no or limited available data.

Recently, a drug targeted at an HTT-metal interaction was brought to clinical trial. Hydroxyquinoline (PBT2), a compound that reduces copper binding to the Huntingtin protein, progressed through Phase II clinical trials with 109 patients. The medication was considered safe and well received by subjects, but lack of significant improvement in cognition or function prevented the drug from continuing to Phase III trials.[122,203] Yet, the influence of environmental factors on disease progression suggests that the aberrant properties of mutant HTT can be mitigated, and exploration of these factors, such as the gene environment interaction between HTT and metals, may reveal further therapeutic targets.

Autophagy and metals in Huntington's disease

Disturbances in macroautophagy have recently been implicated as a cause of pathology in many neurodegenerative diseases, including HD.[204] Cells transport waste products, including metalloproteins, between organelles and from within the cytoplasm to outside of the cell membrane via autophagosomes that envelope and contain toxic products such as misfolded proteins and damaged organelles.[205] Interestingly, *HTT* shares structural similarity with a yeast autophagy gene, Atg11, which has similarities to both a GABA receptor and an autophagic scaffold.[57] In HD, autophagosomes are frequently devoid of cargo,[206] though their number and form is unaffected, suggesting that there is a defect in the cargo-recognition function. This abnormality may allow for the buildup of aggregates of HTT and other toxic products, especially Fe-containing proteins, which may contribute to the metal dyshomeostasis seen in HD (described below).

In a *Drosophila* model of HD, reducing wild-type HTT function disturbs macroautophagy, and conditionally knocking out *Htt* in adult mice also causes signs of autophagosomal dysfunction, including accumulation of p62, which is an autophagic receptor

protein[24]. Selective autophagy is the process by which particular proteins are engulfed by double-membrane vesicles for transport between intracellular compartments.[207] Ochaba et al., found that HTT is necessary for selective autophagy in both *Drosophila* and mouse, and that mutant HTT causes a deficit in protein clearance that is likely related to this reduction in selective autophagy.[24,208] Htt knockout in wild-type mouse brain leads to accumulation of both p62- and ubiquitin- containing aggregates, which may indicate breakdown of the selective autophagic process which disposes of these products.[24,209] Clearance of the Fe-binding protein ferritin occurs through selective autophagy, and ferritin clearance is impaired by mutant HTT in patients with HD and in mouse models.[102,210,211] This obstruction of ferritin processing could lead to the increased intracellular Fe-storage abnormalities seen in HD (discussed below).

One integral protein to the membrane of the autophagosome is the Clathrin Light Chain (CLC), which is known to be regulated by Huntingtin Interacting Protein-1 (HIP1).[212] CLC forms clathrin-coated vesicles that are part of the endosomal recycling system as well as the autophagosome. This pathway is also related to Fe homeostasis, through transferrin, a protein that binds and transports Fe. The transferrin receptor is taken up by the rapid recycling endosomal G-clathrin vesicles which are mediated by CLC,[213] a pathway which links the HTT interacting proteins with both autophagy, transferrin receptor recycling and metal homeostasis.

Metal dyshomeostasis itself may be the root cause of macroautophagy alterations in HD. Zhang et al., found that Mn exposure increased autophagy acutely in wild-type rats post-exposure, but thereafter inhibited autophagy, when measured up to 28 days later.[214] And, in cultured dopaminergic neurons, Mn nanoparticles activated autophagic cell death.[215] Furthermore, Cu exposure leads to the autophagosomal destruction of mitochondria (mitophagy) and related apoptosis when Cu is complexed with dopamine.[216] Fe also has an

effect on autophagy, with some studies showing autophagic increases after Fe accumulation, and other data demonstrating Fe-induced reductions.[217] The interaction between metal homeostasis and macroautophagy has not yet been studied in the context of HD, though both pathways are clearly involved in the disease process.

Macroautophagy proteins can regulate cell cycle progression, mitosis, and selective autophagic clearance.[218-220] Other vesicular transport systems such as microvesicles and exosomes may also connect metal homeostasis with HD. There is new interest in this interplay between metals, HTT and macroautophagy.

Exosomes and metal in Huntington's disease

Exosomes are very small vesicles (50nm or less in diameter) in the extracellular space, that contain proteins and waste products, including metals.[221] These exosomes originate in the endosome and contain transferrin receptors, among other proteins, and may also play a role in intracellular metal homeostasis and metal transport between organelles. In addition to carrying metals and metal receptors, exosomes have been found to deliver toxic trinucleotide RNA's, and fragments of polyglutamine proteins from one cell to another, spreading these fragments in a prion-like fashion.[222] HTT has been associated with exosomal protein in several studies, suggesting that it either plays a part in exosomal regulation, or that exosomes serve to recycle or dispose of HTT.[222-224] Exosomal contents may prove to serve as a biomarker, both for metal exposure as well as for clinical treatment trials.

Iron

HD has been associated with altered Fe homeostasis in a number of *ex vivo* and *in vivo* human studies, focusing mainly on the vulnerable basal ganglia structures. Post-mortem analysis of patient brains has shown increased Fe levels in HD caudate, putamen, and globus

pallidus,[198-200] which is consistent with the macroautophagy deficits mentioned above. Mice expressing mutant HTT fragments show increased Fe buildup in brain as the disease progresses.[225,226] In human patients with HD, there is also abnormal accumulation of striatal Fe and Cu as symptoms progress.[201]

Correlation of MRI signal (field mapping evolution measurements) with ICPMS measurements of transition metals points to abnormal iron deposition in HD caudate, putamen, globus pallidus, and cortex at different disease stages, including pre-manifest HD, suggesting a role for Fe as a biomarker for the disease and implicating Fe dysregulation in HD pathogenesis[198,202,227-234] **(Figure 1-7)**. Imaging studies correlating T2 measures with CAG repeat number and clinical features in HD patients suggest that longer CAG tracts may be associated with higher amounts of toxic forms of Fe in certain vulnerable basal ganglia structures.[230,231] Furthermore, nuclear inclusions of fragments of the mutant polyQ protein are associated with Fe-dependent oxidation.[235]

More recent magnetic resonance studies have examined the relationship between brain atrophy and Fe deposition in HD. One study reported that increased Fe accumulation in early-manifest HD basal ganglia and atrophy of those regions occurred independently of each other.[232] Another study of pre-symptomatic HD subjects found that both excessive Fe accumulation and volumetric losses in the basal ganglia which began at the pre-symptomatic disease stage intensified with disease progression and CAG repeat number.[234] A recent imaging study by van Bergen et al,[202] confirmed increased Fe levels in the caudate nucleus, putamen, and globus pallidus of subjects with pre-manifest HD, showing significant atrophy in the caudate nucleus and putamen which was inversely correlated with Fe levels in those regions. The investigators also reported significantly decreased Fe in hippocampus and substantia nigra

of pre-manifest HD patients**.** Thus, while the role of Fe in HD neuropathology remains under investigation, the links between altered Fe homeostasis in HD brain and other clinical and biological features of the disease suggest that Fe may play a role in HD pathogenesis and/or serve as a tool for studying HD.

The mechanisms leading to Fe accumulation in HD brain are unknown, but may be related to any or all of three known Fe-related proteins: ferritin (the Fe storage protein), transferrin (a protein that binds Fe) or ferroportin (a transmembrane protein that moves Fe across membranes). *Ex vivo* and imaging studies have shown increased levels of ferritin, in post-mortem and earlier-stage HD basal ganglia and cortex, particularly in microglia with morphologic abnormalities,[200,210] though ferritin was decreased in the serum of patients.[236] This low serum ferritin is characteristic of a similar autosomal dominant progressive movement disorder known as neuroferritinopathy, or adult-onset basal ganglia disease, which is caused by a mutation in the ferritin light chain (FTL) gene. The FTL mutation results in abnormal Fe and ferritin accumulation in the basal ganglia, and the symptoms of motor dysfunction are very similar to thost of HD.[237-241]

The HTT protein is intimately connected with cellular Fe metabolism, but the exact relationship and direction of the Fe-HTT regulation, is unclear. HTT co-fractionates with the transferrin receptor (TfR)[242] and some data indicates that HTT itself is an Fe-responsive protein.[101] On the other hand, reduction of HTT expression in zebrafish leads to increased TfR1 expression in hypochromic blood.[102] Upon exposure to bioavailable Fe, this phenotype is reversed, suggesting a functional role of wild-type huntingtin in making endocytosed Fe accessible, perhaps releasing Fe from endocytic vesicles.

Supplemental Fe may be detrimental in HD, even in the prodromal phases, as it has been shown in two different HD mouse models that supplementation with Fe in the neonatal period causes more severe striatal degeneration to develop.[243,244] Furthermore, HTT aggregates are increased with Fe-dependent oxidation and protected with deferoxamine, an Fe chelator.[225] Cu is also implicated in HD pathology, as both Cu and Fe exposures have been linked to increased aggregation of mutant HTT[226] and a Cu/Fe chelator, clioquinol, an anti-fungal drug, reduced mutant HTT aggregates while also rescuing the HD behavioral phenotype in R6/2 mice.[245] There is also a connection between Cu and Fe, in that Cu treatment induces ferroportin expression, allowing for Fe efflux from cultured macrophage cells,[246] though Cu deficiency has no impact.[247]

Copper

The role of Cu and Cu-binding proteins in patients with HD is still under investigation. Dexter et al., reported increased Cu levels in post-mortem HD putamen,[199] however, a more recent study by Rosas et al. using field mapping evolution measurements (obtained through MRI) correlated with direct ICPMS analysis of dissected tissue, did not find elevated Cu levels in HD brain[198] (**Figure 1-7**). Indirect evidence that Cu accumulation may be high is found in analysis of gene expression data from post-mortem HD patient brain tissue revealed upregulation of genes encoding Cu-binding proteins, including metallothioneins 1 and 2 (MT1 and MT2) and ceruloplasmin.[248,249] Though those studies were post-mortem, another study of oxidative damage in the cerebrospinal fluid (CSF) of living patients found increased lipoperoxidation in the CSF of those with HD along with decreased Cu/Zn-dependent superoxide dismutase (SOD1) activity and decreased ceruloplasmin ferroxidase activity, which

was correlated to motor assessments.[250] While these findings suggest that free Cu may be increased in HD CSF, the investigators did not report significantly higher levels of free Cu.

Rodents exposed to quinolinic acid exhibit striatal deficits that resemble those seen in HD due to neuronal death by depletion of GABA.[251] These QUIN-HD model rats accumulate excess Cu in the striatum, which may be linked to the agonistic effect of quinolinic acid on NMDA-type glutamate receptors.[252] Cu is released after activation of NMDA receptors, and their stimulation increases trafficking of a Cu-specific transporter, ATP7A, from the late Golgi into neuronal dendrites, resulting in local Cu accumulation.[253] Surprisingly, pre-treatment of rats with Cu-supplemented drinking water before exposure to quinolinic acid prevents some of the HD-related symptoms.[254]

Though HTT interacts indirectly with Fe through Fe-binding proteins and transporters, the connection between HTT and Cu is direct. Experiments *in vitro* show that Cu^{2+} interacts with wild-type HTT, decreasing the solubility of HTT protein fragments[76], and increasing aggregation. Previously, aggregates were thought to be inert, but it has now been shown that Cu also binds with HTT after aggregation, possible further exacerbating their insolubility.[91] Fewer aggregates form when Cu influx transporters (DmATP7 and Ctr1B) are blocked in *Drosophila* HD models.[76,255] Furthermore, there are two residues on the HTT protein which may bind Cu (Met8 and His82), and when these sites are mutated in HD Drosophila models, the toxic effects of mutant HTT are prevented.[255] Copper binds directly to the N-terminal region of the HTT protein[226], but a correlation with number of repeats and the strength of Cu binding has not been found, It appears that neither the Cu alone, nor the polyQ extension on HTT exon 1 alone caused HD symptoms, but the combination of the HD mutation and Cu exposure was toxic, suggesting that Cu-related treatments could be of benefit to HD patients.

Calcium

Ca is very important in HD, both on a regional and molecular level. Intracellular Ca^{2+} modulates many biological functions through its role as a second messenger,[256] thus it is tightly regulated by intracellular sequestration through Ca buffering proteins (such as calbindin), and by the presence of storage pools in the mitochondria and endoplasmic reticulum (ER).[257] Neuronal Ca levels were much higher in R6/2 mice (a mouse model which bears the first exon of mutant human *HTT*) than in their wild-type littermates after symptoms had begun.[258]

Optimal intracellular Ca concentration is controlled by AMPA receptors, glutamate-gated NMDA receptors, voltage-gated Ca channels, and Store-Operated Calcium Entry (SOCE) channels.[257] In cultured neurons from HD model mice, there is increased intracellular Ca response to glutamate challenge, leading to oxidative stress which can cause apoptosis.[259-263] Interestingly, it is chiefly the duration of Ca response that is altered, rather than the total Ca, implicating abnormalities in cellular Ca handling rather than influx.[257]

Subcellularly, Ca can be released from pools stored in the mitochondria or in the ER, and there is indirect evidence that HTT may be involved in the regulation of these Ca stores. The HTT protein directly binds with the mitochondrial membrane,[264] and the polyQ expansion reduces mitochondrial sequestration of Ca, suggesting a role in controlling mitochondrial Ca transport. There is also direct binding of the HTT protein with Huntington Associated Protein 1 (HAP1) and inositol tri-phosphate (IP3) which causes IP3 to interact with the IP3 receptor on the ER membrane.[265] The IP3 receptor is a Ca channel that is activated by IP3, allowing for the release of Ca in response to mGluR1/5 receptor activation. Mutant HTT binds to the type 1 IP3 receptor (InsP3R1), increasing its activity and reducing Ca levels in the ER.[262,266]

The store-operated calcium (SOC) release pathway is also affected in HD. Stroma Interacting Molecule 2 (STIM2) is a plasma membrane protein located in the ER that participates in SOC release as a Ca sensor.[267] When ER Ca decreases, STIM2 interacts with SOC entry channels to resupply the ER with Ca. Bezprozvanny and colleagues found that STIM2 expression is elevated in HD model mouse striatum, possibly as a compensatory mechanism to release the excess Ca accumulation caused by the abnormal sensitivity of the InsP3R1 when it is bound to mutant HTT.[268] Further, depletion of Ca from the ER activates the SOC pathway in neuronal spines in the HD mouse model, perhaps leading to the reduction in spine density found in aged HD model mice compared to wild-type. Indeed, reducing expression of either InsP3R1 or STIM2 reversed the dendritic spine abnormalities in HD mouse cortical-striatal cell cultures compared to wild-type.

Thus, the levels of Ca in neurons and within neuronal organelles contributes to HD abnormalities. Ca dyshomeostsis may also play a role in the HD associated alterations in the bioavailabilities of other metals as well. The homeostasis of both Ca and Mn are disrupted in HD, and the two metals are closely related in many biological pathways, often transported through the same channels, though sometimes moving in opposite directions

Manganese

Overexposure to Mn causes preferential accumulation in the mitochondria of the brain and liver,[269] especially in the basal ganglia of rats[270] and humans,[191] the region also most affected in both HD and PD. This distribution is different than that depicted in **Figure 1-7**, which refers to metal accumulation in HD, rather than overexposure. Mn also appears to selectively accumulate in the mitochondria of these regions[269] and causes apoptosis from mitochondrial cytochrome c release[271,272] in a caspase-dependent pathway.[273] Subtoxic Mn

exposure causes greater susceptibility to 1-methyl-4-phenylpyridinium (MPP), a mitochondrial toxin which targets nigral dopaminergic neurons and is used to create a common PD model. This MPP+ related apoptosis can be reversed by n-acetyl creatine.[274] In HD, it is possible that mutant HTT causes normal levels of bioactive agents to become neurotoxic to selected populations of neurons.

Overexposure to Mn increases risk of a Parkinsonian phenotype referred to as manganism.[275,276] This condition is similar to HD in that it is a progressive neurodegenerative condition which primarily affects the basal ganglia motor pathways. However, there is a loss of nigrostriatal dopaminergic pathways in PD, while there is deterioration of the striatal GABAergic MSN's in HD, and motor symptoms differ.[277] Surprisingly, in HD models, studies utilizing immortalized striatal cells and striatum of knock-in mouse models of HD have demonstrated a resistance to the toxic effects of Mn.[193,278,279] Emerging evidence from our laboratory aimed at examining Mn transport dynamics in the immortalized striatal cell line model of HD has revealed a significant decrease in instantaneous Mn uptake and storage capablilites in mutant *HTT* cells compared to wildtype following Mn exposure, though efflux rate appears to be equal in both.[280] It is possible that mutant HTT interacts with constituents of the neuronal Mn transport system and dysregulates Mn kinetics. This gene-environment interaction between mutant HTT and Mn may serve to explain how xenobiotics influence genetic functions. A reduction of Mn in neurons would alter the normal neuronal and glial functions of proteins that cannot function without sufficient Mn, and their byproducts would be reduced in HD. A review of studies on manganoproteins in Chapter III shows either directly or indirectly that they are all reduced in the presence of mutant HTT.

To study the effect of Mn on HD pathology, we generated a novel HD model which we

hypothesized would more rapidly show pathology than the existing mouse models. This model, the BAC225, will be described in Chapter II.

References

1. Novak MJ, Tabrizi SJ. Huntington's disease. *BMJ* 2010; **340**: c3109.
2. The Huntington's Disease Collaborative Research Group. A novel gene containing a trinucleotide repeat that is expanded and unstable on Huntington's disease chromosomes. *Cell* 1993; **72**(6): 971-83.
3. Chopra R, Shakkottai VG. The role for alterations in neuronal activity in the pathogenesis of polyglutamine repeat disorders. *Neurotherapeutics* 2014; **11**(4): 751-63.
4. Squitieri F, Jankovic J. Huntington's disease: How intermediate are intermediate repeat lengths? *Movement Disorders* 2012; **27**(14): 1714-7.
5. Orr HT, Zoghbi HY. Trinucleotide repeat disorders. *Annu Rev Neurosci* 2007; **30**: 575-621.
6. Wolfe KJ, Cyr DM. Amyloid in neurodegenerative diseases: friend or foe? Seminars in cell & developmental biology; 2011: Elsevier; 2011. p. 476-81.
7. Hannan AJ. Review: Environmental enrichment and brain repair: harnessing the therapeutic effects of cognitive stimulation and physical activity to enhance experience-dependent plasticity. *Neuropathology and applied neurobiology* 2014; **40**(1): 13-25.
8. Babenko O, Kovalchuk I, Metz GA. Epigenetic programming of neurodegenerative diseases by an adverse environment. *Brain research* 2012; **1444**: 96-111.
9. Kremer B, Goldberg P, Andrew SE, et al. A worldwide study of the Huntington's disease mutation. The sensitivity and specificity of measuring CAG repeats. *N Engl J Med* 1994; **330**(20): 1401-6.
10. Schmitt I, Bachner D, Megow D, et al. Expression of the Huntington disease gene in rodents: cloning the rat homologue and evidence for downregulation in non-neuronal tissues during development. *Hum Mol Genet* 1995; **4**(7): 1173-82.
11. Barnes GT, Duyao MP, Ambrose CM, et al. Mouse Huntington's disease gene homolog (Hdh). *Somat Cell Mol Genet* 1994; **20**(2): 87-97.
12. Ross CA, Aylward EH, Wild EJ, et al. Huntington disease: natural history, biomarkers and prospects for therapeutics. *Nat Rev Neurol* 2014; **10**(4): 204-16.
13. Squitieri F, Jankovic J. Huntington's disease: how intermediate are intermediate repeat lengths? *Mov Disord* 2012; **27**(14): 1714-7.
14. Kay C, Collins JA, Miedzybrodzka Z, et al. Huntington disease reduced penetrance alleles occur at high frequency in the general population. *Neurology* 2016; **87**(3): 282-8.
15. Pringsheim T, Wiltshire K, Day L, Dykeman J, Steeves T, Jette N. The incidence and prevalence of Huntington's disease: a systematic review and meta-analysis. *Mov Disord* 2012; **27**(9): 1083-91.
16. Walker FO. Huntington's disease. *Lancet* 2007; **369**(9557): 218-28.
17. Dorner JL, Miller BR, Barton SJ, Brock TJ, Rebec GV. Sex differences in behavior and striatal ascorbate release in the 140 CAG knock-in mouse model of Huntington's disease. *Behav Brain Res* 2007; **178**(1): 90-7.
18. Zielonka D, Marinus J, Roos RA, et al. The influence of gender on phenotype and disease progression in patients with Huntington's disease. *Parkinsonism Relat Disord* 2013; **19**(2): 192-7.
19. Cattaneo E, Rigamonti D, Goffredo D, Zuccato C, Squitieri F, Sipione S. Loss of normal huntingtin function: new developments in Huntington's disease research. *Trends Neurosci* 2001; **24**(3): 182-8.

20. Cattaneo E, Zuccato C, Tartari M. Normal huntingtin function: an alternative approach to Huntington's disease. *Nat Rev Neurosci* 2005; **6**(12): 919-30.
21. Nasir J, Floresco SB, O'Kusky JR, et al. Targeted disruption of the Huntington's disease gene results in embryonic lethality and behavioral and morphological changes in heterozygotes. *Cell* 1995; **81**(5): 811-23.
22. Zuccato C, Valenza M, Cattaneo E. Molecular mechanisms and potential therapeutical targets in Huntington's disease. *Physiol Rev* 2010; **90**(3): 905-81.
23. Wang N, Gray M, Lu XH, et al. Neuronal targets for reducing mutant huntingtin expression to ameliorate disease in a mouse model of Huntington's disease. *Nat Med* 2014; **20**(5): 536-41.
24. Ochaba J, Lukacsovich T, Csikos G, et al. Potential function for the Huntingtin protein as a scaffold for selective autophagy. *Proc Natl Acad Sci U S A* 2014; **111**(47): 16889-94.
25. Wong YC, Holzbaur EL. The regulation of autophagosome dynamics by huntingtin and HAP1 is disrupted by expression of mutant huntingtin, leading to defective cargo degradation. *J Neurosci* 2014; **34**(4): 1293-305.
26. Trushina E, Dyer RB, Badger JD, 2nd, et al. Mutant huntingtin impairs axonal trafficking in mammalian neurons in vivo and in vitro. *Mol Cell Biol* 2004; **24**(18): 8195-209.
27. Gauthier LR, Charrin BC, Borrell-Pages M, et al. Huntingtin controls neurotrophic support and survival of neurons by enhancing BDNF vesicular transport along microtubules. *Cell* 2004; **118**(1): 127-38.
28. Zala D, Hinckelmann MV, Saudou F. Huntingtin's function in axonal transport is conserved in Drosophila melanogaster. *PLoS One* 2013; **8**(3): e60162.
29. Squitieri F, Almqvist EW, Cannella M, Cislaghi G, Hayden MR. Predictive testing for persons at risk for homozygosity for CAG expansion in the Huntington disease gene. *Clin Genet* 2003; **64**(6): 524-5.
30. Zeitlin S, Liu JP, Chapman DL, Papaioannou VE, Efstratiadis A. Increased apoptosis and early embryonic lethality in mice nullizygous for the Huntington's disease gene homologue. *Nat Genet* 1995; **11**(2): 155-63.
31. Lopes F, Barbosa M, Ameur A, et al. Identification of novel genetic causes of Rett syndrome-like phenotypes. *J Med Genet* 2016; **53**(3): 190-9.
32. Rodan LH, Cohen J, Fatemi A, et al. A novel neurodevelopmental disorder associated with compound heterozygous variants in the huntingtin gene. *Eur J Hum Genet* 2016.
33. Ho AK, Gilbert AS, Mason SL, Goodman AO, Barker RA. Health-related quality of life in Huntington's disease: Which factors matter most? *Mov Disord* 2009; **24**(4): 574-8.
34. D Lo HR, Hersch S. Biomarkers to Enable the Development of Neuroportective Therapies for Huntington's Disease. Neurobiology of Huntington's Disease. Boca Raton: CRC Press; 2011.
35. Duff K, Beglinger LJ, Theriault D, Allison J, Paulsen JS. Cognitive deficits in Huntington's disease on the Repeatable Battery for the Assessment of Neuropsychological Status. *J Clin Exp Neuropsychol* 2010; **32**(3): 231-8.
36. Thompson JC, Harris J, Sollom AC, et al. Longitudinal evaluation of neuropsychiatric symptoms in Huntington's disease. *J Neuropsychiatry Clin Neurosci* 2012; **24**(1): 53-60.
37. Stack EC, Dedeoglu A, Smith KM, et al. Neuroprotective effects of synaptic modulation in Huntington's disease R6/2 mice. *J Neurosci* 2007; **27**(47): 12908-15.

38. Douaud G, Gaura V, Ribeiro MJ, et al. Distribution of grey matter atrophy in Huntington's disease patients: a combined ROI-based and voxel-based morphometric study. *Neuroimage* 2006; **32**(4): 1562-75.
39. Boutell JM, Thomas P, Neal JW, et al. Aberrant interactions of transcriptional repressor proteins with the Huntington's disease gene product, huntingtin. *Hum Mol Genet* 1999; **8**(9): 1647-55.
40. Sassone J, Colciago C, Cislaghi G, Silani V, Ciammola A. Huntington's disease: the current state of research with peripheral tissues. *Exp Neurol* 2009; **219**(2): 385-97.
41. Kirkwood SC, Su JL, Conneally P, Foroud T. Progression of symptoms in the early and middle stages of Huntington disease. *Arch Neurol* 2001; **58**(2): 273-8.
42. Gusella JF, MacDonald ME. Huntington's disease: the case for genetic modifiers. *Genome Med* 2009; **1**(8): 80.
43. Rosenblatt A, Brinkman RR, Liang KY, et al. Familial influence on age of onset among siblings with Huntington disease. *Am J Med Genet* 2001; **105**(5): 399-403.
44. Friedman JH, Trieschmann ME, Myers RH, Fernandez HH. Monozygotic twins discordant for Huntington disease after 7 years. *Arch Neurol* 2005; **62**(6): 995-7.
45. Heemskerk AW, Roos RA. Aspiration pneumonia and death in Huntington's disease. *PLoS Curr* 2012; **4**: RRN1293.
46. Saudou F, Humbert S. The Biology of Huntingtin. *Neuron* 2016; **89**(5): 910-26.
47. Squitieri F, Frati L, Ciarmiello A, Lastoria S, Quarrell O. Juvenile Huntington's disease: does a dosage-effect pathogenic mechanism differ from the classical adult disease? *Mech Ageing Dev* 2006; **127**(2): 208-12.
48. Andresen JM, Gayan J, Djousse L, et al. The relationship between CAG repeat length and age of onset differs for Huntington's disease patients with juvenile onset or adult onset. *Ann Hum Genet* 2007; **71**(Pt 3): 295-301.
49. Quarrell OW, Nance MA, Nopoulos P, Paulsen JS, Smith JA, Squitieri F. Managing juvenile Huntington's disease. *Neurodegener Dis Manag* 2013; **3**(3).
50. Spires TL, Hannan AJ. Nature, nurture and neurology: gene-environment interactions in neurodegenerative disease. FEBS Anniversary Prize Lecture delivered on 27 June 2004 at the 29th FEBS Congress in Warsaw. *FEBS J* 2005; **272**(10): 2347-61.
51. Moughamian AJ, Osborn GE, Lazarus JE, Maday S, Holzbaur EL. Ordered recruitment of dynactin to the microtubule plus-end is required for efficient initiation of retrograde axonal transport. *J Neurosci* 2013; **33**(32): 13190-203.
52. Cornett J, Cao F, Wang CE, et al. Polyglutamine expansion of huntingtin impairs its nuclear export. *Nat Genet* 2005; **37**(2): 198-204.
53. Valor LM. Transcription, epigenetics and ameliorative strategies in Huntington's Disease: a genome-wide perspective. *Mol Neurobiol* 2015; **51**(1): 406-23.
54. Benn CL, Sun T, Sadri-Vakili G, et al. Huntingtin modulates transcription, occupies gene promoters in vivo, and binds directly to DNA in a polyglutamine-dependent manner. *J Neurosci* 2008; **28**(42): 10720-33.
55. Bae BI, Xu H, Igarashi S, et al. p53 mediates cellular dysfunction and behavioral abnormalities in Huntington's disease. *Neuron* 2005; **47**(1): 29-41.
56. Saudou F, Finkbeiner S, Devys D, Greenberg ME. Huntingtin acts in the nucleus to induce apoptosis but death does not correlate with the formation of intranuclear inclusions. *Cell* 1998; **95**(1): 55-66.

57. Steffan JS. Does Huntingtin play a role in selective macroautophagy? *Cell Cycle* 2010; **9**(17): 3401-13.
58. Higgins MK, McMahon HT. Snap-shots of clathrin-mediated endocytosis. *Trends Biochem Sci* 2002; **27**(5): 257-63.
59. Davranche A, Aviolat H, Zeder-Lutz G, et al. Huntingtin affinity for partners is not changed by polyglutamine length: aggregation itself triggers aberrant interactions. *Hum Mol Genet* 2011; **20**(14): 2795-806.
60. Harjes P, Wanker EE. The hunt for huntingtin function: interaction partners tell many different stories. *Trends Biochem Sci* 2003; **28**(8): 425-33.
61. Kaltenbach LS, Romero E, Becklin RR, et al. Huntingtin interacting proteins are genetic modifiers of neurodegeneration. *PLoS Genet* 2007; **3**(5): e82.
62. Culver BP, Savas JN, Park SK, et al. Proteomic analysis of wild-type and mutant huntingtin-associated proteins in mouse brains identifies unique interactions and involvement in protein synthesis. *J Biol Chem* 2012; **287**(26): 21599-614.
63. Goehler H, Lalowski M, Stelzl U, et al. A protein interaction network links GIT1, an enhancer of huntingtin aggregation, to Huntington's disease. *Mol Cell* 2004; **15**(6): 853-65.
64. Kim MW, Chelliah Y, Kim SW, Otwinowski Z, Bezprozvanny I. Secondary structure of Huntingtin amino-terminal region. *Structure* 2009; **17**(9): 1205-12.
65. Warby SC, Doty CN, Graham RK, Shively J, Singaraja RR, Hayden MR. Phosphorylation of huntingtin reduces the accumulation of its nuclear fragments. *Mol Cell Neurosci* 2009; **40**(2): 121-7.
66. Squitieri F, Gellera C, Cannella M, et al. Homozygosity for CAG mutation in Huntington disease is associated with a more severe clinical course. *Brain* 2003; **126**(Pt 4): 946-55.
67. Mangiarini L, Sathasivam K, Seller M, et al. Exon 1 of the HD gene with an expanded CAG repeat is sufficient to cause a progressive neurological phenotype in transgenic mice. *Cell* 1996; **87**(3): 493-506.
68. Steffan JS, Agrawal N, Pallos J, et al. SUMO modification of Huntingtin and Huntington's disease pathology. *Science* 2004; **304**(5667): 100-4.
69. Kalchman MA, Graham RK, Xia G, et al. Huntingtin is ubiquitinated and interacts with a specific ubiquitin-conjugating enzyme. *J Biol Chem* 1996; **271**(32): 19385-94.
70. Steffan JS, Bodai L, Pallos J, et al. Histone deacetylase inhibitors arrest polyglutamine-dependent neurodegeneration in Drosophila. *Nature* 2001; **413**(6857): 739-43.
71. Jeong H, Then F, Melia TJ, Jr., et al. Acetylation targets mutant huntingtin to autophagosomes for degradation. *Cell* 2009; **137**(1): 60-72.
72. Yanai A, Huang K, Kang R, et al. Palmitoylation of huntingtin by HIP14 is essential for its trafficking and function. *Nat Neurosci* 2006; **9**(6): 824-31.
73. Martin DD, Heit RJ, Yap MC, Davidson MW, Hayden MR, Berthiaume LG. Identification of a post-translationally myristoylated autophagy-inducing domain released by caspase cleavage of huntingtin. *Hum Mol Genet* 2014; **23**(12): 3166-79.
74. Jones L, Hughes A. Pathogenic mechanisms in Huntington's disease. *Int Rev Neurobiol* 2011; **98**: 373-418.
75. Ratovitski T, Gucek M, Jiang H, et al. Mutant huntingtin N-terminal fragments of specific size mediate aggregation and toxicity in neuronal cells. *J Biol Chem* 2009; **284**(16): 10855-67.

76. Fox JH, Connor T, Stiles M, et al. Cysteine oxidation within N-terminal mutant huntingtin promotes oligomerization and delays clearance of soluble protein. *J Biol Chem* 2011; **286**(20): 18320-30.
77. Wagster MV, Hedreen JC, Peyser CE, Folstein SE, Ross CA. Selective loss of [3H]kainic acid and [3H]AMPA binding in layer VI of frontal cortex in Huntington's disease. *Exp Neurol* 1994; **127**(1): 70-5.
78. Hedreen JC, Peyser CE, Folstein SE, Ross CA. Neuronal loss in layers V and VI of cerebral cortex in Huntington's disease. *Neurosci Lett* 1991; **133**(2): 257-61.
79. Younes L, Ratnanather JT, Brown T, et al. Regionally selective atrophy of subcortical structures in prodromal HD as revealed by statistical shape analysis. *Hum Brain Mapp* 2014; **35**(3): 792-809.
80. Raymond LA, Andre VM, Cepeda C, Gladding CM, Milnerwood AJ, Levine MS. Pathophysiology of Huntington's disease: time-dependent alterations in synaptic and receptor function. *Neuroscience* 2011; **198**: 252-73.
81. Soares-Cunha C, Coimbra B, Sousa N, Rodrigues AJ. Reappraising striatal D1- and D2-neurons in reward and aversion. *Neurosci Biobehav Rev* 2016; **68**: 370-86.
82. Paulson HL, Albin RL. Huntington's Disease: Clinical Features and Routes to Therapy. In: Lo DC, Hughes RE, eds. Neurobiology of Huntington's Disease: Applications to Drug Discovery. Boca Raton (FL); 2011.
83. Caron NS, Desmond CR, Xia J, Truant R. Polyglutamine domain flexibility mediates the proximity between flanking sequences in huntingtin. *Proc Natl Acad Sci U S A* 2013; **110**(36): 14610-5.
84. DiFiglia M, Sapp E, Chase K, et al. Huntingtin is a cytoplasmic protein associated with vesicles in human and rat brain neurons. *Neuron* 1995; **14**(5): 1075-81.
85. Sharp AH, Loev SJ, Schilling G, et al. Widespread expression of Huntington's disease gene (IT15) protein product. *Neuron* 1995; **14**(5): 1065-74.
86. Atwal RS, Xia J, Pinchev D, Taylor J, Epand RM, Truant R. Huntingtin has a membrane association signal that can modulate huntingtin aggregation, nuclear entry and toxicity. *Hum Mol Genet* 2007; **16**(21): 2600-15.
87. Thompson LM, Aiken CT, Kaltenbach LS, et al. IKK phosphorylates Huntingtin and targets it for degradation by the proteasome and lysosome. *J Cell Biol* 2009; **187**(7): 1083-99.
88. Ehrnhoefer DE, Sutton L, Hayden MR. Small changes, big impact: posttranslational modifications and function of huntingtin in Huntington disease. *Neuroscientist* 2011; **17**(5): 475-92.
89. Poirier MA, Jiang H, Ross CA. A structure-based analysis of huntingtin mutant polyglutamine aggregation and toxicity: evidence for a compact beta-sheet structure. *Hum Mol Genet* 2005; **14**(6): 765-74.
90. Arrasate M, Finkbeiner S. Protein aggregates in Huntington's disease. *Exp Neurol* 2012; **238**(1): 1-11.
91. Mitomi Y, Nomura T, Kurosawa M, Nukina N, Furukawa Y. Post-aggregation oxidation of mutant huntingtin controls the interactions between aggregates. *J Biol Chem* 2012; **287**(41): 34764-75.
92. Zhao T, Hong Y, Li S, Li XJ. Compartment-Dependent Degradation of Mutant Huntingtin Accounts for Its Preferential Accumulation in Neuronal Processes. *J Neurosci* 2016; **36**(32): 8317-28.

93. Tao T, Tartakoff AM. Nuclear relocation of normal huntingtin. *Traffic* 2001; **2**(6): 385-94.
94. Velier J, Kim M, Schwarz C, et al. Wild-type and mutant huntingtins function in vesicle trafficking in the secretory and endocytic pathways. *Exp Neurol* 1998; **152**(1): 34-40.
95. Gutekunst CA, Levey AI, Heilman CJ, et al. Identification and localization of huntingtin in brain and human lymphoblastoid cell lines with anti-fusion protein antibodies. *Proc Natl Acad Sci U S A* 1995; **92**(19): 8710-4.
96. Hoffner G, Kahlem P, Djian P. Perinuclear localization of huntingtin as a consequence of its binding to microtubules through an interaction with beta-tubulin: relevance to Huntington's disease. *J Cell Sci* 2002; **115**(Pt 5): 941-8.
97. Kegel KB, Sapp E, Yoder J, et al. Huntingtin associates with acidic phospholipids at the plasma membrane. *J Biol Chem* 2005; **280**(43): 36464-73.
98. Engelender S, Sharp AH, Colomer V, et al. Huntingtin-associated protein 1 (HAP1) interacts with the p150Glued subunit of dynactin. *Hum Mol Genet* 1997; **6**(13): 2205-12.
99. Li SH, Gutekunst CA, Hersch SM, Li XJ. Interaction of huntingtin-associated protein with dynactin P150Glued. *J Neurosci* 1998; **18**(4): 1261-9.
100. Qin ZH, Wang Y, Sapp E, et al. Huntingtin bodies sequester vesicle-associated proteins by a polyproline-dependent interaction. *J Neurosci* 2004; **24**(1): 269-81.
101. Hilditch-Maguire P, Trettel F, Passani LA, Auerbach A, Persichetti F, MacDonald ME. Huntingtin: an iron-regulated protein essential for normal nuclear and perinuclear organelles. *Hum Mol Genet* 2000; **9**(19): 2789-97.
102. Lumsden AL, Henshall TL, Dayan S, Lardelli MT, Richards RI. Huntingtin-deficient zebrafish exhibit defects in iron utilization and development. *Hum Mol Genet* 2007; **16**(16): 1905-20.
103. Lazarus JE, Moughamian AJ, Tokito MK, Holzbaur EL. Dynactin subunit p150(Glued) is a neuron-specific anti-catastrophe factor. *PLoS Biol* 2013; **11**(7): e1001611.
104. Rubinsztein DC. Lessons from animal models of Huntington's disease. *Trends Genet* 2002; **18**(4): 202-9.
105. Ramaswamy S, McBride JL, Kordower JH. Animal models of Huntington's disease. *ILAR J* 2007; **48**(4): 356-73.
106. Li XJ, Li S. Influence of species differences on the neuropathology of transgenic Huntington's disease animal models. *J Genet Genomics* 2012; **39**(6): 239-45.
107. Ruzo A, Ismailoglu I, Popowski M, et al. Discovery of novel isoforms of huntingtin reveals a new hominid-specific exon. *PLoS One* 2015; **10**(5): e0127687.
108. Kazemi-Esfarjani P, Benzer S. Genetic suppression of polyglutamine toxicity in Drosophila. *Science* 2000; **287**(5459): 1837-40.
109. Fernandez-Funez P, Nino-Rosales ML, de Gouyon B, et al. Identification of genes that modify ataxin-1-induced neurodegeneration. *Nature* 2000; **408**(6808): 101-6.
110. Marsh JL, Walker H, Theisen H, et al. Expanded polyglutamine peptides alone are intrinsically cytotoxic and cause neurodegeneration in Drosophila. *Human molecular genetics* 2000; **9**(1): 13-25.
111. Warrick JM, Chan HE, Gray-Board GL, Chai Y, Paulson HL, Bonini NM. Suppression of polyglutamine-mediated neurodegeneration in Drosophila by the molecular chaperone HSP70. *Nature genetics* 1999; **23**(4): 425-8.

112. Brand AH, Perrimon N. Targeted gene expression as a means of altering cell fates and generating dominant phenotypes. *development* 1993; **118**(2): 401-15.
113. Lee W-CM, Yoshihara M, Littleton JT. Cytoplasmic aggregates trap polyglutamine-containing proteins and block axonal transport in a Drosophila model of Huntington's disease. *Proceedings of the National Academy of Sciences of the United States of America* 2004; **101**(9): 3224-9.
114. Pallos J, Bodai L, Lukacsovich T, et al. Inhibition of specific HDACs and sirtuins suppresses pathogenesis in a Drosophila model of Huntington's disease. *Human molecular genetics* 2008; **17**(23): 3767-75.
115. Lu B, Al-Ramahi I, Valencia A, et al. Identification of NUB1 as a suppressor of mutant Huntingtin toxicity via enhanced protein clearance. *Nature neuroscience* 2013; **16**(5): 562-70.
116. Faber PW, Alter JR, MacDonald ME, Hart AC. Polyglutamine-mediated dysfunction and apoptotic death of a Caenorhabditis elegans sensory neuron. *Proceedings of the National Academy of Sciences* 1999; **96**(1): 179-84.
117. Parker JA, Connolly JB, Wellington C, Hayden M, Dausset J, Neri C. Expanded polyglutamines in Caenorhabditis elegans cause axonal abnormalities and severe dysfunction of PLM mechanosensory neurons without cell death. *Proceedings of the National Academy of Sciences* 2001; **98**(23): 13318-23.
118. Martinez-Finley EJ, Avila DS, Chakraborty S, Aschner M. Insights from Caenorhabditis elegans on the role of metals in neurodegenerative diseases. *Metallomics* 2011; **3**(3): 271-9.
119. Gidalevitz T, Wang N, Deravaj T, Alexander-Floyd J, Morimoto RI. Natural genetic variation determines susceptibility to aggregation or toxicity in a C. elegans model for polyglutamine disease. *BMC biology* 2013; **11**(1): 100.
120. Cherny RA, Ayton S, Finkelstein DI, Bush AI, McColl G, Massa SM. PBT2 reduces toxicity in a C. elegans model of polyQ aggregation and extends lifespan, reduces striatal atrophy and improves motor performance in the R6/2 mouse model of Huntington's disease. *Journal of Huntington's Disease* 2012; **1**(2): 211-9.
121. Prana. Prana announces successful phase 2 results in Huntington Disease trial. Melbourne & New York: Prana Biotechnology; 2014.
122. Huntington Study Group Reach HDI. Safety, tolerability, and efficacy of PBT2 in Huntington's disease: a phase 2, randomised, double-blind, placebo-controlled trial. *Lancet Neurol* 2015; **14**(1): 39-47.
123. Chan AW, Xu Y, Jiang J, et al. A two years longitudinal study of a transgenic Huntington disease monkey. *BMC neuroscience* 2014; **15**(1): 36.
124. Ferrante RJ, Kowall NW, Cipolloni P, Storey E, Beal MF. Excitotoxin lesions in primates as a model for Huntington's disease: histopathologic and neurochemical characterization. *Experimental neurology* 1993; **119**(1): 46-71.
125. Brouillet E, Hantraye P, Ferrante RJ, et al. Chronic mitochondrial energy impairment produces selective striatal degeneration and abnormal choreiform movements in primates. *Proceedings of the National Academy of Sciences* 1995; **92**(15): 7105-9.
126. Dal-Pan A, Pifferi F, Marchal J, Picq J-L, Aujard F, Consortium R. Cognitive performances are selectively enhanced during chronic caloric restriction or resveratrol supplementation in a primate. *PloS one* 2011; **6**(1): e16581.

127. Verina T, Kiihl SF, Schneider JS, Guilarte TR. Manganese exposure induces microglia activation and dystrophy in the substantia nigra of non-human primates. *Neurotoxicology* 2011; **32**(2): 215-26.
128. Morton AJ, Rudiger SR, Wood NI, et al. Early and progressive circadian abnormalities in Huntington's disease sheep are unmasked by social environment. *Human molecular genetics* 2014: ddu047.
129. Crook ZR, Housman D. Huntington's disease: can mice lead the way to treatment? *Neuron* 2011; **69**(3): 423-35.
130. Menalled LB, Chesselet MF. Mouse models of Huntington's disease. *Trends Pharmacol Sci* 2002; **23**(1): 32-9.
131. Slow EJ, Graham RK, Osmand AP, et al. Absence of behavioral abnormalities and neurodegeneration in vivo despite widespread neuronal huntingtin inclusions. *Proc Natl Acad Sci U S A* 2005; **102**(32): 11402-7.
132. Pouladi MA, Xie Y, Skotte NH, et al. Full-length huntingtin levels modulate body weight by influencing insulin-like growth factor 1 expression. *Hum Mol Genet* 2010; **19**(8): 1528-38.
133. Van Raamsdonk JM, Gibson WT, Pearson J, et al. Body weight is modulated by levels of full-length huntingtin. *Hum Mol Genet* 2006; **15**(9): 1513-23.
134. Tereshchenko A, McHugh M, Lee JK, et al. Abnormal Weight and Body Mass Index in Children with Juvenile Huntington's Disease. *J Huntingtons Dis* 2015; **4**(3): 231-8.
135. Hamilton JM, Wolfson T, Peavy GM, Jacobson MW, Corey-Bloom J, Huntington Study G. Rate and correlates of weight change in Huntington's disease. *J Neurol Neurosurg Psychiatry* 2004; **75**(2): 209-12.
136. Aziz NA, Pijl H, Frolich M, van der Graaf AW, Roelfsema F, Roos RA. Leptin secretion rate increases with higher CAG repeat number in Huntington's disease patients. *Clin Endocrinol (Oxf)* 2010; **73**(2): 206-11.
137. Gray M, Shirasaki DI, Cepeda C, et al. Full-length human mutant huntingtin with a stable polyglutamine repeat can elicit progressive and selective neuropathogenesis in BACHD mice. *J Neurosci* 2008; **28**(24): 6182-95.
138. Menalled LB, Sison JD, Wu Y, et al. Early motor dysfunction and striosomal distribution of huntingtin microaggregates in Huntington's disease knock-in mice. *J Neurosci* 2002; **22**(18): 8266-76.
139. Lin CH, Tallaksen-Greene S, Chien WM, et al. Neurological abnormalities in a knock-in mouse model of Huntington's disease. *Hum Mol Genet* 2001; **10**(2): 137-44.
140. van Dellen A, Blakemore C, Deacon R, York D, Hannan AJ. Delaying the onset of Huntington's in mice. *Nature* 2000; **404**(6779): 721-2.
141. Carter RJ, Hunt MJ, Morton AJ. Environmental stimulation increases survival in mice transgenic for exon 1 of the Huntington's disease gene. *Mov Disord* 2000; **15**(5): 925-37.
142. Hockly E, Cordery PM, Woodman B, et al. Environmental enrichment slows disease progression in R6/2 Huntington's disease mice. *Ann Neurol* 2002; **51**(2): 235-42.
143. Wood NI, Glynn D, Morton AJ. "Brain training" improves cognitive performance and survival in a transgenic mouse model of Huntington's disease. *Neurobiol Dis* 2011; **42**(3): 427-37.
144. Turner CA, Lewis MH. Environmental enrichment: effects on stereotyped behavior and neurotrophin levels. *Physiol Behav* 2003; **80**(2-3): 259-66.

145. Laviola G, Hannan AJ, Macri S, Solinas M, Jaber M. Effects of enriched environment on animal models of neurodegenerative diseases and psychiatric disorders. *Neurobiol Dis* 2008; **31**(2): 159-68.
146. Ferris LT, Williams JS, Shen CL. The effect of acute exercise on serum brain-derived neurotrophic factor levels and cognitive function. *Med Sci Sports Exerc* 2007; **39**(4): 728-34.
147. Saylor AJ, McGinty JF. An intrastriatal brain-derived neurotrophic factor infusion restores striatal gene expression in Bdnf heterozygous mice. *Brain Struct Funct* 2010; **215**(2): 97-104.
148. Altar CA, Cai N, Bliven T, et al. Anterograde transport of brain-derived neurotrophic factor and its role in the brain. *Nature* 1997; **389**(6653): 856-60.
149. Huang EJ, Reichardt LF. Neurotrophins: roles in neuronal development and function. *Annu Rev Neurosci* 2001; **24**: 677-736.
150. Molteni R, Ying Z, Gomez-Pinilla F. Differential effects of acute and chronic exercise on plasticity-related genes in the rat hippocampus revealed by microarray. *Eur J Neurosci* 2002; **16**(6): 1107-16.
151. Ding Q, Ying Z, Gomez-Pinilla F. Exercise influences hippocampal plasticity by modulating brain-derived neurotrophic factor processing. *Neuroscience* 2011; **192**: 773-80.
152. Spires TL, Grote HE, Varshney NK, et al. Environmental enrichment rescues protein deficits in a mouse model of Huntington's disease, indicating a possible disease mechanism. *J Neurosci* 2004; **24**(9): 2270-6.
153. Zuccato C, Marullo M, Conforti P, MacDonald ME, Tartari M, Cattaneo E. Systematic assessment of BDNF and its receptor levels in human cortices affected by Huntington's disease. *Brain Pathol* 2008; **18**(2): 225-38.
154. Ciammola A, Sassone J, Cannella M, et al. Low brain-derived neurotrophic factor (BDNF) levels in serum of Huntington's disease patients. *Am J Med Genet B Neuropsychiatr Genet* 2007; **144B**(4): 574-7.
155. Laske C, Stellos K, Hoffmann N, et al. Higher BDNF serum levels predict slower cognitive decline in Alzheimer's disease patients. *Int J Neuropsychopharmacol* 2011; **14**(3): 399-404.
156. Shimojo M. Huntingtin regulates RE1-silencing transcription factor/neuron-restrictive silencer factor (REST/NRSF) nuclear trafficking indirectly through a complex with REST/NRSF-interacting LIM domain protein (RILP) and dynactin p150 Glued. *J Biol Chem* 2008; **283**(50): 34880-6.
157. Zala D, Hinckelmann MV, Yu H, et al. Vesicular glycolysis provides on-board energy for fast axonal transport. *Cell* 2013; **152**(3): 479-91.
158. Zuccato C, Tartari M, Crotti A, et al. Huntingtin interacts with REST/NRSF to modulate the transcription of NRSE-controlled neuronal genes. *Nat Genet* 2003; **35**(1): 76-83.
159. Wu CL, Hwang CS, Chen SD, Yin JH, Yang DI. Neuroprotective mechanisms of brain-derived neurotrophic factor against 3-nitropropionic acid toxicity: therapeutic implications for Huntington's disease. *Ann N Y Acad Sci* 2010; **1201**: 8-12.
160. Canals JM, Pineda JR, Torres-Peraza JF, et al. Brain-derived neurotrophic factor regulates the onset and severity of motor dysfunction associated with enkephalinergic neuronal degeneration in Huntington's disease. *J Neurosci* 2004; **24**(35): 7727-39.

161. Hurlbert MS, Zhou W, Wasmeier C, Kaddis FG, Hutton JC, Freed CR. Mice transgenic for an expanded CAG repeat in the Huntington's disease gene develop diabetes. *Diabetes* 1999; **48**(3): 649-51.
162. Farrer LA, Meaney FJ. An anthropometric assessment of Huntington's disease patients and families. *Am J Phys Anthropol* 1985; **67**(3): 185-94.
163. Pratley RE, Salbe AD, Ravussin E, Caviness JN. Higher sedentary energy expenditure in patients with Huntington's disease. *Ann Neurol* 2000; **47**(1): 64-70.
164. Goodman AO, Barker RA. Body composition in premanifest Huntington's disease reveals lower bone density compared to controls. *PLoS Curr* 2011; **3**: RRN1214.
165. Hult S, Soylu R, Bjorklund T, et al. Mutant huntingtin causes metabolic imbalance by disruption of hypothalamic neurocircuits. *Cell Metab* 2011; **13**(4): 428-39.
166. Duan W, Guo Z, Jiang H, Ware M, Li XJ, Mattson MP. Dietary restriction normalizes glucose metabolism and BDNF levels, slows disease progression, and increases survival in huntingtin mutant mice. *Proc Natl Acad Sci U S A* 2003; **100**(5): 2911-6.
167. Bjorkqvist M, Petersen A, Bacos K, et al. Progressive alterations in the hypothalamic-pituitary-adrenal axis in the R6/2 transgenic mouse model of Huntington's disease. *Hum Mol Genet* 2006; **15**(10): 1713-21.
168. Clifford JJ, Drago J, Natoli AL, et al. Essential fatty acids given from conception prevent topographies of motor deficit in a transgenic model of Huntington's disease. *Neuroscience* 2002; **109**(1): 81-8.
169. Vaddadi KS, Soosai E, Chiu E, Dingjan P. A randomised, placebo-controlled, double blind study of treatment of Huntington's disease with unsaturated fatty acids. *Neuroreport* 2002; **13**(1): 29-33.
170. Miyazawa D, Yasui Y, Yamada K, Ohara N, Okuyama H. Regional differences of the mouse brain in response to an alpha-linolenic acid-restricted diet: Neurotrophin content and protein kinase activity. *Life Sci* 2010; **87**(15-16): 490-4.
171. Weindruch R. The retardation of aging by caloric restriction: studies in rodents and primates. *Toxicol Pathol* 1996; **24**(6): 742-5.
172. Steinkraus KA, Smith ED, Davis C, et al. Dietary restriction suppresses proteotoxicity and enhances longevity by an hsf-1-dependent mechanism in Caenorhabditis elegans. *Aging Cell* 2008; **7**(3): 394-404.
173. Martinez-Finley EJ, Avila DS, Chakraborty S, Aschner M. Insights from Caenorhabditis elegans on the role of metals in neurodegenerative diseases. *Metallomics* 2011; **3**(3): 271-9.
174. Lin MT, Beal MF. Mitochondrial dysfunction and oxidative stress in neurodegenerative diseases. *Nature* 2006; **443**(7113): 787-95.
175. Browne SE, Bowling AC, MacGarvey U, et al. Oxidative damage and metabolic dysfunction in Huntington's disease: selective vulnerability of the basal ganglia. *Ann Neurol* 1997; **41**(5): 646-53.
176. Damiano M, Galvan L, Deglon N, Brouillet E. Mitochondria in Huntington's disease. *Biochim Biophys Acta* 2010; **1802**(1): 52-61.
177. Beal MF, Brouillet E, Jenkins BG, et al. Neurochemical and histologic characterization of striatal excitotoxic lesions produced by the mitochondrial toxin 3-nitropropionic acid. *J Neurosci* 1993; **13**(10): 4181-92.

178. Brouillet E, Guyot MC, Mittoux V, et al. Partial inhibition of brain succinate dehydrogenase by 3-nitropropionic acid is sufficient to initiate striatal degeneration in rat. *J Neurochem* 1998; **70**(2): 794-805.
179. Napolitano M, Centonze D, Gubellini P, et al. Inhibition of mitochondrial complex II alters striatal expression of genes involved in glutamatergic and dopaminergic signaling: possible implications for Huntington's disease. *Neurobiol Dis* 2004; **15**(2): 407-14.
180. Cowan CM, Raymond LA. Selective neuronal degeneration in Huntington's disease. *Curr Top Dev Biol* 2006; **75**: 25-71.
181. Walaas SI, Hemmings HC, Jr., Greengard P, Nairn AC. Beyond the dopamine receptor: regulation and roles of serine/threonine protein phosphatases. *Front Neuroanat* 2011; **5**: 50.
182. Beal MF. Mitochondria take center stage in aging and neurodegeneration. *Ann Neurol* 2005; **58**(4): 495-505.
183. Goswami A, Dikshit P, Mishra A, Mulherkar S, Nukina N, Jana NR. Oxidative stress promotes mutant huntingtin aggregation and mutant huntingtin-dependent cell death by mimicking proteasomal malfunction. *Biochem Biophys Res Commun* 2006; **342**(1): 184-90.
184. Yang L, Calingasan NY, Wille EJ, et al. Combination therapy with coenzyme Q10 and creatine produces additive neuroprotective effects in models of Parkinson's and Huntington's diseases. *Journal of Neurochemistry* 2009; **109**(5): 1427-39.
185. Dusek P, Roos PM, Litwin T, Schneider SA, Flaten TP, Aaseth J. The neurotoxicity of iron, copper and manganese in Parkinson's and Wilson's diseases. *J Trace Elem Med Biol* 2015; **31**: 193-203.
186. Su FC, Goutman SA, Chernyak S, et al. Association of Environmental Toxins With Amyotrophic Lateral Sclerosis. *JAMA Neurol* 2016.
187. James SA, Volitakis I, Adlard PA, et al. Elevated labile Cu is associated with oxidative pathology in Alzheimer disease. *Free Radic Biol Med* 2012; **52**(2): 298-302.
188. Wright RO, Baccarelli A. Metals and neurotoxicology. *J Nutr* 2007; **137**(12): 2809-13.
189. Mates JM, Segura JA, Alonso FJ, Marquez J. Roles of dioxins and heavy metals in cancer and neurological diseases using ROS-mediated mechanisms. *Free Radic Biol Med* 2010; **49**(9): 1328-41.
190. Migliore L, Coppede F. Genetics, environmental factors and the emerging role of epigenetics in neurodegenerative diseases. *Mutat Res* 2009; **667**(1-2): 82-97.
191. Bowman AB, Kwakye GF, Herrero Hernandez E, Aschner M. Role of manganese in neurodegenerative diseases. *J Trace Elem Med Biol* 2011; **25**(4): 191-203.
192. Park JS, Koentjoro B, Veivers D, Mackay-Sim A, Sue CM. Parkinson's disease-associated human ATP13A2 (PARK9) deficiency causes zinc dyshomeostasis and mitochondrial dysfunction. *Hum Mol Genet* 2014; **23**(11): 2802-15.
193. Williams BB, Kwakye GF, Wegrzynowicz M, et al. Altered manganese homeostasis and manganese toxicity in a Huntington's disease striatal cell model are not explained by defects in the iron transport system. *Toxicol Sci* 2010; **117**(1): 169-79.
194. Dodd CA, Ward DL, Klein BG. Basal Ganglia accumulation and motor assessment following manganese chloride exposure in the C57BL/6 mouse. *Int J Toxicol* 2005; **24**(6): 389-97.

195. Brouillet E, Hantraye P, Ferrante RJ, et al. Chronic mitochondrial energy impairment produces selective striatal degeneration and abnormal choreiform movements in primates. *Proc Natl Acad Sci U S A* 1995; **92**(15): 7105-9.
196. Beal MF. Bioenergetic approaches for neuroprotection in Parkinson's disease. *Ann Neurol* 2003; **53 Suppl 3**: S39-47; discussion S-8.
197. Tarohda T, Yamamoto M, Amamo R. Regional distribution of manganese, iron, copper, and zinc in the rat brain during development. *Anal Bioanal Chem* 2004; **380**(2): 240-6.
198. Rosas HD, Chen YI, Doros G, et al. Alterations in brain transition metals in Huntington disease: an evolving and intricate story. *Arch Neurol* 2012; **69**(7): 887-93.
199. Dexter DT, Carayon A, Javoy-Agid F, et al. Alterations in the levels of iron, ferritin and other trace metals in Parkinson's disease and other neurodegenerative diseases affecting the basal ganglia. *Brain* 1991; **114 (Pt 4)**: 1953-75.
200. Chen JC, Hardy PA, Kucharczyk W, et al. MR of human postmortem brain tissue: correlative study between T2 and assays of iron and ferritin in Parkinson and Huntington disease. *AJNR Am J Neuroradiol* 1993; **14**(2): 275-81.
201. Dal-Pan A, Pifferi F, Marchal J, Picq JL, Aujard F, Consortium R. Cognitive performances are selectively enhanced during chronic caloric restriction or resveratrol supplementation in a primate. *PLoS One* 2011; **6**(1): e16581.
202. van Bergen JM, Hua J, Unschuld PG, et al. Quantitative Susceptibility Mapping Suggests Altered Brain Iron in Premanifest Huntington Disease. *AJNR Am J Neuroradiol* 2016; **37**(5): 789-96.
203. Shannon KM, Fraint A. Therapeutic advances in Huntington's Disease. *Mov Disord* 2015; **30**(11): 1539-46.
204. Zhang Z, Miah M, Culbreth M, Aschner M. Autophagy in Neurodegenerative Diseases and Metal Neurotoxicity. *Neurochem Res* 2016; **41**(1-2): 409-22.
205. Ohsumi Y. Historical landmarks of autophagy research. *Cell Res* 2014; **24**(1): 9-23.
206. Martinez-Vicente M, Talloczy Z, Wong E, et al. Cargo recognition failure is responsible for inefficient autophagy in Huntington's disease. *Nat Neurosci* 2010; **13**(5): 567-76.
207. Stolz A, Ernst A, Dikic I. Cargo recognition and trafficking in selective autophagy. *Nat Cell Biol* 2014; **16**(6): 495-501.
208. Ochaba J, Monteys AM, O'Rourke JG, et al. PIAS1 Regulates Mutant Huntingtin Accumulation and Huntington's Disease-Associated Phenotypes In Vivo. *Neuron* 2016; **90**(3): 507-20.
209. Lamark T, Johansen T. Aggrephagy: selective disposal of protein aggregates by macroautophagy. *Int J Cell Biol* 2012; **2012**: 736905.
210. Simmons DA, Casale M, Alcon B, Pham N, Narayan N, Lynch G. Ferritin accumulation in dystrophic microglia is an early event in the development of Huntington's disease. *Glia* 2007; **55**(10): 1074-84.
211. Mancias JD, Wang X, Gygi SP, Harper JW, Kimmelman AC. Quantitative proteomics identifies NCOA4 as the cargo receptor mediating ferritinophagy. *Nature* 2014; **509**(7498): 105-9.
212. Legendre-Guillemin V, Metzler M, Lemaire JF, et al. Huntingtin interacting protein 1 (HIP1) regulates clathrin assembly through direct binding to the regulatory region of the clathrin light chain. *J Biol Chem* 2005; **280**(7): 6101-8.

213. Majeed SR, Vasudevan L, Chen CY, et al. Clathrin light chains are required for the gyrating-clathrin recycling pathway and thereby promote cell migration. *Nat Commun* 2014; **5**: 3891.
214. Zhang J, Cao R, Cai T, et al. The role of autophagy dysregulation in manganese-induced dopaminergic neurodegeneration. *Neurotox Res* 2013; **24**(4): 478-90.
215. Afeseh Ngwa H, Kanthasamy A, Gu Y, Fang N, Anantharam V, Kanthasamy AG. Manganese nanoparticle activates mitochondrial dependent apoptotic signaling and autophagy in dopaminergic neuronal cells. *Toxicol Appl Pharmacol* 2011; **256**(3): 227-40.
216. Paris I, Perez-Pastene C, Couve E, Caviedes P, Ledoux S, Segura-Aguilar J. Copper dopamine complex induces mitochondrial autophagy preceding caspase-independent apoptotic cell death. *J Biol Chem* 2009; **284**(20): 13306-15.
217. Castino R, Fiorentino I, Cagnin M, Giovia A, Isidoro C. Chelation of lysosomal iron protects dopaminergic SH-SY5Y neuroblastoma cells from hydrogen peroxide toxicity by precluding autophagy and Akt dephosphorylation. *Toxicol Sci* 2011; **123**(2): 523-41.
218. Dotiwala F, Eapen VV, Harrison JC, et al. DNA damage checkpoint triggers autophagy to regulate the initiation of anaphase. *Proc Natl Acad Sci U S A* 2013; **110**(1): E41-9.
219. Maskey D, Yousefi S, Schmid I, et al. ATG5 is induced by DNA-damaging agents and promotes mitotic catastrophe independent of autophagy. *Nat Commun* 2013; **4**: 2130.
220. Pohl C, Jentsch S. Midbody ring disposal by autophagy is a post-abscission event of cytokinesis. *Nat Cell Biol* 2009; **11**(1): 65-70.
221. Bellingham SA, Guo B, Hill AF. The secret life of extracellular vesicles in metal homeostasis and neurodegeneration. *Biol Cell* 2015; **107**(11): 389-418.
222. Zhang X, Abels ER, Redzic JS, Margulis J, Finkbeiner S, Breakefield XO. Potential Transfer of Polyglutamine and CAG-Repeat RNA in Extracellular Vesicles in Huntington's Disease: Background and Evaluation in Cell Culture. *Cell Mol Neurobiol* 2016; **36**(3): 459-70.
223. Lee M, Liu T, Im W, Kim M. Exosomes from adipose-derived stem cells ameliorate phenotype of Huntington's disease in vitro model. *Eur J Neurosci* 2016; **44**(4): 2114-9.
224. Jeon I, Cicchetti F, Cisbani G, et al. Human-to-mouse prion-like propagation of mutant huntingtin protein. *Acta Neuropathol* 2016.
225. Chen J, Marks E, Lai B, et al. Iron accumulates in Huntington's disease neurons: protection by deferoxamine. *PLoS One* 2013; **8**(10): e77023.
226. Fox JH, Kama JA, Lieberman G, et al. Mechanisms of copper ion mediated Huntington's disease progression. *PLoS One* 2007; **2**(3): e334.
227. Dominguez JF, Ng AC, Poudel G, et al. Iron accumulation in the basal ganglia in Huntington's disease: cross-sectional data from the IMAGE-HD study. *J Neurol Neurosurg Psychiatry* 2016; **87**(5): 545-9.
228. Bartzokis G, Cummings J, Perlman S, Hance DB, Mintz J. Increased basal ganglia iron levels in Huntington disease. *Arch Neurol* 1999; **56**(5): 569-74.
229. Bartzokis G, Lu PH, Tishler TA, et al. Myelin breakdown and iron changes in Huntington's disease: pathogenesis and treatment implications. *Neurochem Res* 2007; **32**(10): 1655-64.
230. Vymazal J, Klempir J, Jech R, et al. MR relaxometry in Huntington's disease: correlation between imaging, genetic and clinical parameters. *J Neurol Sci* 2007; **263**(1-2): 20-5.

231. Jurgens CK, Jasinschi R, Ekin A, et al. MRI T2 Hypointensities in basal ganglia of premanifest Huntington's disease. *PLoS Curr* 2010; **2**.
232. Dumas EM, Versluis MJ, van den Bogaard SJ, et al. Elevated brain iron is independent from atrophy in Huntington's Disease. *Neuroimage* 2012; **61**(3): 558-64.
233. Sanchez-Castaneda C, Cherubini A, Elifani F, et al. Seeking Huntington disease biomarkers by multimodal, cross-sectional basal ganglia imaging. *Hum Brain Mapp* 2013; **34**(7): 1625-35.
234. Sanchez-Castaneda C, Squitieri F, Di Paola M, Dayan M, Petrollini M, Sabatini U. The role of iron in gray matter degeneration in Huntington's disease: a magnetic resonance imaging study. *Hum Brain Mapp* 2015; **36**(1): 50-66.
235. Firdaus WJ, Wyttenbach A, Giuliano P, Kretz-Remy C, Currie RW, Arrigo AP. Huntingtin inclusion bodies are iron-dependent centers of oxidative events. *FEBS J* 2006; **273**(23): 5428-41.
236. Verina T, Kiihl SF, Schneider JS, Guilarte TR. Manganese exposure induces microglia activation and dystrophy in the substantia nigra of non-human primates. *Neurotoxicology* 2011; **32**(2): 215-26.
237. Bonilla E, Estevez J, Suarez H, et al. Serum ferritin deficiency in Huntington's disease patients. *Neurosci Lett* 1991; **129**(1): 22-4.
238. Curtis AR, Fey C, Morris CM, et al. Mutation in the gene encoding ferritin light polypeptide causes dominant adult-onset basal ganglia disease. *Nat Genet* 2001; **28**(4): 350-4.
239. Levi S, Cozzi A, Arosio P. Neuroferritinopathy: a neurodegenerative disorder associated with L-ferritin mutation. *Best Pract Res Clin Haematol* 2005; **18**(2): 265-76.
240. Chinnery PF, Crompton DE, Birchall D, et al. Clinical features and natural history of neuroferritinopathy caused by the FTL1 460InsA mutation. *Brain* 2007; **130**(Pt 1): 110-9.
241. Martino D, Stamelou M, Bhatia KP. The differential diagnosis of Huntington's disease-like syndromes: 'red flags' for the clinician. *J Neurol Neurosurg Psychiatry* 2013; **84**(6): 650-6.
242. Kegel KB, Kim M, Sapp E, et al. Huntingtin expression stimulates endosomal-lysosomal activity, endosome tubulation, and autophagy. *J Neurosci* 2000; **20**(19): 7268-78.
243. Berggren KL, Lu Z, Fox JA, Dudenhoeffer M, Agrawal S, Fox JH. Neonatal Iron Supplementation Induces Striatal Atrophy in Female YAC128 Huntington's Disease Mice. *J Huntingtons Dis* 2016; **5**(1): 53-63.
244. Berggren KL, Chen J, Fox J, et al. Neonatal iron supplementation potentiates oxidative stress, energetic dysfunction and neurodegeneration in the R6/2 mouse model of Huntington's disease. *Redox Biol* 2015; **4**: 363-74.
245. Nguyen T, Hamby A, Massa SM. Clioquinol down-regulates mutant huntingtin expression in vitro and mitigates pathology in a Huntington's disease mouse model. *Proc Natl Acad Sci U S A* 2005; **102**(33): 11840-5.
246. Chung J, Haile DJ, Wessling-Resnick M. Copper-induced ferroportin-1 expression in J774 macrophages is associated with increased iron efflux. *Proc Natl Acad Sci U S A* 2004; **101**(9): 2700-5.
247. Prohaska JR, Broderius M. Copper deficiency has minimal impact on ferroportin expression or function. *Biometals* 2012; **25**(4): 633-42.

248. Hodges A, Strand AD, Aragaki AK, et al. Regional and cellular gene expression changes in human Huntington's disease brain. *Hum Mol Genet* 2006; **15**(6): 965-77.
249. Hands SL, Mason R, Sajjad MU, Giorgini F, Wyttenbach A. Metallothioneins and copper metabolism are candidate therapeutic targets in Huntington's disease. *Biochem Soc Trans* 2010; **38**(2): 552-8.
250. Boll MC, Alcaraz-Zubeldia M, Montes S, Rios C. Free copper, ferroxidase and SOD1 activities, lipid peroxidation and NO(x) content in the CSF. A different marker profile in four neurodegenerative diseases. *Neurochem Res* 2008; **33**(9): 1717-23.
251. Sanberg PR, Calderon SF, Giordano M, Tew JM, Norman AB. The quinolinic acid model of Huntington's disease: locomotor abnormalities. *Exp Neurol* 1989; **105**(1): 45-53.
252. Santamaria A, Rios C, Perez P, et al. Quinolinic acid neurotoxicity: in vivo increased copper and manganese content in rat corpus striatum after quinolinate intrastriatal injection. *Toxicol Lett* 1996; **87**(2-3): 113-9.
253. Schlief ML, West T, Craig AM, Holtzman DM, Gitlin JD. Role of the Menkes copper-transporting ATPase in NMDA receptor-mediated neuronal toxicity. *Proc Natl Acad Sci U S A* 2006; **103**(40): 14919-24.
254. Martinez-Lazcano JC, Montes S, Sanchez-Mendoza MA, et al. Sub-chronic copper pretreatment reduces oxidative damage in an experimental Huntington's disease model. *Biol Trace Elem Res* 2014; **162**(1-3): 211-8.
255. Xiao G, Fan Q, Wang X, Zhou B. Huntington disease arises from a combinatory toxicity of polyglutamine and copper binding. *Proc Natl Acad Sci U S A* 2013; **110**(37): 14995-5000.
256. Zhou RP, Wu XS, Wang ZS, Xie YY, Ge JF, Chen FH. Novel Insights into Acid-Sensing Ion Channels: Implications for Degenerative Diseases. *Aging Dis* 2016; **7**(4): 491-501.
257. Raymond LA. Striatal synaptic dysfunction and altered calcium regulation in Huntington disease. *Biochem Biophys Res Commun* 2016.
258. Kolodziejczyk K, Raymond LA. Differential changes in thalamic and cortical excitatory synapses onto striatal spiny projection neurons in a Huntington disease mouse model. *Neurobiol Dis* 2016; **86**: 62-74.
259. Chen X, Wu J, Lvovskaya S, Herndon E, Supnet C, Bezprozvanny I. Dantrolene is neuroprotective in Huntington's disease transgenic mouse model. *Mol Neurodegener* 2011; **6**: 81.
260. Fernandes HB, Baimbridge KG, Church J, Hayden MR, Raymond LA. Mitochondrial sensitivity and altered calcium handling underlie enhanced NMDA-induced apoptosis in YAC128 model of Huntington's disease. *J Neurosci* 2007; **27**(50): 13614-23.
261. Rosenstock TR, Bertoncini CR, Teles AV, Hirata H, Fernandes MJ, Smaili SS. Glutamate-induced alterations in Ca2+ signaling are modulated by mitochondrial Ca2+ handling capacity in brain slices of R6/1 transgenic mice. *Eur J Neurosci* 2010; **32**(1): 60-70.
262. Tang TS, Slow E, Lupu V, et al. Disturbed Ca2+ signaling and apoptosis of medium spiny neurons in Huntington's disease. *Proc Natl Acad Sci U S A* 2005; **102**(7): 2602-7.
263. Zhang H, Li Q, Graham RK, Slow E, Hayden MR, Bezprozvanny I. Full length mutant huntingtin is required for altered Ca2+ signaling and apoptosis of striatal neurons in the YAC mouse model of Huntington's disease. *Neurobiol Dis* 2008; **31**(1): 80-8.
264. Panov AV, Gutekunst CA, Leavitt BR, et al. Early mitochondrial calcium defects in Huntington's disease are a direct effect of polyglutamines. *Nat Neurosci* 2002; **5**(8): 731-6.

265. Parent A, Fortin M, Cote PY, Cicchetti F. Calcium-binding proteins in primate basal ganglia. *Neurosci Res* 1996; **25**(4): 309-34.
266. Tang TS, Tu H, Chan EY, et al. Huntingtin and huntingtin-associated protein 1 influence neuronal calcium signaling mediated by inositol-(1,4,5) triphosphate receptor type 1. *Neuron* 2003; **39**(2): 227-39.
267. Rana A, Yen M, Sadaghiani AM, et al. Alternative splicing converts STIM2 from an activator to an inhibitor of store-operated calcium channels. *J Cell Biol* 2015; **209**(5): 653-69.
268. Wu J, Ryskamp DA, Liang X, et al. Enhanced Store-Operated Calcium Entry Leads to Striatal Synaptic Loss in a Huntington's Disease Mouse Model. *J Neurosci* 2016; **36**(1): 125-41.
269. Gavin CE, Gunter KK, Gunter TE. Manganese and calcium efflux kinetics in brain mitochondria. Relevance to manganese toxicity. *Biochem J* 1990; **266**(2): 329-34.
270. Prohaska JR. Functions of trace elements in brain metabolism. *Physiol Rev* 1987; **67**(3): 858-901.
271. Prabhakaran K, Chapman GD, Gunasekar PG. BNIP3 up-regulation and mitochondrial dysfunction in manganese-induced neurotoxicity. *Neurotoxicology* 2009; **30**(3): 414-22.
272. Choo YS, Johnson GV, MacDonald M, Detloff PJ, Lesort M. Mutant huntingtin directly increases susceptibility of mitochondria to the calcium-induced permeability transition and cytochrome c release. *Hum Mol Genet* 2004; **13**(14): 1407-20.
273. Tamm C, Sabri F, Ceccatelli S. Mitochondrial-mediated apoptosis in neural stem cells exposed to manganese. *Toxicol Sci* 2008; **101**(2): 310-20.
274. Wang RG, Zhu XZ. Subtoxic concentration of manganese synergistically potentiates 1-methyl-4-phenylpyridinium-induced neurotoxicity in PC12 cells. *Brain Res* 2003; **961**(1): 131-8.
275. Gorrell JM, DiMonte D, Graham D. The role of the environment in Parkinson's disease. *Environ Health Perspect* 1996; **104**(6): 652-4.
276. Racette BA, McGee-Minnich L, Moerlein SM, Mink JW, Videen TO, Perlmutter JS. Welding-related parkinsonism: clinical features, treatment, and pathophysiology. *Neurology* 2001; **56**(1): 8-13.
277. Saxena S, Caroni P. Selective neuronal vulnerability in neurodegenerative diseases: from stressor thresholds to degeneration. *Neuron* 2011; **71**(1): 35-48.
278. Williams BB, Li D, Wegrzynowicz M, et al. Disease-toxicant screen reveals a neuroprotective interaction between Huntington's disease and manganese exposure. *J Neurochem* 2010; **112**(1): 227-37.
279. Madison JL, Wegrzynowicz M, Aschner M, Bowman AB. Gender and manganese exposure interactions on mouse striatal neuron morphology. *Neurotoxicology* 2011; **32**(6): 896-906.
280. Kwakye G. Development of a Novel High Throughput Assay: Impaired Manganese Transport Kinetics and Homeostasis in Huntington's Disease [Dissertation]. Nashville, TN: Vanderbilt University; 2011.

Chapter II

Effect of Expanded CAG Repeat on BAC Mouse Model

Note: This chapter has been derived from the following publications:

Wegrzynowicz M, Bichell TJ, Soares BD, Loth M, McGlothan J, Alikhan F, Hua K, Coughlin J, Holt H, Jetter C, Mori S, Pomper M, Osmand A, Guilarte T, Bowman AB. Novel BAC Mouse Model of Huntington's Disease with 225 CAG Repeats Exhibits an Early Widespread and Stable Degenerative Phenotype. *J Huntingtons Dis* 2015; **4**(1): 17-36. (Wegrzynowicz and Bichell contributed equally to this manuscript).

Author contributions: MW, TJVB and ABB wrote the manuscript. MW and ABB generated the genetic construct. MW, CJ and TJVB maintained the mouse colony. BS, ML, JM, FA and TG performed the TSPO and DR binding experiments with tissue provided by MW. KH and JC performed the MRIs with tissue provided by MW. TJVB performed the PCR and the QRT-PCR on tissue collected by MW and TJVB. MW, TJVB, HH, CJ performed the behavior experiments and/or analyzed data. SM, MP and AO performed the IHSC experiments with tissue collected and perfused by TJVB. AO, TG and ABB conceptualized and advised on the study.

Background

Typical adult-onset HD is characterized by selective degeneration of neurons within the striatum, cortex and hypothalamus with relative sparing of the cerebellum and hippocampus.[1]Additionally, several peripheral tissues (endocrine tissues, cardiac and skeletal muscle) have been suggested to contribute to HD pathogenesis.[2] The juvenile form of the disease, due to longer CAG repeat lengths (> ~60 repeats), presents with more extensive neuropathology that includes cerebellar degeneration and can display clinical manifestations distinct from adult-onset HD.[3,4] Surprisingly, published mouse models expressing the full-length *Htt* gene with CAG repeat lengths well beyond those associated with adult-onset HD, such as the YAC128 model, exhibit selective neurodegenerative phenotypes more similar to adult-onset HD than the juvenile form (for review see [5]). Though the knock-in mouse models reported to date parallel the human genetic disorder, bearing mutations at the endogenous *Htt* locus, they display very mild

symptoms, akin to the pre-symptomatic stage of human adult-onset HD, and none of these models reproduce the full spectrum of HD symptoms and pathologies.

A diverse collection of animal models available, differing in number of CAG repeats, transgene length, transgene locus and polyglutamine (polyQ)/wild-type (WT) HTT ratio may therefore be fundamental for successful studies of the pathological mechanisms of HD and for evaluating the efficacy of interventional strategies. To determine if very long repeat lengths in the mouse are capable of producing phenotypes associated with the juvenile form of HD we generated a novel model mouse expressing full-length mouse *Htt* with ~225 CAG repeats under the control of mouse *Htt* promoter, using a bacterial artificial chromosome (BAC) system.

In many respects, the C57BL/6J-Tg(BAC225Htt)1Bow model we constructed (hereafter referred to as the BAC-225Q mouse) exhibits a phenotype consistent with juvenile-onset HD and/or late stage of adult-onset HD at a very early age. The BAC-225Q mouse exhibits very early motor behavior abnormalities (the most rapid onset amongst full-length *Htt* models of HD), sudden and extreme loss of body weight, severe aggregate load, and widespread neurodegeneration. Very early striatal pathology was observed prior to detectable volume loss, including reactive gliosis and loss of dopamine receptors in medium spiny neurons. Additionally, an increase in plasma concentrations of markers of energy metabolism deficiency and systemic inflammation is observed in BAC-225Q mice. The model is also noteworthy as despite the early onset of neuropathological and motor phenotypes (<3 months), little or no progression of phenotypic severity was observed with age through at least 10 to 15 months of age. These features make BAC-225Q mice a reliable mouse model of HD, useful particularly in studies of the juvenile form of disease, the metabolic phenotypes in HD and on the relationship between regional neuropathology and general HD symptoms.

Method of generation of the C57BL/6J-Tg(BAC225Htt)1Bow mouse

The BAC-225Q transgenic animals were generated by pronuclear injection of fertilized C57BL6/J eggs with a modified bacteria artificial chromosome (BAC RP24-165D1 obtained from CHORI BACPAC resources) covering ~202kb of the *mus musculus Htt* genomic locus (containing the entire *Htt* locus plus partial sequence of the flanking genes *Grk4* (last 5 out of a total of 16 exons) and *Rgs12* (first exon only) modified to expand the normal CAG repeat to a length of ~225 repeats within the full-length *Htt* gene by a subcloning/BAC recombineering strategy[6] Detailed information on break points of BAC RP24-165D1 is available on the UCSC genome browser (http://genome.ucsc.edu/index.html).

Briefly, the recombineering strategy began by subcloning a 266-CAG repeat from the mutant *Atxn7* locus by PCR using genomic DNA of the SCA7 knock-in mouse model,[7] HindIII and PvuII restriction enzyme recognition sites were engineered into the primers to allow restriction enzyme cloning into the genomic DNA flanking exon 1 of the mouse *Htt* gene. This construct was used as a targeting vector via BAC recombineering using GalK positive and negative selection in the RP24-165D1 BAC. Restriction mapping of BAC fragments and sequencing of the expanded CAG repeat from the BAC was used to validate appropriate targeting. The Vanderbilt Transgenic Shared Resource generated three female BAC positive transgenic founders that were mated to C57BL/6 male mice to test for germline transmission using uncut BAC vector prepared via the Qiagen Large Construct Kit (Qiagen). One of the three founders transmitted the transgenic allele to establish the BAC-225Q line. Expression of full-length mutant Huntingtin protein was confirmed in transgene positive animals by western blotting. BAC-225Q transgenic animals were maintained in their original genetic background (C57BL/6J) and

the transgene was transmitted to the offspring from a hemizygous transgenic parent by crossing it with a non-transgenic animal.

As only a single transgenic line was generated we were not able to test whether any particular phenotypes displayed position effects. To minimize position effects we used only hemizygous transgenic mice for all experiments to ensure at least one functional allele for any genes disrupted from the transgene insertion. Genotyping and analysis of CAG repeat length was performed using genomic DNA isolated from the tail with the following primers, flanking the CAG repeat within Htt: F: 5'-CCCATTCATTGCCTTGCTG-3', and R: 5'-GCGGCTGAGGGGGTTGA-3'. Agarose gel electrophoresis demonstrated a calculated CAG repeat length in the BAC-225Q animals of between 220–230 repeats. The length of the CAG repeat in the transgene has not detectably changed since transmission from the original founder across >10 generations, suggesting a stable repeat with no detectable intergenerational expansion or contraction (**Figure 2-1)**. Furthermore, of over 1000 transgenic positive progeny we have seen only a handful of animals with an observable small increase or decrease in the CAG repeat containing PCR product used to genotype the animals. Thus, while expansions and contractions are still possible, they were rare events (less than 1 in 200 animals). The basis for the repeat stability is unclear though possible explanations include the genomic location of the transgene insertion site, or relatively low expression level of the transgene mRNA (see results section). Mice were weighed weekly, from four to 43 weeks of age, 2–4 hours before the end of the light phase of the light cycle.

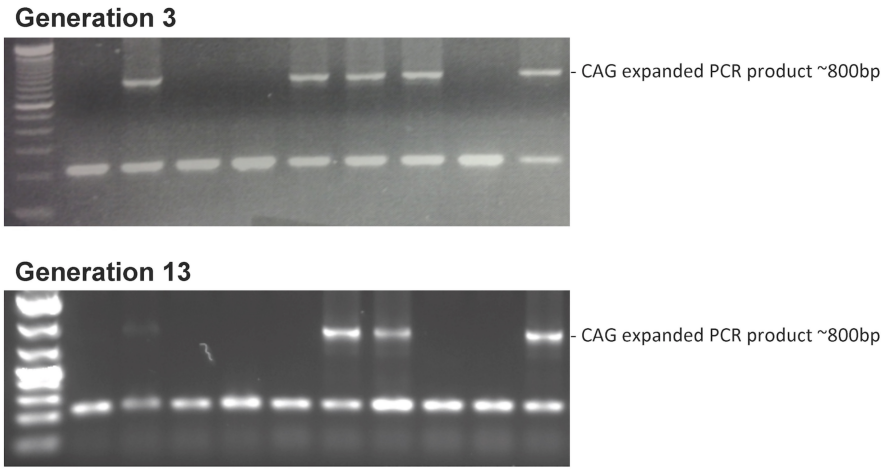

Figure 2-1. Representative PCR genotyping over the CAG repeat in *Htt* exon 1 shows stable CAG repeat length. Genomic DNA from progeny of a BAC-225Q transgenic animal crossed to WT C57Bl/6 animal in an early generation (Top panel) versus pups from a litter 10 generations later (Bottom panel). Top panel DNA ladder is Life Technologies 100bp DNA ladder; bottom panel is Invitrogen 1Kb plus DNA ladder. Note highly similar sizes of CAG expanded allele band from all transgenic animals; a consistent band mobility was seen in nearly all genotyping reactions across 5+ years maintaining this line.

Methods and materials for phenotyping BAC225 mouse

Western blotting

Western blotting was performed as described[8]. Briefly, tissue was homogenized on ice in RIPA buffer (50 mM Tris, 150 mM NaCl, 0.1% sodium dodecyl sulfate (SDS), 1% IGEPAL CA-630, 12 mM deoxycholic acid, pH 8.0) supplemented with 1% protease inhibitor cocktail (Sigma). Homogenates were centrifuged at 14,000 x g, for 10 minutes, at 4^{O}C. Protein content was measured by DC assay (Bio-Rad). Samples were mixed with sample buffer (60 mM Tris, 6% SDS, 30% glycerol, 15% β-mercaptoethanol, 0.015% bromophenol blue, pH 6.8) and incubated at 95^{O}C for 5 minutes. The electrophoresis was run using 15 x 22 cm, 10% polyacrylamide gels, overnight at 1050 V x hour with CBS Scientific Vertical Electrophoresis System in running buffer (0.1% SDS, 20 mM Tris-HCl and 192 mM glycine). Next, proteins were transferred to 0.2 μm

pore Protran nitrocellulose membrane (Whatman) in transfer buffer (20 mM Tris-HCl, 192 mM Glycine, 10% methanol), at 500 mA, at 4^{O}C for 3 h, using CBS Scientific Electrophoretic Blotting System or the iBlot transfer system. The membrane was blocked with 5% milk in TBST buffer (150 mM NaCl, 56 mM Tris-HCl, 44 mM Trizma base, 0.05% Tween-20) for 3 hours at room temperature (RT) or with Odyssey Blocking Buffer (LI-COR part 927-400000) for 90 mins at RT. The blocked membranes were incubated with mouse anti-HTT 1HU-4C8 antibody (MAB2166, Millipore, 1:5,000 – 1:20,000) or mouse anti-polyglutamine expanded 1C2 antibody (MAB1574, Millipore, 1:5000) diluted in 5% milk in TBST overnight at room temperature. Anti-mouse secondary antibody (Jackson ImmunoResearch Laboratories) was used at 1:10,000 – 1:15,000 dilutions in 5% milk in TBST or in Odyssey Blocking Buffer with 0.1%Tween. The blots were visualized with West Dura Extended Duration Chemiluminescent Substrate (Thermo Fisher Scientific) or using the Li-Cor Odyssey infrared system. Blot quantification was performed with ImageJ (NIH), with the background correction calculated using a signal ratio error model.[9]

Rotarod

Three cohorts of animals were used for the rotarod test (a rotating balance-beam-like rod which measures rodent abilities such as motor coordination and endurance). The first cohort was examined at 3, 4, 5, 6, 7, 8, 9, 12 and 15 months, the second cohort at 6, 7 and 12 months, and the third cohort at 1.5, 2 and 2.5 months of age. Animals were tested at Vanderbilt Murine Neurobehavioral Core using an Ugo Basile Accelerating Rotarod. Three 10-minute trials per day with a 30 minute interval were performed for 4 consecutive days during the light phase of the light cycle for a total of 12 trials per age point. A single trial consisted of 5 minutes of acceleration phase (from 2 to 40 rpm), followed by 5 minutes of constant phase (40 rpm). For each animal, the average of all the 12 trials was calculated per age point and this value was used

to calculate the average for each experimental group and for statistical purposes. ANOVA showed a significant effect of gender on rotarod performance, thus males and females were analyzed separately. All experiments, designed to minimize animal pain, were carried out with the approval from Vanderbilt University Medical Center Institutional Animal Care and Use Committee.

Open field

Open field behavior testing was performed during the dark phase of the light cycle at the Vanderbilt Murine Neurobehavioral Core. Male and female animals, at the age of 3, 6, 9 and 12 months were placed in the ENV-510 open field test chambers (27 cm x 27 cm x 20.3 cm; MED Associates) and monitored for 30 minutes in the dark. The chambers housed 16 infrared beams monitoring X-Y-Z coordinates every 50 milliseconds. Animals were scored for total distance travelled, vertical counts, jump counts and average velocity. Data were recorded and analyzed in Activity Monitor 5.0 (MED Associates). There was no significant influence of gender by ANOVA on open field performance, thus male and female data were pooled for analysis.

Leptin and cytokine measurements in plasma

Blood samples were collected using a submandibular bleeding method[10] with Goldenrod mouse bleeding lancets from mice at 2, 3, 5, 6, 8 and 10 months of age, 2-4 hours before the end of the light phase of the light cycle. Blood was collected to EDTA coated tubes and samples were centrifuged at 1850 x g, for 15 minutes, at 4^{O}C. Plasma was snap frozen in liquid nitrogen and stored at -80^{O}C. Leptin and cytokines (IL-4, IL-6, MIP2, KC, IFNγ, TNFα) were measured by the Vanderbilt Hormone Assay Core using Mouse Adipokine Kit and Mouse Cytokine / Chemokine Kit Panel 1 (Millipore), respectively, according to the manufacturer's recommendations. Luminex 100 with Xponent 3.1 software was used to quantify the assays. ANOVA failed to find a

significant difference by gender, thus male and female data were combined for analysis to maximize statistical power.

Volumetric MRI

Mice were perfused with 4% PFA and heads were postfixed in PFA solution. Before imaging, samples were placed in a plastic tube with Fomblin Profludropolyether to prevent dehydration. Samples were imaged using a 9.4 Tesla scanner (vertical bore, Bruker Biospin) using a 15 mm volume coil. 3D T2-weighted Rapid Acquisition with Refocused Echoes (RARE) sequence was used, with the following parameters: RARE factor of 8, Effective Echo Time (TE) = 43.82 ms, Repetition Time = 2000 ms, FOV = 25.6 mm x 14.4 mm x 10 mm, number of average = 4. The image had a matrix size of 256 x 144 x 100, which was zero-filled to 256 x 256 x 128. Signals from tissue outside of the brain were removed from acquired subject image by skull stripping. After initial affine alignment, the intensity-corrected subject T2-weighted image and the atlas T2-weighted image[11] were submitted to a Linux cluster running Large Deformation Diffeomorphic Metric Mapping (LDDMM)[12] using the DiffeoMap software package (www.mristudio.org, X. Li, H. Jiang, and S. Mori, Johns Hopkins University). A topology-preserving mapping between the subject and atlas T2-weighted image was generated by single-channel LDDMM, and inverse mapping (from atlas space to subject space) was applied to the predefined structural segmentations in the atlas space. The segmentation quality of striatum was inspected and manual touch-up was applied when necessary. The volume of the whole brain and the inverse transformed structures were reported in DiffeoMap.

k

Immunohistochemistry

Animals were anesthetized with isoflurane and transcardially perfused with 4% paraformaldehyde (PFA) in 0.1 M phosphate buffer, pH 7.4. The brains were post-fixed in 4% PFA at 4^{O}C for 24 h, immersed in sucrose solutions (15%, 20% and 30%) and frozen. Frozen brains were thawed in cryoprotectant (20% glycerol/2% DMSO) and multiple brains were embedded in a gelatin block and post-fixed in formaldehyde containing cryoprotectant; sections were freeze cut at 35μm, transferred to cryoprotectant, and stored at −20°C (Neuroscience Associates). Sections were stained under free-floating conditions for GFAP (glial fibrillary acidic protein; DAKO, 1:100,000), for Iba-1 (WAKO, 1:40,000), and for polyglutamine, following formic acid antigen retrieval, with biotinylated-4H7H7 (80 ng/ml).[13] The following general protocol was used: sections were blocked by reacting aldehyde sites with ethanolamine and reducing Schiff bases with ascorbic acid and treating with 0.5% Triton X-100 in PBS, followed by overnight incubation in primary antibody; for glial staining sections were washed, reacted with biotinylated anti-rabbit IgG (Vector), followed by Elite ABC reagent (Vector); peroxidase reactivity was detected with nickel-enhanced DAB using glucose-glucose oxidase to generate hydrogen peroxide in Tris-imidazole buffer. Biotinylated-4H7H7 localization was visualized by reaction with Elite ABC reagent followed by tyramide amplification using biotin-PEG-tyramide and a second reaction with Elite ABC reagent, and the peroxidase detected as above. Sections were mounted on glass slides, dehydrated and processed through alcohols and xylene substitute and cover-slipped with xylene substitute mountant (Shandon). When required mounted sections were lightly counterstained with thionin for Nissl substance.

High resolution digital images were collected on a Nikon Eclipse Ni microscope and minimally manipulated in Photoshop CS5 using consistent adjustments. Staining intensity was

quantified in Photoshop by inverting gray scale images, selecting regions of interest with the lasso tool and using the median intensity determined by the Histogram tool.

Tissue preparation

For Nissl and acetylcholinesterase staining, animals were sacrificed by cervical dislocation, and freshly isolated brains were quickly frozen on dry ice. For immunohistochemistry, animals were deeply anesthetized with isoflurane and transcardially perfused with 4% paraformaldehyde (PFA) in 0.1 M phosphate buffer, pH 7.4. The brains were isolated from the skulls, post-fixed in 4% PFA at 4^{O}C for 24 h, immersed in sucrose solutions (15%, 20% and 30%) and frozen on dry ice. Before sectioning, the brains were transferred to a cryostat and allowed to come to -15^{0}C for 30 min. Forty μm sections were collected on uncoated slides (for Nissl and acetylcholinesterase staining) or in PBS (for Htt immunostaining).

Nissl staining

Cresyl violet solution (0.5%) in 400 mM acetic buffer, pH 3.9 was stirred for 7 days at RT using a magnetic stirrer and filtered through filter paper prior to use. Sections collected on slides were incubated in histoclear (2 x 5 min.), 100% EtOH (2 x 5 min.), 95% EtOH (5 min.), 70% EtOH (5 min.), H_2O (5 s), cresyl violet solution (45 min.), H_2O (5 min.), 70% EtOH (5 min.), 95% EtOH (5 min.), 100% EtOH (2 x 5 min.), histoclear (2 x 5 min.) and coverslipped using DPX mounting medium (Sigma).

Acetylcholinesterase staining

The sections collected on the slides were incubated overnight in the incubation solution (4 mM S-acetylthiocholine iodide, 85 μM ethoproprazine, 50 mM sodium acetate, 4 mM $CuSO_4$, 16 mM Gly, pH 5.0) at RT. The next day, they were rinsed in H_2O, incubated in 1% Na_2S x 9 H_2O in acetic buffer, pH 7.5 for 10 min., rinsed with H_2O and incubated in formalin overnight. Next, the

slices were air-dried, dipped in 100% EtOH and histoclear and coverslipped using DPX mounting medium.

HTT immunostaining

Following 2 h blocking with 5% normal goat serum (NGS, Jackson ImmunoResearch) in PBS with 0.1% Tween-20 (PBST), free floating sections were incubated overnight at RT with primary antibodies diluted in PBST: mouse MAB 2166 (1:1000), mouse HU-4E6 (MAB 2170, Millipore, 1:1,000), mouse 3B5H10 (Sigma, 1:500) and mouse MW1 (DSHB, University of Iowa, 1:1,000). Next, the sections were incubated for 3 h at RT with DyLight 488-conjugated goat anti-mouse secondary antibody (Jackson ImmunoResearch) diluted at 1: 400 in PBST with NGS. Sections were mounted using ProLong Gold Antifade Reagent with DAPI (Invitrogen) and analyzed with a Zeiss Observer.Z1 epifluorescent microscope equipped with Axiovision software (Carl Zeiss).

TSPO and dopamine receptor autoradiography

Translocator Protein 18kDa (TSPO) and dopamine receptors (D1, D2) were visualized using quantitative receptor autoradiography. Fresh-frozen brains were sectioned (20 μm) on a freezing cryostat and thaw-mounted onto poly-L-lysine-coated slides (Sigma). [^{3}H]-DPA-713 (83 Ci/mmol; Quotient Bioresearch) autoradiography was used to measure TSPO. Slides were dried at 37°C for 30 min, followed by a prewash in 50 mM Tris-HCl buffer (pH 7.4) for 5 minutes at room temperature. Sections were then incubated in 0.5 nM [^{3}H]-DPA-713 buffer for 30 minutes at room temperature. Non-specific binding was assessed in adjacent sections incubated in the presence of 10 mM PK11195 (Sigma). The reaction was terminated by two 3-minute washes in cold buffer (4°C) and two dips in cold water (4°C). Sections were apposed to Kodak Bio-Max MR films (Sigma) with [^{3}H]-Microscales (Perkin Elmer) for 4 weeks.

[H^3]-SCH-23390 (84.3 Ci/mmol; Perkin Elmer) autoradiography was used to measure D1 dopamine receptors. Sections were dried at 37°C for 30 min, followed by a preincubation for 20 min. at room temperature in 50 mM Tris buffer, pH 7.4, containing 120 mM NaCl, 5 mM KCl, 2 mM CaCl2, 1 mM MgCl2. Sections were then incubated at room temperature for 30 min in the same buffer (pH 7.4) containing 1 mM ascorbic acid, 40 nM ketanserin (Sigma), and 1 nM [H^3]-SCH-23390. Non-specific binding was defined in adjacent sections incubated in the presence of 5 μM (+)-butaclamol (Sigma). After incubation, sections were rinsed twice for 20 seconds each in cold buffer containing 1 mM ascorbic acid (pH 7.4, 4°C), then dipped in cold distilled H2O (4°C), and dried under a stream of cool air. Sections were apposed to Kodak Bio-Max MR films (Sigma) with [^{3}H]-Microscales (Perkin Elmer) for 5 weeks.

[H^3]-Spiperone (85.4 Ci/mmol; Perkin Elmer) autoradiography was used to measure D2 dopamine receptors. Sections were dried at 37°C for 30 min, followed by a prewash for 5 minutes at 36°C in 50 mM Tris buffer, pH 7.1, containing 120 mM NaCl, 5 mM KCl, 2 mM CaCl2, 1 mM MgCl2. Sections were then incubated at 36°C for 30 min in the same buffer (pH 7.1) containing 40 nM ketanserin (Sigma), and 1.4 nM [H^3]-Spiperone. Non-specific binding was assessed in adjacent sections incubated in the presence of 1 μM (+)-butaclamol (Sigma). After incubation, sections were rinsed three times for 20 seconds each in cold buffer (4°C), then dipped in cold distilled H2O (4°C), and dried under a stream of cool air. Sections were apposed to Kodak Bio-Max MR films (Sigma) with [^{3}H]-Microscales (Perkin Elmer) for 4 weeks. All images were acquired and quantified using the MCID software (InterFocus Imaging Ltd.).

Statistics

Two-way univariate and multivariate ANOVA was performed using SPSS Statistics 19 (IBM). Student's t-test was used for pairwise comparisons between experimental groups (Excel 2008; Microsoft).

Results

Mutant HTT protein is widely expressed in brain of BAC-225Q mice and forms abundant protein aggregates throughout the brain

The polyQ-expanded HTT was identified by western blotting with 1HU-4C8 (MAB 2166) antibody as a novel band specific to transgenic tissue, retarded in migration above the WT HTT band, and was present in all examined brain regions of all the analyzed BAC-225Q animals, but not in WT littermates (**Figure 2-2A**). The levels of transgenic protein were approximately 50% lower than those of WT protein in BAC-225Q animals in all analyzed regions, when compared to full-length protein present as a monomer on SDS gel, and no difference in this ratio was found between striata from 3- and 12-month-old mice (**Figure 2-2A**), indicating that there is not a substantial decrease of the extractable expanded mutant Htt protein relative to WT HTT protein over this time frame. Examination of cortical protein extracts in full uncut western blots probed with anti-polyglutamine MAB1574 (1C2 clone) demonstrated the expression of mutant polyglutamine expanded HTT in the BAC-225Q animals, and no abundant HTT protein fragments were seen in either 3-month or 15-month BAC-225Q transgenic animals (**Figure 2-2B**). Furthermore, the levels of extractable mutant HTT protein were similar between 3-month and 15-month BAC-225Q cortex. To determine how mRNA expression levels of the mutant *Htt* transgenic allele versus the endogenous WT *Htt* alleles compared to the relative expression levels of the mutant versus WT HTT protein seen by western, we assessed total mouse *Htt* mRNA levels in striata of 3-month and 15-month old animals by quantitative RT-PCR

(**Figure 2-3)**. This also allowed us to test whether mRNA expression of the mutant *Htt* transgene was altered by age. Two-way ANOVA demonstrated a significant ~10% increase in total *Htt* mRNA expression in BAC-225Q animals versus WT ($p=0.004$), with no significant difference by age ($p=0.834$).

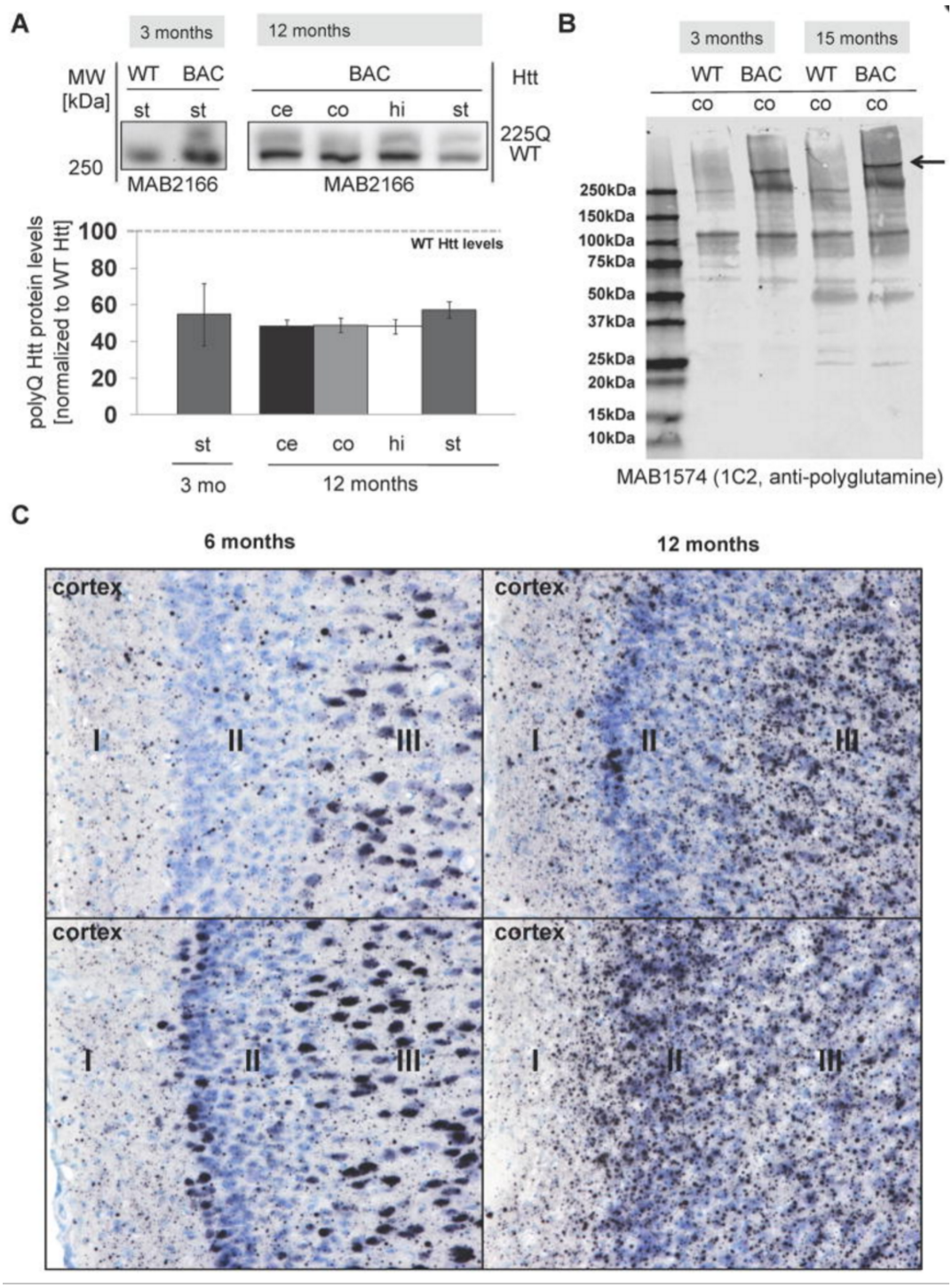

Figure 2-2. Transgenic polyQ HTT protein is widely expressed in brain of BAC-225Q mice, and accumulates as large neuropil aggregates, legend on following page.

Figure 2-2. Transgenic polyQ HTT protein is widely expressed in brain of BAC-225Q mice, and accumulates as large neuropil aggregates. (A) The levels of total HTT protein (MAB2166, n=3) were measured by western blotting for HTT protein. Transgenic polyQ HTT is expressed at about half the level of endogenous HTT in striatum (st) of 3-month old animals and cerebellum (ce), cortex (co), hippocampus (hi) and striatum of 12-month old animals. (B) Full uncut gel western blots of cortex extracts from 3-month-old animals were probed for poly-glutamine proteins (MAB1574, clone 1C2). Aside from the full-length mutant HTT protein band (indicated by arrow) no other abundant BAC-225Q specific protein fragments were detected between WT and BAC animals at either 3-months or 15-months of age. Analysis of the same protein extracts with anti-Htt MAB2166 confirmed the absence of mutant HTT protein fragments in the BAC-225Q cortex (data not shown). (C) Mutant HTT immunostaining was performed in cortex of 6-month (left) and 12-month old (right) BAC-225Q mice and WT mice (not shown) with 4H7H7 antibody. Representative fields from two animals (upper and lower) are shown of cortical layers I, II and III. Animals in upper fields had a relatively lower aggregate abundance compared to the animals in the lower fields. Nuclear accumulation is abundant in 6-month old animals, with sparse neuropil aggregates; in contrast 12-month-old animals exhibit extensive and larger neuropil aggregates with concomitant decrease in nuclear immmunoreactivity. All fields are 225μm x 170μm.

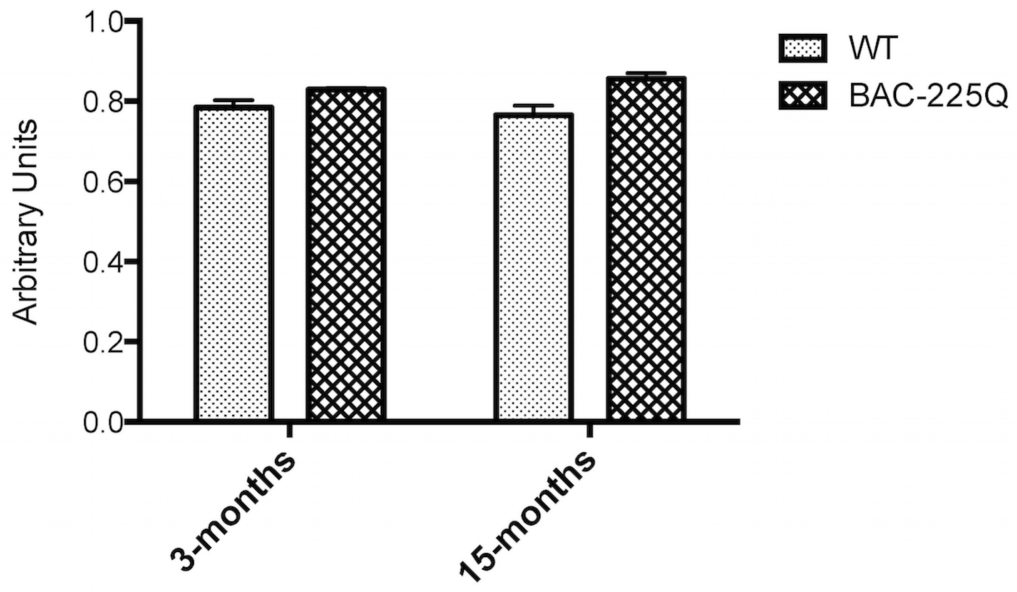

Figure 2-3. QRT-PCR for total mouse *Htt* expression in striatum at 3-months and 15-months of age. Quantitative RT-PCR with random hexamers for the first strand reaction was performed on total RNA from striatum of WT and BAC-225Q striatum using the standard methods of our laboratory. Primers for amplification were not over the CAG repeat in exon 1, Primer 1: 5'-GGAGCTGCAGGTGTTCTTTC-3', and Primer 2: 5'-CTGTTGAAGGGCCAGAGAAG-3'. Two-way ANOVA detects a significant increase in total *Htt* expression levels in the BAC-225Q mice versus WT ($p=0.004$); while no significant difference in age was observed. The BAC-225Q transgenic animals have ~10% increase in total Htt expression.

Table 2-1. Distribution of mutant HTT aggregates at 6 months

Diffuse nuclear or neuropil aggregate levels were scored from (-) absent, (tr) trace, to (+, ++, +++, or ++++) for increasing abundance. (High) and (Low) indicate representative animals with relatively high or low aggregate density representing the variability between animals of the same sex.

Neuroanatomical location		Male				Female			
		High		Low		High		Low	
		Nuclear	Neuropil	Nuclear	Neuropil	Nuclear	Neuropil	Nuclear	Neuropil
Olfactory system	Anterior olfactory nucleus	++	++	+	++	++	++	tr	++
	Lateral olfactory tract	-	++++	-	++	-	++++	-	+++
Cortex	Frontal cortex	+++	++	tr	+	++	+	-	++
	Primary motor cortex	+++	++	+	+	++	+	tr	++
	Secondary motor cortex	+++	+++	+	+	++	++	+	++
	Cingulate cortex	+++	+++	+	+	++	++	+	++
	Primary somatosensory cortex	+++	++	+	+	+++	+	tr	+
	Piriform cortex	++++	++	+	+	++++	++	+++	+
	Secondary somatosensory cortex	++	++	+	+	+++	+	tr	+
	Retrosplenial cortex	+++	+++	+	+	++	++	tr	+++
	Temporal association cortex	++	+++	tr	++	+	+++	-	+++
	Primary visual cortex	++	+++	+	+	++	++	-	++
Striatum	Nucleus accumbens	+++	+	+	+	+++	+	+	+
	Ventral pallidum	-	++	-	tr	-	++	-	++
	Caudate/putamen	++++	tr	++	tr	++++	tr	+	tr
	Globus pallidus	-	tr	-	tr	-	+	-	+
Septum	Septohippocampal nucleus	tr	++	-	++	-	++	-	+++
	Lateral septal nucleus	tr	++	-	+	-	++	-	++
Bed nucleus of the stria	Medial	tr	++++	-	++	tr	+++	-	++
Hypothalamus	Magnocellular preoptic nucleus	++	+	+	+	+++	++	tr	+
	Ventromedial hypothalamic nuclei	-	++	-	++	-	+++	-	++
	Lateral hypothalamic area	tr	+	-	+	-	+	-	+
	Premammilary nucleus	-	++	-	+++	-	++	-	++
Thalamus	Laterodorsal	++	++	tr	+	++	++	++	++

	thalamic nuclei								
	Ventral thalamic nuclei	+++	+	+	++	+++	++	++	++
	Medial habenular nucleus	+	++	**tr**	-	+	+	**tr**	-
Geniculate	**Dorsal lateral geniculate nucleus**	++	+	+	+	++	++	+	+
	Pregeniculate nucleus	+	++	-	+	-	++	-	++
	Medial geniculate	++	+	+	+	++	+	**tr**	+
Amygdala	**Central amygdaloid nucleus**	+	++	-	++	**tr**	+++	-	+++
	Basolateral amygdaloid nucleus	+++	++	+	+	++	++	-	++
	Basomedial amygdaloid nucleus	++	+++	+	++	+	+++	-	+++
Hippocampus	**CA1**	++++	-	++	-	++++	-	**tr**	-
	CA2	++	-	+	-	++	-	**tr**	-
	CA3	+++	-	+	-	+++	-	-	-
	Polymorphic layer (CA4)	+	++++	-	+++	+	++++	+	+++
	Dentate gyrus	+	-	-	-	+	-	-	-
	Subiculum	+++	+++	+	+++	++	+++	**tr**	+++
Colliculi	**Superior colliculus superficial gray**	+	++	-	++	**tr**	++	-	++
	Inferior colliculus	+	++	-	++	+	+++	-	++
Mesencephalon	**Red nucleus**	+	+	-	+	-	-	-	-
	Pontine nucleus	+	++	+	++	+	++	**tr**	++
	Olivary nuclei	++	+	-	+	+	++	-	++
Cerebellum	**Purkinje cell layer**	+++	-	++	-	+++	-	+++	-
	Cerebellar nuclei	-	+++	-	+++	-	++++	-	+++

An important hallmark of HD is accumulation of HTT aggregates in brain. To identify Htt inclusions we carried out immunohistochemical analysis of brains of 6- and 12-month-old BAC-225Q mice and WT littermates using 4H7H7 antibody (**Figure 2-2C**). We detected an extensive deposition of polyglutamine-containing aggregates in transgenic animals only; staining was variable but predominantly of neuropil aggregates, with additional neuronal nuclear staining only at 6 months of age. We noted a high degree of animal-to-animal variability in the relative abundance of mutant HTT aggregates (**Table 2-1**). We quantified the abundance of aggregates in two representative animals of both sexes, one with relatively high and another relatively low

aggregate loads at 6 months (**Table 2-1**). The most affected regions at 6 months were the hippocampus and associated cortex, and the bed nucleus of the stria terminalis, cerebellar nuclei and Purkinje cells, both superior and inferior colliculi. Striatum at 6 months, however, exhibited minimal neuropil aggregates, but widespread neuronal nuclear staining. These, and additional selected regions with semi-quantitative analysis are shown in **(Figure 2-4** and **Table 2-1).** There are variable numbers of neuropil aggregates and some neuronal nuclear staining throughout the cerebrum. Studies at 12 months were limited to analysis of cortical regions where a marked reduction in the extent of neuronal nuclear staining was seen together with an increase in the number and size of neuropil aggregates (**Figure 2-2C**).

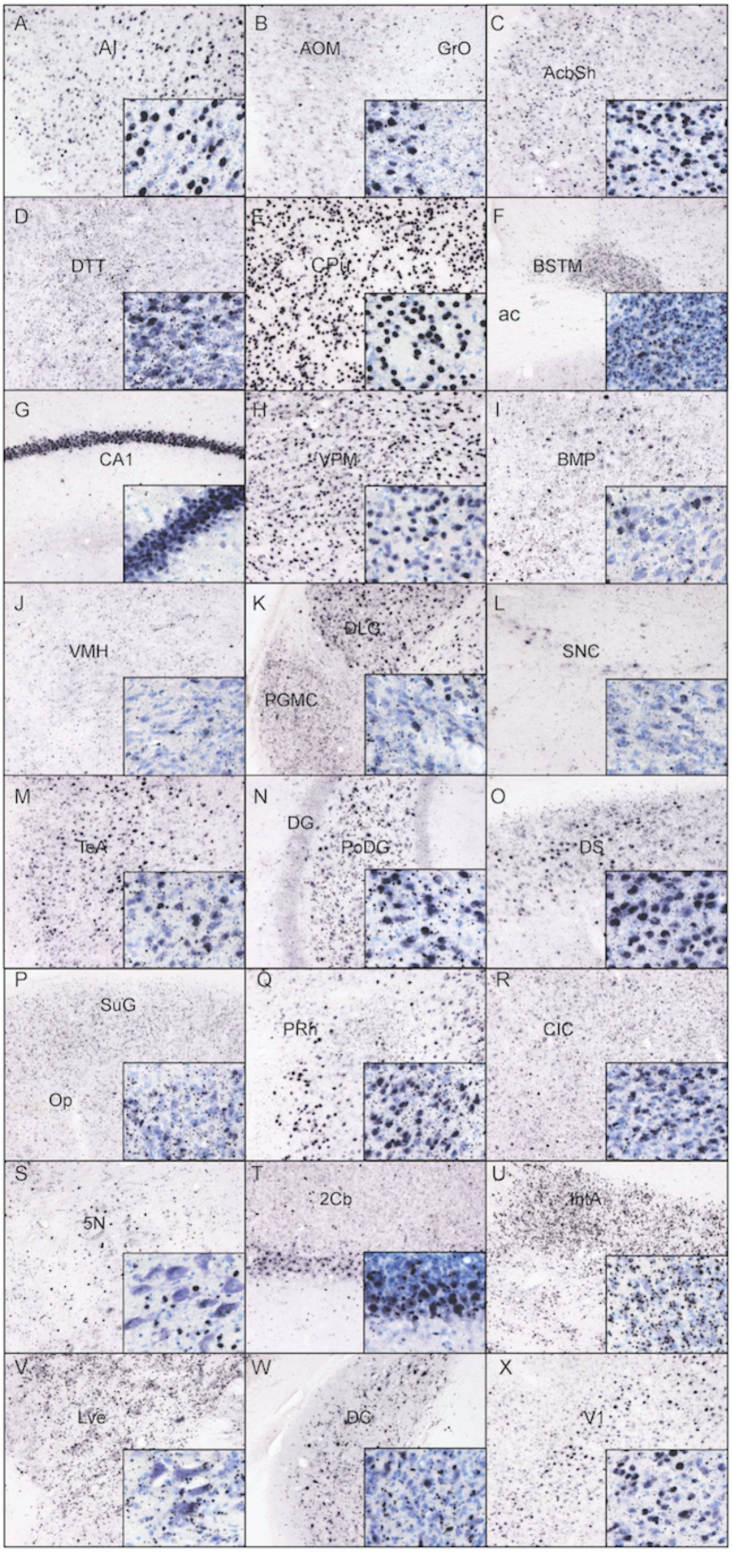

Figure 2-4 Mutant Htt immunostaining (4H7H7) in 6-month-old BAC-225Q mice, legend on following page .

Figure 2-4. Mutant Htt immunostaining (4H7H7) in 6-month-old BAC-225Q mice; field and abbreviations defined: A1, agranular insular cortex (A), AOM, anterior olfactory area, medial (B)/ AcbSh, nucleus accumbens, shell (C); DTT, dorsal taenia tecta (D); CPu, caudate putamen (E); BSTM, bed nucleus of the stria terminalis, medial (F)/ CA1, CA1 field of hippocampus (G); VPM, ventral posteromedial thalamic nucleus (H); BMP, basomedial amygdaloid nucleus, posterior (I); VMH, ventromedial hypothalamic nucleus (J); DLG, dorsal lateral geniculate, and PGMC, pregeniculate nucleus, magnocellular (K); SNC, substantia nigra pars compacta (L); TeA, temporal association cortex (M); PoDG, polymorphic layer of the dentate gyrus, and DG, dentate gyrus of hippogampus (N)/ DS, dorsal subiculum (O)/ SuG, superficial gray layer of the superior colliculus, and Op, optic nerve layer of the superior colliculus (P)/ PRh, perirhinal cortex (Q); CIC, central nucleus of the inferior colliculus (R); 5N, motor trigeminal nucleus (S); 2Cb, lobule 2 of the cerebellar vermis (T); IntA, interposed cerebellar nucleus, anterior part (U); Lve, lateral vestibular nucleus (V); DC, dorsal cochlear nucleus (W); V1, primary visual cortex (X). Field size: A-X: 450u x 340u; insets: 115u x 85u.

BAC-225Q mice are characterized by reduced body weight and early behavioral abnormalities

HD patients experience weight loss[14] and we observed marked reductions in body weight in BAC-225Q mice compared to WT littermates (**Figure 2-5**). In females this reduction was detected before 2 months of age, and was initially driven by slower weight gain and then by total arrest of weight gain. Weight deficiency in males appeared after body weight of BAC-225Q males had reached a plateau (~4.5 months) (**Figure 2-5**). In both WT males and females, body weight continuously increased until the tenth month of age, resulting in strong differences between WT and transgenic mice (transgenic males were 23% lighter and females were 16% lighter than WT).

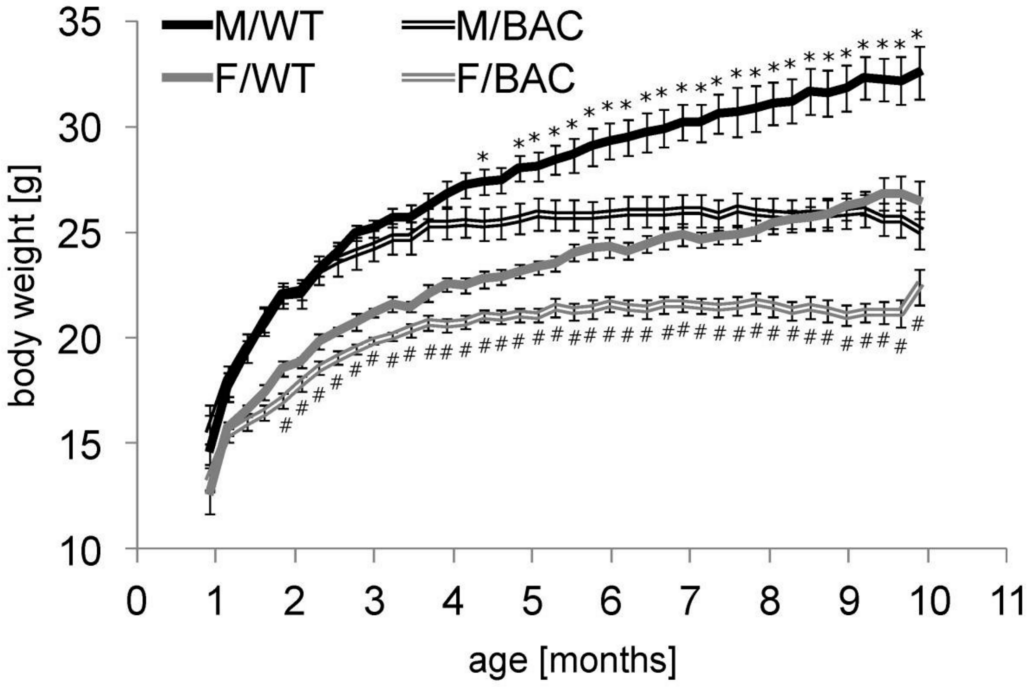

Figure 2-5. Decreased body weight in BAC-225Q mice relative to WT. Body weight of BAC-225Q animals and their WT littermates was measured from 1st to 10th month of age (n=9–15). Progressively decreased weight is observed in both BAC-225Q males (from 4.5 months, *t-test, $p<0.05$) and females (from 2 months, #t-test, $p<0.05$), when compared to WT mice. Three-way ANOVA reveals effect of genotype ($F(1,1862)=737.03$, $p<0.001$), effect of gender ($F(1,1862)=1877.94$, $p<0.001$), effect of age ($F(38,1862)=63.856$, $p<0.001$ and genotype-age interaction ($F(38, 1862)=7.742$, $p<0.001$).

To monitor motor performance of BAC-225Q animals we used the accelerating rotarod test. The first cohort of animals was examined at 3, 4, 5, 6, 7, 8, 9, 12 and 15 months of age. We identified a deficiency in rotarod performance beginning at 3 months of age (performance time loss by 28% in males (**Figure 2-6A**) and 19% in females (data not shown)), but unexpectedly this phenotype was found to be static until 6 to 7 months of age, then regressive at later ages (**Figure 2-6A**). Nevertheless, ANOVA analyses showed a strong effect of genotype on rotarod performance for both males and females. We also found a difference between genders in age-dependent regress of motor deficiency – females were significantly impaired only at 3 and 4

months of age (data not shown). In males the difference between BAC-225Q and WT mice was observed until 9 months of age, but was absent in 12- and 15-month-old animals (**Figure 2-6A**). Despite this apparent recovery in older animals, no genotype-age interaction was found by ANOVA, suggesting that a continued trend toward motor deficiency was present. The loss of rotarod phenotype in BAC-225Q mice at older ages could suggest a training effect, however, we performed rotarod with another cohort of animals, in which the first session was carried out using 6-month-old, rotarod-naïve mice, and then these animals were further tested only at 7 and 12 months of age. In this case, despite a different experimental paradigm than in the first cohort, we obtained the same results – a decreased latency to fall at 6 and 7, but not at 12 months of age in BAC-225Q males, and normal rotarod performance at 6, 7 and 12 months in BAC-225Q females (data not shown). This strongly suggests that factors other than motor skill learning are responsible for the loss of rotarod impairment at later ages in BAC-225Q animals. One possibility is the reduced body weight of the mutant animals compared with WT, as lower body weight is known to be associated with improved performance on rotarod.[15,16]

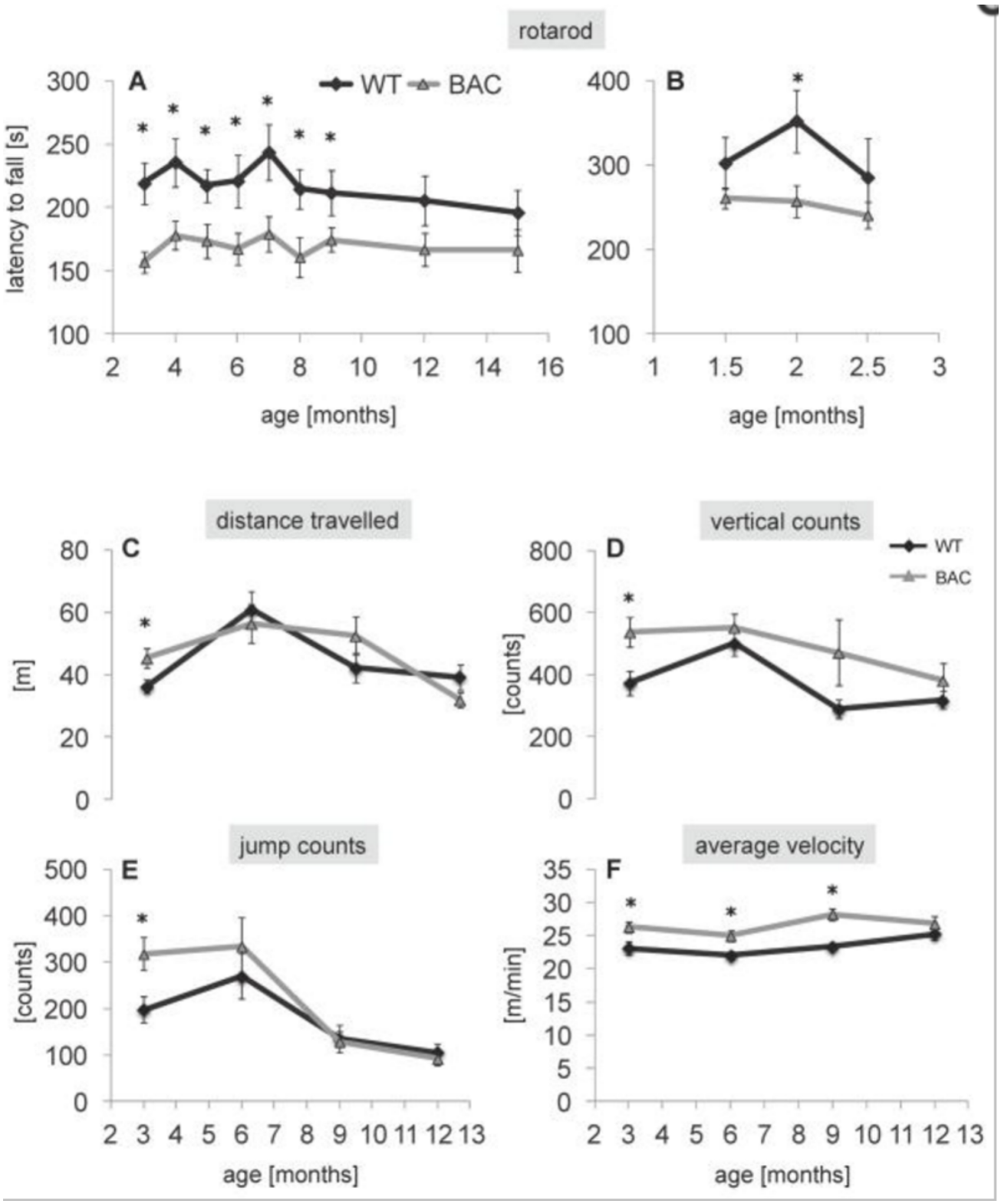

Figure 2-6. Behavioral abnormalities in BAC-225Q mice, legend on following page.

Figure 2-6. Behavioral abnormalities in BAC-225Q mice. (A) Motor performance was evaluated using accelerating rotarod in 3- to 15-month-old males (n=9–10). Performance of BAC-225Q animals is impaired relative to WT littermates starting from 3 months of age (*t-test, $p<0.05$). Unexpectedly, this impairment is absent in the aged mice, at 12 and 15 months, and at the earlier time points, between 3rd and 9th month, the rotarod performance deficiency, though present, is not progressive. These observations are confirmed by ANOVA that identifies effect of genotype ($F(1,170)=44.744$, $p<0.001$), but not effect of age or genotype-age interaction. (B) Since the rotarod deficit was identified at the earliest examined time point, 3 months of age, another cohort of animals was assessed from 1.5 to 2.5 months (n=9–13). Of the three examined time points, statistically significant difference between BAC-225Q and WT mice is found only at 2 months of age (*t-test, $p=0.021$), however two-way ANOVA reveals strong effect of genotype on rotarod performance between 1.5 and 2.5 months ($F(1,66)=8.048$, $p=0.006$). (C–F) Early hyperactive behavior followed by normalization of the symptoms in BAC-225Q mice. Spontaneous locomotor activity of 3- to 12-month-old mice was examined in open field test (n=16–27). At 3 months of age, (C) longer distance travelled (*t-test, $p=0.42$) as well as (D) increased vertical counts (*t-test, $p=0.023$), (E) jump counts (*t-test, $p=0.023$), and (F) average velocity (*t-test, $p=0.022$) are observed in BAC-225Q animals compared to WT littermates. These alterations, except (F) average velocity at 6 and 9 months of age (*t-test, $p=0.12$, $p<0.001$, respectively) are not found in the later time points. Two-way multivariate ANOVA reveals effect of age on total distance travelled ($F(3,151)=10.015$, $p<0.001$), vertical counts ($F(3,151)=5.454$, $p=0.001$), jump counts ($F(3,151)=13.939$, $p<0.001$), and average velocity ($F(1,151)=20.099$, $p<0.001$). Effect of genotype is found for vertical counts ($F(1,151)=8.964$, $p=0.003$) and average velocity ($F(3,151)=3.356$, $p=0.021$).

Because we identified a rotarod performance decline at age 3 months, we examined one more cohort of mice at a younger age. The analyses at 1.5, 2 and 2.5 months also showed strong effects of genotype for both genders, however the impairment was stronger in females (significant differences at all the three analyzed time points; data not shown) than in males (significant differences were restricted to the 2 months time point only, but the trend was present at 1.5 and 2.5 months) (**Figure 2-6B**). Of note, the rotarod performance impairment in these younger BAC-225Q mice occurs prior to the significant differences in body weight between genotypes.

To determine if there was a relationship between Htt aggregate load and rotarod performance within the BAC-225Q animals we assessed aggregate load in three paired sets of transgenic animals for which we had acquired rotarod data ahead of sacrificing for immunohistochemical analysis. We examined two pairs of animals at 6-months of age (rotarod performance between 1.5 and 2.5 months of age), and one pair of animals at 12 months of age (rotarod performance at 6 and 7 months of age). We focused on the aggregate load of the lateral olfactory tract – as unlike other regions of the brain the lateral olfactory tract had almost exclusively neuropil aggregates at both ages, with minimal nuclear accumulation. In all instances the animal with the higher aggregate load had relatively poor rotarod performance in the preceding months. Paired t-test analysis demonstrated a significant ($p=0.011$) difference in the ratio of average aggregate load over the average rotarod performance in the animals with relatively higher aggregate load versus the animal with a lower intensity aggregate staining.

To examine spontaneous motor activity we performed the open field test. At 3 months we observed hyperactivity as reflected by increase in total distance travelled, vertical and jump counts, and average velocity in BAC-225Q mice (**Figure 2-6C-F**). This early spontaneous behavioral impairment regressed in older animals.

Summarizing, we identified very early abnormalities in BAC-225Q mice, represented by reduced body weight and behavioral impairment. The body weight deficiency was progressive, and may have been responsible for regression of behavioral impairment, observed at later time points.

Blood markers of HD in BAC-225Q mice

Two important groups of markers identified in blood of HD patients are those related to inflammation and disturbed energy metabolism.[17-19] We analyzed the levels of several such biomarkers in BAC-225Q mouse plasma versus WT between 2 and 10 months of age to determine if they show an association with pathology in this HD model. Of six cytokines measured, two (IL-4 and MIP2) were below the detection limit in BAC-225Q mice and WT littermates, and we did not observe any genotype-dependent alterations for three others (IFNγ, IL-6 and TNFα) between 2 and 10 months of age (data not shown). However, we identified alterations in the concentrations of keratinocyte chemoattractant (KC), a murine functional homologue of human IL-8.[20] We observed increased levels of KC in plasma of 10-month-old BAC-225Q mice compared to WT littermates, and trend toward an increase at 6 months mice (**Figure 2-7A**).

Besides cytokines, we examined plasma levels of leptin, a central regulator of energy metabolism,[21] and found its levels increased in BAC-225Q mice starting from 6 months of age (**Figure 2-7B**). The significant changes in leptin levels (6 months) occur after a decrease in body weight is observed in BAC-225Q mice (5 months or younger), though whether it represents a cause or effect of the weight phenotype is unclear.

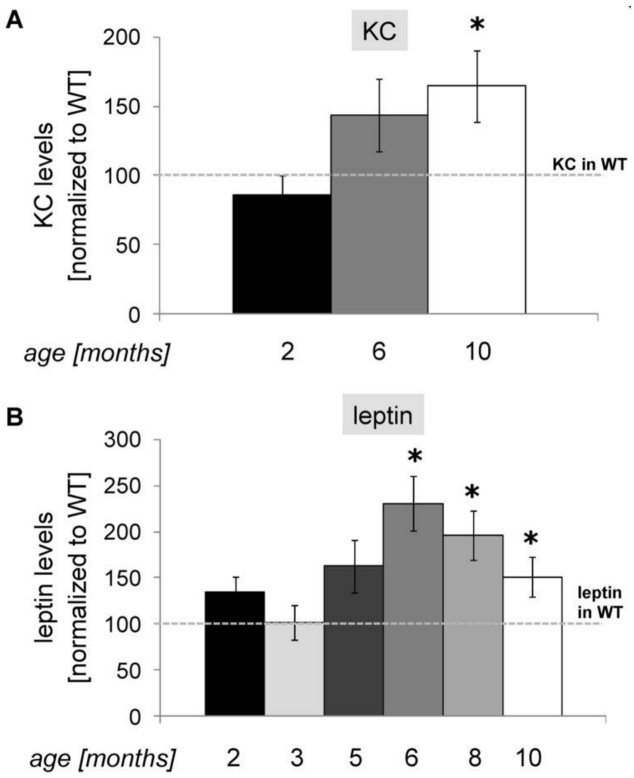

Figure 2-7. Increase in plasma levels of KC and leptin in BAC-225Q mice. The levels of seven HD-associated blood markers were measured in plasma of BAC-225Q mice. IL-4 and MIP2 are below detection limit, for IFNγ, IL-6 and TNFα no differences are found between BAC-225Q and WT mice, but levels of pro-inflammatory chemokine, KC (mouse homologue of human IL-8), and of energy metabolism-regulating hormone, leptin, are altered (n=12-18, n=12–17, respectively, gender balanced). (A) Plasma concentrations of KC are elevated in 10-month-old BAC-225Q animals (*t-test, p=0.014). (B) Leptin levels are increased in BAC-225Q mice at 6, 8 and 10 months of age (*t-test, p<0.001, p=0.002, p=0.038, respectively).

BAC-225Q mice display widespread brain atrophy

To investigate the effect of transgene expression on brain volume we analyzed fixed brains from 3- and 10-month-old female mice using volumetric MRI measurements. We found that total brain volume was decreased by 6.4% in 3 month-old BAC-225Q animals (**Figure 2-8A**). This was an effect of widespread atrophy as we were not able to distinguish any particularly affected region(s). At this age, 13 of a total of 27 brain regions examined, exhibited significantly

decreased volumes in BAC-225Q mice compared to WT littermates (**Figure 2-7A)**. The affected regions included both gray and white matter. Importantly, volume of the striatum, a primary site of neurodegeneration in adult-onset HD in humans,[22] was not changed at this age. The widespread brain atrophy was progressive – at 10 months we observed total brain volume loss by 12% and found 19 of 27 regions to be significantly reduced (**Figure 2-8B**). At this time point we also observed a 10% loss of striatal volume in striatum as well as decreased neocortex volume (another prominent site of neurodegeneration in HD.[23-25] Other regions affected at 10 months, but not at 3 months included cingulum, stria medullaris, fasciculus retroflexus, fornix, anterior commissure and corpus callosum/external capsule, suggesting a pronounced effect on white matter tracts (**Figure 2-8**). This early, widespread pathology suggest that this mouse model recapitulates features of juvenile-onset HD more so than adult-onset HD.

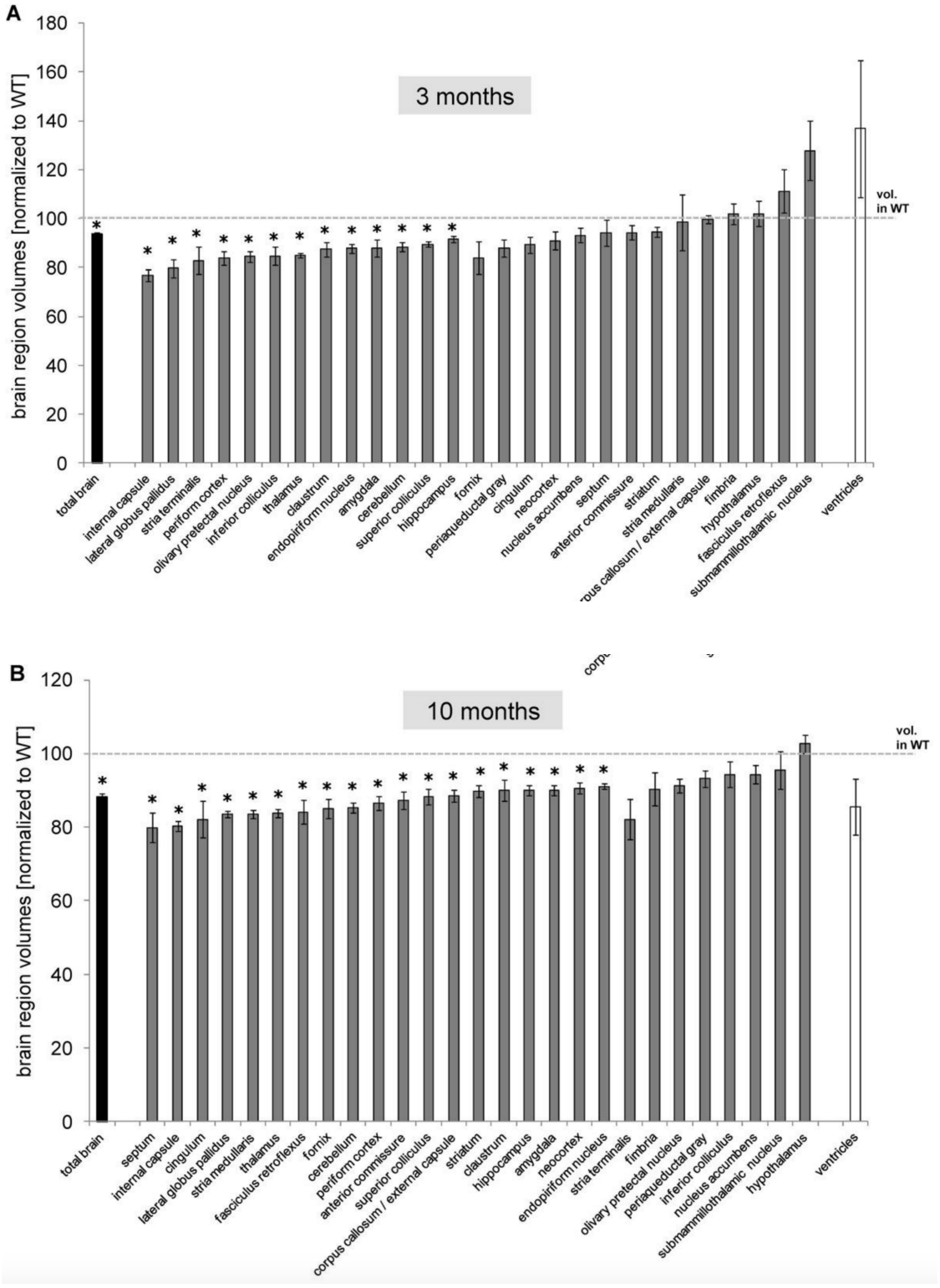

Figure 2-8. Progressive loss of brain volume in BAC-225Q mice (legend on following page).

Figure 2-8. Progressive loss of brain volume in BAC-225Q mice. Brain volumes were measured using MRI volumetric analysis in BAC-225Q mice at 3 and 10 months of age (n=4). (A) Total brain volume (*t-test, $p=0.039$) and volumes of 13 out of 27 analyzed brain regions (*t-test, $p<0.05$) are decreased in BAC-225Q mice compared to WT littermates at 3 months of age. (B) At 10 months of age a loss of total brain volume is more prominent (*t-test, $p=0.001$) and 19 brain regions with decreased volumes (*t-test, $p<0.05$) are identified.

Glial cell activation and neuroinflammation often accompanies neurodegeneration. We analyzed gliosis in BAC-225Q mouse brain by immunohistochemical detection of astrocyte- and microglia-specific markers, GFAP and Iba1, respectively. This analysis revealed no significant increase in gliosis at 6 months (data not shown), but showed a significant increase in staining for markers of both astrogliosis and microgliosis in cortex at 12 months (**Figure 2-9**).

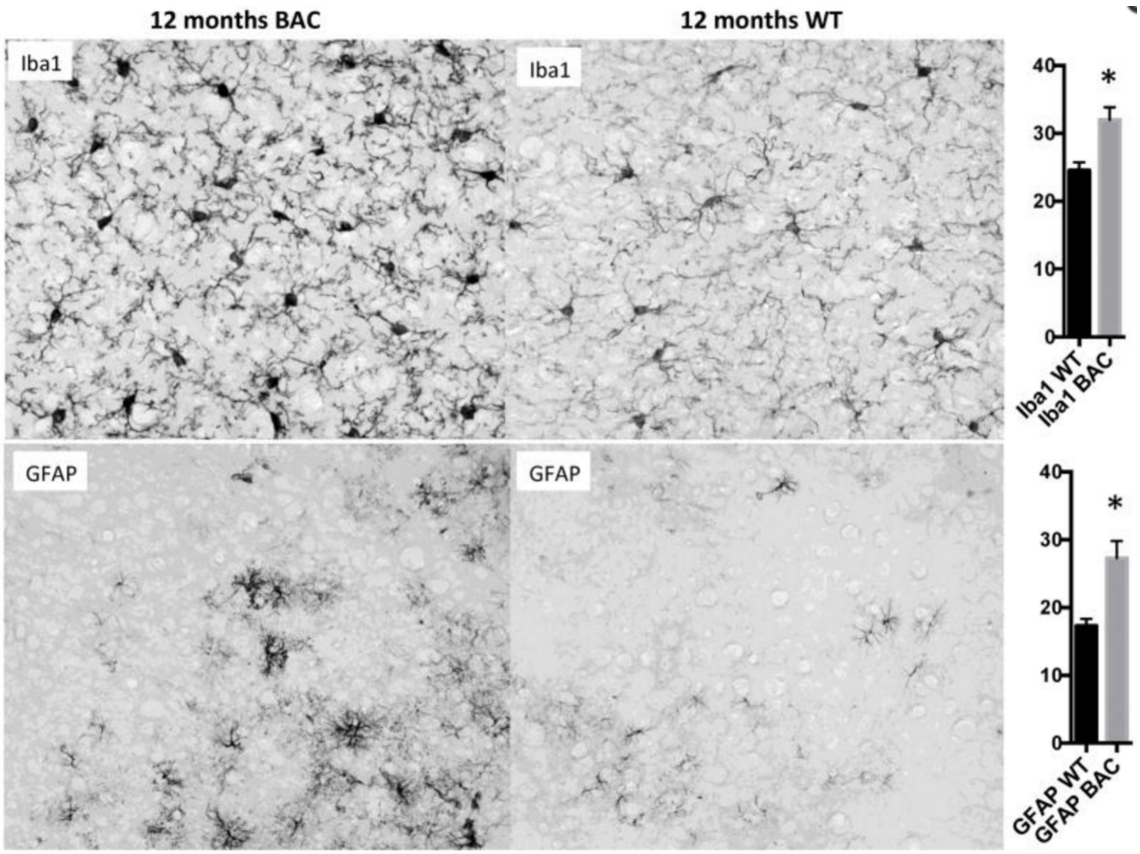

Figure 2-9. Gliosis in 12-month old BAC-225Q mouse brain versus WT mouse brain. Microgliosis and astrogliosis were analyzed by immunohistochemical detection of Iba1 and GFAP, respectively. S1 cortex is shown, with quantification in arbitrary units (* $p<0.01$ t-test, n=6, 3 animals per genotype, left and right hemispheres). All fields are 200µm x 160µm.

In addition to conventional immunohistochemistry we performed TSPO (Translocator Protein 18 kDA, formerly known as Peripheral Benzodiazepine Receptor (PBR)) autoradiography in several brain regions of BAC-225Q animals. TSPO is a sensitive marker of neuroinflammation and active gliosis.[26] Additionally, to confirm and validate TSPO autoradiography as a marker of neurodegeneration in HD animals, we also performed this assay in an established HD mouse model, YAC128 (JAX, #004938, Bar Harbor, ME, USA), and compared region- and age-specific changes in TSPO activation between both models. YAC128 mice have been shown to display late, adult-onset HD-like pathology characterized by loss of striatal and cortical volumes

beginning at 9 to 12 months, respectively, selective striatal neuronal loss from 12 months, rotarod performance deficits from 6 months, and hypoactivity on open field from 12 months[27]. In contrast, as shown in this manuscript, the BAC-225Q animals display early (< 3 months) and more widespread neuropathology. The YAC128 mice are in an FVB genetic background,[27] so each line was compared to WT littermates of its own background strain. In BAC-225Q mice, we observed TSPO up-regulation in every analyzed region except hippocampus (**Figure 2-10A**). Interestingly, in some of these regions, the TSPO phenotype was present in spite of an absence of volume loss as measured by MRI (striatum at 3 months and periaqueductal gray and hypothalamus at both time points); in contrast, other regions with volume loss were not accompanied by TSPO up-regulation (thalamus and globus pallidus at 3 months, hippocampus at both time points). These findings suggest that despite widespread and uniform volume loss, there may be regional differences in the mechanisms contributing/accompanying neurodegeneration in BAC-225Q animals. In YAC128 mice, TSPO was up-regulated in striatum at 10 months and thalamus at 6 and 10 months (**Figure 2-10B**). These results indicate a juvenile-like, widespread and early pathology in the BAC-225Q HD model, and validate adult-like, region-specific and late pathology in the YAC128 HD model.

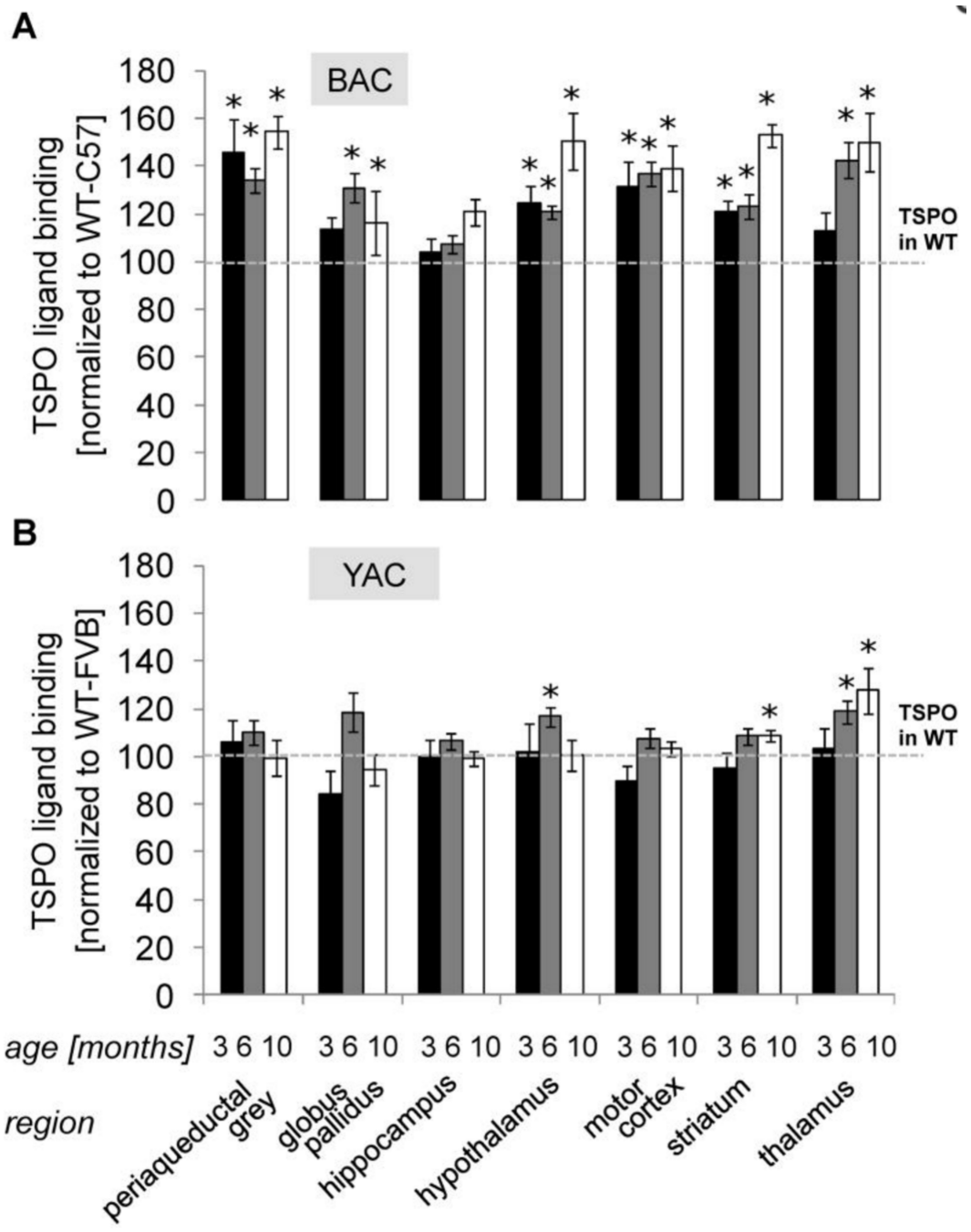

Figure 2-10. Early, widespread up-regulation of TSPO, a neuroinflammation biomarker, in brain of BAC-225Q animals, and late, region-specific up-regulation in YAC128 mice, an established model of adult-onset HD (legend on following page).

Figure 2-10. Early, widespread up-regulation of TSPO, a neuroinflammation biomarker, in brain of BAC-225Q animals, and late, region-specific up-regulation in YAC128 mice, an established model of adult-onset HD. (A) Binding of [^{3}H]-DPA-713, a ligand of neuroinflammation biomarker, TSPO, was measured in BAC-225Q mice using autoradiography (n=6-8). TSPO is up-regulated in all examined regions except hippocampus. In most of the analyzed regions TSPO pathology starts early – increased ligand binding is observed at 3, 6 and 10 months in periaqueductal gray (*t-test, p=0.017, p<0.001, p<0.001, respectively), hypothalamus (p=0.013, p=0.021, p=0.015, respectively), motor cortex (p=0.018, p<0.001, p<0.001, respectively) and striatum, (p=0.011, p=0.003, p<0.001, respectively) and at 6 and 9 months in globus pallidus (p<0.001, p=0.017, respectively) and thalamus (p<0.001, p=0.003, respectively). (B) To validate TSPO as a marker of ongoing neurodegeneration in HD models, autoradiography experiments were performed also in the most commonly used transgenic model of adult-onset HD, YAC128 mice (n=7–10). Only three regions with increased binding of [^{3}H]-DPA-713 are found, and TSPO phenotype is observed later than in BAC-225Q animals – at 6 months in hypothalamus (*t-test, p=0.026), at 6 and 10 months in thalamus (*t-test, p=0.021, p=0.036, respectively) and at 10 months in striatum (p=0.048). These findings confirm juvenile-like, widespread degeneration in BAC225Q mice and more specific, adult-like degeneration in YAC128 mice.

Striatum is a primary site of pathology in HD[22,28] and we observed a two-stage pattern of neurodegeneration of this region in the BAC-225Q model (TSPO activation starting at 3 months and volume loss at 10 months). Striatal medium spiny neurons (MSNs) are particularly prone to degeneration in HD.[22] Two main subtypes of MSNs are distinguished by expression of D1 or D2 dopamine receptors, with the latter being more vulnerable in adult-onset HD. To examine MSN subtype involvement in BAC-225Q mouse pathology, we performed a radioligand binding assay in striata of 3, 6 and 10-month-old animals (**Figure 2-11A**). YAC128 mice, characterized by striatal MSN loss[27], were also included in this experiment as a positive control and comparison. D1 receptor ligand binding was found to be decreased in BAC-225Q mice at 6 months, however not significantly different than control at 10 months. No alteration in D1 receptor binding was observed in YAC128 mice (**Figure 2-11**) at either age point. In both models we observed a statistically significant decrease in D2 receptor levels at 6 and 10 months, however BAC-225Q mice exhibited a greater change at both time points (loss of ~30% signal vs loss of ~15% signal

in YAC128 mice). In HD patients, striatal neuropathology follows a specific pattern – from caudal to rostral striatum[22]. We analyzed dopamine receptors in striatal subdivisions in BAC-225Q mice, and found a similar spatio-temporal pattern of changes in radioligand binding - starting with D1 loss at 3 months in caudal striatum, followed by a decrease in both receptors at 6 months in all the subdivisions, and a loss of D2 ligand binding at 10 months in the rostral subdivision (**Figure 2-11B**). In YAC128 animals similar changes were seen, but limited only to D2 receptors, and delayed compared to BAC-225Q mice (**Figure 2-11B**).

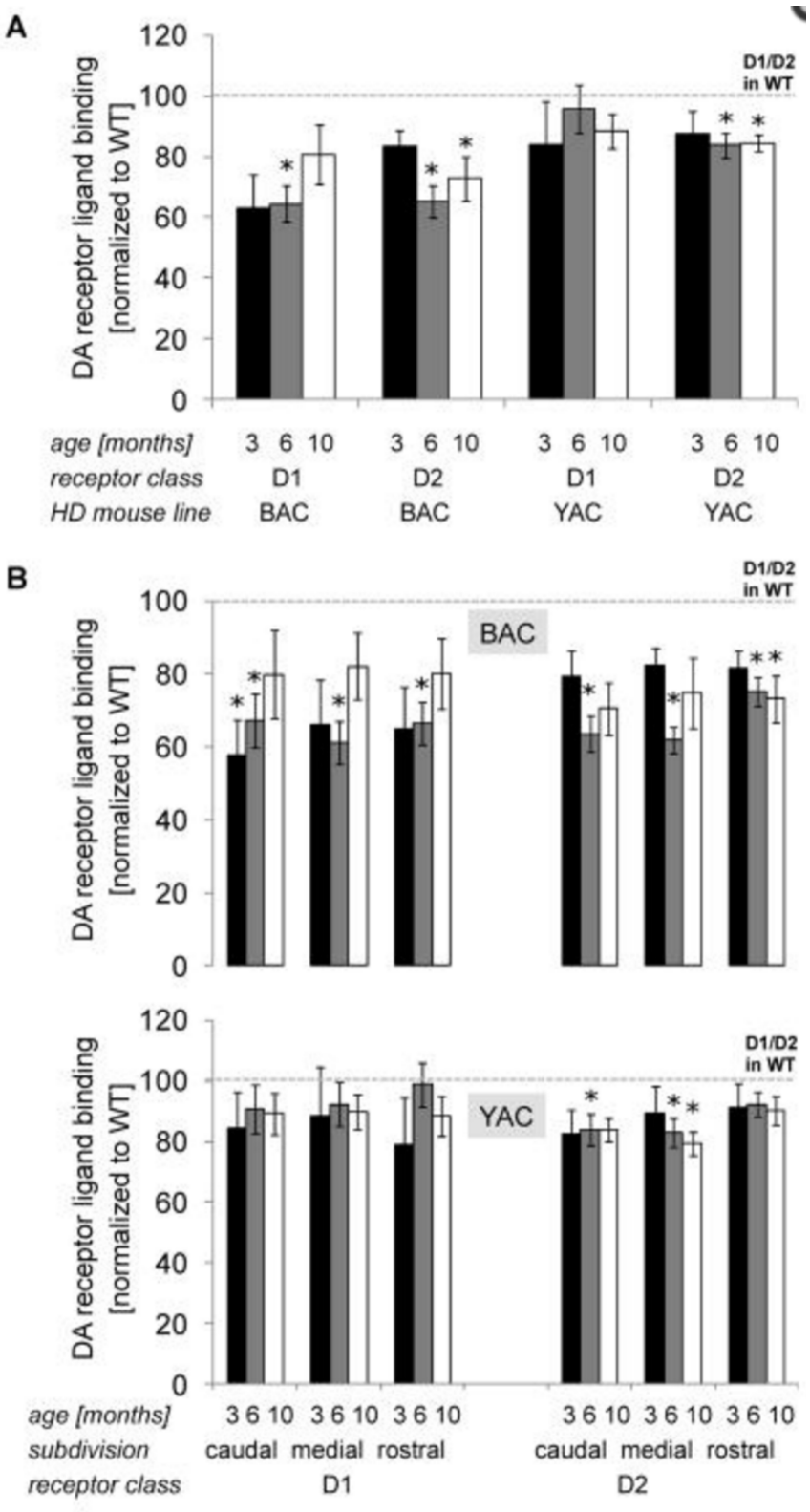

Figure 2-11. Loss of ligand binding to dopamine receptors in HD mice, (legend on following page).

Figure 2-11. Loss of ligand binding to dopamine receptors in HD mice. (A) Autoradiography experiments using [^{3}H]-SCH1337, D1 receptor ligand and [^{3}H]-spiperone, D2 receptor ligand, were performed in striata of BAC-225Q (n=4-12) and YAC128 animals (n=5–12). In BAC-225Q mice loss of ligand binding to D1 receptor is found at 6 months of age (*t-test, p=0.002), and to D2 receptor - at 6 and 10 months of age (*t-test, p<0.001; p=0.035, respectively). In YAC128 animals only loss of D2 ligand binding is observed (*t-test, p=0.011; p=0.03, at 6 and 10 months respectively). (B) Dopamine receptor ligand binding in striatum was assessed also in spatiotemporal manner. In BAC-225Q mice, the impairment of either receptor is age- and subregion-dependent, starting from D1 ligand binding decrease at 3 months in caudal striatum (*t-test, p=0.039), followed by loss of both receptor types at 6 months in all the three subdivisions (*t-test, p=0.021; p<0.001; p=0.003 for D1, and p<0.001; p<0.001; p=0.006 for D2 in respectively, caudal, medial and rostral striatum), and finally D2 loss at 10 months in rostral striatum (*t-test, p=0.014). In YAC128 animals the pattern of D2 receptor pathology appeared to be similar, but delayed compared to BAC-225Q mice. Loss of D2 ligand binding is observed at 6 months of age in caudal and medial striatum (*t-test, p=0.024, p=0.022, respectively), and at 10 months in medial striatum (*t-test, p=0.012). No changes in D2 receptor binding in rostral subdivision is found up to 10 months of age and no D1 pathology is observed in any part of striatum.

To summarize, we observed early, widespread and progressive loss of brain volumes and found activation of the neuroinflammation marker, TSPO, in BAC-225Q mice. Striatal volume was not affected to a greater degree than other brain regions, though early loss of D1 and D2 dopamine receptors was observed in this region.

Discussion

In this study, we generated and characterized a novel transgenic model of HD, BAC-225Q, that expresses full-length murine *Htt* with ~225 CAG repeats under control of the mouse *Htt* promoter/enhancer contained within the BAC transgene. Expression of CAG-repeat expanded full-length mouse *Htt* under the native mouse promoter ensures that expression of the transgene is controlled by the same cellular mechanisms as expression of WT *Htt* in the same animal (as it is in HD patients); contrary to other models in which the human *HTT* promoter (R6/1, R6/2,[29] YAC72,[30] YAC128,[27] BACHD[31] or the prion promoter (N171-82Q)[32] is used.

Additionally, by using mouse *Htt* rather than the human gene, this model avoids the potential confounder of unexpected protein-protein interactions between human HTT and native mouse proteins. Of note, other models that express CAG-expanded mouse *Htt*, like the KI HD models, exhibit late behavioral and neuropathological phenotype.[33-36] By expressing the mouse *Htt* gene with an expanded repeat of ~225 CAGs, we hypothesized that this new model would exhibit earlier phenotypes than previously published full-length mouse *Htt* models with shorter CAG repeat lengths. We demonstrate here early and widespread neuropathological phenotypes, with similarities to the neurodegenerative features of juvenile HD. The phenotypes in BAC-225Q animals are detected much earlier than in the Q200 heterozygous knock-in model.[36] Similar to BAC-225Q, the Q200 model expresses mouse transgenic *Htt* with comparable CAG repeat length under the mouse promoter, and would be expected to exhibit similar pathology. Q200 mice are characterized by weight loss (observed only in females) and some locomotor deficits at 11 months of age (but not rotarod performance which was unaffected up to 18 months). Similar to BAC-225Q animals, Q200 mice displayed loss of both D1 and D2 receptors, but without loss of striatal volume or MSN number up to 18 months of age. Also gliosis was observed later in the Q200 mice, with minimal astrogliosis at 9 months of age. Interestingly, inconsistent with CAG repeat length, but consistent with late phenotype onset, Q200 knock-in mice exhibit specific striatal and cortical, adult-onset pathology in contrast to the widespread pathology observed in the BAC-225Q animals.[36]

Despite many juvenile onset HD-like phenotypes, the early motor phenotypes of BAC-225Q mice have similarity to the adult-onset form of HD. The initial hyperactivity of BAC-225Q mice (**Figure 2-6C-F**) is consistent with the initial motor changes observed in adult-onset HD patients who typically display chorea, restlessness and involuntary movements as the first motor

symptoms of HD[37](Roos 2010). In HD patients, this is believed to be a consequence of impairment to the indirect pathway (D2-receptor expressing MSNs) at early stages of adult-onset HD that precedes impairment of the direct pathway (D1-receptor expressing MSNs).[22,38-41]

Juvenile HD is typically not associated with early hyperactivity – instead motor deficits in these patients manifest more often as bradykinesia and dystonia correlating with early degeneration of MSNs in both the direct and indirect pathways.[38,42,43] Juvenile HD is similar though to late stage adult-onset HD, at which time both populations of MSNs are degenerating and hypokinetic motor symptoms prevail.[22,38] Despite the initial hyperactivity, the BAC-225Q model showed concurrent and similarly decreased binding of both D1- and D2-receptor ligands in the striatum consistent with neuropathology of both direct and indirect pathways, while the YAC128 model demonstrated a more selective decrease in D2-receptor ligand binding (**Figure 2-11**). Loss of both D1- and D2-receptor classes is more consistent with juvenile HD-like striatal pathology in the BAC-225Q model, in contrast to early adult HD-like striatal pathology (D2-receptor selective loss) in the YAC128 model. Thus the basis for the hyperactive motor phenotypes in the BAC-225Q model in face of concurrent direct and indirect pathway involvement is unclear, but may represent differences in basal ganglia function in humans versus mice.

In addition to hyperactivity, BAC-225Q mice also displayed early locomotor deficiency, detected by the rotarod test, which, however, unexpectedly was found to be regressive with age (**Figure 2-6A**). Similarly, spontaneous motor behavior, after initial hyperactivity, was restored at 6 months (**Figure 2-6C-E**). This is in contrast with HD patients, who display worsening of motor symptoms over time.[1] One factor that may influence the motor phenotype of BAC-225Q mice is body weight loss (**Figure 2-5**). It was shown that decreased body weight correlates negatively

with latency to fall in rotarod experiments[15] and is associated with higher motor performance in open field testing.[15] Finally, high levels of neuropil HTT aggregates and loss of diffuse nuclear Htt aggregate staining between 6 months and 12 months (**Figure 2-2C**) correlates with the amelioration of the motor phenotype in BAC-225Q mice. It has been hypothesized that formation of large inclusions of polyglutamine expanded HTT is a mechanism of cellular defense against a more toxic oligomeric species rather than a direct cause of pathology[44,45]. BAC-225Q mice display extensive aggregation compared to many full-length Htt models, and the aggregates are notably larger in size. For example BACHD animals, in which the transgene is expressed under the human *HTT* promoter, have much lower aggregate density and are characterized by progressive behavioral and neuropathological phenotypes[31] despite a regional distribution pattern of aggregates similar to what we observed in BAC-225Q mice. In this context, we hypothesize that after reaching toxic levels of HTT accumulation, manifesting as locomotor impairment and neuropathological phenotypes, BAC-225Q animals initiate efficient sequestration of toxic intermediates into neuropil aggregates between 6 months and 12 months of age, protecting them against further progression of pathological phenotypes. This mechanism may be related to the very large *Htt* CAG repeat in BAC-225Q animals, as it was previously demonstrated in the R6/2 mouse model that there exists a limit to which the relationship between length of polyQ tract and severity of the phenotype is linearly proportional, with the possibility that exceptionally long CAG repeats result in less severe pathogenicity accompanied by increased formation of large aggregates.[46] However, given the observation that individual BAC-225Q animals with more extensive neuropil aggregation have relatively poor rotarod performance, a role for clearing total mutant HTT accumulation also appears to correlate with improved performance.

The body weight phenotype in BAC-225Q mice, manifested as a failure to gain weight from about 4 months of age onward, is consistent with human HD pathology, where progressive inexplicable loss of weight is a non-neurological hallmark of HD.[14,47,48] Of note, our data on the surface contradicts reports showing that expression of full-length human *HTT* increases body weight in a level-dependent but polyQ tract length-independent manner.[49,50] Despite over-expression of total *Htt* in our model (two WT alleles, and the mutant transgenic allele) we do not observe a weight gain phenotype. In fact, our model expressing mutant mouse Htt, in addition to both copies of the endogenous mouse *Htt* gene, results in failure to gain appropriate weight (**Figure 2-5**), consistent with human weight loss phenotype, suggests the weight gain phenotype of mouse models expressing human *HTT*[31,49,51] may be attributed specifically to the expression of the human isoform of *HTT* in the mouse. In support of this idea, a weight loss phenotype is also observed in the zQ175 knock-in model.[52] Furthermore, the weight gain phenotype of transgenic mouse models may also be mouse strain-dependent, as the YAC128 transgenic construct in the C57BL/6 strain does not alter body weight.[53]

Leptin is a major regulator of body weight, a hormone which induces a long-term inhibition of food intake, and whose levels are often altered in diseases manifested by body weight alterations.[54,55] There are conflicting reports on the levels of circulating leptin in HD patients, with both decreases[17,19] and increases (in a CAG length dependent manner being reported[56]. We found that leptin concentrations were elevated in the plasma of BAC-225Q mice (**Figure 2-7**), which may be partially responsible for the decrease in body weight in this model. However it should be noted that weight deficiency was observed starting from an earlier time point (**Figure 2-5**) than the increase in leptin levels (**Figure 2-7**). Leptin acts in the brain on the hypothalamus and it was recently suggested that this region may also exhibit early changes in

HD pathology.[57,58] In BAC-225Q mice, we identified up-regulation of TSPO in the hypothalamus (**Figure 2-10**) suggestive of neuropathology in this region, which may be related to impaired leptin homeostasis.

Despite widespread *HTT* expression throughout the brain[59] adult-onset HD is characterized by brain region selectivity with striatal degeneration being the most prominent.[22] However, as more sensitive techniques of brain imaging are employed, other regions of degeneration have been identified including cerebral cortex, globus pallidus, thalamus, hypothalamus, white matter and others, even at the presymptomatic stage.[58,60-62] Additionally, it was shown that longer CAG repeat number correlates with more widespread neurodegeneration and that in juvenile HD, the extent of the atrophy in other brain regions, including cerebral cortex, hippocampus, amygdala, brainstem and cerebellum, is comparable to that seen in striatum.[63] In BAC-225Q mice we found predominant aggregation of Htt in hippocampus and cerebellum (**Figure 2-4**), and using volumetric MRI, we identified early and widespread volume loss in several brain regions affected in the juvenile form of HD (**Figure 2-8**). We also detected astrogliosis and microgliosis by immunohistochemistry (**Figure 2-9**) as well as TSPO up-regulation with autoradiography in most of the analyzed brain regions (**Figure 2-10A**), often prior to detection of regional brain volume loss by MRI (**Figure 2-8**). This suggests that gliosis and neuroinflammation, may precede loss of brain volume in HD pathobiology. Importantly, the TSPO data are consistent with human studies in which patients show elevated TSPO levels not only at symptomatic,[64,65] but also at presymptomatic stages of HD.[66] Importantly, the extent of TSPO activation in HD patient striatum was similar to the values found in BAC-225Q mice (increases of 30–85% versus 25–60%, respectively). Therefore, TSPO up-regulation appears to be an early and sensitive marker of regional brain impairment in HD. This relationship is also

confirmed by our findings in the YAC128 model, where increased TSPO levels were found in striatum at 10 months (**Figure 2-10B**), which is proximate to the age when striatal loss is first observed in this model.[27] Additionally, our TSPO analysis in YAC128 mice confirmed that this model has a later, milder and less widespread neurodegenerative pathology compared to the BAC-225Q. Summarizing, TSPO up-regulation clearly elucidates a widespread, neurodegenerative-like phenotype in BAC-225Q mice.

To summarize, we have characterized a novel mouse model expressing mouse *Htt* with ~225 CAG repeats. This model reveals an early phenotype including body weight deficiency, motor behavioral abnormalities, widespread Htt aggregation especially in hippocampus and associated cortex, brain atrophy and gliosis, as well as striatal pathology in both direct, and indirect pathway MSNs. Additionally, neurological symptoms in these animals are accompanied by changes in specific blood biomarkers of HD. These features of the BAC-225Q model suggest it may have utility for studies on the juvenile form or possibly late-stages of adult-onset HD, as well as the metabolic disturbances, regional vulnerability to mutant HTT pathology, and early striatal dysfunction prior to neurodegeneration. Consistent with its large CAG-repeat length, this model shows an earlier age-of-onset relative to previously published full-length *Htt* mouse models. Despite this early onset and continued expression of the mutant *Htt* transgene, the BAC-225Q model shows a predominantly non-progressive phenotype, which may provide a stable early time point for the study of wide-spread HD-associated neuropathology relative to existing full-length *Htt* models with much later ages-of-onset.

References

1. Walker FO. Huntington's Disease. *Semin Neurol* 2007; **27**(2): 143-50.
2. Sassone J, Colciago C, Cislaghi G, Silani V, Ciammola A. Huntington's disease: the current state of research with peripheral tissues. *Exp Neurol* 2009; **219**(2): 385-97.
3. Squitieri F, Frati L, Ciarmiello A, Lastoria S, Quarrell O. Juvenile Huntington's disease: does a dosage-effect pathogenic mechanism differ from the classical adult disease? *Mech Ageing Dev* 2006; **127**(2): 208-12.
4. Andresen JM, Gayan J, Djousse L, et al. The relationship between CAG repeat length and age of onset differs for Huntington's disease patients with juvenile onset or adult onset. *Ann Hum Genet* 2007; **71**(Pt 3): 295-301.
5. Crook ZR, Housman D. Huntington's disease: can mice lead the way to treatment? *Neuron* 2011; **69**(3): 423-35.
6. Warming S, Costantino N, Court DL, Jenkins NA, Copeland NG. Simple and highly efficient BAC recombineering using galK selection. *Nucleic Acids Res* 2005; **33**(4): e36.
7. Yoo SY, Pennesi ME, Weeber EJ, et al. SCA7 knockin mice model human SCA7 and reveal gradual accumulation of mutant ataxin-7 in neurons and abnormalities in short-term plasticity. *Neuron* 2003; **37**(3): 383-401.
8. Wegrzynowicz M, Holt HK, Friedman DB, Bowman AB. Changes in the striatal proteome of YAC128Q mice exhibit gene-environment interactions between mutant huntingtin and manganese. *J Proteome Res* 2012; **11**(2): 1118-32.
9. Kreutz C, Bartolome Rodriguez MM, Maiwald T, et al. An error model for protein quantification. *Bioinformatics* 2007; **23**(20): 2747-53.
10. Golde WT, Gollobin P, Rodriguez LL. A rapid, simple, and humane method for submandibular bleeding of mice using a lancet. *Lab Anim (NY)* 2005; **34**(9): 39-43.
11. Aggarwal M, Zhang J, Miller MI, Sidman RL, Mori S. Magnetic resonance imaging and micro-computed tomography combined atlas of developing and adult mouse brains for stereotaxic surgery. *Neuroscience* 2009; **162**(4): 1339-50.
12. Miller MI, Trouve A, Younes L. On the metrics and euler-lagrange equations of computational anatomy. *Annu Rev Biomed Eng* 2002; **4**: 375-405.
13. Gu X, Greiner ER, Mishra R, et al. Serines 13 and 16 are critical determinants of full-length human mutant huntingtin induced disease pathogenesis in HD mice. *Neuron* 2009; **64**(6): 828-40.
14. van der Burg JM, Bjorkqvist M, Brundin P. Beyond the brain: widespread pathology in Huntington's disease. *Lancet Neurol* 2009; **8**(8): 765-74.
15. McFadyen MP, Kusek G, Bolivar VJ, Flaherty L. Differences among eight inbred strains of mice in motor ability and motor learning on a rotorod. *Genes Brain Behav* 2003; **2**(4): 214-9.
16. Gafni J, Papanikolaou T, Degiacomo F, et al. Caspase-6 activity in a BACHD mouse modulates steady-state levels of mutant huntingtin protein but is not necessary for production of a 586 amino acid proteolytic fragment. *J Neurosci* 2012; **32**(22): 7454-65.
17. Mochel F, Charles P, Seguin F, et al. Early energy deficit in Huntington disease: identification of a plasma biomarker traceable during disease progression. *PLoS One* 2007; **2**(7): e647.

18. Bjorkqvist M, Wild EJ, Thiele J, et al. A novel pathogenic pathway of immune activation detectable before clinical onset in Huntington's disease. *J Exp Med* 2008; **205**(8): 1869-77.
19. Popovic V, Svetel M, Djurovic M, et al. Circulating and cerebrospinal fluid ghrelin and leptin: potential role in altered body weight in Huntington's disease. *Eur J Endocrinol* 2004; **151**(4): 451-5.
20. Bozic CR, Gerard NP, von Uexkull-Guldenband C, et al. The murine interleukin 8 type B receptor homologue and its ligands. Expression and biological characterization. *J Biol Chem* 1994; **269**(47): 29355-8.
21. Henry BA, Clarke IJ. Adipose tissue hormones and the regulation of food intake. *J Neuroendocrinol* 2008; **20**(6): 842-9.
22. Vonsattel JP, Myers RH, Stevens TJ, Ferrante RJ, Bird ED, Richardson EP, Jr. Neuropathological classification of Huntington's disease. *J Neuropathol Exp Neurol* 1985; **44**(6): 559-77.
23. Hedreen JC, Peyser CE, Folstein SE, Ross CA. Neuronal loss in layers V and VI of cerebral cortex in Huntington's disease. *Neurosci Lett* 1991; **133**(2): 257-61.
24. Nopoulos PC, Aylward EH, Ross CA, et al. Cerebral cortex structure in prodromal Huntington disease. *Neurobiol Dis* 2010; **40**(3): 544-54.
25. Nopoulos PC, Aylward EH, Ross CA, et al. Smaller intracranial volume in prodromal Huntington's disease: evidence for abnormal neurodevelopment. *Brain* 2011; **134**(Pt 1): 137-42.
26. Chen MK, Guilarte TR. Translocator protein 18 kDa (TSPO): molecular sensor of brain injury and repair. *Pharmacol Ther* 2008; **118**(1): 1-17.
27. Slow EJ, van Raamsdonk J, Rogers D, et al. Selective striatal neuronal loss in a YAC128 mouse model of Huntington disease. *Hum Mol Genet* 2003; **12**(13): 1555-67.
28. Vonsattel JP, Keller C, Cortes Ramirez EP. Huntington's disease - neuropathology. *Handb Clin Neurol* 2011; **100**: 83-100.
29. Mangiarini L, Sathasivam K, Seller M, et al. Exon 1 of the HD gene with an expanded CAG repeat is sufficient to cause a progressive neurological phenotype in transgenic mice. *Cell* 1996; **87**(3): 493-506.
30. Hodgson JG, Agopyan N, Gutekunst CA, et al. A YAC mouse model for Huntington's disease with full-length mutant huntingtin, cytoplasmic toxicity, and selective striatal neurodegeneration. *Neuron* 1999; **23**(1): 181-92.
31. Gray M, Shirasaki DI, Cepeda C, et al. Full-length human mutant huntingtin with a stable polyglutamine repeat can elicit progressive and selective neuropathogenesis in BACHD mice. *J Neurosci* 2008; **28**(24): 6182-95.
32. Schilling G, Becher MW, Sharp AH, et al. Intranuclear inclusions and neuritic aggregates in transgenic mice expressing a mutant N-terminal fragment of huntingtin. *Hum Mol Genet* 1999; **8**(3): 397-407.
33. Wheeler VC, Auerbach W, White JK, et al. Length-dependent gametic CAG repeat instability in the Huntington's disease knock-in mouse. *Hum Mol Genet* 1999; **8**(1): 115-22.
34. Shelbourne PF, Killeen N, Hevner RF, et al. A Huntington's disease CAG expansion at the murine Hdh locus is unstable and associated with behavioural abnormalities in mice. *Hum Mol Genet* 1999; **8**(5): 763-74.

35. Yu ZX, Li SH, Evans J, Pillarisetti A, Li H, Li XJ. Mutant huntingtin causes context-dependent neurodegeneration in mice with Huntington's disease. *J Neurosci* 2003; **23**(6): 2193-202.
36. Heng MY, Duong DK, Albin RL, et al. Early autophagic response in a novel knock-in model of Huntington disease. *Hum Mol Genet* 2010; **19**(19): 3702-20.
37. Roos RA. Huntington's disease: a clinical review. *Orphanet J Rare Dis* 2010; **5**: 40.
38. Albin RL, Reiner A, Anderson KD, Penney JB, Young AB. Striatal and nigral neuron subpopulations in rigid Huntington's disease: implications for the functional anatomy of chorea and rigidity-akinesia. *Ann Neurol* 1990; **27**(4): 357-65.
39. Andrews TC, Weeks RA, Turjanski N, et al. Huntington's disease progression. PET and clinical observations. *Brain* 1999; **122 (Pt 12)**: 2353-63.
40. Lawrence AD, Weeks RA, Brooks DJ, et al. The relationship between striatal dopamine receptor binding and cognitive performance in Huntington's disease. *Brain* 1998; **121 (Pt 7)**: 1343-55.
41. Weeks RA, Piccini P, Harding AE, Brooks DJ. Striatal D1 and D2 dopamine receptor loss in asymptomatic mutation carriers of Huntington's disease. *Ann Neurol* 1996; **40**(1): 49-54.
42. Louis ED, Anderson KE, Moskowitz C, Thorne DZ, Marder K. Dystonia-predominant adult-onset Huntington disease: association between motor phenotype and age of onset in adults. *Arch Neurol* 2000; **57**(9): 1326-30.
43. Gonzalez-Alegre P, Afifi AK. Clinical characteristics of childhood-onset (juvenile) Huntington disease: report of 12 patients and review of the literature. *J Child Neurol* 2006; **21**(3): 223-9.
44. Kuemmerle S, Gutekunst CA, Klein AM, et al. Huntington aggregates may not predict neuronal death in Huntington's disease. *Ann Neurol* 1999; **46**(6): 842-9.
45. Romero E, Cha GH, Verstreken P, et al. Suppression of neurodegeneration and increased neurotransmission caused by expanded full-length huntingtin accumulating in the cytoplasm. *Neuron* 2008; **57**(1): 27-40.
46. Cummings DM, Alaghband Y, Hickey MA, et al. A critical window of CAG repeat-length correlates with phenotype severity in the R6/2 mouse model of Huntington's disease. *J Neurophysiol* 2012; **107**(2): 677-91.
47. Sanberg PR, Fibiger HC, Mark RF. Body weight and dietary factors in Huntington's disease patients compared with matched controls. *Med J Aust* 1981; **1**(8): 407-9.
48. Stoy N, McKay E. Weight loss in Huntington's disease. *Ann Neurol* 2000; **48**(1): 130-1.
49. Pouladi MA, Xie Y, Skotte NH, et al. Full-length huntingtin levels modulate body weight by influencing insulin-like growth factor 1 expression. *Hum Mol Genet* 2010; **19**(8): 1528-38.
50. Van Raamsdonk JM, Gibson WT, Pearson J, et al. Body weight is modulated by levels of full-length huntingtin. *Hum Mol Genet* 2006; **15**(9): 1513-23.
51. Pouladi MA, Stanek LM, Xie Y, et al. Marked differences in neurochemistry and aggregates despite similar behavioural and neuropathological features of Huntington disease in the full-length BACHD and YAC128 mice. *Hum Mol Genet* 2012; **21**(10): 2219-32.
52. Menalled LB, Kudwa AE, Miller S, et al. Comprehensive behavioral and molecular characterization of a new knock-in mouse model of Huntington's disease: zQ175. *PLoS One* 2012; **7**(12): e49838.

53. Van Raamsdonk JM, Metzler M, Slow E, et al. Phenotypic abnormalities in the YAC128 mouse model of Huntington disease are penetrant on multiple genetic backgrounds and modulated by strain. *Neurobiol Dis* 2007; **26**(1): 189-200.
54. Li MD. Leptin and beyond: an odyssey to the central control of body weight. *Yale J Biol Med* 2011; **84**(1): 1-7.
55. Klok MD, Jakobsdottir S, Drent ML. The role of leptin and ghrelin in the regulation of food intake and body weight in humans: a review. *Obes Rev* 2007; **8**(1): 21-34.
56. Aziz NA, Pijl H, Frolich M, van der Graaf AW, Roelfsema F, Roos RA. Leptin secretion rate increases with higher CAG repeat number in Huntington's disease patients. *Clin Endocrinol (Oxf)* 2010; **73**(2): 206-11.
57. Gabery S, Murphy K, Schultz K, et al. Changes in key hypothalamic neuropeptide populations in Huntington disease revealed by neuropathological analyses. *Acta Neuropathol* 2010; **120**(6): 777-88.
58. Politis M, Pavese N, Tai YF, Tabrizi SJ, Barker RA, Piccini P. Hypothalamic involvement in Huntington's disease: an in vivo PET study. *Brain* 2008; **131**(Pt 11): 2860-9.
59. Sipione S, Cattaneo E. Modeling Huntington's disease in cells, flies, and mice. *Mol Neurobiol* 2001; **23**(1): 21-51.
60. Di Paola M, Luders E, Cherubini A, et al. Multimodal MRI analysis of the corpus callosum reveals white matter differences in presymptomatic and early Huntington's disease. *Cereb Cortex* 2012; **22**(12): 2858-66.
61. Douaud G, Gaura V, Ribeiro MJ, et al. Distribution of grey matter atrophy in Huntington's disease patients: a combined ROI-based and voxel-based morphometric study. *Neuroimage* 2006; **32**(4): 1562-75.
62. Paulsen JS, Nopoulos PC, Aylward E, et al. Striatal and white matter predictors of estimated diagnosis for Huntington disease. *Brain Res Bull* 2010; **82**(3-4): 201-7.
63. Rosas HD, Koroshetz WJ, Chen YI, et al. Evidence for more widespread cerebral pathology in early HD: an MRI-based morphometric analysis. *Neurology* 2003; **60**(10): 1615-20.
64. Messmer K, Reynolds GP. Increased peripheral benzodiazepine binding sites in the brain of patients with Huntington's disease. *Neurosci Lett* 1998; **241**(1): 53-6.
65. Pavese N, Gerhard A, Tai YF, et al. Microglial activation correlates with severity in Huntington disease: a clinical and PET study. *Neurology* 2006; **66**(11): 1638-43.
66. Tai YF, Pavese N, Gerhard A, et al. Microglial activation in presymptomatic Huntington's disease gene carriers. *Brain* 2007; **130**(Pt 7): 1759-66.

Chapter III

Manganese in HD

Note: Much of this chapter has been derived from the following publications:

Bichell TJ. Gene-Environment Interactions in Huntington's Disease. *Vanderbilt Reviews Neuroscience* 2012; **4**(2012): 9.

Tidball AM, Bichell TJ, Bowman AB. Manganese and Huntington's Disease. In: Costa L, Aschner M, eds. Manganese in Health and Disease: Royal Society of Chemistry; 2014.

Bichell TJ, Uhouse M, Bradley E, Bowman AB. Gene-Environment Interactions in Huntington's Disease. In: Aschner M, Costa LG, eds. Environmental Factors in Neurodevelopmental and Neurodegenerative Disorders. London: Elsevier, Inc.; 2015: 451.

Bichell TJ, Halbesma T, Tipps KG, Bowman AB. Metal Biology Associated with Huntington's Disease. In: White A, Aschner M, Costa L, Bush A, eds. Biometals in Neurodegenerative Diseases: Mechanisms and Therapeutics. In Press: Elsevier; 2016.

Background on metals in HD and pilot data

Mn exposure has long been associated with motor pathway damage, suggesting that the metal is involved in the functioning of neuronal systems that control movement. In general, it is an excess of Mn that is considered to be pathogenic. For example, chronic exposure to Mn through vocations such as welding or smelting increases the risk of Manganism, a neurodegenerative Parkinsonian condition affecting the nigrostriatal dopaminergic pathways.[1,2] Even populations exposed to subtoxic levels of airborne Mn from nearby industries exhibit subtle, though not significant, effects on motor pathways, as measured by postural sway score.[3] In HD, it is likely the inverse. Interestingly though excess Cu and Fe are associated with the toxicity of mutant HTT, it is most likely a deficit of Mn that is associated with HD, especially in the crucial brain regions that are most susceptible to neurodegeneration in the disorder.

Confusingly, there is overlap between the symptoms of Mn toxicity and the toxicity of mutant HTT. For example, mutant HTT decreases BDNF transcription[4] and reduces BDNF transport.[5] Mn exposure decreases phosphorylation of serine 421 on HTT, which controls BDNF transport[6]. In wild-type mice, Mn exposure decreases BDNF production,[6] and Mn exposure also causes reduction in the spine density and dendritic length of MSNs.[7] These BDNF and dendritic spine alterations caused by the toxicity of Mn exposure are the same phenotypes which are seen in HD, suggesting that an inverted U-curve of dose response, may explain the relationship between Mn exposure and neuronal function[8,9] (**Figure 3-1**).

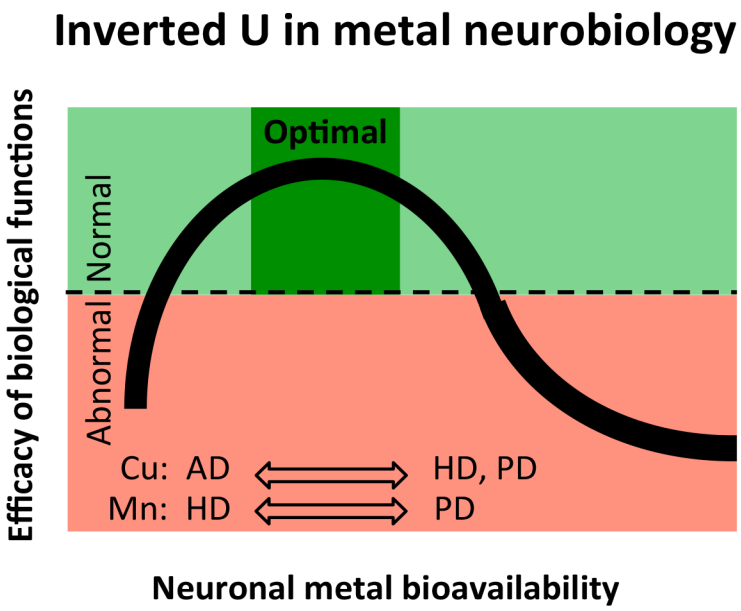

Figure 3-1. The biological response to metal concentration in neuronal tissues follows an inverted U. Low concentrations as well as high concentrations cause damage or dysfunction, and the efficacy of biological functions is only optimal at a narrow range.

There is evidence that the deficiency portion of the homeostasis curve is invoked in HD. In the presence of mutant HTT, Mn bioavailability decreases: cultured striatal cell models of HD reveal a deficiency of Mn and studies of mouse models find a reduction of striatal Mn

bioavailabilty.[10,11] Still, though these HD models reveal Mn dyshomeostasis, there is limited evidence of a brain regional Mn deficit in human HD patients. Post-mortem analysis by Dexter et al., did not reveal significant alterations of Mn levels in the basal ganglia compared to normal controls,[12,13] but the sample size included only six females and 4 males, and the study was done before genetic confirmation of HD was possible. More recently, Rosas et al., reported decreased Mn in cortical regions of post mortem HD brain,[13] but not striatum. This suggests a sub-regional, cell-type, or even sub-cellular Mn dyshomeostasis.

In any case, there is substantial disagreement in the literature about the regional location of Mn in normal brain, chiefly because most methods for measuring Mn in tissues have resolution which is too low.[14] For this reason, most studies measure regional Mn deposition following excess exposure, with almost no studies of Mn localizations in conditions of a deficiency of the metal, and the distribution may be very different depending upon tissue concentration.

Bowman lab members found no difference between genotypes in baseline accumulation of Mn between striatum and cortex, though excess exposure revealed a Mn accumulation deficit in the HD striatum, but not in cortex (**Figure 3-2**). Mn exposure did not affect the deposition of other metals in striatum, except that Fe accumulation increased along with Mn exposure in wild-type, but that increase was not seen in the HD mutants (**Figure 3-3**). To obtain dry weight measurements, tubes were weighed, then frozen tissue added, and exposed to 95^{o}C for 48 hours, or until constant mass was obtained. Manganese levels were measured by ICPMS.

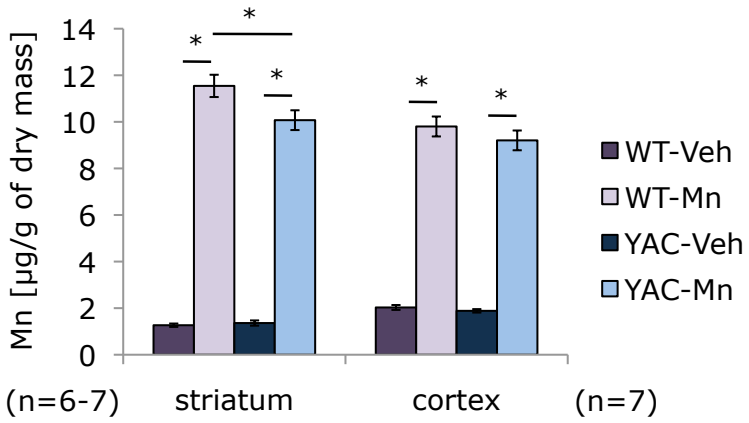

	F	sig.	F	sig.
genotype	F(1,27)=4.13	**0.054**	F(1,28)=1.45	**0.24**
treatment	F(1,27)=783.43	**< 0.001**	F(1,28)=599.57	**< 0.001**
genotype x treatment	F(1,27)=5.32	**0.03**	F(1,28 =0.54	**0.47**

Figure 3-2. The decrease in net striatal Mn accumulation in the YAC128Q mouse model of HD at age 12 weeks was not seen in cortex. Experiment by M. Wegrzynowicz

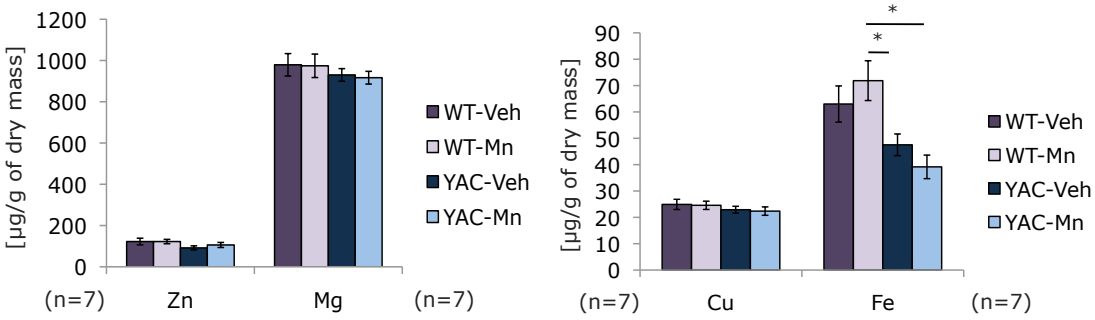

Fe		
	F	**sig.**
genotype	F(1,28) = 16.42	**0.001**
treatment	F(1,28) = 0.002	**0.967**
genotype x treatment	F(1,28) = 2.097	**0.162**

Figure 3-3. The alterations in Mn bioavailability were not reflected in similar reductions in other metals at baseline, but Mn exposure increased net striatal Fe accumulation in the WT mouse exposed to Mn at age 12 weeks but not the YAC128Q. There was no striatal increase in other metals. Experiment by M. Wegrzynowicz

Manganese deposition: brain regions, cell-types and cellular organelles

Regional deposition

Mn is paramagnetic, and therefore provides enhanced signal intensity in T1-weighted MRI,[15] allowing for imaging of Mn deposits *in vivo*, but the resolution of these images is not fine enough to distinguish deposits of manganese in deficiency conditions.[14] The results gathered through MRI[16] are different from those seen via other techniques such as x-ray fluorescence,[14] atomic absorption spectroscopy[17], or inductively coupled plasma mass spectroscopy[18]. This discrepancy may be due to the speciation of manganese (Mn^{2+} vs. Mn^{3+}) or to Mn-binding interactions,[15] MRI measurements following Mn exposure generally document elevated Mn accumulating in the hippocampus, while other methods record Mn deposits to be chiefly in the globus pallidus and substantia nigra.[16]

In normal human brain without excess Mn exposure, most studies agree that there is more Mn found in the basal ganglia than in other brain regions, particularly in the caudate and putamen,[19] which is the region of most profound degeneration in HD. In the hippocampus, Mn is most concentrated (often with Zn) in the CA2/3 region, while Fe was localized in CA1 and Dentate Gyrus, with a negative correlation between the depositions of Cu and Mn.[15]

In normal rats there are slight differences, ie, the highest levels of Mn are thought to be in the globus pallidus and the striatum, followed by the hypothalamus.[17,20] After chronic Mn treatment, the globus pallidus collects the most Mn, with cortex and striatum collecting slightly less.[21] An ICP-MS study of HD patients found a slight decrease in Mn deposition in two subregions of the cortex, but not in the basal ganglia, whereas another study found no differences in Mn deposition between HD and controls[12,13] (**Figure 1-7**). Robison et al., exposed rats to one month of Mn, either by injection or in the diet, and found a specific accumulation of Mn in the

dopaminergic neurons of the substantia nigra pars compacta (SNc),[20] which are the neurons that degenerate in Parkinson's disease.

Aside from the difficulty in measuring Mn deposits at the sub-regional level, it has been even more difficult to tease out whether Mn bioavailability is altered in particular subregions or cell types in HD. The cell-type or subcellular localization under condition of Mn deficiency has not been studied.

Cell-type deposition

In general, it had been thought that astrocytes accounted for most of the Mn in brain, primarily because astrocytes are rich in glutamine synthetase (GS), a glia-specific enzyme that can bind as many as 4 Mn^{2+} ions per subunit, with 15 subunits in each enzyme.[22] However, GS can also bind Mg^{2+}, and other ions, as well as Mn^{2+} as a co-factor.[23] With over-exposure to Mn, as when Mn is injected intra-cerebrally in rats, the metal collects in astrocyte-rich regions, but immunohistochemical images show that the most intense staining for astrocytes co-localizes with the lowest concentrations of Mn.[15]

Morello et al., found that, under normal conditions, Mn accumulates equally in rat neurons and astrocytes.[21] In chick embryos, Wedler found that neurons store more Mn than astrocytes[24] and Tholey et al., found that there is more Mn and Cu in neurons than astrocytes, but more Fe and Zn in astrocytes than neurons.[25] Robison found that sites of high Mn accumulation do not correspond to the sites where Cu accumulates, postulating that this anti-correlation suggests that astrocytes are not the storehouse for Mn under normal conditions,[15] though they may accumulate more Mn under toxic exposures. However, technical limitations have prevented robust quantitative measurements of cellular Mn levels (e.g. astrocytes versus neuron) *in vivo*, and the above studies rely on *ex vivo* or cultured brain cells.

Because manganese is biologically important, both as an enzymatic cofactor and in reduction of reactive oxygen species, knowing where Mn is located in cells, cell types and brain regions is crucial to elucidating its role in HD pathology. There is no known direct reporter protein for Mn, like there is for Fe (the iron storage protein ferritin), but diverse methodologies have been used to measure the metal in tissues and cell cultures, including graphite furnace, inductively-coupled mass spectroscopy (ICPMS),[21,26] energy dispersive X-ray fluorescence,[25] x-ray fluorescence,[20] synchrotron radiation X-ray and fluorescence (SRXRF).[27] As tissues and cells are prepared for assay, subcellular conditions change and may cause movement of metals between compartments, or changes in Mn levels within organelles, which might also alter measurement.

Sub-cellular deposition

There is also disagreement in the literature about where Mn collects within cells. Many studies indicate that Mn preferentially accumulates in mitochondria, but other data show that Mn is found primarily in the Golgi apparatus, the ER, or the nucleus. These differences can partially be explained by the relative amounts of Mn in experimental conditions, because different biological transport and storage mechanisms may be activated when excessive Mn exposure occurs. Acute vs. chronic exposure to Mn may also stimulate alternative homeostatic processes.

Several researchers agree that exposure to excess Mn results in preferential accumulation in mitochondria in both liver and brain,[18] with greatest mitochondrial accumulation in the basal ganglia.[28,29] This excess of Mn leads to mitochondrial cytochrome c release,[30,31] which activates caspase-dependent apoptotic pathways[32] leading to increased cell death.

In cases of normal Mn levels, most studies agree that Mn is not stored in mitochondria. It appears that Mn is lowest in the mitochondria, intermediate in the cytoplasm and highest in the Golgi[26,33,34] in yeast studies under normal conditions. In rats, without excess Mn exposure, Mn is

highest in the nucleolus, and lowest in the mitochondria.[20,21] In chick embryos Mn is concentrated in the cytosol and microsomes[25], rather than the mitochondria. In hippocampal CA3, Mn was distributed diffusely and localized separately from Fe, which was found in small foci.[15]

In fact, the Golgi may be the site of Mn storage under normal conditions. In cultured dopaminergic cells and in cultured pheochromocytoma cells, Mn accumulated preferentially in the Golgi apparatus.[35,36] In cultured PC12 cells, Mn was observed in the Golgi apparatus at 100uM exposures, which was confirmed when the Golgi was ruptured with brefeldin A, redistributing Mn into the cytosol.[20]

As with excess exposure to Mn, chronic exposure to Mn also causes a shift in Mn storage, with the mitochondria of astrocytes accumulating the most Mn, followed by neuronal mitochondria, with the lowest accumulation in the nuclei of both cell types.[21,37] Because the level and duration of Mn exposure clearly affects the intracellular localization of Mn deposits, this suggests that there is tight biological regulation of Mn transport and storage pools.

Manganese transporters

At least 15 metal transporters are known to move Mn across cell membranes,[38] usually along with other metals. Mn often travels through the same channels as Fe, including the divalent metal transporter 1 (DMT1) and the transferrin receptor. Indeed, Mn exposure causes alterations in protein expression of ferroportin-a (FPN), a cytoplasmic Fe^{2+} exporter, as well as inducing FPN to localize to the cell membrane.[39] Further evidence that Mn is moved with Fe comes from "flatiron mice: which are ferroportin deficient. Flatiron mice have both increased Mn and Fe in the olfactory bulb, and both reduced Mn and Fe in bone.[40] There is a further association between Mn and Fe in HD, through the cell stress response. Nath et al, established that HTT plays a role in the cell stress pathway, by observing the accumulation of HTT in the early endosomes of live

cells under conditions of stress,[41] arresting recycling endosome function. During this process, HTT localized in cytosolic puncta, called Hungtingtin stress bodies (HSB's). HSBs colocalize with transferrin as well as Rab5C, a protein of the early endosome. This sequestration of transferrin in the early endosome blocks it from moving to the recycling endosome with its cargo of Fe. Though there seem to be many connections between Fe transport and Mn dyshomeostasis, Williams et al found no increase in net Mn uptake even when cultured HD model cells were exposed to saturating levels of Fe.[11] The relationship between Fe transporters and Mn in HD remains enigmatic.

Mn^{2+} is also transported by the divalent metal/bicarbonate ion symporters ZIP8 and ZIP14, several Ca channels, the solute carrier-39 (SLC39) family of Zn transporters, by the Mg transporter hip14 and the transient receptor potential melastatin 7 (TRPM7) channel.[38] It is thought that Mn^{2+} is transported into the mitochondria via the Ca^{2+} uniporter.[42,43] Efflux of Mn from the mitochondria is processed through both slow and fast mechanisms (reviewed by Bowman et al[29]) in addition to the ferroportin-1 iron transporter. Surprisingly, there were no significant alterations in gene expression for transferrin in the blood of HD patients, nor for SLC11A2 (DMT1), though there was a trend towards reduced expression in patients compared to controls,[44] and if there are mRNA expression differences in brain subregions, these might not be detectable in blood samples. In addition, the same study found no changes in expression of the transferrin receptor (TfR), nor SLC39A8 (ZIP8).

Definitive links to other neurodegenerative disorders, but not to HD, have been found between mutations in many of these metal transporters,[38,45] for example in the case of PARK9 (also known as ATP13A2) and SLC30A1, which are both associated with forms of Parkinson's disease. Mutations in PARK9 cause a severe parkinsonian condition, Kufor-Rakeb syndrome,[46]

and mutations in SLC30A10 cause Parkinson's disease,[47] but neither are associated with HD. Two other known metal transporters, Huntington Interacting Protein-14 (HIP14) and Huntington Interacting Protein-14-Like (HIP14L) may prove to connect Mn transport issues to HD pathology because these proteins are known to palmitoylate HTT which is necessary for its proper function,[48] and mutant HTT has reduced palmytoylation.[49,50]

Many valuable studies of Mn transporters have been performed in yeast models. PARK9 is a mammalian homologue to the yeast protein, Ypk1, which was first identified in *Sacchromyces cerevisiae* as a Mn transporter on the vacuole.[51] There is evidence that another yeast protein, Spf1 (mammalian homologue is ATP13A1), located on the ER of *Sacchromyces cerevisiae*, influences Mn homeostasis,[26] but it is only now being characterized.

Mtm1p is another interesting carrier protein with a mammalian homolog SLC25A39, which was first identified in yeast. Mtm1p was originally thought to be the Mn chaperone for mitochondrial Sod2 based on impaired activation of MnSOD in a genetic yeast knockout.[52,53] Mtm1p has now been shown to be involved in mitochondrial Fe homeostasis as well, in complex with pyridoxal 5′-phosphate (PLP) or Vitamin B6 as the carrier substrate.[54,55] Vitamin B6 is an electrophilic catalyst, which stabilizes reactions by binding to substrates covalently. Interestingly, the harmonizome database indeed shows SLC25A39 to be reduced in HD.[56]

The *Drosophila* ortholog for SLC25A39 (shawn) is a susceptibility loci for epilepsy, and mutants display vesicle trafficking defects, as well as changes in metal homeostasis.[57] Cytosolic Mn was increased in shawn mutants while mitochondrial Ca was increased, free Fe^{2+} accumulated, and aconitase activity was decreased. Aconitase is an interesting enzyme with two distinct functions: in mitochondria it converts citrate into isocitrate with Fe/S as a cofactor, but in the cytosol, it acts as an iron regulatory protein.[58] As cytosolic Fe levels drop, aconitase unbinds

from its Fe/S cofactor and binds instead to the messenger RNA for ferritin and the transferrin receptor, inhibiting the formation of ferritin so that iron can be released from storage.[59,60] Furthermore, aconitase is a transglutaminase 2 substrate, and increased transglutaminase activity in HD may incorporate aconitase into inactive polymers, causing further mitochondrial dysfunction.[61]

Though aconitase is an Fe-dependent enzyme that may impact Mn homeostasis, there are many other enzymes that are Mn-dependent, and may be impacted by metal dysregulation. Striatal Mn deficiency in HD may restrict the activity of these essential enzymatic functions.

Mn-dependent and Mn-utilizing enzymes

Enzymes known to use Mn as a co-factor include glutamine synthetase (GS), superoxide dismutase 2 (SOD2), arginase 1 and 2 (ARG1, ARG2), ataxia telangiectasia mutated (ATM), meiotic recombination 11 (MRE-11) and Fanconi's associated nuclease 1 (FAN1).[62]A reduction of bioavailable Mn would alter the normal neuronal and glial functions of proteins that cannot function without sufficient Mn. Indeed, all manganoproteins that have been examined to date show reductions in the presence of mutant HTT, either directly or indirectly. Most eukaryotic enzymes bind to both Cu and Zn, while those from mitochondria and prokaryotes rely on Mn and Fe as co-factors, suggesting that Mn and Fe dyshomeostasis may be much more influential than that of other metals in HD, though some enzymes can substitute for other transition metals as cofactors in deficiency conditions. If derangement of Mn homeostasis is one of the root causes of HD, the fact that the symptoms take so long to develop may be because so many of the Mn-utilizing enzymes can function with other metals, albeit less efficiently, or less effectively.

The following enzymes are known to incorporate Mn as a cofactor, although some of these enzymes also bind to other metals as well.

GS - glutamine synthetase

GS converts glutamate to glutamine in astrocytes, and glial dysfunction is a recognized part of the pathogenesis of HD.[63,64] A reduction in GS activity may contribute to the increased neurotoxicity in medium spiny neurons[65]. Indeed, there is reduced GS in both HD animal models and patients[66,67] and decreased activity of GS, has been reported in post-mortem HD patient brain[66]. GS is reduced in HD patients even when the glial marker, GFAP, is not reduced.[66] Insufficient manganese may increase glutamate trafficking, glutamatergic signaling, and excitotoxicity,[65] leading to the increased seizure susceptibility observed in Mn-deficient individuals.[68]

A study in cultured rat astrocytes found that acute exposure to Mn reduced GS activity and increased GS protein,[69] while another 3-week exposure showed no change between exposed rats and controls,[70] and a 13-week chronic exposure reduced GS immunostaining and enzyme activity in striatum and globus pallidus, but not in motor cortex.[37] The investigators of this last study controlled for GFAP and did not see a commensurate decrease in astrocyte number, suggesting that the reduction in GS was due to enzymatic insufficiency rather than astrocytic cell death. Other studies in rats exposed to airborne Mn^{2+} for 90 days or more did not show significant changes in protein or mRNA expression of GS, even though Mn^{2+} accumulation increased.[71] This suggests that in a condition of Mn deficit GS activity may revert to another cofactor, if necessary.

Interestingly, many other metals, such as Mg, Fe and cobalt (Co) are able to bind with GS,[23] but at different pH levels, with Fe binding at a lower pH than the other metals. The optimal pH for GS enzymatic activity varies between 4.8 and 8.5, depending on the concentration and combination of metals present, and Ca inhibits GS activity at all pH values,[23] However, GS can

also bind Mg, cadmium, and Fe as well as Mn as a co-factor, and though Mg^{2+} binds less tightly than Mn^{2+} to the enzyme, it speeds its activity, depending upon the pH.[23]

Unpublished work in our lab by Michal Wegrzynowycz and Hunter Holt did not find a difference in GS activity after the same Mn treatment protocol peformed in the ARG experiments described below.

SOD2 - Mn-dependent superoxide dismutase

SOD2 (also known as MnSOD) acts to detoxify superoxides into hydrogen peroxide and O_2.[72] MnSOD is a mitochondrial protein that requires four Mn ions per tetramer. In HD brain tissue, a reduction in SOD2 is known to cause oxidative stress and worsen the severity of HD symptoms[73] and the expression level of MnSOD drastically changes its redox capacity.[74] Loss of Mn-SOD activity increases sensitivity to mitochondrial complex 2 inhibitors (such as 3-nitroproprionic acid), which is associated with HD-like striatal degeneration.[75,76] HD models are hypersensitive to 3-nitroproprionic acid (3-NPA) and other complex II inhibitors,[245] an effect which is especially pronounced in older HD model mice.[77] These SOD2-related alterations further implicate a reduction in the bioavailability of Mn as an enzymatic co-factor, as a cause for the HD-related susceptibility to neuronal death.

Interestingly, Luk et al found that Mn^{2+} can only bind to MnSOD when the peptide is newly synthesized and unfolded, and it is only the newly synthesized form of MnSOD that can enter mitochondria.[53] This suggests that Mn^{2+} associates with MnSOD as part of its import into mitochondria in an unfolded state. MnSOD is twice as active at a pH of 10 that at a pH of 7.8,[78] suggesting that gradations in acid-base balance could have an effect on efficiency of the enzyme.

PC - pyruvate carboxylase

(PC) catalyzes the conversion of pyruvate to oxaloacetate and is implicated as an intermediary in many pathways, including gluconeogenesis and the TCA cycle, earning the classification of an anaplerotic enzyme.[79-81] Pyruvate carboxylase relies on either Mn or Mg, as well as thiamine pyrophosphate as cofactors, and dysregulated activity of the enzyme has wide-ranging implications. Deficiencies of pyruvate carboxylase activity can cause acidosis through a build up of lactate in the blood,[82] a serious medical condition. Minor reductions in pyruvate carboxylase can reduce the availability of TCA cycle precursors, which has been hypothesized to contribute to the reduced ATP levels seen in Huntington's disease models.[83-86] In patients, two downstream metabolites have been identified as potential biomarkers for Huntington's disease; N-acetyl aspartate (a metabolite of oxaloacetate), and lactate. The concentration of both N-acetyl aspartate and lactate together have been identified as potential biomarkers for HD, as the concentration of both increases in correlation with the duration since symptom onset.[87,88] Pyruvate carboxylase deficiency has also been linked to dysfunction of the urea cycle,[89] as has arginase. A region specific deficiency of manganese could reduce the availability of pyruvate carboxylase in the fragile medium spiny neurons of the striatum, leading to derangements in these basic energetic cycles, which may explain some of the degeneration of neurons in this region.

PPMs - metalloprotein phosphatases

PPMs include a subset of serine/threonine protein phosphatases that require both Mn^{2+} and Mg^{2+} ions to perform the vital function of dephosphorylation at the serine and threonine sites, which is a crucial regulatory step for myriad neuronal proteins.[90] One such manganese-dependent enzyme, protein phosphatase 1 (PP1) dephosphorylates serine in AKT and P53, two signaling pathways implicated in Huntington's disease.[91,92] In addition, some of PPM/PP2C family

members have been identified as mediators in a G-protein coupled receptor dopamine signaling pathway, through the striatal dopamine D2 receptor (D2R),[93] D2R activation decreases dephosporylation of Huntingtin on its AKT site through the PPM/PP2C family, independent of B-arrestin, and this can then downregulate AKT activation and reduce AKT's phosphorylation of Huntingtin at Serine-421, known to be necessary fro proper anterograde vesicular transport,[93] This connection between the manganese-dependent PPM and the AKT pathway through Huntingtin could have far ranging downstream effects, and AKT is already known to have reduced phosphorylation in HD models.[94] Exposure to 3-nitroproprionic acid which causes neurodegeneration similar to Huntington's disease, also results in reduced striatal PPM gene expression.[95] Evidence that metalloprotein phosphatases are reduced in Huntington's disease is lacking, but pathways that would be affected by such a reduction in dephosphatase activity have shown derangements that could stem from such a deficiency

ATM – ataxia telangiectasia mutated

A mutation in ATM causes ataxia telangiectasia (A-T), a disorder that leads to impaired immune system and motor skills, as well as cancer from DNA damage. Notably, Cu levels are significantly higher and Zn levels significantly lower in patients with A-T. The normal role of ATM is in repairing DNA damage and reacting to persistent oxidative stress.[96,97] ATM functions by phosphorylating either H2AX (which activates the DNA repair machinery) or p53 (which activates the cell death pathway), depending on the extent of DNA damage detected. In HD neuroprogenitor cell culture, a deficit of Mn-dependent activation of ATM kinase can be corrected by increasing Mn bioavailability pharmacologically.[98] This correction in ATM activation leads to normalization of the p53 signaling pathway, which has broad implications for

HD pathology. Interestingly, acidic pH not only induces DNA damage, but also appears to induce ATM kinase activity as measured by H2AX phosphorylation.[99]

Improper ATM signaling could invoke the p53 response over the DNA repair response, over-inducing the cell death pathway and leading to neurodegeneration. In fact recent work shows that reducing ATM expression (in cells, flies and mice) prevents symptoms of HD, suggesting that the Mn deficit in HD striatum might actually have a paradoxical protective effect.[100]

MRE-11 – meiotic recombination 11, and FAN1 – Fanconi's associated nuclease 1

Like ATM, MRE-11 and FAN1 are part of the DNA repair pathway, and both are Mn dependent enzymes linked with DNA damage in HD. MRE-11 associates with ATM and complexes with Ras-Proximate 1 (RAP1) to maintain telomere length,[101] while FAN1 functions to remove the interstrand DNA crosslinks that impede double-stranded repair.[62,102] Pathological double-stranded DNA repair is found in HD and in other polyglutamine expansion diseases.[103] Recently, a genome wide association study of 1462 patients with HD and other polyglutamine spinocerebellar ataxias (SCAs) revealed that a single-nucleotide polymorphisms (SNP) from FAN1 was a genetic modifier for the age of onset.[104] Both Mn and Mg can serve as co-factors for FAN1,[62] but MRE-11 is not active when Mg is substituted for Mn.[105]

MRE11 is a manganese binding nuclear enzyme that is an integral part of the protein complex of Rad50- Mre11A- Nbs1 known as the MRN complex.[106] This MRN complex is another part of the DNA damage repair mechanism, correcting double stranded breaks through the homologous recombination pathway.[107] The Mre11A protein functions as a nuclease by cleaving DNA with both exonuclease and endonuclease activity, required for both DNA repair and genomic stability.[108,109] As part of the MRN complex, Mre11A also assists in DNA damage

response signaling by activating ATM kinase.[109,110] Research has shown that Mre11A can also be activated by magnesium, but nuclease activity appears to be highly variable and limited in regards to temperature, direction of nuclease activity, and substrate length.[106-108,111] In response to irradiation, Mre11 expression is higher in HD fibroblasts, and takes a longer time to return to baseline.[112] It appears that manganese is crucial to Mre11a's activity, and decreased manganese availability in Huntington's disease may result in the reduced ability to repair DNA double-strand breaks, and thus lead to increased genomic instability.

POLI - DNA polymerase iota

POLI is yet another manganese dependent enzyme that is involved with translesion synthesis.[113] When a DNA lesion is present, translesion synthesis is necessary for a cell to continue DNA replication. POLI marks the site by inserting a nucleotide directly across from the DNA lesion.[113] Although historically it was thought that DNA polymerases utilized the divalent cation of magnesium, it is now apparent that certain polymerases, such as DNA polymerase iota, may preferentially utilize manganese, as shown by greater activation in Mn^{2+}-containing rather than Mg^{2+}-containing solutions.[114] Additionally, when Mn was substituted for Mg, the efficiency of nucleotide incorporation in DNA translesion synthesis was enhanced.[115] This increased kinetic activity may be the result of a stronger stabilizing effect by Mn^{2+}, allowing an enhanced rate of conformational change.[115] In theory, HD models may have altered translesion synthesis resulting from a deficiency of available manganese. If reduced manganese leads to inefficiency in DNA repair, these lesions can lead to senescence or apoptosis in affected cells.

AGMAT- agmatinase

Agmatine has recently been identified as a neurotransmitter, which binds to the imidazoline receptor and may be especially important in the cortex in the context of

schizophrenia,[116] though it is most abundant in hypothalamus and hippocampus.[117] Agmatine is a result of the decarboxylation of L-arginine, and is hydrolyzed by agmatinases into urea and putrecine, which is further metabolized into the other polyamines.[117]

Though agmatine and polyamines are found in brain, they may be synthesized by other routes, as the mitochondrial enzyme agmatinase was shown to have very scant brain activity.[118] Morris et al predicted that mouse agmatinase would be inactive because it lacks the catalytically active domains on the enzyme,[119] though these domains are conserved in the human protein. Bernstein et al., found agmatinase to be present in rodent interneurons, highly expressed in purkinje cells[120] and in the post-mortem hippocampi of patients with affective disorders.[121] In addition, an agmatinase-like protein (ALP) was discovered by Uribe et al., in rodent brain,[122]k and was later identified as a truncated isoform of Lim and Calponin Homology Domain 1 (LIMCH1).[117] Both AGMAT and LIMCH1 require Mn as a cofactor.[123] [122,124]

Because agmatinase is a regulator of polyamines, and polyamines have been connected to aggregate load,[125] agmatinases may prove to be important Mn-dependent enzymes in HD though the polyamines may also be synthesized through ornithine decarboxylase activity to cleave arginine.[126] The maximal activity of agmatinase is at a pH of 8.5,[118]

ARG1 and ARG2 – arginases

ARG1 and ARG2: Arginase 1 (ARG1) and Arginase 2 (ARG2) are manganese-dependent urea cycle enzyme isoforms that both convert L-arginine to L-ornithine and urea, but each has unique tissue and subcellular distribution and localization. ARG1 is highly concentrated in the cytosol of the liver and serves as an integral part of the urea cycle, whereas ARG2 is broadly expressed across the body and is located in the mitochondria. Both isoforms require two Mn^{2+} ions to form the activated binuclear manganese complex, and perform at maximal velocity

between pH 9.0-9.5.[127] ARG2 is implicated in the neuronal metabolism of arginine, where it competes with nitric oxide synthase for substrate, thereby regulating nitric oxide production.[128] Metabolic pathways downstream of arginase are known to be disrupted in Huntington's disease models. For example, arginine is metabolized by either nitric oxide synthase or arginase, so a lack of arginase could push the balance towards the nitric oxide synthase pathway and alterations in nitric oxide signaling and nitric oxide synthase have been identified in Huntington's disease models.[129-131] The urea cycle is deficient in Huntington's disease and has been linked to increased blood citrulline levels.[132] Patients with Huntington's disease have an abnormal growth hormone response to arginine infusion,[133] and a Huntington's disease mouse model fed with diets high in arginine has an earlier disease onset,[134] suggesting that arginine is not being metabolized properly. The only study which directly measured arginase in Huntington's disease models focused on circadian gene transcription, but not in striatum. Interestingly, ARG1 is transcribed in a circadian manner by the liver, but in R6/2 model mice, the gene transcription becomes arrhythmic.[135] Arginase 1 also has a neuroprotective role; it has been found to prevent neuronal death in trophic factor-deprived cell cultures.[136] All of these indirect links between arginase levels and Huntington's disease point to arginase as a potential regional indicator for manganese. All of the evidence linking abnormalities in Mn-dependent enzymes to HD mentioned above strongly supports the data showing that there is reduced Mn bioavailability contributing to pathologies seen in the disease.

Although it is not yet clear which of these known manganoproteins are most affected by manganese deficiency, a striatal specific reduction in manganese such as is indicated by current evidence in Huntington's disease models clearly could have widespread repercussions for cellular processes. A proteomics study of gene-environmental interactions between manganese and

mutant *HTT* in the YAC128 model mouse showed that manganese exposure caused disruptions in proteins involved in glycolysis, excitotoxicity and cytoskeletal dynamics, but the enzymes listed above were not amongst the affected proteins.[137] The proteins which were most likely to represent markers of the mutant *HTT*/manganese interaction were UBQLN1 (a ubiquilin), ENO1 (enolase) and SAE1 (a sumoylation factor). Beyond the proteins that are directly affected by changes in the availability of manganese in Huntington's disease, it is important to understand how manganese is transported and handled between and inside neurons, to understand the gene-environment interaction between manganese and mutant *HTT*.

For a further discussion of the arginases, agmatinases and the urea cycle in HD, please see **Chapter 5**.

References

1. Saxena S, Caroni P. Selective neuronal vulnerability in neurodegenerative diseases: from stressor thresholds to degeneration. *Neuron* 2011; **71**(1): 35-48.
2. Racette BA, Aschner M, Guilarte TR, Dydak U, Criswell SR, Zheng W. Pathophysiology of manganese-associated neurotoxicity. *Neurotoxicology* 2012; **33**(4): 881-6.
3. Kim Y, Bowler RM, Abdelouahab N, Harris M, Gocheva V, Roels HA. Motor function in adults of an Ohio community with environmental manganese exposure. *Neurotoxicology* 2011; **32**(5): 606-14.
4. Zuccato C, Tartari M, Crotti A, et al. Huntingtin interacts with REST/NRSF to modulate the transcription of NRSE-controlled neuronal genes. *Nat Genet* 2003; **35**(1): 76-83.
5. Colin E, Zala D, Liot G, et al. Huntingtin phosphorylation acts as a molecular switch for anterograde/retrograde transport in neurons. *EMBO J* 2008; **27**(15): 2124-34.
6. Stansfield KH, Bichell TJ, Bowman AB, Guilarte TR. BDNF and Huntingtin protein modifications by manganese: implications for striatal medium spiny neuron pathology in manganese neurotoxicity. *J Neurochem* 2014; **131**(5): 655-66.
7. Madison JL, Wegrzynowicz M, Aschner M, Bowman AB. Disease-toxicant interactions in manganese exposed Huntington disease mice: early changes in striatal neuron morphology and dopamine metabolism. *PLoS One* 2012; **7**(2): e31024.
8. Calabrese EJ. Hormesis is central to toxicology, pharmacology and risk assessment. *Hum Exp Toxicol* 2010; **29**(4): 249-61.
9. Calabrese EJ, Baldwin LA. Hormesis: U-shaped dose responses and their centrality in toxicology. *Trends Pharmacol Sci* 2001; **22**(6): 285-91.
10. Williams BB, Li D, Wegrzynowicz M, et al. Disease-toxicant screen reveals a neuroprotective interaction between Huntington's disease and manganese exposure. *J Neurochem* 2010; **112**(1): 227-37.
11. Williams BB, Kwakye GF, Wegrzynowicz M, et al. Altered manganese homeostasis and manganese toxicity in a Huntington's disease striatal cell model are not explained by defects in the iron transport system. *Toxicol Sci* 2010; **117**(1): 169-79.
12. Dexter DT, Carayon A, Javoy-Agid F, et al. Alterations in the levels of iron, ferritin and other trace metals in Parkinson's disease and other neurodegenerative diseases affecting the basal ganglia. *Brain* 1991; **114 (Pt 4)**: 1953-75.
13. Rosas HD, Chen YI, Doros G, et al. Alterations in brain transition metals in Huntington disease: an evolving and intricate story. *Arch Neurol* 2012; **69**(7): 887-93.
14. Robison G, Zakharova T, Fu S, et al. X-ray fluorescence imaging: a new tool for studying manganese neurotoxicity. *PLoS One* 2012; **7**(11): e48899.
15. Robison G, Zakharova T, Fu S, et al. X-ray fluorescence imaging of the hippocampal formation after manganese exposure. *Metallomics* 2013; **5**(11): 1554-65.
16. Mok SI, Munasinghe JP, Young WS. Infusion-based manganese-enhanced MRI: a new imaging technique to visualize the mouse brain. *Brain Struct Funct* 2012; **217**(1): 107-14.
17. Bonilla E. Flameless atomic absorption spectrophotometric determination of manganese in rat brain and other tissues. *Clin Chem* 1978; **24**(3): 471-4.
18. Tarohda T, Yamamoto M, Amamo R. Regional distribution of manganese, iron, copper, and zinc in the rat brain during development. *Anal Bioanal Chem* 2004; **380**(2): 240-6.

19. Larsen NA, Pakkenberg H, Damsgaard E, Heydorn K. Topographical distribution of arsenic, manganese, and selenium in the normal human brain. *J Neurol Sci* 1979; **42**(3): 407-16.
20. Robison G, Sullivan B, Cannon JR, Pushkar Y. Identification of dopaminergic neurons of the substantia nigra pars compacta as a target of manganese accumulation. *Metallomics* 2015; **7**(5): 748-55.
21. Morello M, Canini A, Mattioli P, et al. Sub-cellular localization of manganese in the basal ganglia of normal and manganese-treated rats An electron spectroscopy imaging and electron energy-loss spectroscopy study. *Neurotoxicology* 2008; **29**(1): 60-72.
22. Krajewski WW, Collins R, Holmberg-Schiavone L, Jones TA, Karlberg T, Mowbray SL. Crystal structures of mammalian glutamine synthetases illustrate substrate-induced conformational changes and provide opportunities for drug and herbicide design. *J Mol Biol* 2008; **375**(1): 217-28.
23. Monder C. Metal ion interactions and glutamine synthetase activity. *Biochemistry* 1965; **4**(12): 2677-86.
24. Wedler FC. The Role of Glia in Neurotoxicity. Boca Raton, FL: CRC Press; 1996.
25. Tholey G, Sena AH, Ledig M. Specific insulin-mediated regulation of glutamine synthetase in cultured chick astroglial cells. *J Neurochem* 1986; **47**(5): 1490-2.
26. Cohen Y, Megyeri M, Chen OC, et al. The yeast p5 type ATPase, spf1, regulates manganese transport into the endoplasmic reticulum. *PLoS One* 2013; **8**(12): e85519.
27. Colvin RA, Lai B, Holmes WR, Lee D. Understanding metal homeostasis in primary cultured neurons. Studies using single neuron subcellular and quantitative metallomics. *Metallomics* 2015; **7**(7): 1111-23.
28. Prohaska JR. Functions of trace elements in brain metabolism. *Physiol Rev* 1987; **67**(3): 858-901.
29. Bowman AB, Kwakye GF, Herrero Hernandez E, Aschner M. Role of manganese in neurodegenerative diseases. *J Trace Elem Med Biol* 2011; **25**(4): 191-203.
30. Prabhakaran K, Chapman GD, Gunasekar PG. BNIP3 up-regulation and mitochondrial dysfunction in manganese-induced neurotoxicity. *Neurotoxicology* 2009; **30**(3): 414-22.
31. Choo YS, Johnson GV, MacDonald M, Detloff PJ, Lesort M. Mutant huntingtin directly increases susceptibility of mitochondria to the calcium-induced permeability transition and cytochrome c release. *Hum Mol Genet* 2004; **13**(14): 1407-20.
32. Tamm C, Sabri F, Ceccatelli S. Mitochondrial-mediated apoptosis in neural stem cells exposed to manganese. *Toxicol Sci* 2008; **101**(2): 310-20.
33. Garcia-Rodriguez N, Manzano-Lopez J, Munoz-Bravo M, Fernandez-Garcia E, Muniz M, Wellinger RE. Manganese redistribution by calcium-stimulated vesicle trafficking bypasses the need for P-type ATPase function. *J Biol Chem* 2015; **290**(15): 9335-47.
34. Pierrel F, Cobine PA, Winge DR. Metal Ion availability in mitochondria. *Biometals* 2007; **20**(3-4): 675-82.
35. Carmona A, Roudeau S, Perrin L, Veronesi G, Ortega R. Environmental manganese compounds accumulate as Mn(II) within the Golgi apparatus of dopamine cells: relationship between speciation, subcellular distribution, and cytotoxicity. *Metallomics* 2014; **6**(4): 822-32.
36. Carmona A, Deves G, Roudeau S, Cloetens P, Bohic S, Ortega R. Manganese accumulates within golgi apparatus in dopaminergic cells as revealed by synchrotron X-ray fluorescence nanoimaging. *ACS Chem Neurosci* 2010; **1**(3): 194-203.

37. Morello M, Zatta P, Zambenedetti P, et al. Manganese intoxication decreases the expression of manganoproteins in the rat basal ganglia: an immunohistochemical study. *Brain Res Bull* 2007; **74**(6): 406-15.
38. Horning KJ, Caito SW, Tipps KG, Bowman AB, Aschner M. Manganese Is Essential for Neuronal Health. *Annu Rev Nutr* 2015; **35**: 71-108.
39. Eller M, Williams DR. alpha-Synuclein in Parkinson disease and other neurodegenerative disorders. *Clin Chem Lab Med* 2011; **49**(3): 403-8.
40. Seo YA, Elkhader JA, Wessling-Resnick M. Distribution of manganese and other biometals in flatiron mice. *Biometals* 2016; **29**(1): 147-55.
41. Nath S, Munsie LN, Truant R. A huntingtin-mediated fast stress response halting endosomal trafficking is defective in Huntington's disease. *Hum Mol Genet* 2015; **24**(2): 450-62.
42. Gunter TE, Puskin JS. Manganous ion as a spin label in studies of mitochondrial uptake of manganese. *Biophys J* 1972; **12**(6): 625-35.
43. Liccione JJ, Maines MD. Selective vulnerability of glutathione metabolism and cellular defense mechanisms in rat striatum to manganese. *J Pharmacol Exp Ther* 1988; **247**(1): 156-61.
44. Szeliga M, Rozycka A, Jedrak P, et al. Expression of RNAs Coding for Metal Transporters in Blood of Patients with Huntington's Disease. *Neurochem Res* 2016; **41**(1-2): 101-6.
45. Ugolino J, Fang S, Kubisch C, Monteiro MJ. Mutant Atp13a2 proteins involved in parkinsonism are degraded by ER-associated degradation and sensitize cells to ER-stress induced cell death. *Hum Mol Genet* 2011; **20**(18): 3565-77.
46. Tan J, Zhang T, Jiang L, et al. Regulation of intracellular manganese homeostasis by Kufor-Rakeb syndrome-associated ATP13A2 protein. *J Biol Chem* 2011; **286**(34): 29654-62.
47. Chen P, Bowman AB, Mukhopadhyay S, Aschner M. SLC30A10: A novel manganese transporter. *Worm* 2015; **4**(3): e1042648.
48. Goytain A, Hines RM, Quamme GA. Huntingtin-interacting proteins, HIP14 and HIP14L, mediate dual functions, palmitoyl acyltransferase and Mg2+ transport. *J Biol Chem* 2008; **283**(48): 33365-74.
49. Singaraja RR, Huang K, Sanders SS, et al. Altered palmitoylation and neuropathological deficits in mice lacking HIP14. *Hum Mol Genet* 2011; **20**(20): 3899-909.
50. Ohyama T, Verstreken P, Ly CV, et al. Huntingtin-interacting protein 14, a palmitoyl transferase required for exocytosis and targeting of CSP to synaptic vesicles. *J Cell Biol* 2007; **179**(7): 1481-96.
51. Wiederhold E, Gandhi T, Permentier HP, Breitling R, Poolman B, Slotboom DJ. The yeast vacuolar membrane proteome. *Mol Cell Proteomics* 2009; **8**(2): 380-92.
52. Luk E, Carroll M, Baker M, Culotta VC. Manganese activation of superoxide dismutase 2 in Saccharomyces cerevisiae requires MTM1, a member of the mitochondrial carrier family. *Proc Natl Acad Sci U S A* 2003; **100**(18): 10353-7.
53. Luk E, Yang M, Jensen LT, Bourbonnais Y, Culotta VC. Manganese activation of superoxide dismutase 2 in the mitochondria of Saccharomyces cerevisiae. *J Biol Chem* 2005; **280**(24): 22715-20.
54. Yang M, Cobine PA, Molik S, et al. The effects of mitochondrial iron homeostasis on cofactor specificity of superoxide dismutase 2. *EMBO J* 2006; **25**(8): 1775-83.

55. Park J, McCormick SP, Chakrabarti M, Lindahl PA. Insights into the iron-ome and manganese-ome of Deltamtm1 Saccharomyces cerevisiae mitochondria. *Metallomics* 2013; **5**(6): 656-72.
56. Rouillard AD, Gundersen GW, Fernandez NF, et al. The harmonizome: a collection of processed datasets gathered to serve and mine knowledge about genes and proteins. *Database (Oxford)* 2016; **2016**.
57. Slabbaert JR, Kuenen S, Swerts J, et al. Shawn, the Drosophila Homolog of SLC25A39/40, Is a Mitochondrial Carrier That Promotes Neuronal Survival. *J Neurosci* 2016; **36**(6): 1914-29.
58. Artymiuk PJ, Green J. The double life of aconitase. *Structure* 2006; **14**(1): 2-4.
59. Jeffery CJ. Molecular mechanisms for multitasking: recent crystal structures of moonlighting proteins. *Curr Opin Struct Biol* 2004; **14**(6): 663-8.
60. Copley SD. Enzymes with extra talents: moonlighting functions and catalytic promiscuity. *Curr Opin Chem Biol* 2003; **7**(2): 265-72.
61. Kim SY, Marekov L, Bubber P, et al. Mitochondrial aconitase is a transglutaminase 2 substrate: transglutamination is a probable mechanism contributing to high-molecular-weight aggregates of aconitase and loss of aconitase activity in Huntington disease brain. *Neurochem Res* 2005; **30**(10): 1245-55.
62. Kratz K, Schopf B, Kaden S, et al. Deficiency of FANCD2-associated nuclease KIAA1018/FAN1 sensitizes cells to interstrand crosslinking agents. *Cell* 2010; **142**(1): 77-88.
63. Lobsiger CS, Cleveland DW. Glial cells as intrinsic components of non-cell-autonomous neurodegenerative disease. *Nat Neurosci* 2007; **10**(11): 1355-60.
64. Behrens PF, Franz P, Woodman B, Lindenberg KS, Landwehrmeyer GB. Impaired glutamate transport and glutamate-glutamine cycling: downstream effects of the Huntington mutation. *Brain* 2002; **125**(Pt 8): 1908-22.
65. Maciejewski PK, Rothman DL. Proposed cycles for functional glutamate trafficking in synaptic neurotransmission. *Neurochem Int* 2008; **52**(4-5): 809-25.
66. Butterworth J. Changes in nine enzyme markers for neurons, glia, and endothelial cells in agonal state and Huntington's disease caudate nucleus. *J Neurochem* 1986; **47**(2): 583-7.
67. Carter CJ. Loss of glutamine synthetase activity in the brain in Huntington's disease. *Lancet* 1981; **1**(8223): 782-3.
68. Eid T, Williamson A, Lee TS, Petroff OA, de Lanerolle NC. Glutamate and astrocytes--key players in human mesial temporal lobe epilepsy? *Epilepsia* 2008; **49 Suppl 2**: 42-52.
69. Chen CJ, Liao SL. Oxidative stress involves in astrocytic alterations induced by manganese. *Exp Neurol* 2002; **175**(1): 216-25.
70. Weber S, Dorman DC, Lash LH, Erikson K, Vrana KE, Aschner M. Effects of manganese (Mn) on the developing rat brain: oxidative-stress related endpoints. *Neurotoxicology* 2002; **23**(2): 169-75.
71. Taylor MD, Erikson KM, Dobson AW, Fitsanakis VA, Dorman DC, Aschner M. Effects of inhaled manganese on biomarkers of oxidative stress in the rat brain. *Neurotoxicology* 2006; **27**(5): 788-97.
72. Zelko IN, Mariani TJ, Folz RJ. Superoxide dismutase multigene family: a comparison of the CuZn-SOD (SOD1), Mn-SOD (SOD2), and EC-SOD (SOD3) gene structures, evolution, and expression. *Free Radic Biol Med* 2002; **33**(3): 337-49.

73. Kim J, Moody JP, Edgerly CK, et al. Mitochondrial loss, dysfunction and altered dynamics in Huntington's disease. *Hum Mol Genet* 2010; **19**(20): 3919-35.
74. Ansenberger-Fricano K, Ganini D, Mao M, et al. The peroxidase activity of mitochondrial superoxide dismutase. *Free Radic Biol Med* 2013; **54**: 116-24.
75. Andreassen OA, Ferrante RJ, Dedeoglu A, et al. Mice with a partial deficiency of manganese superoxide dismutase show increased vulnerability to the mitochondrial toxins malonate, 3-nitropropionic acid, and MPTP. *Exp Neurol* 2001; **167**(1): 189-95.
76. Bogdanov MB, Ferrante RJ, Kuemmerle S, Klivenyi P, Beal MF. Increased vulnerability to 3-nitropropionic acid in an animal model of Huntington's disease. *J Neurochem* 1998; **71**(6): 2642-4.
77. Hickey MA, Morton AJ. Mice transgenic for the Huntington's disease mutation are resistant to chronic 3-nitropropionic acid-induced striatal toxicity. *J Neurochem* 2000; **75**(5): 2163-71.
78. Crapo JD, McCord JM, Fridovich I. Preparation and assay of superoxide dismutases. *Methods Enzymol* 1978; **53**: 382-93.
79. Scrutton MC, Utter MF, Mildvan AS. Pyruvate carboxylase VI. The presence of tightly bound manganese. *Journal of Biological Chemistry* 1966; **241**(15): 3480-7.
80. Scrutton MC, Utter MF. Pyruvate carboxylase III. Some physical and chemical properties of the highly purified enzyme. *Journal of Biological Chemistry* 1965; **240**(1): 1-9.
81. Mildvan AS, Scrutton MC, Utter MF. Pyruvate carboxylase VII. A possible role for tightly bound manganese. *Journal of Biological Chemistry* 1966; **241**(15): 3488-98.
82. Mochel F, DeLonlay P, Touati G, et al. Pyruvate carboxylase deficiency: clinical and biochemical response to anaplerotic diet therapy. *Molecular genetics and metabolism* 2005; **84**(4): 305-12.
83. Gines S, Seong IS, Fossale E, et al. Specific progressive cAMP reduction implicates energy deficit in presymptomatic Huntington's disease knock-in mice. *Human molecular genetics* 2003; **12**(5): 497-508.
84. Weydt P, Pineda VV, Torrence AE, et al. Thermoregulatory and metabolic defects in Huntington's disease transgenic mice implicate PGC-1α in Huntington's disease neurodegeneration. *Cell metabolism* 2006; **4**(5): 349-62.
85. Mochel F, Durant B, Meng X, et al. Early alterations of brain cellular energy homeostasis in Huntington disease models. *Journal of Biological Chemistry* 2012; **287**(2): 1361-70.
86. Seong IS, Ivanova E, Lee J-M, et al. HD CAG repeat implicates a dominant property of huntingtin in mitochondrial energy metabolism. *Human molecular genetics* 2005; **14**(19): 2871-80.
87. Harms L, Meierkord H, Timm G, Pfeiffer L, Ludolph A. Decreased N-acetyl-aspartate/choline ratio and increased lactate in the frontal lobe of patients with Huntington's disease: a proton magnetic resonance spectroscopy study. *Journal of Neurology, Neurosurgery & Psychiatry* 1997; **62**(1): 27-30.
88. Jenkins BG, Koroshetz WJ, Beal MF, Rosen BR. Evidence for irnnairment of energy metabofism in vivo in Huntington's disease using localized 1H NMR spectroscopy. *Neurology* 1993; **43**(12): 2689-.
89. Ortez C, Jou C, Cortès-Saladelafont E, et al. Infantile parkinsonism and gabaergic hypotransmission in a patient with pyruvate carboxylase deficiency. *Gene* 2013; **532**(2): 302-6.

90. Woźniak-Celmer E, Ołdziej S, Ciarkowski J. Theoretical models of catalytic domains of protein phosphatases 1 and 2A with Zn2+ and Mn2+ metal dications and putative bioligands in their catalytic centers. *Acta biochimica Polonica* 2000; **48**(1): 35-52.
91. Xiao L, Gong L, Yuan D, et al. Protein phosphatase-1 regulates Akt1 signal transduction pathway to control gene expression, cell survival and differentiation. *Cell Death & Differentiation* 2010; **17**(9): 1448-62.
92. Li DW, Liu J, Schmid P, et al. Protein serine/threonine phosphatase-1 dephosphorylates p53 at Ser-15 and Ser-37 to modulate its transcriptional and apoptotic activities. *Oncogene* 2006; **25**(21): 3006-22.
93. Marion S, Urs NM, Peterson SM, et al. Dopamine D2 Receptor Relies upon PPM/PP2C Protein Phosphatases to Dephosphorylate Huntingtin Protein. *Journal of Biological Chemistry* 2014; **289**(17): 11715-24.
94. Williams BB, Kwakye GF, Wegrzynowicz M, et al. Altered manganese homeostasis and manganese toxicity in a Huntington's disease striatal cell model are not due to defects in the iron transport system. *Toxicological Sciences* 2010: kfq174.
95. Napolitano M, Centonze D, Gubellini P, et al. Inhibition of mitochondrial complex II alters striatal expression of genes involved in glutamatergic and dopaminergic signaling: possible implications for Huntington's disease. *Neurobiology of disease* 2004; **15**(2): 407-14.
96. Guo Z, Deshpande R, Paull TT. ATM activation in the presence of oxidative stress. *Cell Cycle* 2010; **9**(24): 4805-11.
97. Squadrone S, Brizio P, Mancini C, et al. Blood metal levels and related antioxidant enzyme activities in patients with ataxia telangiectasia. *Neurobiol Dis* 2015; **81**: 162-7.
98. Tidball AM, Bryan MR, Uhouse MA, et al. A novel manganese-dependent ATM-p53 signaling pathway is selectively impaired in patient-based neuroprogenitor and murine striatal models of Huntington's disease. *Hum Mol Genet* 2015; **24**(7): 1929-44.
99. Xiao H, Li TK, Yang JM, Liu LF. Acidic pH induces topoisomerase II-mediated DNA damage. *Proc Natl Acad Sci U S A* 2003; **100**(9): 5205-10.
100. Lu XH, Mattis VB, Wang N, et al. Targeting ATM ameliorates mutant Huntingtin toxicity in cell and animal models of Huntington's disease. *Sci Transl Med* 2014; **6**(268): 268ra178.
101. O'Connor MS, Safari A, Liu D, Qin J, Songyang Z. The human Rap1 protein complex and modulation of telomere length. *J Biol Chem* 2004; **279**(27): 28585-91.
102. Yoshikiyo K, Kratz K, Hirota K, et al. KIAA1018/FAN1 nuclease protects cells against genomic instability induced by interstrand cross-linking agents. *Proc Natl Acad Sci U S A* 2010; **107**(50): 21553-7.
103. Shiwaku H, Okazawa H. Impaired DNA damage repair as a common feature of neurodegenerative diseases and psychiatric disorders. *Curr Mol Med* 2015; **15**(2): 119-28.
104. Bettencourt C, Hensman-Moss D, Flower M, et al. DNA repair pathways underlie a common genetic mechanism modulating onset in polyglutamine diseases. *Ann Neurol* 2016; **79**(6): 983-90.
105. Hopfner KP, Karcher A, Shin D, Fairley C, Tainer JA, Carney JP. Mre11 and Rad50 from Pyrococcus furiosus: cloning and biochemical characterization reveal an evolutionarily conserved multiprotein machine. *J Bacteriol* 2000; **182**(21): 6036-41.
106. Trujillo KM, Yuan S-SF, Eva Y-HL, Sung P. Nuclease activities in a complex of human recombination and DNA repair factors Rad50, Mre11, and p95. *Journal of Biological Chemistry* 1998; **273**(34): 21447-50.

107. Hopkins BB, Paull TT. The< i> P. furiosus</i> Mre11/Rad50 Complex Promotes 5′ Strand Resection at a DNA Double-Strand Break. *Cell* 2008; **135**(2): 250-60.
108. Paull TT, Gellert M. The 3′ to 5′ exonuclease activity of Mre11 facilitates repair of DNA double-strand breaks. *Molecular cell* 1998; **1**(7): 969-79.
109. Buis J, Wu Y, Deng Y, et al. Mre11 nuclease activity has essential roles in DNA repair and genomic stability distinct from ATM activation. *Cell* 2008; **135**(1): 85-96.
110. Lee J-H, Paull TT. ATM activation by DNA double-strand breaks through the Mre11-Rad50-Nbs1 complex. *Science* 2005; **308**(5721): 551-4.
111. Hopfner K-P, Karcher A, Shin DS, et al. Structural biology of Rad50 ATPase: ATP-driven conformational control in DNA double-strand break repair and the ABC-ATPase superfamily. *Cell* 2000; **101**(7): 789-800.
112. Ferlazzo ML, Sonzogni L, Granzotto A, et al. Mutations of the Huntington's Disease Protein Impact on the ATM-Dependent Signaling and Repair Pathways of the Radiation-Induced DNA Double-Strand Breaks: Corrective Effect of Statins and Bisphosphonates. *Molecular neurobiology* 2014; **49**(3): 1200-11.
113. Waters LS, Minesinger BK, Wiltrout ME, D'Souza S, Woodruff RV, Walker GC. Eukaryotic translesion polymerases and their roles and regulation in DNA damage tolerance. *Microbiology and Molecular Biology Reviews* 2009; **73**(1): 134-54.
114. Frank EG, Woodgate R. Increased catalytic activity and altered fidelity of human DNA polymerase ι in the presence of manganese. *Journal of Biological Chemistry* 2007; **282**(34): 24689-96.
115. Hays H, Berdis AJ. Manganese substantially alters the dynamics of translesion DNA synthesis. *Biochemistry* 2002; **41**(15): 4771-8.
116. Liu P, Jing Y, Collie ND, Dean B, Bilkey DK, Zhang H. Altered brain arginine metabolism in schizophrenia. *Transl Psychiatry* 2016; **6**: e871.
117. Garcia D, Ordenes P, Benitez J, et al. Cloning of two LIMCH1 isoforms: characterization of their distribution in rat brain and their agmatinase activity. *Histochem Cell Biol* 2016; **145**(3): 305-13.
118. Sastre M, Regunathan S, Galea E, Reis DJ. Agmatinase activity in rat brain: a metabolic pathway for the degradation of agmatine. *J Neurochem* 1996; **67**(4): 1761-5.
119. Morris SM, Jr. Vertebrate agmatinases: what role do they play in agmatine catabolism? *Ann N Y Acad Sci* 2003; **1009**: 30-3.
120. Bernstein HG, Stich C, Jager K, et al. Agmatinase, an inactivator of the putative endogenous antidepressant agmatine, is strongly upregulated in hippocampal interneurons of subjects with mood disorders. *Neuropharmacology* 2012; **62**(1): 237-46.
121. Bernstein HG, Derst C, Stich C, et al. The agmatine-degrading enzyme agmatinase: a key to agmatine signaling in rat and human brain? *Amino Acids* 2011; **40**(2): 453-65.
122. Cofre J, Montes P, Vallejos A, et al. Further insight into the inhibitory action of a LIM/double zinc-finger motif of an agmatinase-like protein. *J Inorg Biochem* 2014; **132**: 92-5.
123. Mella C, Martinez F, de Los Angeles Garcia M, et al. Expression and localization of an agmatinase-like protein in the rat brain. *Histochem Cell Biol* 2010; **134**(2): 137-44.
124. Quinones M, Cofre J, Benitez J, et al. Insight on the interaction of an agmatinase-like protein with Mn(2+) activator ions. *J Inorg Biochem* 2015; **145**: 65-9.
125. Minois N, Carmona-Gutierrez D, Madeo F. Polyamines in aging and disease. *Aging (Albany NY)* 2011; **3**(8): 716-32.

126. Peters D, Berger J, Langnaese K, et al. Arginase and Arginine Decarboxylase - Where Do the Putative Gate Keepers of Polyamine Synthesis Reside in Rat Brain? *PLoS One* 2013; **8**(6): e66735.
127. Ash DE. Structure and function of arginases. *The Journal of nutrition* 2004; **134**(10): 2760S-4S.
128. Morris Jr SM. Recent advances in arginine metabolism: roles and regulation of the arginases. *British journal of pharmacology* 2009; **157**(6): 922-30.
129. Deckel AW, Tang V, Nuttal D, Gary K, Elder R. Altered neuronal nitric oxide synthase expression contributes to disease progression in Huntington's disease transgenic mice. *Brain research* 2002; **939**(1): 76-86.
130. Deckel AW, Gordinier A, Nuttal D, et al. Reduced activity and protein expression of NOS in R6/2 HD transgenic mice: effects of L-NAME on symptom progression. *Brain research* 2001; **919**(1): 70-81.
131. Nakamura T, Wang L, Wong CC, et al. Transnitrosylation of XIAP regulates caspase-dependent neuronal cell death. *Mol Cell* 2010; **39**(2): 184-95.
132. Chiang M-C, Chen H-M, Lee Y-H, et al. Dysregulation of C/EBPα by mutant Huntingtin causes the urea cycle deficiency in Huntington's disease. *Human molecular genetics* 2007; **16**(5): 483-98.
133. LEOPOLD NA, PODOLSKY S. Exaggerated Growth Hormone Response to Arginine Infusion in Huntington's Disease 1. *The Journal of Clinical Endocrinology & Metabolism* 1975; **41**(1): 160-3.
134. Deckel AW, Volmer P, Weiner R, et al. Dietary arginine alters time of symptom onset in Huntington's disease transgenic mice. *Brain research* 2000; **875**(1): 187-95.
135. Maywood ES, Fraenkel E, McAllister CJ, et al. Disruption of peripheral circadian timekeeping in a mouse model of Huntington's disease and its restoration by temporally scheduled feeding. *The Journal of neuroscience* 2010; **30**(30): 10199-204.
136. Estévez AG, Sahawneh MA, Lange PS, Bae N, Egea M, Ratan RR. Arginase 1 regulation of nitric oxide production is key to survival of trophic factor-deprived motor neurons. *The Journal of neuroscience* 2006; **26**(33): 8512-6.
137. Wegrzynowicz M, Holt HK, Friedman DB, Bowman AB. Changes in the Striatal Proteome of YAC128Q Mice Exhibit Gene–Environment Interactions between Mutant Huntingtin and Manganese. *Journal of proteome research* 2012; **11**(2): 1118-32.

Chapter IV

Validation of Key Methods and Resources for Analysis of the Arginase Pathway in the HD x Mn Interaction

Note: Portions this chapter have been submitted for publication under review as the following:

Bichell TJV, Wegrzynowicz M, Tipps KG, Bradley EM, Uhouse MA, Bryan M, Horning K, Fisher N, Dudek K, Halbesma T, Umashanker P., Stubbs AD, Holt H, Kwakye G, Tidball AM, Colbran RJ, Aschner M, Neely MD, Di Pardo A, Maglione V, Osmand A, Bowman AB. Reduced bioavailable manganese causes striatal urea cycle pathology in Huntington's disease mouse model. *Under Review*.

To explore the downstream effects of striatal Mn dyshomeostasis in living HD model mice, we used 3 different mouse models (one of which we bred in two different strains) and we optimized an arginase enzyme assay to use with tissues from these mice. The following chapter describes the methods employed in the gene-by-environment exploration of arginase in HD.

HD mouse models employed

We had expected the BAC225 mouse model to exhibit more extreme symptoms than other models of HD, but in a more biologically relevant way than the R6/2 mouse (which bears the very toxic exon 1 from human *HTT* only). We identified unique differences between the BAC225 and previous models, including widespread early development of HTT aggregates, but the model did not sicken more rapidly than other, more commonly used models with expanded CAG repeats. Because members of our lab had already made the surprising discovery of Mn dyshomeostasis in HD striatal cell culture models[1-3] as well as in the striatum of the YAC128 mouse model[4], our lab also investigated Mn accumulation in the BAC225 model we had generated as well, but did not find a significant reduction in Mn accumulation in the mutants at the same age (**Figure 4-1**). This finding could be related to progression of disease, as there was

evidence of gliosis via TSPO ligand binding in the BAC225 model before 12 weeks of age and the YAC128 model at 10 months of age (**Figure 2-10**)[5]. The Mn dyshomeostasis seen at 12 weeks in the YAC128 was not seen in the same model at 52 weeks of age, after the onset of symptoms, and after gliotic changes have occurred as well (**Figure 4-2**). This suggests that gliosis may mask a neuronal deficit of Mn accumulation, especially if glia prove to accumulate more Mn than neurons, but evidence is lacking for glial accumulation of Mn in the absence of excess exposure (see discussion below). Though we were unable to detect a deficit of Mn in the region as a whole, we hypothesized that there would be evidence of reduction in Mn-dependent neuronal processes, if there were indeed a reduction of Mn bioavailability in the striatum.

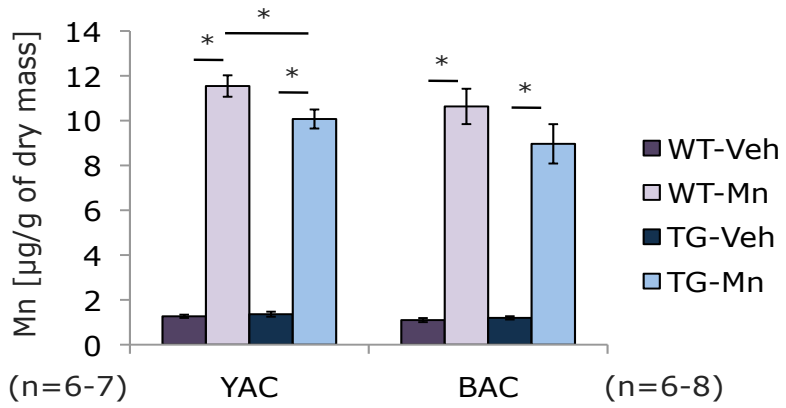

	F	sig.	F	sig.
genotype	F(1,27) = 4.13	**0.054**	F(1,28)=1.98	**0.172**
treatment	F(1,27) = 783.43	**< 0.001**	F(1,28)=240.46	**<0.001**
genotype x treatment	F(1,27) = 5.32	**0.03**	F(1,28)=2.51	**0.126**

Figure 4-1. The significant decrease in net striatal Mn accumulation in the YAC128Q mouse model of HD at age 12 weeks was not significant in BAC mice at the same age To obtain dry weight measurements, tubes were weighed, then frozen tissue added, and exposed to 95°C for 48 hours, or until constant mass was obtained. Manganese levels were measured by ICPMS.Experiment by M. Wegrzynowicz.

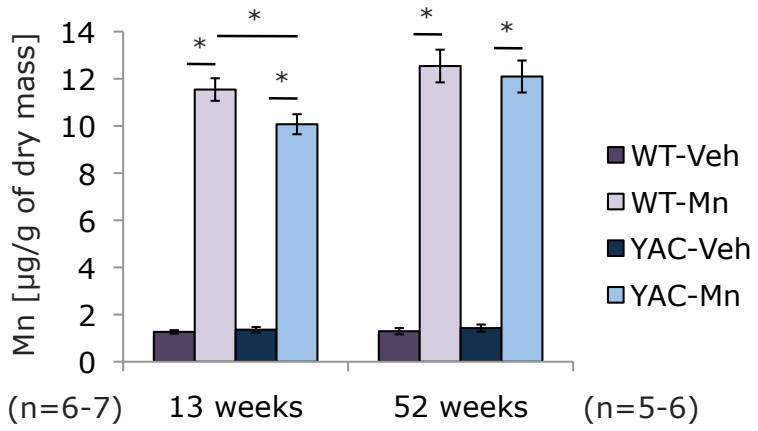

	F	sig.	F	sig.
genotype	F(1,27) = 4.13	**0.054**	F(1,21)=0.22	**0.654**
treatment	F(1,27) = 783.43	**< 0.001**	F(1,21)=505.18	**<0.001**
genotype x treatment	F(1,27) = 5.32	**0.03**	F(1,21)=0.55	**0.47**

Figure 4-2. The decrease in net striatal Mn accumulation in the YAC128Q mouse model of HD at age 12 weeks was not seen at 52 weeks, see methods in Figure 4-1, experiment by M. Wegrzynowicz.

Because we had uncovered Mn dyshomeostasis in the YAC128 model at 12 weeks of age, not in other models, and not in other ages, we proceeded to utizlize the YAC128 for all subsequent experiments. The YAC128 transgene mouse expresses the full-length human *HTT* gene with 128 repeats, inserted via a yeast artificial chromosome[6-8]. The large size of the full-length transgenic model construct allows *HTT* mRNA and protein expression levels to correspond better to the number of transgene copies inserted[8]. Although the YAC128 mouse survives for a normal life span, it has increased weight, develops motor deterioration, has increased N-methyl-D-aspartate (NMDA), AMPA, and metabotropic glutamate receptor (mGluR) binding, and reduced striatal and cortical volume[9].

We duplicated our experiments in both the C57B6/J (C57) strain and the Friends virus B (FVB) strain to insure that our gene-environment effects were not a result of any background genetics or epigenetics. The strains are known to differ in certain traits, for example, the C57 mice develop deafness in adulthood, increase latency to fall from rotarod better, and reduce time to freezing in fear conditioning than FVB[10]. In our experience, the FVB pups have a 1-2 day shorter gestation than the C57 pups, and the FVB dams are excellent mothers, and can foster the C57 orphan pups, but the reverse is not true. Adult male FVB mice often must be housed alone because they become aggressive and are known to injure and kill each other, but that is rare in the C57 strain. C57 mice are known to be more susceptible to pentobarbital, ketamine and nitrous oxide, but not isoflurane[11], while FVB mice are known to be more tumorigenic[12]. We also performed our experiments in males only, because we had seen more variability in Mn accumulation in females in pilot experiments (data not shown), although it would be important to replicate these experiments in females in the future.

Because environmental influences, even minor enhancements to mouse habitats, have been shown to affect the Huntington's disease course, it is crucial that mouse husbandry is uniform across experiments, especially in pre-clinical trials. To this end, Males were weaned with Diet Gel 76A (ClearH2O 72-07-5022) and housed in groups of 2-4, with disposable cardboard houses.

The FVB-Tg(YAC128)53Hay/J mouse line (YAC128Q) was purchased from Jackson Laboratory (Bar Harbor, ME). The C57-YAC128Q line was generated by crossing YAC128Q mice with WT C57BL/6J animals followed by backcrossing with C57BL/6J mice for more than 10 generations. Both lines were maintained in their genetic backgrounds by crossing hemizygous transgenic animals with their WT littermates. Mice were genotyped by PCR

according to the protocol provided by the company (#004938; Jackson Laboratory) and/or by Transnetyx for qPCR-based genotyping (*Htt* Wildtype Forward Primer: GAGAAAGAGAATGTTTAACTCTCCAAGAGA, Reverse Primer: CACATGCACTTTCTACAGCTAGGT, Reporter 1: AAGCAGCTCCAATATC; *Htt* mutant Forward Primer: CCACTTCCCTCTTCTAGTCTGAGA, Reverse Primer: CCACATCTCTCCAGCTCCAAA, Reporter 1: CCCCGCCTCCTCTCG). WT and transgenic littermates were used for experiments. All animal experiments were approved by the Vanderbilt University Medical Center Institutional Animal Care and Use Committee and were designed to minimize pain.

We also collaborated with the Vittorio Magione lab (at the Centre for Neurogenetics and Rare Diseases, IRCC Neuromed, Pozzilli (IS), Italy) to obtain dissected frozen brain tissue from another HD model, the R6/2. These mice were not exposed to Mn, but were dissected at the same 12 week age as previously described in the other lines. The R6/2 and B6CBA colonies were maintained in the animal facility at IRCCS Neuromed. Mice were sacrificed by cervical dislocation and all the procedures were performed in accordance with approved protocols by the IRCCS Neuromed Animal Care Review Board and by "Instituto Superiore di Sanità" (permit number: 1163/2015- PR) and were conducted according to EU Directive 2010/63/EU for animal experiments.

Mn exposure protocol

Manganese exposure followed the previously published sub chronic, 7-day paradigm[13,14]. Briefly, 12-week-old male animals which are at an age that is prior to neurodegeneration and neurogliosis[15] were injected subcutaneously with a 1% solution of $MnCl_2$ x $4H_2O$ in filtered MilliQ water at 50 mg/kg body weight, or with vehicle (filtered

water), on experimental days 0, 3 and 6. Though the HD mice take up less striatal Mn than WT, this exposure paradigm increases Mn levels in both mutant and WT more than 5-fold in the striatum at the time of tissue collection [3]. Mice were then sacrificed by cervical dislocation on day 7, during their 13th week of life; the brain was removed, and placed on ice, rinsed with PBS and rapidly dissected by hemisphere, with all regions kept on ice. First, cerebellum was removed, then hippocampus rolled diagonally away from the midline and removed, revealing the striatum. Striatum was outlined with tips of forceps, and then scooped out. A section of cortex immediately frontal to the striatum was removed and labeled as pre-frontal cortex, and the remaining crescent-shaped edge of visible cortex without attachments to white matter or other layers was also removed. Kidney, heart and liver were also isolated and all tissues were snap-frozen in liquid nitrogen and thereafter stored at -80^{O}C.

Experimental design

Mice were chosen for exposure in a balanced paradigm, as litter size and genotype allowed, so that half of the wild-type littermates and half of the mutants were exposed to Mn, Almost all experiments were performed in male mice only, but some were replicated in female mice.

In addition, for each enzyme activity experiment, samples were chosen to be balanced for weight of dissected frozen striatum as well as for matching to littermates. This helped to control for slightly different dissection techniques that may have removed slightly larger or smaller subsections of striata.

Statistics

General Linear Model (GLM) multivariate or univariate ANOVA was performed using Graphpad Prism or SPSS Statistics 19 (IBM, Armonk, NY). For post-hoc pairwise comparisons between experimental groups, a Student's t-test was used (Excel 2008; Microsoft, Redmond, WA).

Protein experiments

For western blotting, tissue was kept on dry ice and then homogenized in RIPA lysis buffer (50 mM Tris pH8.0, 1mM Ethylenediaminetetraacetic acid [EDTA], 150 mM NaCl, .01% Triton X-100, 1% SDS, 1% sodium deoxycholate, protease inhibitor cocktail [Sigma P8340], 1:100 and phosphatase inhibitor cocktails 2 and 3 [Sigma P5726 and P0044], 1:100) using a 23_G x 1 needle for brain tissue, and glass homogenizers for liver and kidney. Homogenates were then centrifugated at 4° at 13000 rcf for 5 min and supernatant was collected and kept on ice.

Protein content for all experiments was measured using either the DC protein assay kit (Bio-Rad, Hercules, CA) and/or the BCA protein assay (Pierce™ BCA Protein Assay Kit, Thermo), in pellet solubilized with 0.5 M NaOH in the samples prepared for metabolite measurements and in aliquots of supernatants for the samples prepared for activity assays and Western blotting.

Tissue homogenates in RIPA lysis buffer were diluted with sample buffer (4x Laemmlli sample buffer [Bio-Rad 061-0747, 5% β-mercaptoethanol added]), heated for 5 min. at 95^{O}C and 40 mg of protein of each sample loaded onto Mini-Protean TGX Pre-cast gels (4-20% 456-1094). Proteins were transferred for 7-9 min to 0.22μm nitrocellulose membrane (IB301002) using the iBlot™ system. Gels were rinsed with MilliQ water and stained with Coomassie

(Bio-Rad 161-0786) for 45 min, then rinsed 3-5 times with MilliQ water. Membranes were dried, blocked with Odyssey blocking buffer (927-40000 PBS) for 1 hour, and incubated overnight in primary antibodies (in Odyssey blocking buffer with 0.1% Tween-20) at room temperature.

After incubation, antibodies were saved to be re-used. Blots were washed 5 times for 5 min each with 1x TBST buffer (150mM NaCl, 56mM Tris-HCl, 44mM Tris base, 0.05% Tween-20) and incubated in secondary antibodies (in Odyssey blocking buffer with 0.1% Tween-20) for 90 min then washed again with TBST as above. Primary antibodies used are listed in **Table 4-1.**

Table 4-1: Primary Antibodies Used for HD-Urea Cycle Experiments

Protein	Company	Number	Concentration
ARG1	Abcam	ab912795	1:1000
ARG1	Proteintech	16001-1-AP	1:1000
ARG1	Millipore	ABS535	1:1000
ARG2	Abcam	ab81505	1:4000
ARG2	Santa Cruz	sc-20151	1:1000
ARG2	Proteintech	14825-1-AP	1:2000
AGMAT	Santa Cruz	sc-46716	1:1000
LIMCH1	Abcam	ab96178	1:1000
Anti-Polyglutamine-Expansion Diseases Marker (5TF1-1C2)	Millipore	MAB1574	1:5000
ACTIN	Millipore	MAB1501	1:10,000
ACTIN	Sigma	A5441	1:10,000

Secondary antibodies: anti-rabbit, anti-mouse, anti-chicken or anti-goat (Licor IRDye 700 or 800CW) were diluted in Odyssey blocking buffer (previously vortexed with 0.1% Tween-20) at 1:10000. Protein was detected using the Odyssey infrared system and analyzed with ImageStudio (www.licor.com) and normalized to total protein quantified from Coomassie stained gel, or ACTIN signal.

Experiments were performed to assess whether or not GAPDH, UBE3A or ACTIN was most appropriate as a loading control, as there is some evidence that all are affected by mutant HTT or Mn. ACTIN has been used most often in the literature, and it proved to be the most consistent loading control, although it was slightly increased by Mn exposure (representative data **Figure 4-3**). In the case of ARG2, which was increased 2-3 fold after Mn-exposure, an increase in ACTIN would have over-corrected this finding, rather than exaggerating it. Most westerns were normalized to both coomassie and ACTIN to check the accuracy of ACTIN normalization, which did not differ from coomassie

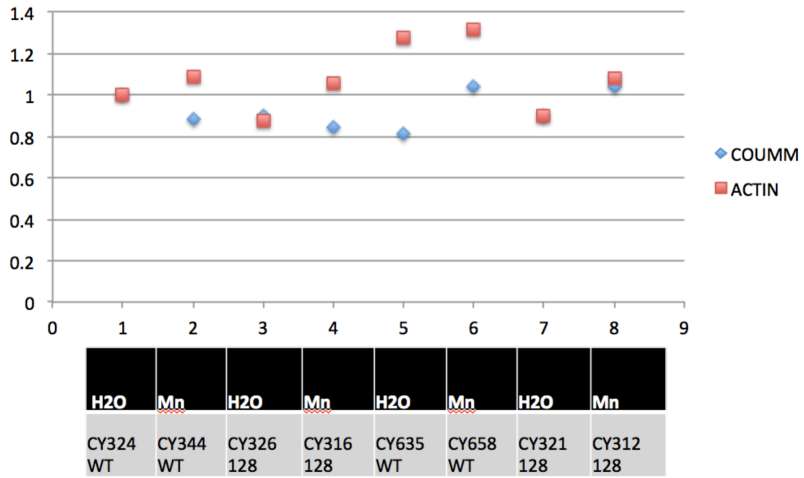

Figure 4-3. Coumassie vs. Actin as a loading control. (Sample data, from western for BDNF blot 2, 3-10-15).

Arginase isoforms in rodent brain

When we began the line of investigation on arginase protein, there were more studies listing ARG1 in mammalian brain than ARG2, although the literature was divided (**Table 4-2**). Many investigators have found ARG1 in mammalian brain tissue, though it is possible that their methods were flawed. Liu et al., showed stable ARG1 protein in human AD brain, and increased ARG2 protein (as well as arginase activity) in post-mortem AD cortex)[16]. Liu's manuscript shows a strong band of ARG1 by western, but they used an antibody that we did not test (Santa Cruz Biotechnology, sc-166920), and the entire blot is not displayed. Using in situ hybridization and immunohistochemistry, Yu et al., found ARG1 to be much more highly expressed than ARG2 in brain, and both arginases were located only in neurons and not in glial cells[17]. Peters et al., found more ARG1 than ARG2 in rat brain with Western blots, but could not locate ARG1 via northern blot[18], suggesting a potential cross-reactivity in the antibody used. Bernstein found that ARG1 was widely expressed in rat brain, especially in interneurons of the hippocampus, but he also found AGMAT (which is likely not expressed in rat brain, and did not double-check for cross-reactivity to ARG2.

Table 4-2: Literature citing brain localization of ARG1 and ARG2

Year	Author	ARG1	ARG2	Species	Notes
2014	Liu et al[16]	Stable in brain	Increased in cortex in AD	Human	Santa Cruz ARG1 antibody
2013	Peters et al[18]	High in brain	Lower than ARG1 in brain	Rat	Not consistent with Northern blot
2012	Choi et al[19]	Not in brain	Yes in brain	Rat	Also in cerebellum
2011	Bernstein et al[20]	High in brain	Not investigated	Rat	Also found AGMAT!
2010	Hansmannel et al[21]	mRNA low in brain	mRNA in brain, increased in AD	Human	
2004	Cederbaum et al[22]	Only embryonic	Yes in brain	Mouse	
2001	Yu et al[17]	Very high in brain	Low in brain	Mouse	Not specific?
1999	Braissant et al[23]	Not much in brain	Yes in brain, esp in Hip	Rat	Also found ARG2 in cerebellum
1997	Morris et al[24]	Not in brain	Yes in brain	Human and rodent	Also found ARG2 in many other tissues

Other investigators have not found ARG1 to be located in brain. For example, Hansmannel et al., showed very low ARG1 mRNA expression in human brain but found that ARG2 increased in Alzheimer's disease (AD) (while glutamine synthetase (GS) was unchanged)[21]. Choi et al found ARG2 in rat brain (including cerebellum) but not ARG1[19]. A 2004 review by Cederbaum et al. noted ARG1 to be relegated to liver and red blood cells, while only ARG2 was the only isozyme found in brain, as well as kidney, gastrointestinal tissue and the prostate. However, this manuscript cites unpublished studies showing expression of ARG1 protein in all brain regions in embryonic rodents, with ARG2 appearing after post-natal day 1, and they do not mention further expression in brain. Morris et al., found

ARG2 in almost every human and rodent tissue, and found ARG1 only in liver[24]

Furthermore, westerns performed by previous Bowman lab personnel had demonstrated the presence of ARG1 in striatum, primarily via the Proteintech antibody (**Figure 4-4**). Unfortunately, we were unable to replicate these experiments.

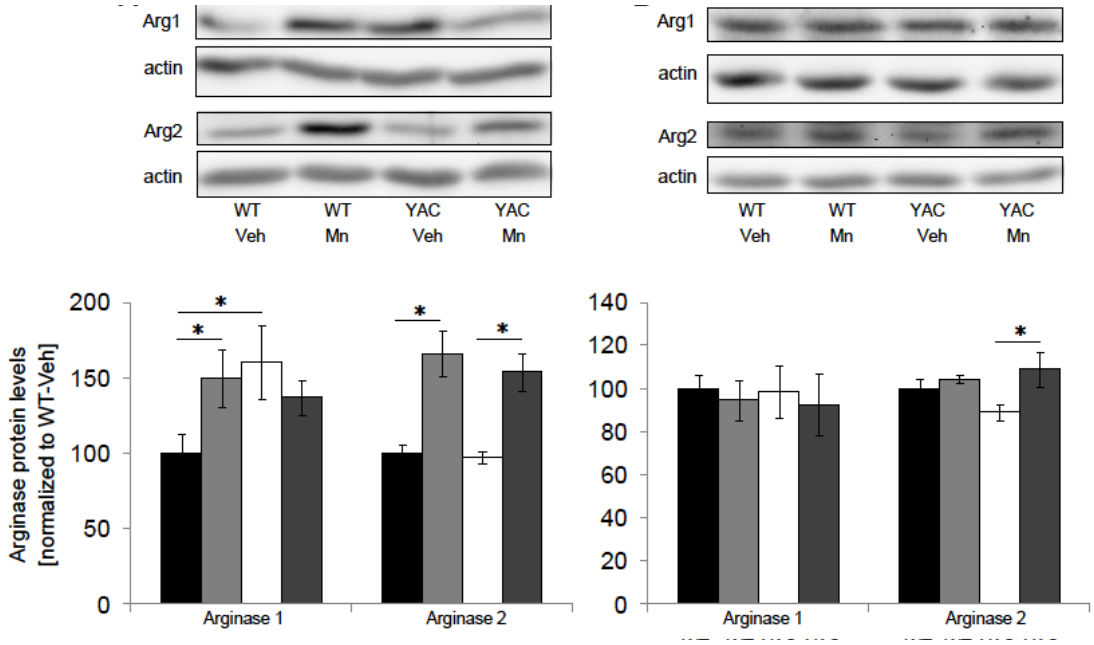

Figure 4-4. Previous western data showed erroneous significant genotype/treatment interaction in ARG1 protein in striatum, but not ARG2 by western blot. Proteintech antibody (experiment by M. Wegrynowicz).

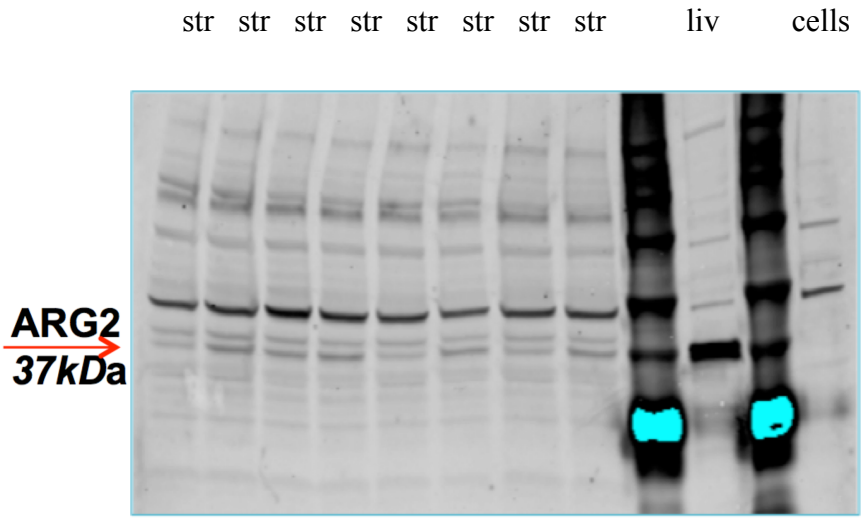

Figure 4-5. ARG2 using liver as control reveals a band at 37kDa in the liver lane as well as a Mn-responsive band in the striatal lanes (Proteintech 14825-1-AP).

Attempts to repeat the original ARG westerns with the Proteintech antibody and with liver as a control revealed a strong, non-specific band at 50kDa, but for both ARG1 and ARG2, though ARG2 is not thought to be present in liver (**Figure 4-5**). It is possible that many published studies locating ARG1 in brain as well as ARG2 were quantifying the nonspecific band located at 50kDa rather than the correct band at 37kDa. It is also possible that many of the antibodies used in the literature bind to both of the isoforms of ARG because they share 59% identical amino acids[18]. In fact, the Proteintech antibody recognizes 354 amino acids of human ARG2, a region which overlaps much of the homologous sequences.

Furthermore, indications that the antibody was binding to both ARG1 and ARG2 came from previous westerns in our lab performed on liver tissue that had noted very similar ARG1 and ARG2 levels, while most studies acknowledge that there is no detectable ARG2 in liver (**Figure 4-6**).

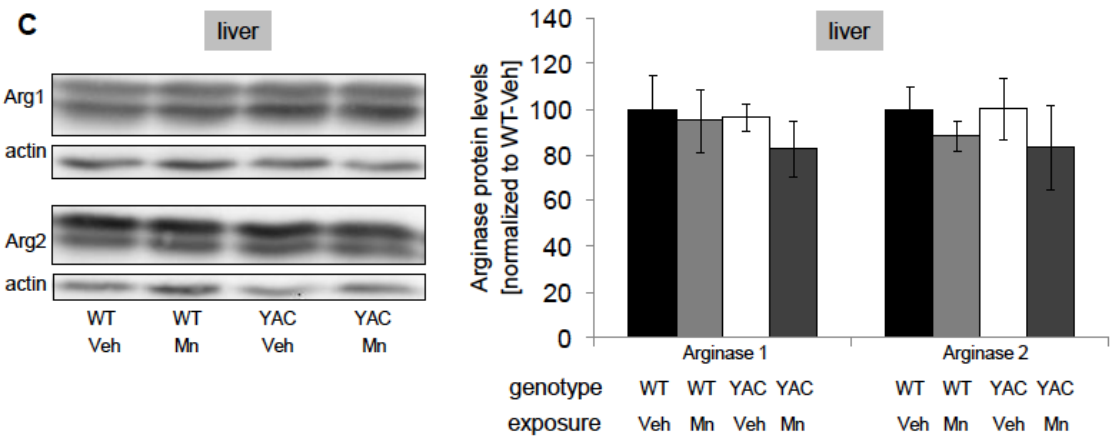

Figure 4-6. ARG1 and ARG2 non-specifically bound in liver, ARG1 Proteintech 16001-1-AP ,ARG2 Proteintech 14825-1-AP,ARG1 Proteintech 16001-1-AP (Experiment by M. Wegrynowicz).

It is also possible that the Proteintech antibody for ARG2 had been contaminated by ARG1 antibody. When we attempted to replicate the significant ARG1 HD x Mn interaction finding shown in **Figure 4-4**, using other antibodies and liver as a control, we were not able to detect ARG1 in striatum (**Figure 4-7 and Figure 4-8**), though it was abundant in liver. Surprisingly though, ARG2 was present in striatum and appeared to be Mn-responsive (**Figure 4-9**)!

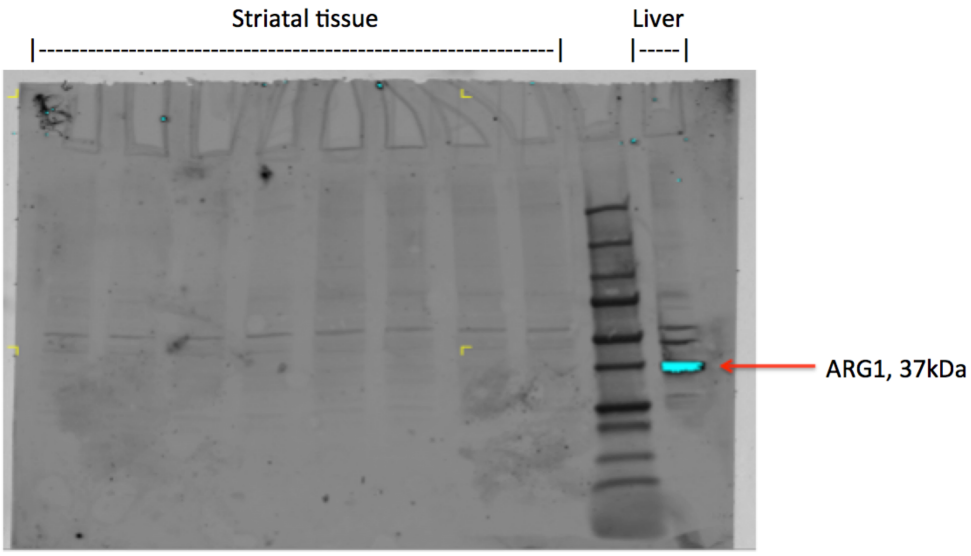

Figure 4-7. ARG1 was detectable in liver at the expected molecular weight, but was not detectable in striatum lanes (Millipore ABS535).

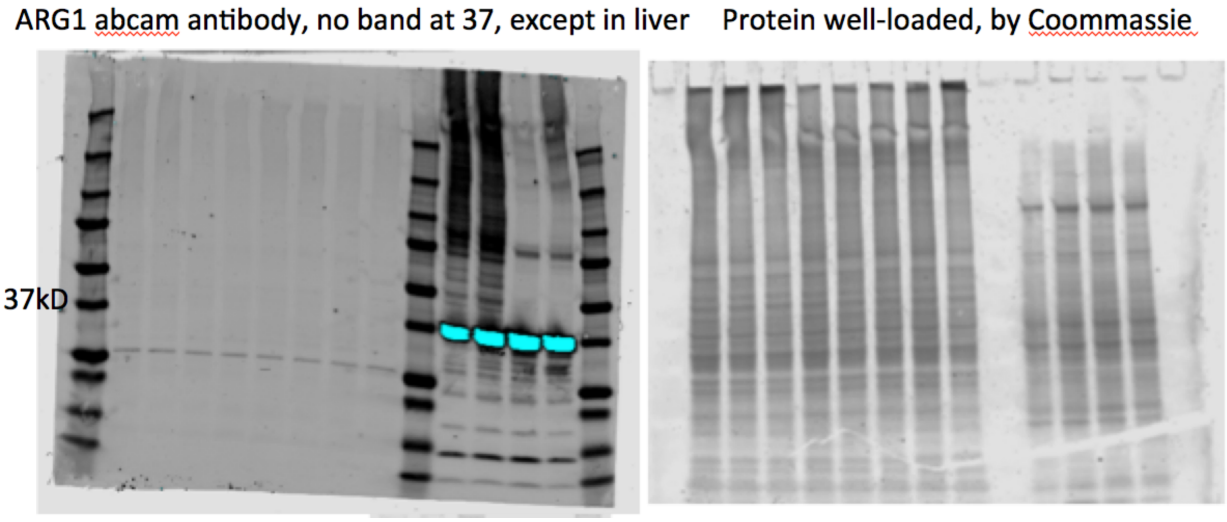

Figure 4-8. ARG1 protein is expressed in liver but not in striatum. The first 8 lanes are loaded with striatal samples, followed by 4 lanes with liver samples. There is a strong 37kDa band in liver lane, no detectable band in striatum lanes (Abcam ab912795).

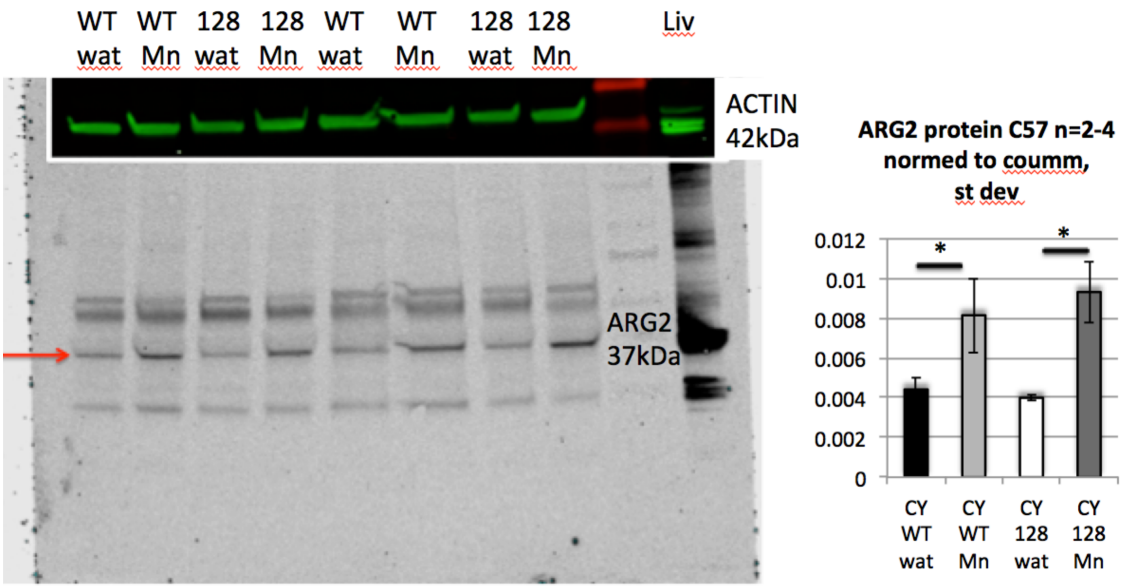

Figure 4-9. ARG2 protein is expressed in striatum and is Mn-responsive, but also appears in liver with abcam antibody There are non-specific bands at 50kDa and at 25kDa as well, Abcam ab81505.

Interestingly, the Allen Brain Atlas shows scant ARG2 in brain, but no ARG1, and there is a strong signal in hippocampal CA2, though not mentioned (**Figure 4-11**), which will be further discussed in Chapter VI.

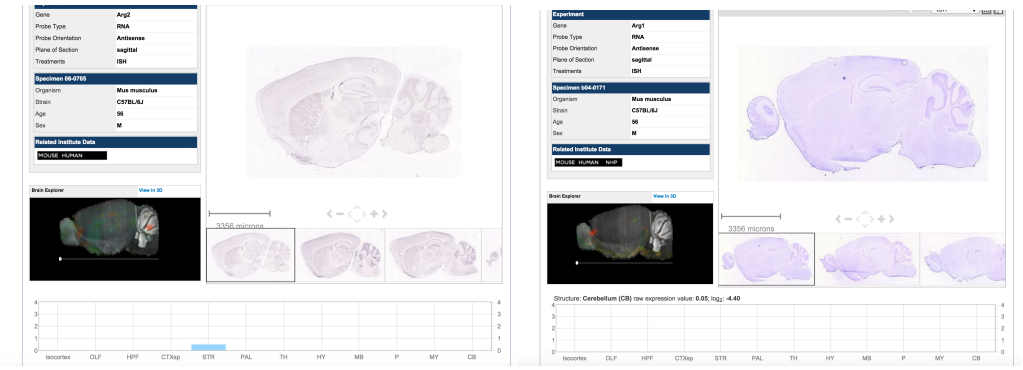

A. B. Image credit: Allen Institute.

Figure 4-10. Allen Brain Atlas[25] shows ARG2 present in striatum and not in other rodent brain regions, while ARG1 is not detectable. A) ARG2, B) ARG1. © 2015 Allen Institute for Brain Science. Allen Brain Atlas API. Available from: brain-map.org/api/index.html

RNA-SEQ evidence on ARG expression in striatum

Subsequent RNA-SEQ studies on striatal samples from mice at the same age following the same Mn-exposure protocol confirmed that *ARG1* gene expression was undetectable in the striatum of this model (**Figure 4-11**), further supporting the idea that the previous western blots had been inaccurate.

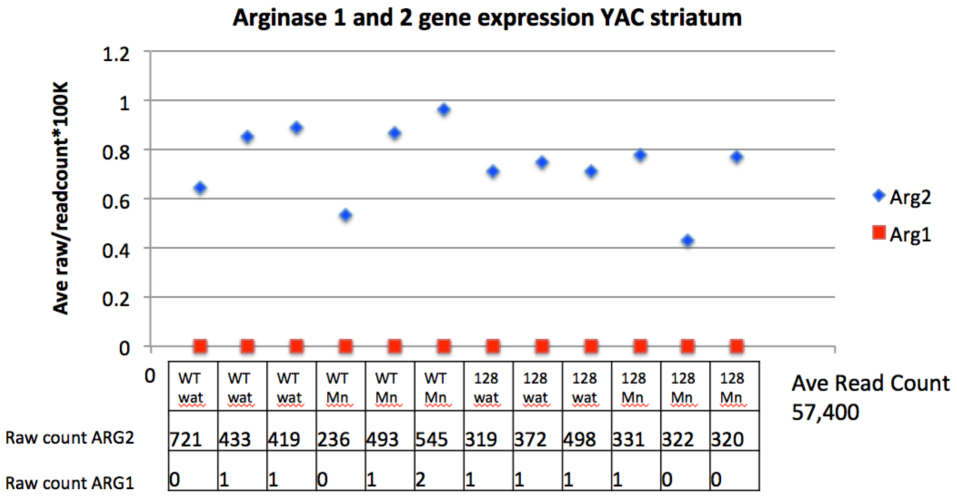

	WT wat	WT wat	WT wat	WT Mn	WT Mn	WT Mn	128 wat	128 wat	128 wat	128 Mn	128 Mn	128 Mn
Raw count ARG2	721	433	419	236	493	545	319	372	498	331	322	320
Raw count ARG1	0	1	1	0	1	2	1	1	1	1	0	0

Figure 4-11. There is no detectable ARG1 gene expression in striatum. ARG2 gene expression is present. Raw RNA-SEQ data on ARG1 and ARG2 gene expression, n=3.

Regional detection of ARG1 and ARG2 protein in mouse tissue

Because ARG1 is known to be present in liver, and ARG2 is known to be located in kidney, those tissues were used as controls to verify the specificity of new protein antibodies for both ARG1 and ARG2 (**Figure 4-12, 4-13**). We found that the Santa Cruz antibody was surprisingly the most specific for ARG2, and the Abcam antibody was most specific for ARG1. The molecular weights of ARG1 and ARG2 are virtually identical, so blots could not be re-used. These controlled westerns confirmed that ARG1 was abundant in liver and was

virtually undetectable in kidney and striatum of both the C57 and FVB background mice dissected at 12 weeks of age (**Figure 4-13**).

Our westerns also confirmed that ARG2 protein was abundantly expressed in kidney, and was easily detectable in striatum (**Figure 4-13**). Surprisingly, ARG2 protein was Mn-responsive, increasing 2-3 fold with Mn-exposure in every tissue where it was detected.

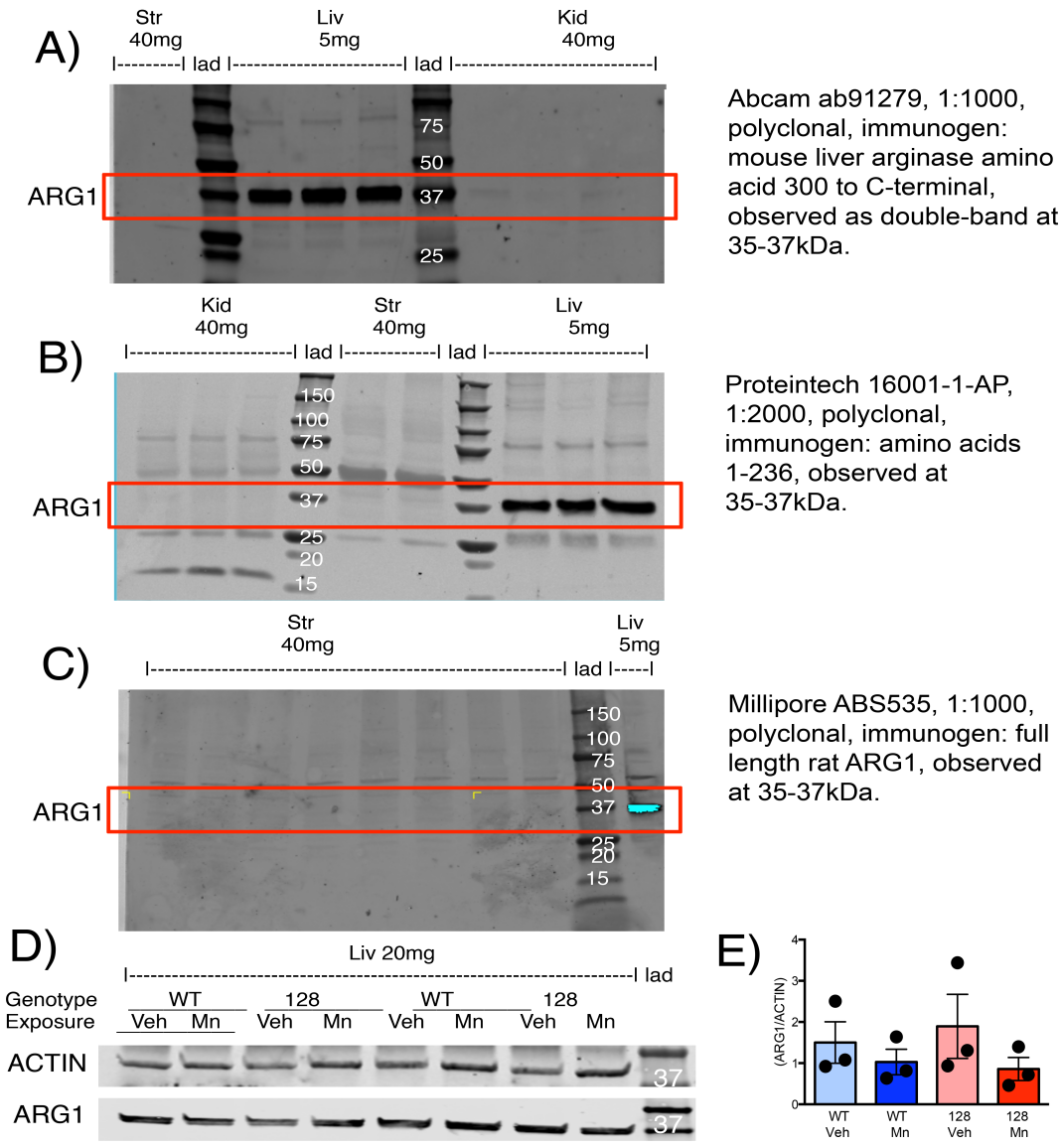

Figure 4-12. ARG1 protein is undetectable in striatum and unaffected by Mn in liver. Shown in **(A)** and **(B)** are the same samples of WT, FVB, vehicle-exposed striatum (Str), liver (Liv) and kidney (Kid) run on different gels with two different ARG1 antibodies **(A)** Abcam, **(B)** Proteintech, and additional striatal samples exposed to Millipore shown in **(C)**, ladder (lad). ARG1 protein is observed as a doublet band at approximately 35-37kDa with all three antibodies in liver tissue and is absent from kidney and striatum. There were strong, non-specific bands at other molecular weights with the Proteintech antibody. **(D)** Mn exposure did not affect hepatic ARG1 protein levels (Abcam ab91279). **(E)** Quantification of ARG1/ACTIN normalized to WT-Vehicle (Veh), n=3. Data presented as ±sem.

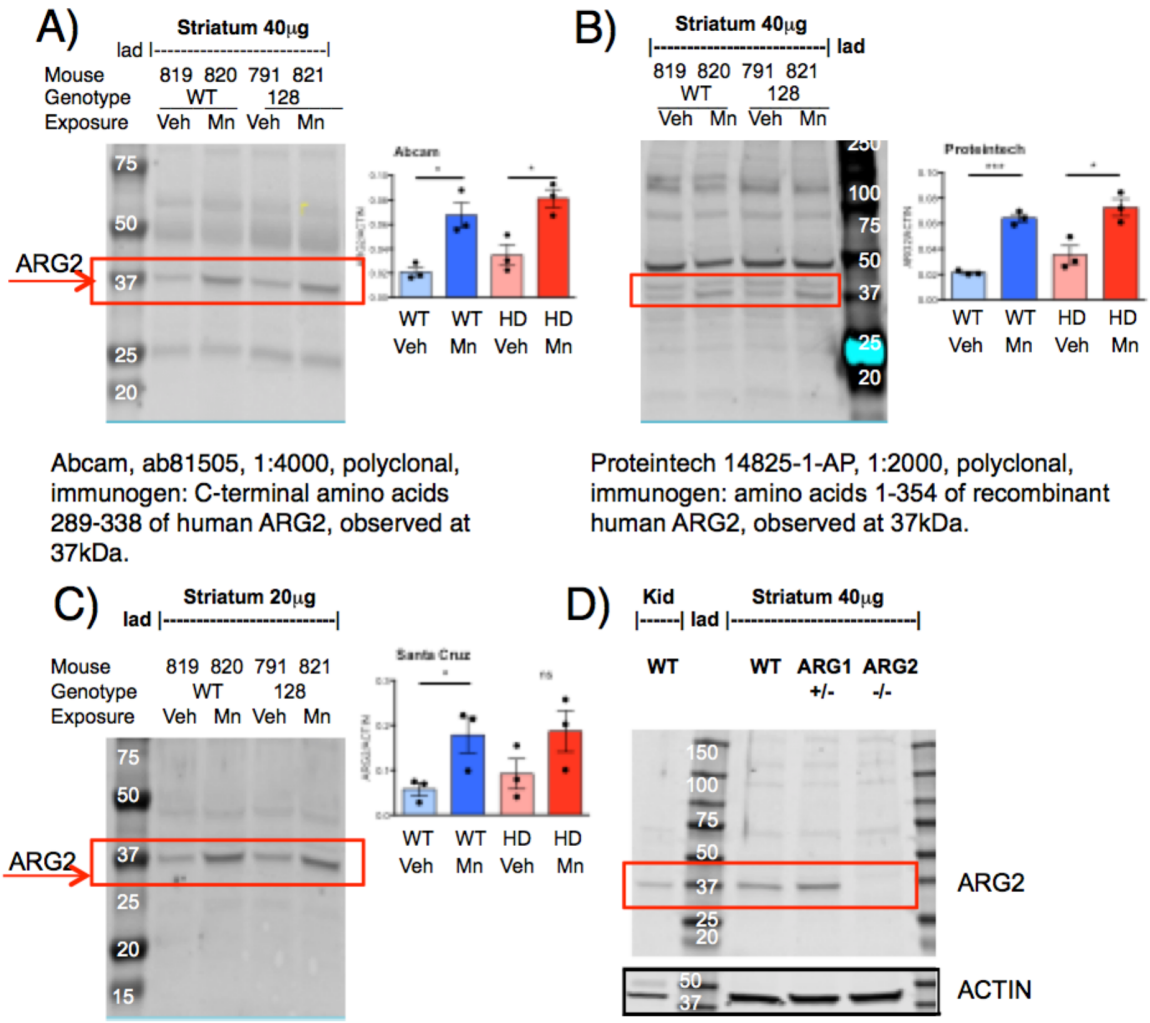

Figure 4-13. ARG2 protein is detectable in striatum with protein levels similar between HD and wild-type; and elevated by Mn-exposure in both genotypes. Shown are representative blots on the same samples run on three different gels and exposed to three different antibodies (A) Abcam, (B) Proteintech, (C) and (D) Santa Cruz; vehicle (Veh). These blots have only one band in common, at 37kDa, and this band shows the same pattern of change for all three after *in vivo* Mn exposure, suggesting that all other bands are non-specific and may be cross-reacting with ARG1. (D) Striatal tissue (40mg) from ARG1 heterozygous knockout[26] and ARG2 homozygous knockout[27] mouse with WT kidney (Kid) (20mg) and striatum for controls. For experiments shown in Figures 5-9, 5-10, 5-11 and 5-12.we used sc-20151 because it had no evidence of cross-reactivity. Quantifications are ARG/ACTIN, normed to WT Veh, FVB, +sem, *post-hoc* binary comparisons by t-test following a significant (p=<.05) ANOVA, *p=<.05, ***p<.001.

Through a recent collaboration with the William and Ruth Caldwell lab, Georgia Regents University, Augusta, GA, we were able to obtain dissected whole brain from two different transgenic arginase deficiency mouse models: an ARG1 heterozygous knockout[26] and an ARG2 homozygous knockout[27]. The Santa Cruz sc-20151 ARG2 antibody was demonstrated to be accurate for ARG2 protein detection with a visible band in the ARG1 het and an absent band in the ARG2 homozygous knockout (**Figure 4-13 D**).

Immunohistochemical experiments

Hoping to visualize a subregional difference in ARG2 protein expression, we continued our collaboration with the Alexander Osmand lab, Department of Biochemistry, University of Tennessee, Knoxville, TN. Mn-exposed 12-week old mice were perfused and whole brains were dissected and fixed in paraformaldehyde and transferred to the Osmand lab for slice preparation and staining.

Free floating formalin-fixed 35m sections were washed and treated with 88% formic acid for 30 min., aldehydes were blocked with ethanolamine acetate pH 9.5 for 1 h followed by the addition of 10 mM ascorbic acid for 10 min. Sections were treated with 0.5% Triton X-100 in PBS (TxPBS) for 50 min. and incubated overnight with a polyclonal rabbit antibody to arginase-2 at 1:5,000 in TxPBS. Sections were washed and incubated with for 90 min in biotinylated anti-rabbit IgG (Vector) at 1 μg/ml in TxPBS. Peroxidase detection of biotinylated secondary antibody was performed with ABC Elite Kit (Vector) with nickel enhanced DAB in the presence of glucose and glucose oxidase in Tris-imidazole buffer after a single round of tyramide amplification using biotin-PEG-tyramide. Sections were mounted on gelatinized glass slides, dried and cover-slipped using Xylene substitute mountant. Digital images of striatum were collected on a Nikon Eclipse Ni microscope equipped with a DS camera.

Gene expression experiments

Arginase 1 (*Arg1*), arginase 2 (*Arg2*), agmatinase (*Agmat*) and the agmatinase-like protein predicted domain of *Limch1* (*Limch1*) transcript levels were measured by quantitative reverse-transcriptase polymerase chain reaction (QRT-PCR). Previous QRT-PCR experiments performed by previous Bowman lab personnel had quantified *Arg1* in striatum, but these experiments, as well as the protein expression experiments detecting ARG1 in striatum, were not replicable. We hypothesized that the standard curve might not have had enough Arg1 gene expression to be reliable, and in addition, that the primer sequences may have been non-specific.

We redesigned the primer sequences for *Arg1*, *Arg2*, and *Actin*, as well as *Agmat* and *Limch1*. The primers were designed specifically to:

1) cross exon boundaries
2) be 18-20 base pairs in size
3) product between 50-120 base pairs
4) Tm 58^{o}C-60^{o}C
5) GC min 30%, max 70%, optimal 50%
6) Max self-complementary
7) Max 3' stability (can only have 1 or 2 Gs or Cs)
8) Max poly x (3-4)

The *Limch1* primer was specifically designed to target the domain which had been shown to transcribe the Agmatinase-Like Protein.

Knowing that *Arg1* might only be present in liver, and *Arg2* might only be present in kidney, we used a mixture of vehicle treated WT liver, kidney and striatal tissue lysates

calculated at a concentration ratio of 1xliver/5xkidney/100xstriatum to prepare the standard for relative quantitation based on estimates of arginase activity in the various tissues.[28,29] Tissue was homogenized in RLT Plus Buffer (Qiagen 1053393) using the needle method as described in the protein preparation methods, and flash frozen in liquid nitrogen. Primer sequences used are listed in **Table 4-3**.

Table 4-3: Primer Sequences Used for QRT-PCR Experiments

Gene	Forward	Reverse
Arg1	5'-TGGCTTGCGAGACGTAGA-3'	5'-CCAATCCCCAGCTTGTCT-3'
Arg2	5'-GGGATGCCACCTAAAAGAC-3'	5'-GCCCACTGAACGAGGATAC-3'
Agmat	5'-CTCTGACCTTGGGTGGAGAC-3'	5'-GAGGTTTGTCCGTGGTGTT-3'
Limch1	5'-GCAGCAACAGCATCGAGATC-3'	5'-CATCCTCTTGGCCGTTCGAT-3'
Actin	5'-CAGCCTTCCTTCTTGGGTAT-3'	5'-CGGATGTCAACGTCACACTT-3'

Frozen homogenates were subjected to RNA purification using RNAeasy Plus Mini kit (QIAGEN 74134) according to manufacturer's protocol. RNA concentrations were determined by absorbance measurements at 260 nm and 280 nm using NanoDrop spectrophotometer (ND-1000 Thermo Fisher Scientific, Waltham, MA). cDNA was reverse-transcribed from isolated RNA with SuperScript III Reverse Transcriptase kit (Invitrogen 18080044), using Mycycler thermocycler (Bio-Rad) according to manufacturer's directions for random hexamers. The qPCR reaction was run on an ABI 7900HT real-time PCR detections system (Invitrogen) using Power SYBR Green Master Mix (Life Technologies Applied Biosystems 4367659) according to the manufacturer's instructions, and the results were analyzed using SDS software (Invitrogen). *Arg1*, *Arg2*, *Agmat*, *Limch1* transcript levels were normalized to the levels of *Actin* as the endogenous active reference control.

Measurement of metabolites via LC-MS

For metabolite measurements, frozen tissues were added to ice cold buffer (100 mM trichloroacetic acid, 10 mM CH_3COONa, 100 µM EDTA, 10.5% MetOH, pH 3.8) and homogenized in Potter-Elvehjem glass/PTFE tissue grinders (Kimble Kontes, Vineland, NJ).

Arginine and its metabolites were measured by liquid chromatography-mass spectrometry (LC-MS). Prior to the analysis, samples were supplemented with internal standard, homoagmatine (hAgm)[30], and purified by centrifugation with Amicon centrifugal filters (Millipore) at 14000 x g, for 10 min., at room temp. The resulting filtrate was then evaporated under N_2 gas and reconstituted with 50% acetonitrile containing 100 mM $NaHCO_3$ (pH 8.0) and derivatized with 20 mM dansyl chloride (Sigma) at $50^{O}C$ for 20 min. Next, samples were diluted with H_2O, centrifuged at 18000 x g, for 10 min at room temp, and transferred to autosampler vials. The LC-MS system was equipped with ThermoPal autosampler, Accela UHP quaternary pump (Thermo Fisher Scientific), Zorbax SB-C18 Rapid Resolution HT column (2.1 mm x 50 mm, 1.8 µm, Agilent Technologies, Santa Clara, CA) with Acquity UPLC in-line 0.2 µm steel filter unit (Waters, Milford, MA), TSQ Quantum Access triple-stage quadrupole mass spectrometer with an electrospray ion source and a 100 µm ID deactivated fused silica capillary (Thermo Fisher Scientific). The autosampler was set at $10^{O}C$ and separations were performed at RT. Mobile phases were composed of 0.5% formic acid in (A) 5% acetonitrile and in (B) 10% 2-propanol / 85% acetonitrile. The flow rate was set at 350 µl/min and the gradient was as follows: B=0%, 3 min; B=0-90%, 3 min; B=90%, 3 min; B=90-0%, 1 min; B=0%, 5 min. MS/MS detection was performed in positive-ion mode. Quantification was based on multiple reaction monitoring detection at a collision energy of 30 V (agmatine (Agm): m/z 364 → 347; hAgm: m/z 378 → 361; Arg: m/z 408 → 391; Orn: m/z

599 → 303; Cit: m/z 409 → 392; putrescine (Put): m/z 555 → 304; spermine (Spm): m/z 1135 → 360, 669, 900; spermidine (Spmd): m/z 845 → 360). Data were acquired with Xcalibur 2.0.7, and analyzed with LCQuan 2.5.6 (Thermo Fisher Scientific).

Development of an optimized arginase enzyme activity assay for striatal tissue

To measure arginase enzymatic activity in dissected striatal tissue samples it was necessary to identify non-radiolabeled assays which had previously been used successfully, ideally with mouse brain tissue. The tiny size of these dissected tissues and the fact that the specific activity of arginase is much lower in brain than in liver or kidney required an exquisitely sensitive assay.[31] From a search of the literature, it was apparent that few arginase assays had been used on mouse brain tissue. Most had relied on liver, or utilized purified enzyme, and in much larger quantities. The assays that had been used with small amounts of tissue were all based on urea (rather than ornithine) as the product of the ARG enzymatic reaction and included protocols from Chan et al. (2009) and Wynn et al. (2011), both derived from Corriza et al..(1994) [31] which had been optimized from an earlier version by.[32] An additional proprietary assay developed by Sigma was directly derived from Jung et al.

Prior members of our lab had measured arginase enzyme activity in pilot experiments with striatal samples using an ornithine output assay (**Figure 4-14**) that included ninhydrin as a colorimetric agent.

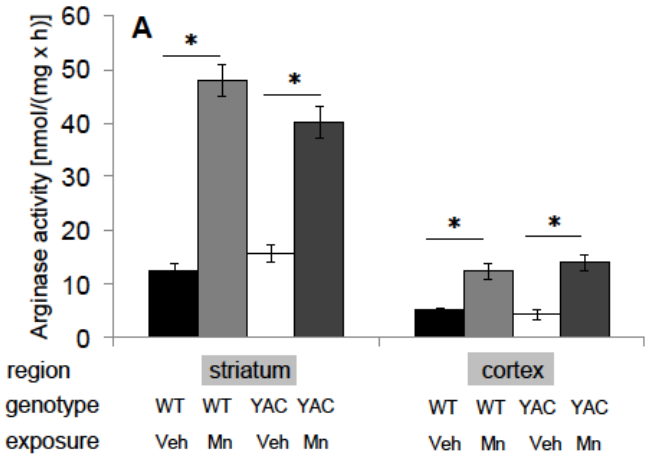

Figure 4-14. Prior data from the Bowman lab showed a significant effect of Mn-exposure in striatal arginase activity as measured by an ornithine assay, with a trend towards an interaction effect, and this interaction effect was also seen in cortex.

Our metabolite experiments had demonstrated an increase of ornithine in the HD model striatum, which resolved after Mn-exposure (See **Figure 5-4, Chapter 5**), a factor which may have interfered with enzyme activity measurement, so we sought to use the byproduct urea as an output instead of ornithine. In addition, a commercial urea assay was available, and had begun to be commonly used.

Summary of existing arginase assays

Corraliza arginase activity assay

The Corraliza assay[31] was developed specifically to measure ARG activity in macrophage cell cultures (approximately 25000 macrophages per sample). The Corraliza assay uses saturating amounts of substrate with small amounts of tissue and is not affected by the presence of citrulline or arginine as previous assays had been.[32]. Activated macrophages express ARG1 and produce citrulline.

As described by Corraliza,et al., previous ARG enzyme assays had used non-saturating

concentrations of arginine or were affected by citrulline, a metabolite of activated macrophages. This is a crucial factor because excess arginine is shunted through the nitric oxide synthase (NOS) pathway where it is metabolized by NOS into NO and citrulline. The optimum pH for ARG activity is very basic: pH 9.7,[33] but prior methods had also been affected by the precipitation of $MnCl_2$ which occurs at the pH of 9.7, and thus to avoid $MnCl_2$ precipitation the reaction was set up to occur at pH 7.5.

To increase the sensitivity of detection, Corraliza et al., reduced the reaction volume and eliminated the previously used stop reagent of perchloric acid. They also reduced the volume of α-isonitrosopropiophenone (ISPF), by increasing its concentration. To stop the reaction they used a small volume of a different acid mixture, instead of perchloric acid. With these modifications, they were able to detect urea concentrations as low as 0.02-0.05/zmol.

Corraliza Arginase Activity Protocol

Reagents

L-arginine, urea and Tris-(hydroxymethyl)-aminomethane (Merck, Darmstadt, Germany).
Protease inhibitors, pepstatin antipain and aprotinin (Boehringer-Mannheim, Mannheim, Germany).
Triton X-100 and ISPF (Sigma, St. Louis, MO 63178, USA)
Sulfuric acid 96%
Ortho-phosphoric acid 85%,
Manganese II chloride and Ethanol absolute (Panreac, Barcelona, Spain).

Method:

1)Wash harvested cells with PBS
2)Add 50ul of 0.1% Triton X-100 containing 5ug pepstatin, 5ug aprotinin and 5ug antipain as protease inhibitors and stir for 30 mins at room temperature
3)Add 50ul of 10mM $MnC1_2$, 50 mM Tris-HCl, pH 7.5
4)Activate enzyme for 10 minutes at 55°C in Eppendorf tubes
5)Initiate reaction by adding 25u1 of 0.5 M arginine, pH 9.7 to a 25ul aliquot of the previously activated lysate.
6)Incubate at 37°C for 60 minutes
7)Stop reaction by the addition of 400ul of an acid mixture containing H_2SO_4, H_3PO_4 and H_2O (1:3:7)
8)Add 25uL 9% ISPF (dissolved in 100% ethanol)
9)Heat at 100°C for 45 min
10)Place in dark for 10 min.
11)Aliquot 200uL samples into 96 well plate
12)Quantify urea produced via colorimetric signal at 540 nm on microplate reader
13)Prepare a calibration curve with increasing amounts of urea between 1.5 and 30ug. Add 400uL of H_2SO_4, H_3PO_4 and H_2O (1:3:7) acid mixture and 25uL ISPF to 100uL urea solution and then aliquot.

Chan arginase activity assay

Chan, et al[34] modified the Corraliza assay to better measure arginase activity in the central nervous system of a mouse model for juvenile Batten disease. Interestingly, like HD, Batten disease is another neurodenerative disorder with a known genetic mutation, though the onset is in childhood and the gene is Ceroid-Lipofuscinosis Neuronal 3 (CLN3). At the time that Chan and colleagues developed their assay, CLN3 was known to be located on the lysosome and was thought to regulate arginine transport. Subsequent research showed that CLN3 is involved in microtubule-dependent, anterograde transport of late endosomes and lysosomes. http://www.genecards.org/cgi-bin/carddisp.pl?gene=CLN3

Using this modified assay, Chan and colleagues found a significant increase in ARG activity in CLN3 mutant mouse cortex compared to wild-type, but only at post-natal day 14 (P14), while they found a decrease in liver ARG activity, but only at P90. These results are questionable, as our arginase gene and protein expression results will demonstrate below (**Chapter 5**). Furthermore, Chan et al., measured OTC activity and protein in mouse cortical tissue, demonstrating a misunderstanding of the urea cycle in brain, which lacks OTC[35]. Interestingly, arginine is transported through the Cationic-transporter family (CAT-1, CAT-3), which are regulated by NMDA receptor activation (and influence the mTOR pathway)[36] and Chan's group did find a large decrease in CAT-1 protein in mutant animals.

The Chan arginase assay protocol differed from the Corraliza protocol slightly at almost every step. These differences may well have affected the sensitivity or reliability of urea detection. While the cells used in the Corraliza protocol were lysed in 0.1% Triton with protease inhibitor cocktail, the tissues used in the Chan protocol were homogenized in 50 mM Tris-HCl, pH 7.4 with the Triton added afterward. Like the Corraliza protocol, the Chan

protocol added 0.1% Triton X-100, but the concentration of Triton was double that of the Corraliza protocol. The Chan protocol activated the ARG with a lower concentration of Mn and used more arginine to start the reaction and incubated longer. The Chan protocol described using a blank reactions, with 25 mM Tris-HCl, pH 9.7 in place of L-arginine to determine background activity. In the Chan protocol, the enzymatic reaction was terminated with a similar addition of 450 ml of acid solution and a similar addition of 9% α–isonitrosopropiophenone then incubated at slightly lower temp 95°C for 30 min instead of 45 min.

Chan Arginase Activity Protocol

1)Homogenize tissue samples in 50 mM Tris-HCl, pH 7.4 containing protease inhibitor cocktail using an Ultra-Turrax T8 disperser (IKA Works, Wilmington, NC, USA) and place on ice.

2)Remove 25uLs tissue homogenate and mix with 50 ul of 0.1% Triton X-100 and incubate at room temperature (RT) for 30 min with shaking.

3)Activate arginase by addition of 50 ul of 25 mMTris-HCl, pH 7.4 and 10 ul of 10 mM $MnCl_2$ and heat at 56°C for 10 min.

4)Start the reaction by the addition of 50 ul of 0.5 M L-arginine (pH 9.7) and incubate for 60–120 min at 37°C.

5)For blank reactions, add 25 uM Tris- HCl, pH 9.7 in place of L-arginine to determine background activity.

6)Terminate reactions by the addition of 450 ul of acid solution (1 H2SO4 : 3 H3PO4 : 7 H2O) followed by the

7)Add colorimetric reagent of 20 ul of 9% aisonitrosopropiophenone (ISPF) (dissolved in 100% ethanol) and incubate at 95°C for 30 min.

8)Cool to RT and determine urea concentration spectrophotometrically by absorbance at 540 nm using a microplate reader (Spectramax M5, Molecular Devices, Sunnyvale, CA, USA) against a standard curve. Express activity as mmol of urea produced per mg of total protein per min.

Wynn arginase activity assay

Like the Chan assay, the Wynn assay was also developed for use in macrophages[37]. Researchers sought a reliable arginase assay to detect enzymatic activity in activated macrophages because ARG1 is a gene that has been used to identify alternative activated macrophages (AAM or M2) and transcription of ARG1 is tightly regulated by exogenous stimuli, including the Th2 cytokines IL-4 and IL-13. Of course, because enzyme activity assays do not differentiate between ARG1 and ARG2, protein and gene expression assays must also be performed to identify which isoform is involved.

The Wynn protocol is optimized (from the Corraliza protocol) to measure urea and therefore indirectly determine arginase activity in whole tissue lysates using a 96 well format. Wynn et al suggested that the hydrolysis portion of the assay can have a variable duration depending on amounts of arginase in the sample, with an extended incubation with substrate for low levels of the arginase enzyme. Wynn and colleagues advised pilot experiments to optimize sample quantity and reaction times, which will differ depending on the type and amount of arginase enzyme in novel cell types and tissues. After extended incubation periods (more than 6 hours), a brown precipitate may form, but Wynn and colleagues did not find this precipitate to interfere with the enzymatic reaction or the detection of urea.

Wynn also advised the use of a multi-channel pipettor to add/mix reagents to improve the uniformity of the colorimetric signal, especially when high concentrations of urea cause the colorimetric assay to develop rapidly. Air bubbles interfere with the readings of the spectrophotometer and should be avoided by careful pipetting

Wynn found that differences in the hydrolysis of arginine have been observed as quickly as 5 to 10 min after incubating activated lysate with arginine substrate solution, and

1 hr is usually more than sufficient. The reaction can be slowed down by diluting all of the activated lysate solutions. The linear range of detection for urea in this assay is reported by the manufacturer of proprietary reagents A and B as 0.01 to 10 mg/ml, but a less sensitive 0.1 mg/ml threshold of detection is common.

According to the Quantichrom packet insert, when the reagents A and B are added to the samples, the reaction proceeds with two steps, 1)the condensation reaction of ortho-phthaldialdedyde with urea, and 2)the rapid reaction with primaquine diphosphate that undergoes rearrangement to yield an intensely colored product, based on a method developed by Jung et al.[38] Ammonium does not interfere with the assay, but high concentrations of hydrogen peroxide (1%) completely block color development and lower concentrations have not been tested.

The Wynn protocol differs from Corraliza in several respects:

1)Activation solution is 1M Mn rather than 10M Mn.

2)Lysis buffer is 0.001% Triton rather than 0.1% Triton x100

3)Colorimetric agent is Quantichrom solution A and B rather than ISPF

4)Standard curve ranges from 20 to 0.04 mg/ml urea rather than 30 to 1.5ug/mL and is made from mixture of lysis buffer, activation solution and substrate solution as well as added urea.

Wynn Arginase Activity Protocol

Reagents
Cultured cells of interest
Iscove's modified DMEM supplemented with 10% fetal bovine serum, penicillin/streptomycin, and L-arginine
1 x PBS

Lysis buffer (see recipe)
Arginase activation solution (see recipe)
Arginase substrate solution (see recipe)
Urea standard solution (see recipe)
Quantichrom urea assay kit (Bioassay Systems, cat. no. DIUR-500)

Whole tissue samples (~100-mg samples)
24-well tissue culture plates
Platform rocker
96-well PCR reaction plate
Thermal cycler
Standard ELISA and PCR plates
Spectrophotometer

To measure arginase activity in cultured cells
1) Set up cultures with ~5 x 10^5 cells per well in Iscove's modified DMEM in 24-well plates. Culture 24 to 48 hr, depending upon arginase expression levels.
2) Remove dead/non-adherent cells by gently aspirating the medium. Rinse wells with 1 ml of PBS and aspirate. Repeat PBS rinse and aspirate fluid completely. Healthy macrophages and fibroblasts should be tightly adherent. If the protocol is done on non-adherent cells such as splenocytes, centrifuge the plate 5 min at 200 x g for each wash/rinse step. After final spin and aspiration, proceed to next step. Supernatants may be retained for other assays.
3) To lyse the cells, add 100 µl lysis buffer per well and gently rock the plate for 15 min at room temperature. Once the cells are lysed, pipet up and down several times and transfer the entire lysate to a 96-well PCR reaction plate. Note: The tissue culture plate with lysis buffer can be frozen overnight at −20°C and thawed at 37°C to enhance the lysis step. Alternatively, the plate can be sealed with paraffin and stored for up to 1 year at −20°C for later use
4) Proceed to Urea Quantification

To measure arginase activity in whole tissues
1) Collect ~100-mg samples of whole tissue and homogenize in 500 µ l of lysis buffer (including the protease inhibitor cocktail). Wynn et al., describe routinely using this technique with normal and fibrotic liver tissues. In theory, it should work with any other tissue of interest. A Precellys 24 (Bertin Technologies) is used to homogenize tissue in MK28 plastic tubes (Bertin Technologies) containing stainless-steel beads. The Precellys is set at 5000 for 15 sec. Other techniques, such as freezing the tissue on dry ice and pulverizing with a mortar and pestle or grinding with a polytron at maximum speed, should also work.

2) Remove debris by centrifuging 20 sec at 5000 x g, room temperature.
3) Dilute samples appropriately in lysis buffer, and proceed to step 4. Homogenized tissue samples, like cell lysates, may be frozen up to 1 year at − 20°C until ready for use.
4) Proceed to Urea Quantification

Urea Quantification

4) Transfer 50 µl of each lysate sample to a new 96-well PCR plate. Add 50 µl of arginase activation solution to each well (providing manganese as a cofactor) and incubate 10 min at 55°C in a thermal cycler.
5) Transfer 25 µl of each activated lysate sample to a new 96-well PCR plate. Add 25 µl arginase substrate solution to each well (providing L-arginine for the enzyme to hydrolyze) and incubate 1hr at 37°C in a thermal cycler. This incubation can be extended up to 24 hr to detect low levels of arginase activity, as long as all samples are incubated for the same duration. A brown precipitate may form after 6 hr of incubation at 37°C, presumably due to reactions with manganese, but does not interfere with enzymatic activity or the subsequent detection of urea.
6) Prepare a blank solution control and a serially diluted urea standard. Use a mix of 1 part lysis buffer, 1 part arginase activation solution, and 2 parts arginase substrate solution as a diluent to match the content of the experimental samples. The concentration of the urea standard must span the range to be measured in the experimental samples. A range from 20 to 0.04 mg/ml, in twofold dilutions, is usually sufficient.
7) Add 5 µl of each reacted sample, the serially diluted urea standard, and the blank solution control to replicate wells of an ELISA plate. Mix together the Quantichrom urea assay kit reagents following manufacturer's instructions at room temperatre (not accurate when chilled), and add 200 µl per well to the ELISA plate.
8) To measure urea concentrations, incubate 2 to 20 min at room temperature in the dark and use a spectrophotometer to read the absorbance at 520 nm. For optimal results, measure absorbance at several time points over the course of the colorimetric reaction.

Arginase activation solution

Mix 50 µl of 1 M MnCl2 (Sigma-Aldrich)
and 250 µl of 1 M Tris·Cl, pH 7.5
in 4.7 ml water to make up a 10 mM MnCl2/50 mM Tris·Cl, pH 7.5 solution.
Store indefinitely at room temperature.

Arginine substrate solution

Add 871 mg of L-arginine to 8.5 ml water.
Adjust pH with ~1 ml of 1 M HCl to pH 9.7 to make up a 0.5 M L-arginine, pH 9.7 solution.
Adjust volume with water to 10 ml.
Store indefinitely at room temperature.

Lysis buffer

0.001% Triton X-100 (Sigma-Aldrich)
1:1000 protease inhibitor cocktail
Mix 5 µl of Triton X-100 in 4.8 ml distilled water and add 200 µl of 25x protease inhibitor cocktail solution (see recipe). Prepare fresh.

Protease inhibitor cocktail solution, 25x

Dissolve 1 Complete Protease Inhibitor Cocktail tablet (Roche) in 2 ml water, vortexing occasionally, to make a 25x solution. Store up to 2 weeks at 4°C, or up to 3 months at −20°C. The protease inhibitor cocktail solution is used for inhibiting serine, cysteine, and metalloproteases.

Solution A

Add 1 part chloramine T solution (Dissolve 7 g of chloramine T in 100 ml deionized water. May be stored for 6 months in the dark at 4°C.) with 4 parts citrate-acetate buffer (to make citrate-acetate buffer: add 57 g sodium acetate.3H2O, 37.5 g sodium citrate.2H2O, 5.5 g H3citrate. H2O to 385 ml of isopropanol (2-propanol), Bring final volume to 1 liter with deionized water. May store indefinitely at room temperature). Prepare fresh before colorization step.

Solution B

Prepare Ehrlich's solution by dissolving 25 g of p-dimethylaminobenzaldehyde with 37.5 ml of 60% perchloric acid. This solution can be stored for up to 8 weeks at 4°C. Mix 15 ml Ehrlich's solution with 65 ml isopropanol. Prepare solution B fresh. Perchloric acid is hazardous and unstable. Consult with the institute's safety officer for appropriate handling and disposal of the solution.

Urea standard solution

Dissolve 500 mg urea (Sigma-Aldrich) into 5 ml of water to make up a 100 mg/ml urea solution. This solution can be stored for up to 1 year at room temperature. Adjust the highest, starting concentration of the urea standard from 100 to 5 mg/ml to match the experimental samples.

Note examples of urea concentrations in biological samples:

The urea concentration (mg/dL) was 12.5 ± 0.9 for commercial 2% reduced fat milk (Kirkland), 35.7 ± 0.1 for Invitrogen fetal bovine serum, 22.1 ± 0.9 for human serum, 22.3 ± 0.2 for human plasma, 31.8 ± 1.1 for rat serum, 42.6 ± 0.1 for rat plasma and 1501 ± 52 for a fresh human urine sample, 0.21 ± 0.03 in a human BAL sample, 0.15 to 2.7 mg/dL in cell culture (from Sigma Quantichrom package insert).

Optimization of the Wynn arginase assay for mouse striatal tissue

Because the literature was in conflict about which arginase was present in brain, it was also not clear what the specific activity of the enzyme might be in our samples. We used the Wynn assay to measure urea in cells and in tissue samples, but obtained unexpected and inconsistent results in both cells and tissue samples between experiments. In retrospect these inconsistent results were due to the lack of arginase in cortical tissue, which is the tissue we had first used, and the very low level of arginase in cells, very close to the limit of detection. We used cortical tissue in these early optimization experiments because it is more abundant, and we did not realize until after the protein experiments, that arginase expression was much lower in cortex than striatum. The cells used were immortalized medium spiny neuron MSN precursers (known as Q7's for the number of CAG repeats in the *Htt* gene) and showed a higher signal for arginase activity than the striatal samples (**Figure 4-15**).

For the arginase enzymatic activity assay, tissue was disrupted on ice with 23_G x 1 needle in lysis buffer (10mM Tris-HCl, in 0.4% Triton-X100 at pH 7.4, supplemented with protease inhibitors: Leupeptin (leupeptin hydrochloride, microbial, Sigma-Aldrich at 1:1000) and Pepstatin-A (microbial, Sigma-Aldrich at 1:1000). The homogenate was centrifuged at 13000 rcf (relative centrifugal force) for 5 min at 4^{O}C and supernatant was used for the activity analysis.

We subsequently realized that the colorimetric reagent continued to change color over time, even when lysate had not been activated or incubated with substrate, though relative amounts of raw absorbance readings did not change.

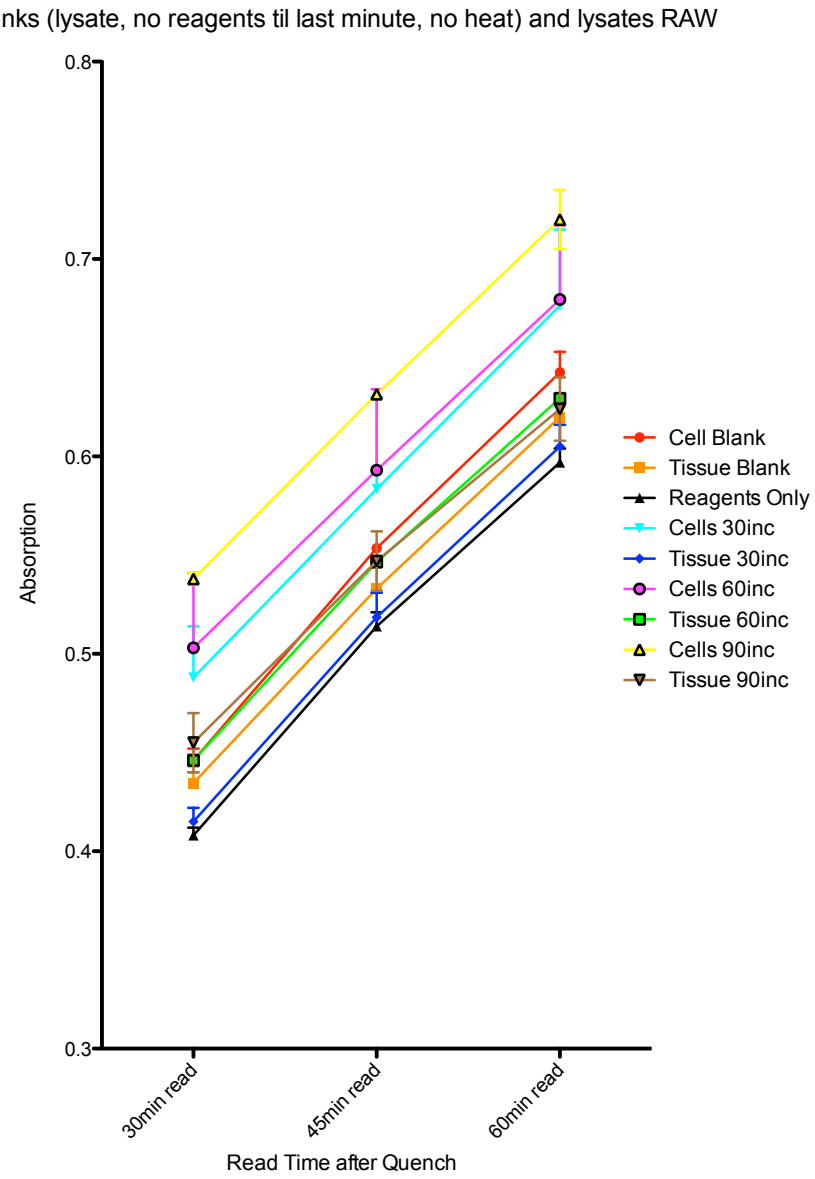

Figure 4-15. Q7 cell lysates and cortical tissue lysates incubated for 30, 60 or 90 mins with substrate at 37°C, then read at either 30, 45 or 60 minutes after plating with colorimetric reagent. Blanks were lysates with activation solution and substrate added just before addition of colorimetric agent, without incubation. Blank tissue sample was not kept on ice.

We then performed an experiment with urea spiked into cell lysates and cortical tissue lysates, read at 30, 45 and 60 mins after addition of the colorimetric assay (**Figure 4-16**). We

found that the 30 minute read was most accurate, with the curve flattening over time after addition of the colorimentric agent, and subsequently determined that a 15 min read was more accurate than a 30 min read. All subsequent experiments were read 15 min after addition of colorimetric agent.

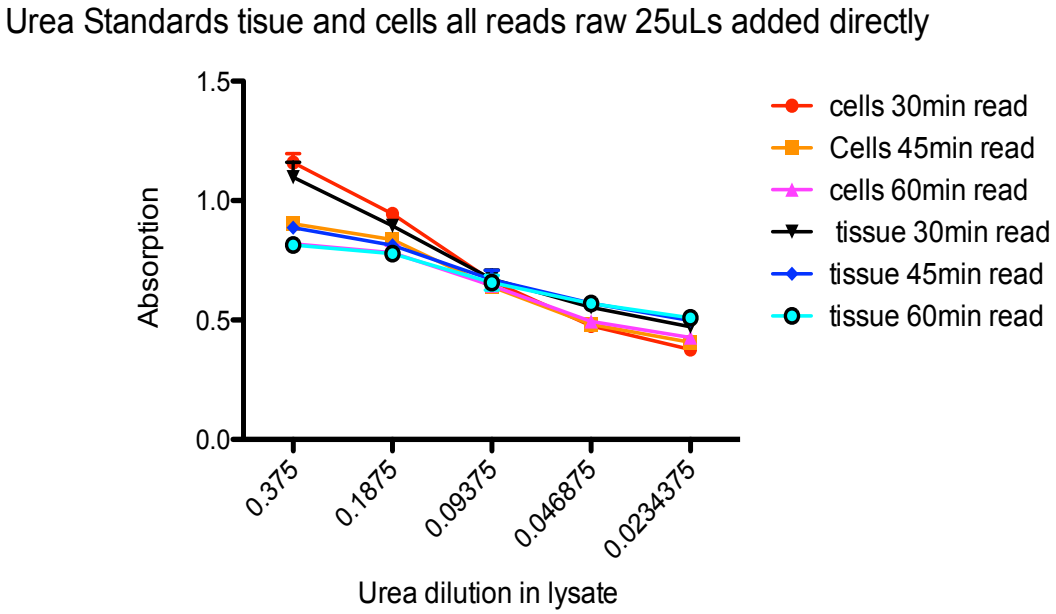

Figure 4-16. Cells lysates and tissue lysates with urea spiked in, read at 30min, 45min or 60min after addition of colorimetric assay.

To account for the amount of biological interference in the OD readings we prepared samples with two kinds of activation solution, one with added Mn (Mn-Supp) and one without Mn (Mn-Unsupp). We then subtracted the readings from the Mn-Unsupp samples from the Mn-Supp samples to obtain the difference (**Figure 4-17**). Again, we confirmed that the earliest reading was the most accurate, as subsequent readings flattened out over time. We also confirmed that the assay was time-dependent (over the time incubated with substrate at 37^{o}) and that signal was higher in cells than in tissue.

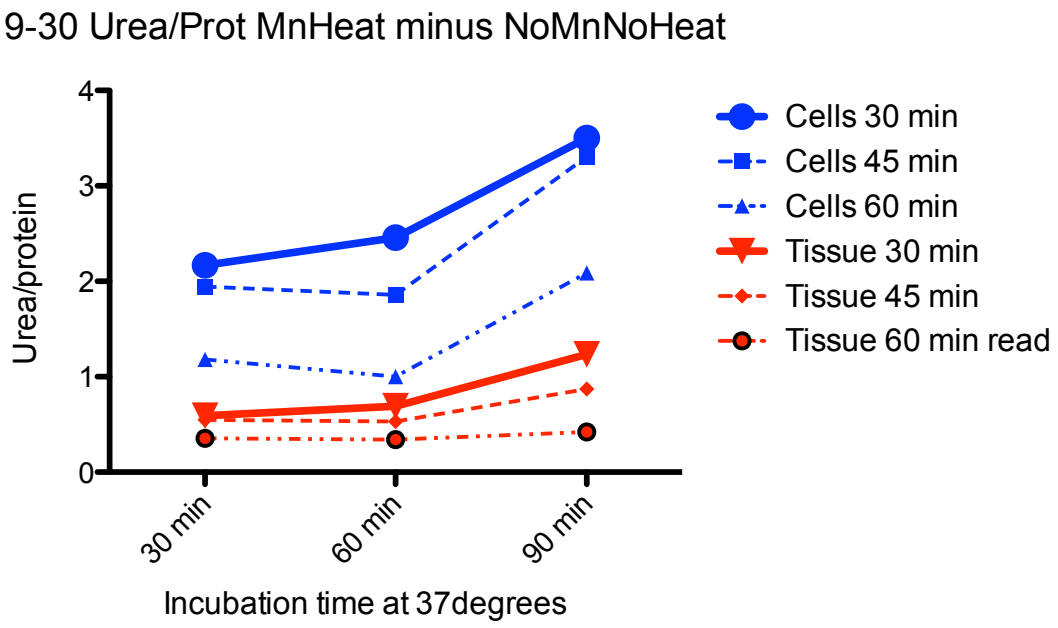

Figure 4-17. Q7 cell lysates and cortical tissue lysates calculated from urea standard curve/protein, read at 30min, 45min or 60min after addition of colorimetric assay.

Striatal samples proved to have more specific enzymatic activity than cortical samples (later confirmed by western blot of protein expression). Ironically, our optimization experiments may have been much more fruitful if we had used kidney instead of cortex, but at that point, we did not realize that the protein in striatum would be ARG2, and we knew that there was much less specific activity of arginase in brain than liver, so we wanted to use brain tissue rather than liver to optimize.

In early optimization experiments, we found that there was an increase in urea over time, in all of the samples, even in the Mn-Unsupp (with only endogenous Mn in the lysate (**Figure 4-18**). We also found that, indeed, activation with Mn-Supp solution *ex vivo* (ie., added to the lysates) produced 2-3 times more enzymatic activity than Mn-Unsupp. Mn-exposure *in vivo* (ie.,

injections to living mice) produced more enzymatic activity as well, but not to the extent that Mn-Supp *ex vivo* could do.

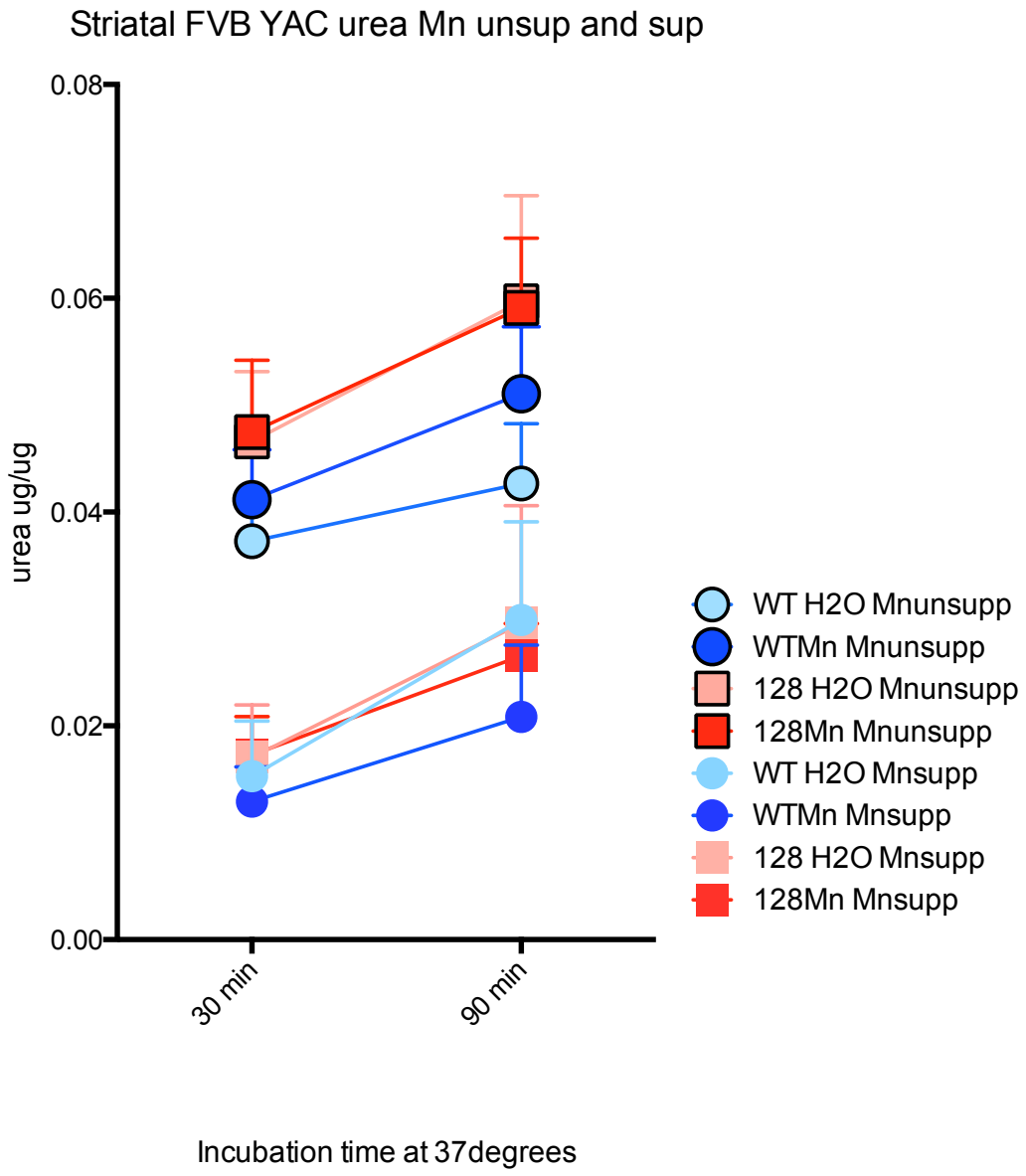

Figure 4-18. Striatal tissue lysates from animals exposed to either Veh or Mn *in vivo*, and either Mn or no Mn supplemented into the activation solution *ex vivo*.

We began to suspect that temperature and time played a larger role than expected in the production of urea, so we began to keep all lysates and reagents on ice, except when they were

in the incubation steps. On the other hand, the colorimetric reagents must be removed from storage in -4^{o} and returned to room temperature, with Reagents A and B kept separately, and mixed shortly before adding to the plate. We had found that the accuracy of the read was also reduced if the colorimetric reagents were too cold (data not shown).

Because timing was so crucial, we realized that loading the plates by genotype could create spurious results. To control for timing and edge effects, we altered the plate design so that genotypes would be intermixed with each other and loaded simulataneously (**Figure 4-19**). The standard wells with the most concentrated urea (2, 3 and 4) were the only wells loaded on an edge. The plates were loaded by column, so Unsupplemented-Vehicle-Treated columns were loaded first, and Supplemented-Mn-Treated columns were loaded last, giving the samples with the most presumed activity, the least amount of time to incubate before reading.

	Unsupp	Unsupp	Supp	Supp	Unsupp	Unsupp	Supp	Supp			
EMPTY	EMPTY	EMPTY	EMPTY	EMPTY	EMPTY	EMPTY	EMPTY	EMPTY	EMPTY	EMPTY	EMPTY
EMPTY	WT Mn 3	WT Mn 3	WT Mn 3	WT Mn 3	128 Mn 3	128 Mn 3	128 Mn 3	128 Mn 3	7	7	10
EMPTY	WT Mn 2	WT Mn 2	WT Mn 2	WT Mn 2	128 Mn 2	128 Mn 2	128 Mn 2	128 Mn 2	6	6	10
EMPTY	Wt Mn 1	WT Mn 1	Wt Mn 1	WT Mn 1	128 Mn 1	128 Mn 1	128 Mn 1	128 Mn 1	5	5	9
EMPTY	WT wat 3	WT wat 3	WT wat 3	WT wat 3	128 wat 3	128 wat 3	128 wat 3	128 wat 3	4	4	9
EMPTY	WT wat 2	WT wat 2	WT wat 2	WT wat 2	128 wat 2	128 wat 2	128 wat 2	128 wat 2	3	3	8
EMPTY	WT wat 1	WT wat 1	WT wat 1	WT wat 1	128 wat 1	128 wat 1	128 wat 1	128 wat 1	2	2	8
EMPTY	EMPTY	EMPTY	EMPTY	EMPTY	EMPTY	EMPTY	EMPTY	EMPTY	EMPTY	EMPTY	EMPTY

	Unsupp	Unsupp	Unsupp	Unsupp	Supp	Supp	Supp	Supp			
EMPTY	EMPTY	EMPTY	EMPTY	EMPTY	EMPTY	EMPTY	EMPTY	EMPTY	EMPTY	EMPTY	EMPTY
EMPTY	128 wat 3	128 wat 3	128 Mn 3	128 Mn 3	128 wat 3	128 wat 3	128 Mn 3	128 Mn 3	10	10	EMPTY
EMPTY	WT wat 3	WT wat 3	WT Mn 3	WT Mn 3	WT wat 3	WT wat 3	WT Mn 3	WT Mn 3	9	9	EMPTY
EMPTY	128 wat 2	128 wat 2	128 Mn 2	128 Mn 2	128 wat 2	128 wat 2	128 Mn 2	128 Mn 2	8	8	EMPTY
EMPTY	WT wat 2	WT wat 2	WT Mn 2	WT Mn 2	WT wat 2	WT wat 2	WT Mn 2	WT Mn 2	7	7	EMPTY
EMPTY	128 wat 1	128 wat 1	128 Mn 1	128 Mn 1	128 wat 1	128 wat 1	128 Mn 1	128 Mn 1	6	6	EMPTY
EMPTY	WT wat 1	WT wat 1	Wt Mn 1	WT Mn 1	WT wat 1	WT wat 1	Wt Mn 1	WT Mn 1	5	5	EMPTY
EMPTY	EMPTY	EMPTY	EMPTY	EMPTY	2	2	3	3	4	4	EMPTY

Figure 4-19. **Plate designs to control for time. A. Badly designed upper plate and B. well-designed lower plate.** The upper plate shows an example of a plate design which could give spurious results if loaded by column, because all wildtype samples precede all mutant samples, and standard wells with the lowest urea have the least time to incubate. The lower plate is well-designed for loading by column to avoid edge effects, and to alternate genotypes to control for timing, duplicating each sample in adjacent columns.

We had been surprised that there were not larger differences in the amounts of urea produced in Mn-exposed animals compared to Veh-exposed animals, so we sought to dialyze out any urea which may have been produced prior to dissection. We used Slide-A-Lyzer® MINI Dialysis Devices, 10K MWCO, 0.5 mL pre-loaded with 14 mL of ice-cold Tris lysis buffer (including the phosphatase cocktails). We added the entire lysed sample in buffer to the dialysis filter tubes, and placed them on ice in -4o on a rocker for 45 min, then transferred each filter tube and contents to a 15cc conical filled with fresh ice-cold Tris lysis buffer, and dialyzed a second time for 45 min.

We found that our experimental results were still sometimes inconsistent, and we attribute some of those inconsistencies to slightly differing pH of our reagents. Arginase binds most tightly to its co-factor Mn and is most efficient at a very basic pH of 9.7[33]. As pH drops, even slightly, it can reduce the output of the enzyme. Future experiments may need to lyse the tissue samples in higher pH and thereby retain the endogenous Mn on the enzyme. This important issue needs further exploration.

To optimize the Wynn assay, we found that the urea standard, including blanks, must be made in dialyzed tissue, because non-tissue blanks (including Lysing buffer, Activation solution and Substrate solution) and changed absorbance over time, and at times had a higher OD than lysates did. After many repeated experiments, we realized that it would have been preferable to use mutant vehicle exposed striatal tissue for the standard curve, as that would have had the lowest endogenous arginase activity, but there was insufficient tissue to make the entire standard curve from the mutant samples. Instead, we mixed all of the vehicle-exposed wild-type and vehicle-exposed mutant lysate which remained after production of the samples, and diluted it to use in the standard curve. Then, we subtracted the value from the wells

without added urea from all of the other values in the standard, and in the sample, as a way to subtract background before the enzymatic activity produced during the assay itself.

Using the optimized Wynn assay, we compared baseline arginase activity in tissue from mice on the FVB background which had neither been exposed *in vivo*, nor supplemented *ex vivo*, and found that striatum exhibited 2-5 times as much arginase activity as cortex, though cortical activity was very close to the bottom of the detectable range (**Figure 4-20**). Furthermore, striatal tissue from mice on the C57B6 background with the HD mutation demonstrated an amount of arginase activity that was below the detectable range, though tissue from wild-types had twice as much arginase activity as that from FVB wild-type mice. In optimizing the Wynn assay, we had attempted to use cortical tissue to optimize the assay because the tissue was more abundant, but in retrospect, this made the task much more difficult, as the amount of enzymatic activity was so low in that tissue.

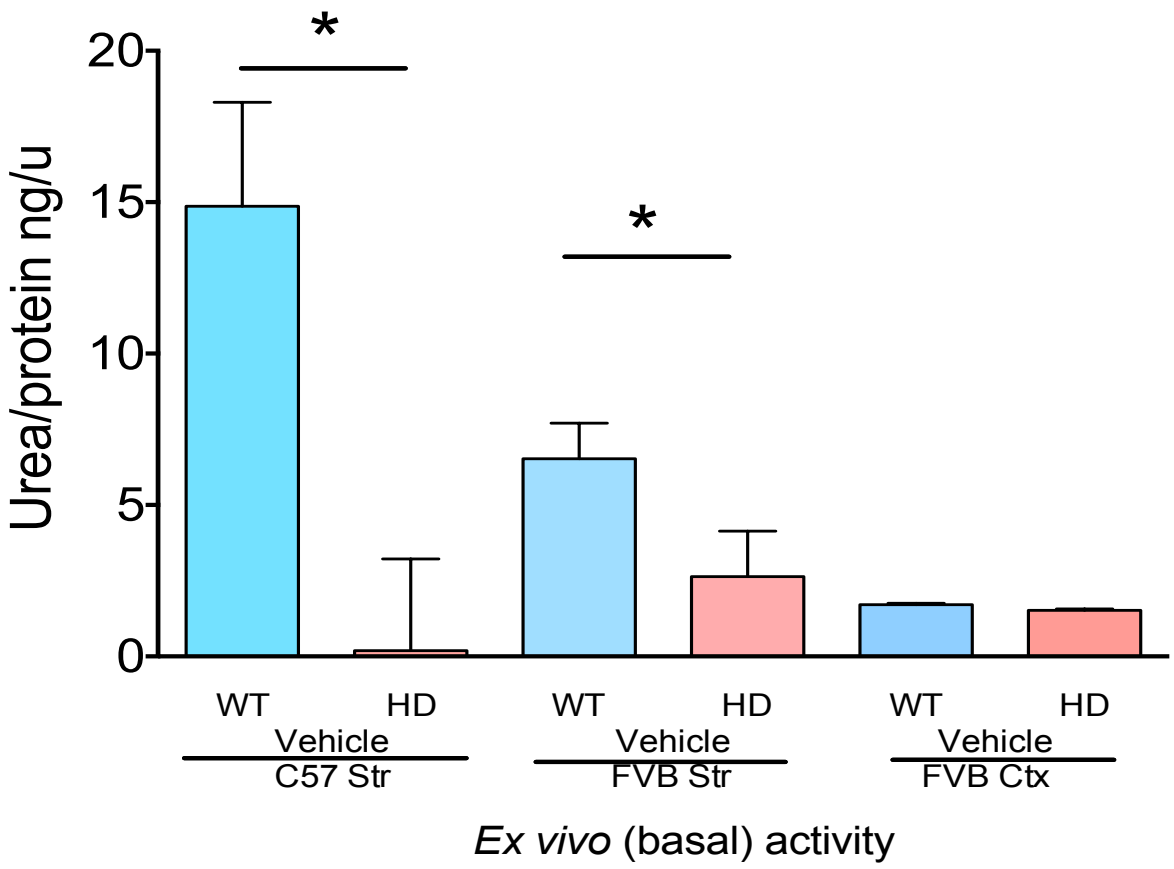

Figure 4-20. Basal deficit in arginase activity in HD striata is significant in both FVB and C57 backgrounds. n=6 for C57 striata, n=12 for FVB striata, n=1 experiment with samples of 3 striata merged for each genotype. These samples were unsupplemented in vitro and unexposed to Mn in vivo.

We also found that cortical arginase activity increased with Mn-exposure *in vivo* and even more so with Mn-supplementation *ex vivo*, indicating the presence of the very small amount of the enzyme, which was supported by our subsequent protein experiments. Mn-activated cortical arginase activity remained lower than striatal baseline, even when mice had been Mn-exposed in vivo (**Figure 4-21**).

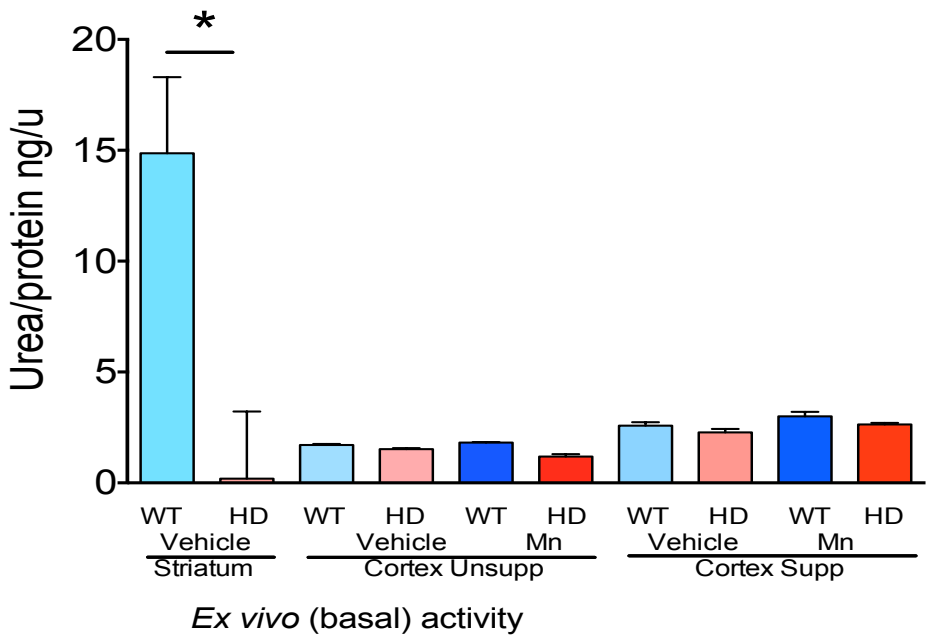

Figure 4-21. Cortical arginase activity less than striatal activity, even in Mn-exposed and Mn-Supplemented. n=6 for C57 striata, and for cortex n=1 experiment with samples of 3 striata merged for each genotype and exposure. These samples were unsupplemented in vitro and unexposed to Mn in vivo.

Our assay was optimized from the Wynn assay in the following ways:

1)We added a dialysis step to remove pre-existing urea

2)We kept all samples and reagents on ice until the stop reaction mix was added

3)We added a Mn-negative (Mn-Unsupp) activation solution so that each sample was measured with only endogenous Mn as well as with the Mn-positive (Mn-Supp) activation solution.

4)We made the urea standard with a mixture of all untreated samples, because we found that there was some kind of biological interference between the lysate and the colorimetric readout, so we wanted to standardize all wells.

5)We loaded duplicate wells for each sample, in a longitudinal design, avoiding edge rows, and used an alternating well design so that we had alternating WT and 128 in each row, with loading horizontal to the row to minimize loading/time effects.

6)We read the plate exactly 15 mins after adding the colorimetric reagent. We read the plate twice, once right side up and once upside down, to be sure that the plate-reader was not dysfunctional. We discarded outlier wells.

7)We subtracted the average zero urea well from every other well when constructing the standard equation and from the samples.

Modified Wynn Arginase Activity Assay Protocol

Reagents

Lysis buffer
1:1000 Protease inhibitor cocktail
10mM Tris-HCl, in 0.4% Triton-X100 at pH 7.4

Protease inhibitor cocktail solution, 25x
Dissolve one Complete Protease Inhibitor Cocktail tablet (Roche 11697498001) in 2 ml water, vortexing occasionally, to make a 25x stock solution. Store up to 2 weeks at 4°C, or up to 3 months at −20°C. The protease inhibitor cocktail solution is used for inhibiting serine, cysteine, and metalloproteases. (Any protease cocktail used should include Leupeptin (leupeptin hydrochloride, microbial, Sigma-Aldrich at 1:1000) and Pepstatin-A (microbial, Sigma-Aldrich at1:1000)

Mn-Supp Arginase activation solution (10 mM $MnCl_2$-4(H_2O)/50 mM Tris-HCl pH 7.5)
Mix 50 µl of 1 M $MnCl_2$-4(H_2O) (Sigma-Aldrich)
and 250 µl of 1 M Tris·Cl, pH 7.5
in 4.7 ml water to make up a 10 mM $MnCl_2$-4(H_2O /50 mM Tris·Cl, pH 7.5 solution.
Store indefinitely at room temperature.

Mn-UnSupp Arginase activation solution (50 mM Tris-HCl ph 7.5)
(50 mM Tris-HCl ph 7.5
Store indefinitely at room temperature.

Arginine substrate solution (0.5 M L-arginine/H_20 pH 9.7)
Add 871 mg of L-arginine to 8.5 ml water.
Adjust pH with ~1 ml of 1 M HCl to pH 9.7 to make up a 0.5 M L-arginine, pH 9.7 solution.
Adjust volume with water to 10 ml.
Store indefinitely at room temperature.

96-well plates (Costar 3370)

Instructions

This assay measures arginase activity on the basis of urea produced from arginine added to tissue homogenate, according to a previously described assay[37], with optimization for mouse striatal tissue homogenates, to permit assessment of enzyme activity in the absence of *ex vivo* supplemented Mn.

Disrupt tissue on ice with 23G x 1 needle in lysis buffer (10mM Tris-HCl, in 0.4% Triton-X100 at pH 7.4, supplemented with protease inhibitors: Leupeptin (leupeptin hydrochloride, microbial, Sigma-Aldrich at 1:1000) and Pepstatin-A (microbial, Sigma-Aldrich at 1:1000).

Centrifuge homogenates at 13000 rcf for 5 min at 4oC and remove supernatant for the activity analysis.

Perform all procedures as quickly as possible, with a maximum of 12 samples (n=3) in a single experiment to minimize the effect of time spent loading plates and tubes. To reduce time:

Design plates to minimize plate- and time-loading effects by alternating wells between genotypes.

Preset two heating blocks to 56^{o}C and 37^{o}C.

Pre-load microcentrifuge tubes with either 20uL of Mn-pos Activation Solution, or 20uL Mn-neg Activation Solution, or 30uL of Arginase Substrate Solution and keep on ice.

Pre-label microcentrifuge tubes and 96-well plates to be loaded quickly with variable-width pipettes.

Prepare tissue samples of approximately 12 mg in 190 uL of lysis buffer (described above), and keep on ice.

Add entire lysed sample in buffer to dialysis filter tubes (Slide-A-Lyzer® MINI Dialysis Devices, 10K MWCO, 0.5 mL) pre-loaded with 14 mL of ice-cold Tris lysis buffer (10mM Tris-HCl, in 0.4% Triton-X100 at pH 7.4)

.

Dialyze samples on a rocker on ice for 45 min, then transfer filter tubes to fresh Tris lysis buffer and dialyze a second time for 45 min.

During dialysis pre-load duplicate micrcentrifuge tubes with one of the following, and keep on ice:

20uL of Mn-pos Activation Solution (10 mM $MnCl_2$-4(H_2O)/50 mM Tris-HCl pH 7.5),

20uL Mn-neg Activation Solution (50 mM Tris-HCl ph 7.5),

30uL of Arginase Substrate Solution (0.5 M L-arginine/H_20 pH 9.7).

After dialysis, move samples into microcentrifuge tubes and keep on ice,

Remove an aliquot and dilute 1:3 into lysis buffer for protein assay.

Begin the enzyme assay by simultaneously adding 20uL of each sample with a variable-width pipette to the microcentrifuge tubes, which had been pre-loaded with 20uL of Mn-pos Activation Solution (Mn-Supp).

Place these tubes immediately in the 56^{o}C heating block for 10 mins.

Add another aliquot of 20uL of each sample to the tubes which had been pre-loaded with 20mL of Mn-neg Activation Solution (Mn-Unsupp), and then place on ice.

At the end of the 10 min incubation period, place both Mn-Supp and Mn-Unsupp tubes in a rack with matching tubes pre-loaded with 30uL of Arginase Substrate Solution

With mulit-channel variable-width pipette, load 30uL from each activated sample (both Mn-Supp and Mn-Unsupp) rapidly into the substrate tubes, and place immediately into the 37^{o}C heating block, to be incubated for 30min.

During this incubation period, prepare the urea standard. Prepare standard on ice in diluted lysate (1:2) from equal amounts of each vehicle-treated sample lysate spiked with urea prepared in Tris lysis buffer and subsequently diluted 1:2 for a range of 1.92mg/mL urea to 0.0075mg/mL with 0mg/mL urea in the final standard tube.

Five minutes before the end of the 37^{o} C incubation period, transfer 20uL of each standard to tubes pre-loaded with 20uL of Mn-neg Activation Solution (Mn-Unsupp) and mix well.

Prepare the Urea Assay Kit mixture A and B (QuantiChrom^{TM} ABIN1000249) and keep at room temperature. Do not chill this mixture

Immediately after mixing, transfer 30uL of each mixture to tubes pre-loaded with 30uL of Arginase Substrate Solution and mix well on ice.

At the end of the 37^{o}C incubation period, arrange sample tubes and standard tubes into a rack matching the design of the 96-well plate. Using multi-channel pipettes transfer 25uL of each sample (and each standard) into duplicate wells.

Add 200uL of the freshly prepared Urea Assay Kit mixture (QuantiChrom^{TM} ABIN1000249) to each well.

Incubate plates in the dark at room temperature for 10-12 min, bubbles were then popped with a needle, and the absorbance was read at 520 nm, exactly 15 min after loading.

After optimization of the modified Wynn assay, we validated it by testing for time-dependence, substrate-dependence and co-factor dependence in kidney and liver tissue homgenates (**Figure 4-22**). We found that this assay was reliable at detecting arginase activity in very small tissue samples within Michaelis-Menten parameters.

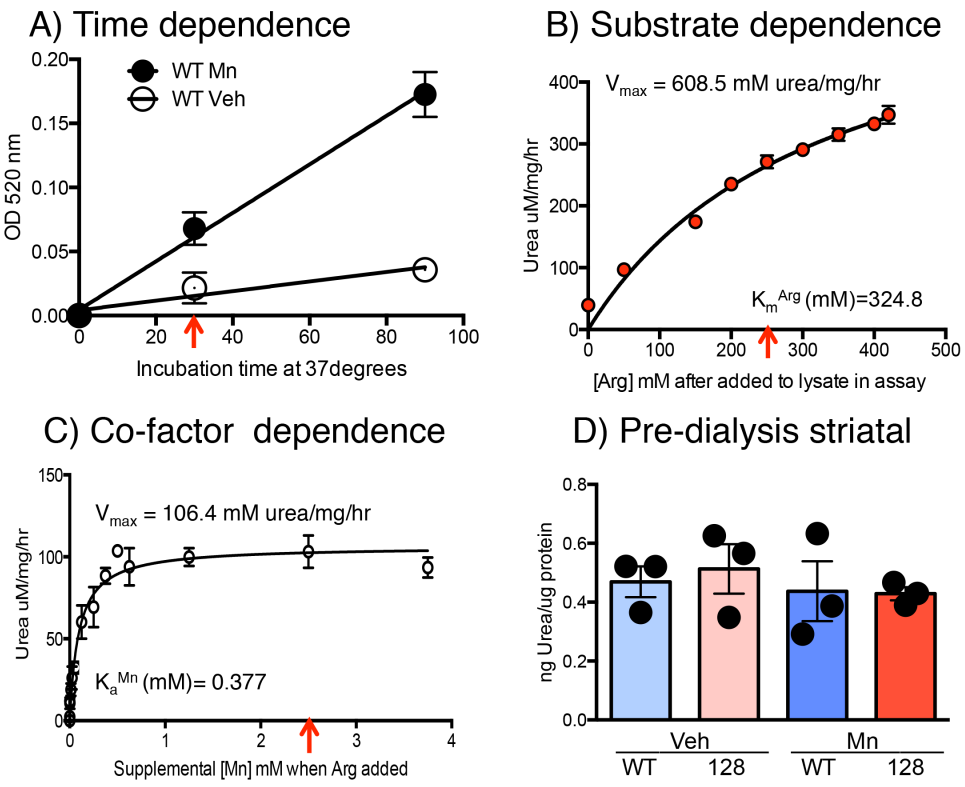

Figure 4-22. The modified Wynn arginase assay[37] is time-, substrate- and co-factor-dependent in tissue lysates. Red arrows in (a-c) indicate parameters used in the assay. (A) Arginase activity is time-dependent (liver tissue, thus primarily ARG1) incubated at 0, 30, and 90 minutes at 37^{o} after addition of substrate solution, subtracting background (raw value at zero time point) from all data points. Significant effect of time by univariate ANOVA: WT Mn [$F(2,6)=146.2$, $p<.0001$], WT Veh [$F(2,6)=15.53$, $p<.0042$]. (B) Arginase activity is arginine-dependent (kidney tissue, thus primarily ARG2), K_m=324.8 mM Arg, V_{max}=608.5 mM urea/mg/hr, urea standards completed without added arginine. (C) Arginase activity is dependent on the co-factor Mn (kidney tissue, thus primarily ARG2). Data shown is arginase activity induced by supplemental Mn, K_a=0.377mM Mn, V_{max}=106.4 mM urea/mg/hr. The increase in arginase activity is not explained simply by the amount of striatal Mn in Mn-exposed animals, because *in vivo* Mn exposure itself is not calculated to raise the concentration of endogenous Mn in the *ex vivo* striatal extracts higher than 0.8 µM in striatum[3]. We used 2.5 mM Mn as in the published assay,[37] which is well above the amount needed to stimulate arginase activity.[39] (D) Extracted urea concentration measured in undialysed striatal samples, FVB, n=3, not significant by two-way ANOVA. Michaelis-Menten parameters calculated with GraphPad Prism.

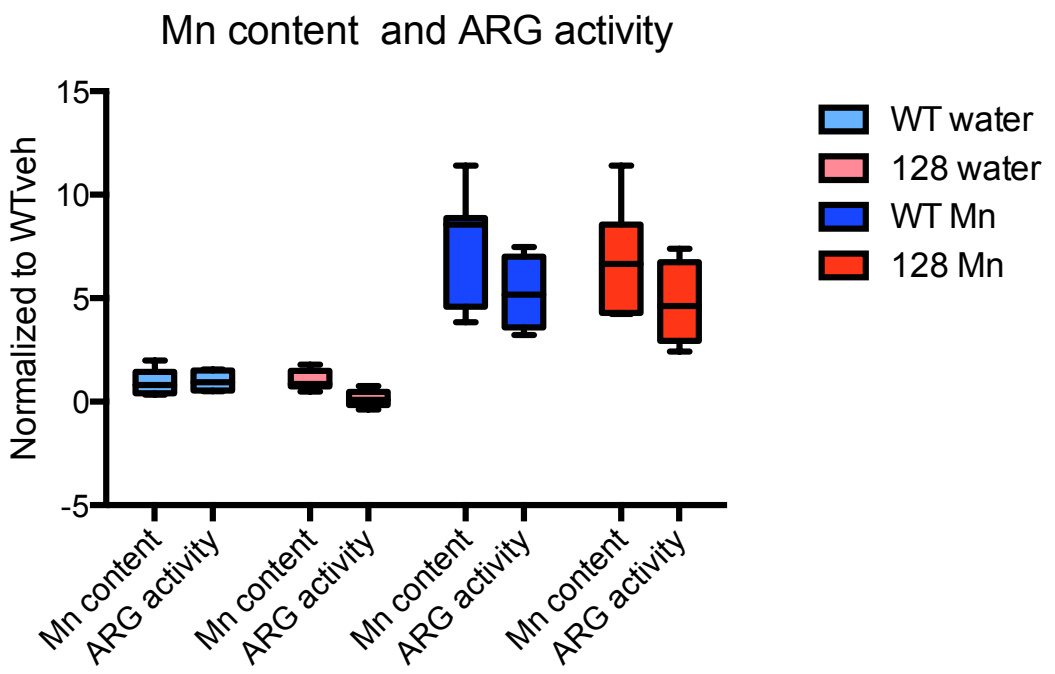

Figure 4-23. Correlation of Mn content as measured by graphite furnace to arginase enzymatic activity as measured by the the Modified Wynn Assay in striatal tissue from FVB mice.

We also found that arginase enzyme activity appears to correlate with Mn content (calculated for different mice with the same genotypes via graphite furnace in prior studies) (**Figure 4-23**).

Agmatinase assay development

We were aware that agmatinase (AGMAT) could play a role in the same pathway as arginase, as a Mn-dependent enzyme, but the literature on agmatinase in rodent brain was even more scanty and conflicting than arginase. By LCMS, we found very low abundance of agmatine (**Figure 5-5**), and by QRT-PCR, we had found almost no mRNA expression of AGMAT in striatal samples although there was detectable genotype-dependent expression of LIMCH1 (**Figure 4-24**) (see discussion about AGMAT and LIMCH1 in **Chapter III**). Still, because agmatinase hydrolyzes agmatine into urea and putrecine, we hoped to optimize the

Wynn urea assay to measure agmatinase activity as well as arginase activity in our striatal samples.

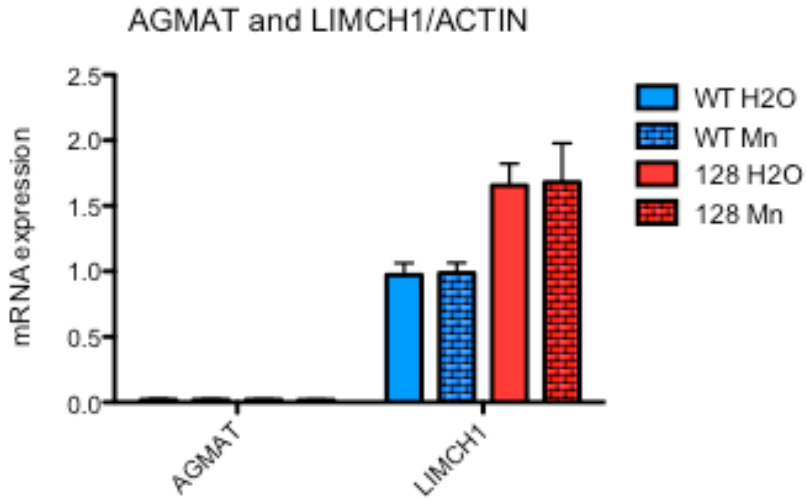

Figure 4-24. AGMAT mRNA expression was undetectable in striatal samples, though LIMCH1 was abundant and increased by genotype, but not affected by Mn exposure. QRT-PCR, n=6, males. Anova for LIMCH1 significant for genotype p=<001. Data presented as means +/- sem.

Most of the handful of researchers studying agmatinase in rodent brain used radioactive 14CO trapping systems to measure agmatinase activity in rodent brain tissue, but Uribe et al,[40].routinely used a urea assay with purified enzyme. The Uribe group uses a protocol with a substrate buffer of 80mM agmatine in 50 mM glycine NaOH at a pH of 9.0, an activation buffer of 2 mM $MnCl_2$ and α-isonitrosopropiophenone as the colorimetric agent,[41] measured by absorbance at 540nm. Incubation is at 37°C. In other papers, the same group used a substrate buffer of 50mM agmatine in 50 mM glycine NaOH at a slightly more basic pH of 9.5.[40]. Because this method was quite similar to the Wynn assay, we altered the arginase protocol to include these an activation buffer of 10mM $MnCl_2$/50mM Tris-Cl, pH 7.5, and a substrate solution of 80 mM agmatine in 50 mM Glycine-NaOH, at a pH of 9.0, but we were

unsuccessful in producing reliable agmatinase activity in striatal samples with this method, However, because of the low agmatine availability and the low agmatinase abundance, it is possible that there is little to no agmatinase activity in striatal tissue from this rodent model.

References

1. Williams BB, Kwakye GF, Wegrzynowicz M, et al. Altered manganese homeostasis and manganese toxicity in a Huntington's disease striatal cell model are not explained by defects in the iron transport system. *Toxicol Sci* 2010; **117**(1): 169-79.
2. Williams BB, Li D, Wegrzynowicz M, et al. Disease-toxicant screen reveals a neuroprotective interaction between Huntington's disease and manganese exposure. *J Neurochem* 2010; **112**(1): 227-37.
3. Madison JL, Wegrzynowicz M, Aschner M, Bowman AB. Disease-toxicant interactions in manganese exposed Huntington disease mice: early changes in striatal neuron morphology and dopamine metabolism. *PLoS One* 2012; **7**(2): e31024.
4. Madison JL, Wegrzynowicz M, Aschner M, Bowman AB. Gender and manganese exposure interactions on mouse striatal neuron morphology. *Neurotoxicology* 2011; **32**(6): 896-906.
5. Wegrzynowicz M, Bichell TJ, Soares BD, et al. Novel BAC Mouse Model of Huntington's Disease with 225 CAG Repeats Exhibits an Early Widespread and Stable Degenerative Phenotype. *J Huntingtons Dis* 2015; **4**(1): 17-36.
6. Hodgson JG, Agopyan N, Gutekunst C-A, et al. A YAC mouse model for Huntington's disease with full-length mutant huntingtin, cytoplasmic toxicity, and selective striatal neurodegeneration. *Neuron* 1999; **23**(1): 181-92.
7. Slow EJ, van Raamsdonk J, Rogers D, et al. Selective striatal neuronal loss in a YAC128 mouse model of Huntington disease. *Human molecular genetics* 2003; **12**(13): 1555-67.
8. Gray M, Shirasaki DI, Cepeda C, et al. Full-length human mutant huntingtin with a stable polyglutamine repeat can elicit progressive and selective neuropathogenesis in BACHD mice. *The journal of neuroscience* 2008; **28**(24): 6182-95.
9. Benn CL, Slow EJ, Farrell LA, et al. Glutamate receptor abnormalities in the YAC128 transgenic mouse model of Huntington's disease. *Neuroscience* 2007; **147**(2): 354-72.
10. Bothe GW, Bolivar VJ, Vedder MJ, Geistfeld JG. Genetic and behavioral differences among five inbred mouse strains commonly used in the production of transgenic and knockout mice. *Genes Brain Behav* 2004; **3**(3): 149-57.
11. Sato Y, Seo N, Kobayashi E. Genetic background differences between FVB and C57BL/6 mice affect hypnotic susceptibility to pentobarbital, ketamine and nitrous oxide, but not isoflurane. *Acta Anaesthesiol Scand* 2006; **50**(5): 553-6.
12. Davie SA, Maglione JE, Manner CK, et al. Effects of FVB/NJ and C57Bl/6J strain backgrounds on mammary tumor phenotype in inducible nitric oxide synthase deficient mice. *Transgenic Res* 2007; **16**(2): 193-201.
13. Wegrzynowicz M, Holt HK, Friedman DB, Bowman AB. Changes in the striatal proteome of YAC128Q mice exhibit gene-environment interactions between mutant huntingtin and manganese. *J Proteome Res* 2012; **11**(2): 1118-32.
14. Dodd CA, Ward DL, Klein BG. Basal Ganglia accumulation and motor assessment following manganese chloride exposure in the C57BL/6 mouse. *Int J Toxicol* 2005; **24**(6): 389-97.
15. Franciosi S, Ryu JK, Shim Y, et al. Age-dependent neurovascular abnormalities and altered microglial morphology in the YAC128 mouse model of Huntington disease. *Neurobiol Dis* 2012; **45**(1): 438-49.

16. Liu P, Fleete MS, Jing Y, et al. Altered arginine metabolism in Alzheimer's disease brains. *Neurobiol Aging* 2014; **35**(9): 1992-2003.
17. Yu H, Iyer RK, Kern RM, Rodriguez WI, Grody WW, Cederbaum SD. Expression of arginase isozymes in mouse brain. *J Neurosci Res* 2001; **66**(3): 406-22.
18. Peters D, Berger J, Langnaese K, et al. Arginase and Arginine Decarboxylase - Where Do the Putative Gate Keepers of Polyamine Synthesis Reside in Rat Brain? *PLoS One* 2013; **8**(6): e66735.
19. Choi S, Park C, Ahn M, Lee JH, Shin T. Immunohistochemical study of arginase 1 and 2 in various tissues of rats. *Acta Histochem* 2012; **114**(5): 487-94.
20. Bernstein HG, Derst C, Stich C, et al. The agmatine-degrading enzyme agmatinase: a key to agmatine signaling in rat and human brain? *Amino Acids* 2011; **40**(2): 453-65.
21. Hansmannel F, Sillaire A, Kamboh MI, et al. Is the urea cycle involved in Alzheimer's disease? *J Alzheimers Dis* 2010; **21**(3): 1013-21.
22. Cederbaum SD, Yu H, Grody WW, Kern RM, Yoo P, Iyer RK. Arginases I and II: do their functions overlap? *Mol Genet Metab* 2004; **81 Suppl 1**: S38-44.
23. Braissant O, Gotoh T, Loup M, Mori M, Bachmann C. L-arginine uptake, the citrulline-NO cycle and arginase II in the rat brain: an in situ hybridization study. *Brain Res Mol Brain Res* 1999; **70**(2): 231-41.
24. Morris SM, Jr., Bhamidipati D, Kepka-Lenhart D. Human type II arginase: sequence analysis and tissue-specific expression. *Gene* 1997; **193**(2): 157-61.
25. Lein ES, Hawrylycz M, Ao N, et al. Genome-wide atlas of gene expression in the adult mouse brain. *Nature* 2007; **445**: 168-75.
26. Iyer RK, Yoo PK, Kern RM, et al. Mouse model for human arginase deficiency. *Mol Cell Biol* 2002; **22**(13): 4491-8.
27. Shi O, Morris SM, Jr., Zoghbi H, Porter CW, O'Brien WE. Generation of a mouse model for arginase II deficiency by targeted disruption of the arginase II gene. *Mol Cell Biol* 2001; **21**(3): 811-3.
28. Konarska L, Tomaszewski L, Rolczyk U. Studies on L-arginase in developing rat small intestine, brain, and kidney. II. Effect of hydrocortisone and thyroxine. *Biochem Med Metab Biol* 1986; **35**(2): 170-8.
29. Spector EB, Rice SC, Moedjono S, Bernard B, Cederbaum SD. Biochemical properties of arginase in human adult and fetal tissues. *Biochem Med* 1982; **28**(2): 165-75.
30. Williams BJ, Du RH, Calcutt MW, Abdolrasulnia R, Christman BW, Blackwell TS. Discovery of an operon that participates in agmatine metabolism and regulates biofilm formation in Pseudomonas aeruginosa. *Mol Microbiol* 2010; **76**(1): 104-19.
31. Corraliza IM, Campo ML, Soler G, Modolell M. Determination of arginase activity in macrophages: a micromethod. *J Immunol Methods* 1994; **174**(1-2): 231-5.
32. Schimke RT. Arginase. In: H. Tabot T, C.W., ed. Methods in Enzymology. London: Academic Press; 1970.
33. Romero PA, Stone E, Lamb C, et al. SCHEMA-designed variants of human Arginase I and II reveal sequence elements important to stability and catalysis. *ACS Synth Biol* 2012; **1**(6): 221-8.
34. Chan CH, Ramirez-Montealegre D, Pearce DA. Altered arginine metabolism in the central nervous system (CNS) of the Cln3-/- mouse model of juvenile Batten disease. *Neuropathol Appl Neurobiol* 2009; **35**(2): 189-207.

35. Wiesinger H. Arginine metabolism and the synthesis of nitric oxide in the nervous system. *Prog Neurobiol* 2001; **64**(4): 365-91.
36. Huang Y, Kang BN, Tian J, et al. The cationic amino acid transporters CAT1 and CAT3 mediate NMDA receptor activation-dependent changes in elaboration of neuronal processes via the mammalian target of rapamycin mTOR pathway. *J Neurosci* 2007; **27**(3): 449-58.
37. Wynn TA, Barron L, Thompson RW, et al. Quantitative assessment of macrophage functions in repair and fibrosis. *Curr Protoc Immunol* 2011; **Chapter 14**: Unit14 22.
38. Jung D, Biggs H, Erikson J, Ledyard PU. New Colorimetric reaction for end-point, continuous-flow, and kinetic measurement of urea. *Clin Chem* 1975; **21**(8): 1136-40.
39. Kuhn NJ, Talbot J, Ward S. pH-sensitive control of arginase by Mn(II) ions at submicromolar concentrations. *Arch Biochem Biophys* 1991; **286**(1): 217-21.
40. Garcia D, Ordenes P, Benitez J, et al. Cloning of two LIMCH1 isoforms: characterization of their distribution in rat brain and their agmatinase activity. *Histochem Cell Biol* 2016; **145**(3): 305-13.
41. Quinones M, Cofre J, Benitez J, et al. Insight on the interaction of an agmatinase-like protein with Mn(2+) activator ions. *J Inorg Biochem* 2015; **145**: 65-9.

Chapter V

Impact of Mn and HD on the Urea Pathway

Note: Much of this chapter have been submitted for publication and is under review as the following:

Bichell TJV, Wegrzynowicz M, Tipps KG, Bradley EM, Uhouse MA, Bryan M, Horning K, Fisher N, Dudek K, Halbesma T, Umashanker P., Stubbs AD, Holt H, Kwakye G, Tidball AM, Colbran RJ, Aschner M, Neely MD, Di Pardo A, Maglione V, Osmand A, Bowman ABB. Reduced bioavailable manganese causes striatal urea cycle pathology in Huntington's disease mouse model. *Under Review*.

Author contributions. Studies were conceived and designed by T.J.V.B., M.W., R.C., M.A., A.O. and A.B.B. Experiments were performed by T.J.V.B., M.W., K.G.T., E.M.B., M.A.U., N.F., K.D., T.H., P.U., A.D.S., H.K.H. and A.O. with contributions from R.C. for enzyme assays; G.K. for western blots; A.M.T. for QRT-PCR; and A.D. and V.M. for R6/2 experiments. Data analysis, interpretation and hypotheses by T.J.V.B., M.W., M.B., K.H., M.D.N., R.C., M.A., A.O. and A.B.B. The paper was written by T.J.V.B., M.W. and A.B.B. and was edited by the other authors.

Urea cycle disruption in HD

Urea, one of the major end products of protein catabolism, is primarily produced in the mammalian liver, and secreted by the kidneys. However, a partial urea cycle also exists in brain. Alterations in Mn bioavailability have the potential to disrupt the urea cycle, affecting at least three of the enzymes involved in the pathway. The neuronal urea cycle contains the Mn^{2+}-dependent enzymes; ARG1, ARG2 and AGMAT. In brain, the urea cycle is only partial; neurons lack the mitochondrial enzymes carbamoylphosphate synthetase (CPS) and ornithine carbamoyltransferase (also known as ornithine transcarbomolase, OTC) and thus brain tissue is incapable synthesizing arginine *de novo*. Neurons are also unable to dispose of waste nitrogen (reviewed by Wiesinger[1]), and urea must be transported out of the region via urea transporters. Arginase hydrolyzes arginine into ornithine and urea, but arginine can also be converted into the signaling peptide, nitric oxide, by nitric oxide synthase (NOS), which will be discussed below (**Figure 5-1**).

Indeed, recent studies have shown dysregulation of urea cycle metabolites in HD patients, both peripherally[2-4] and in post-mortem brain samples[5]. Because of the lack of OTC and CPS in brain, one of the main functions of the neuronal urea cycle is the regulation of nitric oxide[1], which has been shown to be altered in HD[1,6,7]. An HD mouse model on a high-arginine diet exhibits earlier onset of symptoms[8] and patients with HD infused with arginine demonstrate an abnormal growth hormone response[9]. These studies suggest neuronal urea cycle abnormalities in the presence of mutant HTT, however brain arginases and agmatinases have not been examined in HD models (**Figure 5-2 A, B**).

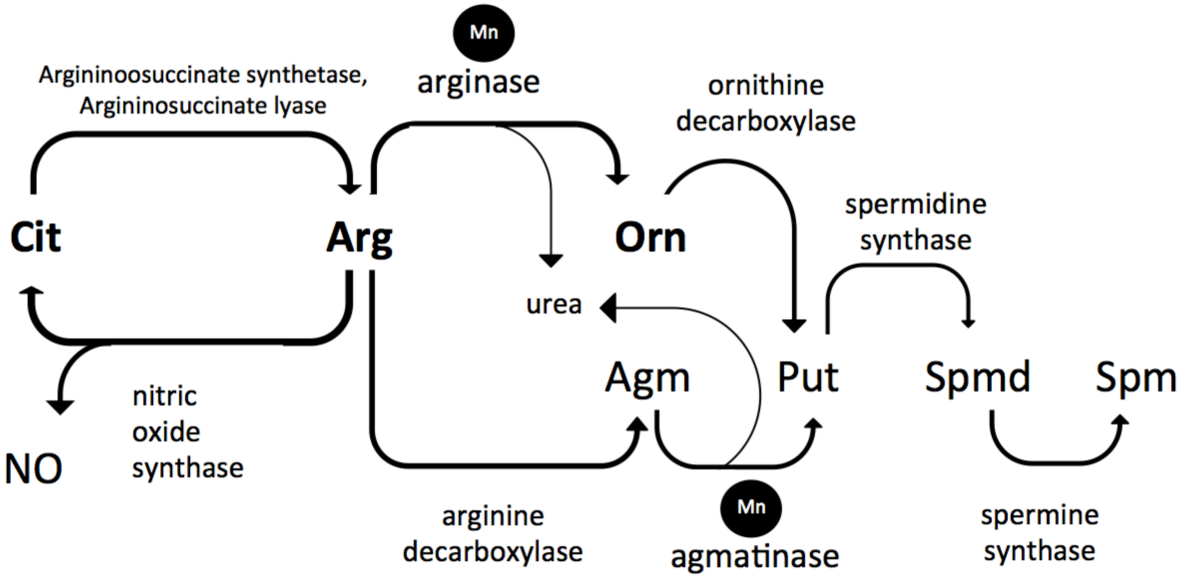

Figure 5-1. The partial urea cycle as it exists in brain, with related nitric oxide and polyamine pathways. Metabolites abbreviated as: Nitric oxide (NO), Citrulline(Cit), Arginine (Arg), Ornithine (Orn), Agmatine (Agm), Putrecine (Put), Spermidine (Spmd), Spermine (Spm).

The urea cycle disregulations found in HD patients reveal an excess of neuronal urea and deficient ornithine[5,10], while a reduction would be expected if deficiency of Mn caused a reduction in ARG activity **(Figure 5-3**). This contradiction could be explained by an alteration

in the ability of urea transporters to remove neuronal urea effectively. Indeed, Solute Carrier Family 14 Member 1 (SLC14A1) a gene for a urea transporter is the most overexpressed gene in HD post-mortem caudate and cortex[11]. In fact, it is possible that excess urea is a signaling mechanism to restrict the influx of Mn, and thereby reduce ARG activity. This issue has not been studied.

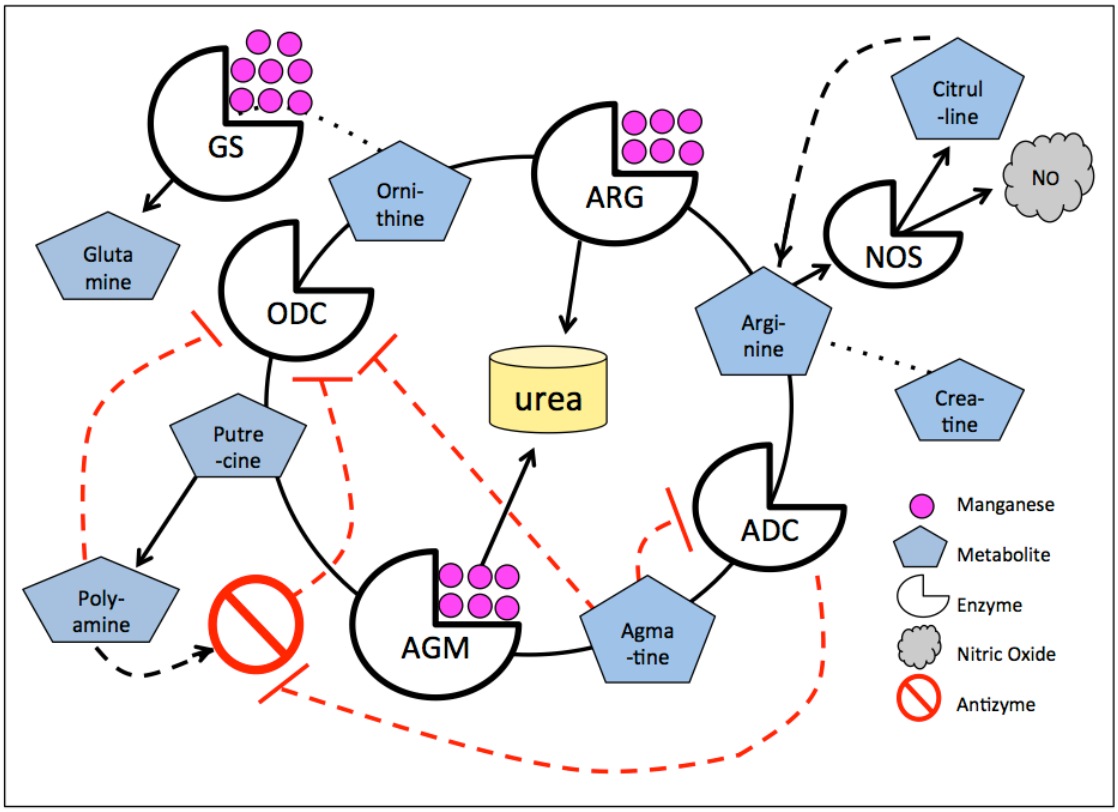

Figure 5-2. The urea cycle is influenced by Mn, which is an essential cofactor for three associated enzymes: Arginases (ARG), Agmatinases (AGM) and Glutamine Synthetase (GS). Arginase pathway related metabolites are altered in HD striatum; and Mn exposure ameliorates this phenotype. (A) Representation of the urea cycle in WT striatum with the presence of adequate Mn (Note: ARG is a homotrimer with 2 Mn ions per monomer, AGM is a hexamer composed of dimers, and GS is composed of 8-12 identical subunits, each with two Mn ions, though Mg can substitute for Mn in GS).

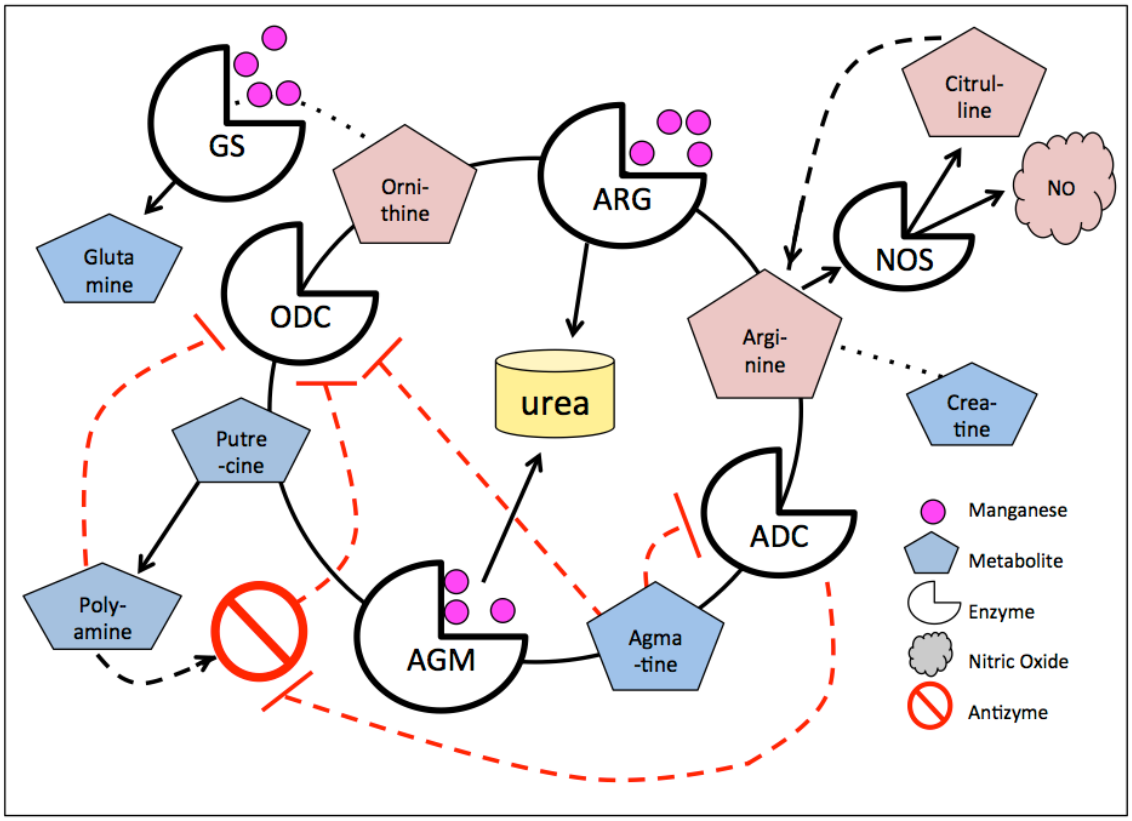

Figure 5-3. In HD, reduced Mn bioavailabilty causes alterations in part of the neuronal urea cycle. Representation of the striatal urea cycle in the HD model with reduced bioavailable Mn, resulting in increased metabolites (indicated in pink).

Agmatine has recently been implicated as a signaling molecule with connections to mood disorders, schizophrenia and aging[12,13], but agmatinase may not be functional in rodent brain, even if it does play a role in human tissue[14]. At any rate, it is unlikely that a Mn-deficiency would affect agmatine levels because the polyamine pathway is so tightly regulated (**Figure 5-2 and Figure 5-3**). The production and activity of ornithine decarboxylase (ODC) is triply controlled: by the polyamines themselves[15], as well as by agmatine[16], and even more so by an antizyme[17] (reviewed by Perez-Leal[18]). ODC is induced by growth-promoting stimuli (insulin, EGF and others) to decarboxylate ornithine to produce putrecine. The polyamines exert a direct translational inhibition on ODC[18] and they also induce synthesis of antizyme

(through an unusual ribosomal frameshift), which binds to ODC and leads to its proteasomal degradation[19].

The location of ARG1 and ARG2 in neurons and brain tissue is disputed, with some studies describing ARG1 in brain, and others ARG2 (see **Chapter 4** for a full discussion of this issue), although many protein antibodies may have cross-reactivity between the two isoforms, which share almost 50% homology[20]. ARG1 is cytosolic and is a marker for microglial activation in many models (though not in mice) and it is found primarily in liver, though it has been implicated in the cortical degeneration in Alzheimer's disease[21]. ARG2 is mitochondrial, and is found primarily in kidney, though ARG2 mRNA expression is upregulated in D2-containing neurons, which are the first to degenerate in HD[22].

Arginase requires six Mn^{2+} ions per homotrimer, and except for Co^{2+}, other essential metals cannot substitute for the co-factor, as they do for most of the other Mn-dependent enzymes. The optimal pH for arginase activity is very alkaline (9.5), with activity dropping precipitously as pH drops, causing the enzyme to become relatively inactive at cytosolic pH (7.2)[23].

AGMAT is difficult to detect in rodent brain but there is an agmatinase-like protein (ALP) that has recently been identified by Uribe, *et al*[24]. ALP is likely to be an isoform of the protein LIM and Calponin Homology Domains 1 (LIMCH1)[24], which is ubiquitous in brain tissue, and may or may not be Mn-dependent[25,26].

We sought to identify whether or not an early, pre-gliostic Mn-deficiency would reduce striatal ARG activity, a condition which could lead to much of the degeneration seen in HD through the disruption of processes downstream of the neuronal urea pathway. We used a well-studied mouse model, the YAC128 to investigate this phenotype *in vivo*. To assure that the

background of the mouse was not a factor, we replicated all of our experiments in two different mouse backgrounds, described in **Chapter 4**.

Indeed, the data contained in experiments described in this chapter link the bioavailability manganese to the neuropathology of HD. This is the first evidence demonstrating that an isolated regional deficit in the bioavailability of an essential nutrient contributes to the selective neuropathology of that region; and further suggests the novel idea that Mn-repletion may be therapeutic for HD patients.

Previous studies have shown that the pathogenic mutation in HD is associated with stark resistance to Mn accumulation/toxicity and reduced molecular responses to Mn in striatal neurons and striatal cell models following Mn exposure (see **Chapter 3**). With this new work, we have sought to understand whether the decreased responsiveness to Mn exposure is a consequence of a basal deficit in bioavailable manganese that contributes to HD neuropathology.

Here we report *in vivo* and *ex vivo* evidence of a urea cycle metabolic phenotype in a prodromal HD mouse model. Further, either *in vivo* or *in vitro* Mn supplementation reverses the urea-cycle pathology by restoring arginase activity. We show that ARG2 is the arginase enzyme present in these mouse brain models, with ARG2 protein levels directly increased by Mn exposure. ARG2 protein is not reduced in the prodromal stage, though enzyme activity is reduced, indicating that altered Mn bioavailability as a cofactor leads to the deficient enzymatic activity. These data support a hypothesis that mutant *HTT* leads to a selective deficiency of neuronal Mn at an early disease stage, contributing to HD striatal urea-cycle pathophysiology through an effect on ARG2.

This is the first study to uncover altered neuronal manganese biology in the absence of an exogenous Mn exposure. This study further identifies a specific neuropathological feature of HD that is reversed by increasing brain Mn levels and directly links this recovery to restoration of a Mn-dependent enzymatic activity. Finally, our findings contribute to an understanding of the importance of neuronal metal handling in general, and in particular, as to its effect on the arginase pathway/urea cycle in the brain.

Urea cycle metabolites are increased in HD model striata and normalized with Mn exposure.

We measured urea cycle related metabolites in striatal brain tissue via liquid chromatography mass spectroscopy (LCMS). We found significantly increased arginine (Arg), citrulline (Cit) and ornithine (Orn) levels in vehicle-exposed HD versus WT striatum **(Figure 5-4)**. All three of these metabolites were normalized in HD striatum by Mn exposure. Mn evoked no change in Cit or Orn in WT, but both WT and HD animals had significantly reduced Arg with Mn. Metabolites further downstream from arginase, including agmatine (Agm), were not affected (**Figure 5-5**). We hypothesized that reduced Mn bioavailability in HD striatum underlies this metabolic phenotype by restricting arginase activity, and that *in vivo* exposure of the HD mice to its cofactor Mn would restore arginase enzymatic activity.

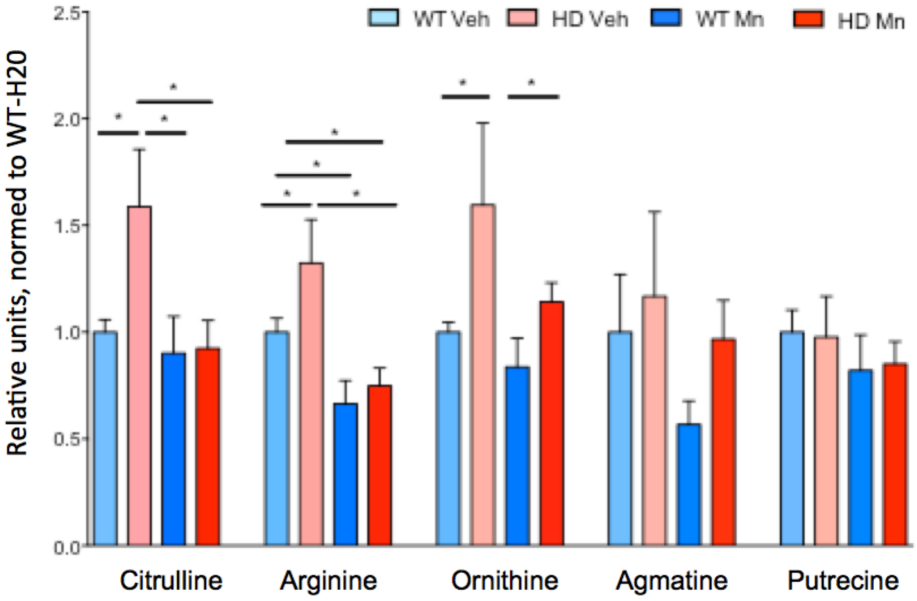

Figure 5-4. Urea cycle metabolites are altered in an HD mouse model and normalized following either *in vivo* Mn exposure or *ex vivo* Mn supplementation. Metabolites measured by LCMS, striatum, n=6-8. Data presented as ±sem, *p< .05, **p< .01, ***p< .001, ****p< .0001, *post-hoc* binary comparisons by t-test following a significant (p=< .05) ANOVA.

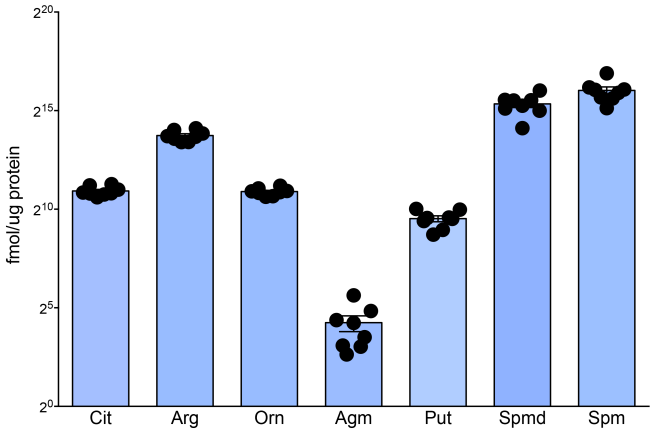

Figure 5-5. Arginine (Arg) is the most abundant of the direct urea cycle metabolites found in striatum and agmatine (Agm) is the least [citrulline (Cit), ornithine (Orn), putrecine (Put)]. Related metabolites, spermidine (Spmd), spermine (Spm), though more abundant, were not significantly affected by genotype or exposure. WT, vehicle-exposed, measured by Laser Coupled Mass Spectroscopy (LCMS), normalized to homo-agmatine, fmol/ug, n=6-8. Data are presented as means ±sem on $\log^2$ scale.

Striatal arginase enzyme activity is reduced in the HD model mice

We directly assessed *ex vivo* arginase activity by customizing an established assay [27] to allow measurement of basal arginase activity in mouse striatal tissue extracts in the absence of *added* Mn **(See Chapter 4)**. Basal arginase activity was approximately 10-fold higher in striatal extracts than in cortical extracts (**Figure 5-6**). Consistent with our hypothesis, basal arginase activity was reduced in striatal extracts from HD mice in both FVB/NJ (FVB) and C57BL/6J (C57) backgrounds **(Figure 5-6 and Figure 5-7A)**, but not in cortical extracts. The deficit in HD striatal arginase activity was rescued by *in vivo* Mn exposure, which increased enzymatic activity in the HD model to levels observed in WT mice **(Figure 5-7 A)**. An inadequate bioavailability of Mn in HD striatum likely underlies this enzymatic deficit, as *in vitro* addition of Mn after tissue extraction eliminated the genotype difference in enzyme activity, increasing arginase activity in both vehicle and Mn exposed animals **(Figure 5-7B, Figure 5-8)**.

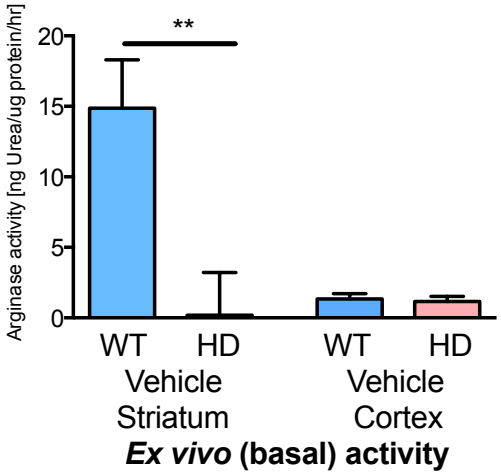

Figure 5-6. Arginase enzymatic activity is altered at baseline in HD model striatum but is higher in striatum than cortex. Vehicle-only striatal arginase activity (n=6 mice, 2 experiments, C57), and cortical (n=2 experiments, mixed C57, FVB, ns). Data presented as ±sem, *p< .05, **p< .01, ***p< .001, ****p< .0001, *post-hoc* binary comparisons by t-test following a significant (p=< .05) ANOVA.

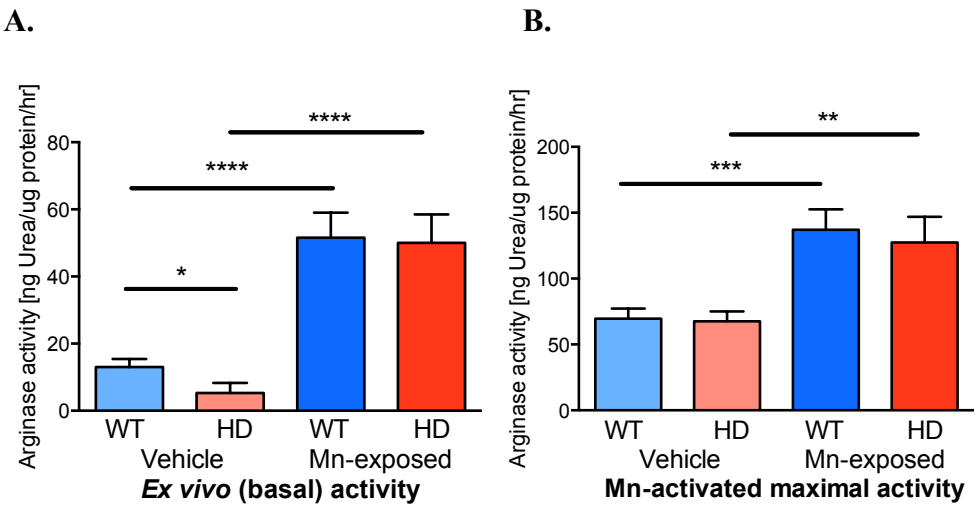

Figure 5-7. Arginase enzyme activity is altered in HD mouse model and normalized following either *in vivo* Mn exposure or *ex vivo* Mn supplementation. (A) Arginase activity, Vehicle (Veh): n=18 mice, 6 experiments), Mn-exposed: n=12 mice, 4 experiments, FVB. (B) Same samples subsequently activated with Mn *ex vivo.* Data presented as ±sem, *p< .05, **p< .01, ***p< .001, ****p< .0001, *post-hoc* binary comparisons by t-test following a significant (p=< .05) ANOVA.

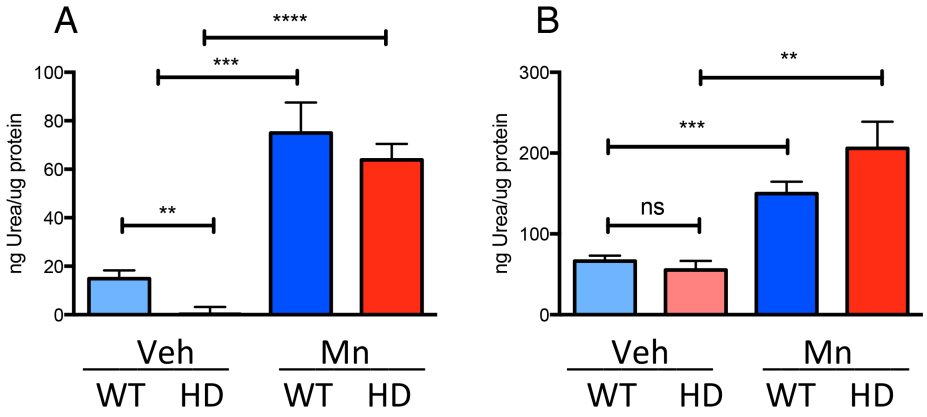

Figure 5-8. Reduced striatal arginase enzyme activity at baseline is also normalized in C57 background following either *in vivo* Mn exposure or *ex vivo* Mn supplementation. (A) Arginase activity, Vehicle (Veh): n=6 mice, 2 experiments). (B) Same samples subsequently activated with Mn *ex vivo.* Data presented as ±sem, *p<.05, **p<.01, ***p<.001, ****p<.0001, *post-hoc* binary comparisons by t-test following a significant (p=<.05) ANOVA.

ARG2 protein increased with Mn exposure, but was not reduced at baseline

To ascertain whether changes in arginase protein levels contribute to changes in enzyme activities at this prodomal stage, we measured striatal ARG1 and ARG2 by western blot. ARG1 was undetectable in all tested brain tissues, while ARG2 was detected in all but cerebellum **(Figure 5-9 A-D, Figure 5-11)**. Striatal ARG2 levels were unaltered in HD mice at this prodromal stage; though surprisingly, *in vivo* Mn exposure increased ARG2 levels in both WT and HD mice (~3-fold in striatum) **(Figure 5-9, A-D, Figure 5-10, Figure 5-11)**. Reflecting the increased enzyme activity levels, ARG2 protein was much more abundant in striatum than in cortex **(Figure 5-9, B)**. The level of ARG2 protein was almost as high in hippocampus as in striatum, and ARG2 was significantly increased by Mn exposure across all brain regions where it was detected. AGMAT was undetectable in these mouse brain tissues, and LIMCH1 was unchanged by Mn-exposure and genotype, corroborating findings on ALP [28] **(Figure 5-9 B, C, Figure 5-11**).

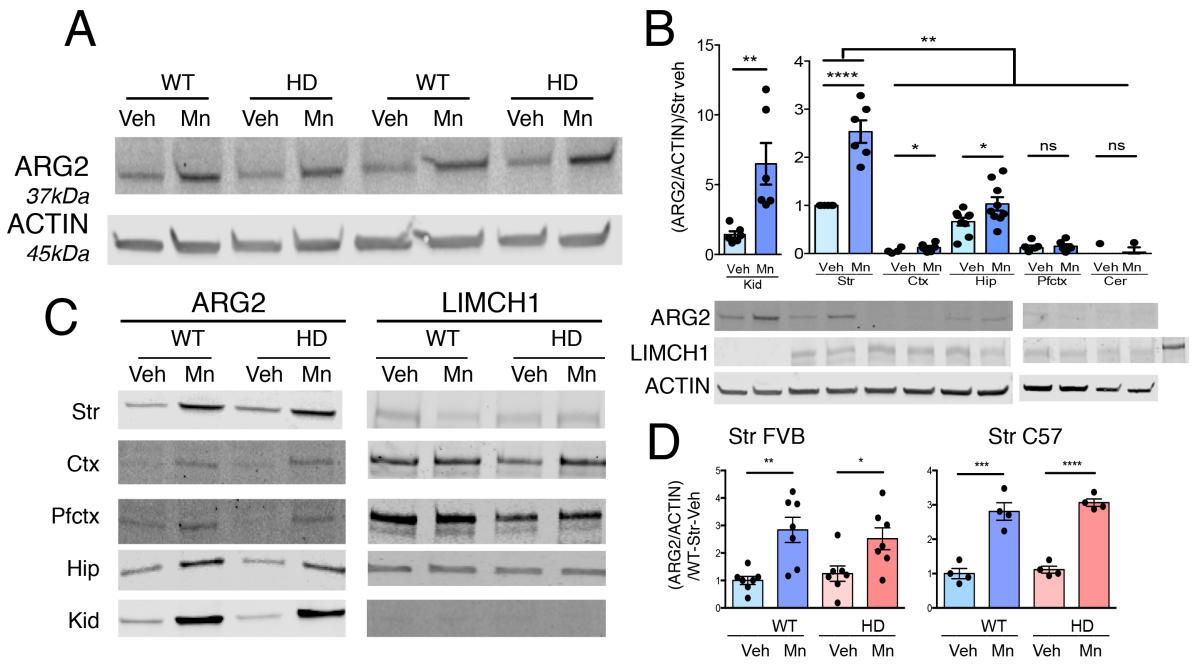

Figure 5-9. ARG2 protein levels are similar in brains of HD and WT mice and elevated by Mn-exposure; ARG1 is undetectable. (A) ARG2, C57 striatum (str). (B) Relative ARG2 protein; WT kidney (Kid), Str, cortex (Ctx), hippocampus (Hip), prefrontal cortex (Pfctx), cerebellum (Cer), FVB, n=6-9. LIMCH1 protein expression is similar across tissues, though neglible in kidney. (C) ARG2 and LIMCH1, FVB. 40mgs each lane. (D) Quantification of ARG2/ACTIN, normed to WT Veh, FVB Str n=7, C57 Str n=4. IHC, representative striatal images closest to average for genotype. (E) Immunohistochemistry (IHC) for ARG2 revealed a substantially increased signal in Mn-exposed striatum in both genotypes and a punctate pattern consistent with its reported mitochondrial localization in other tissues [29]. Data presented as ±sem, *p< .05, **p< .01, ***p< .001, ****p< .0001, *post-hoc* binary comparisons by t-test following a significant (p=< .05) ANOVA.

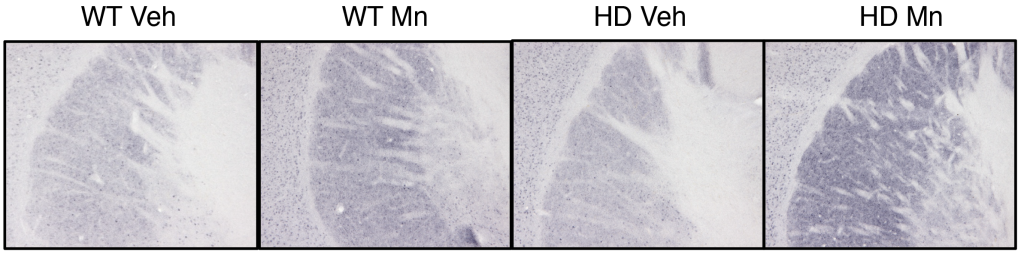

Figure 5-10. Immunohistochemistry (IHC) for ARG2 revealed a substantially increased signal in Mn-exposed striatum in both genotypes and a punctate pattern consistent with its reported mitochondrial localization in other tissues[29,30].

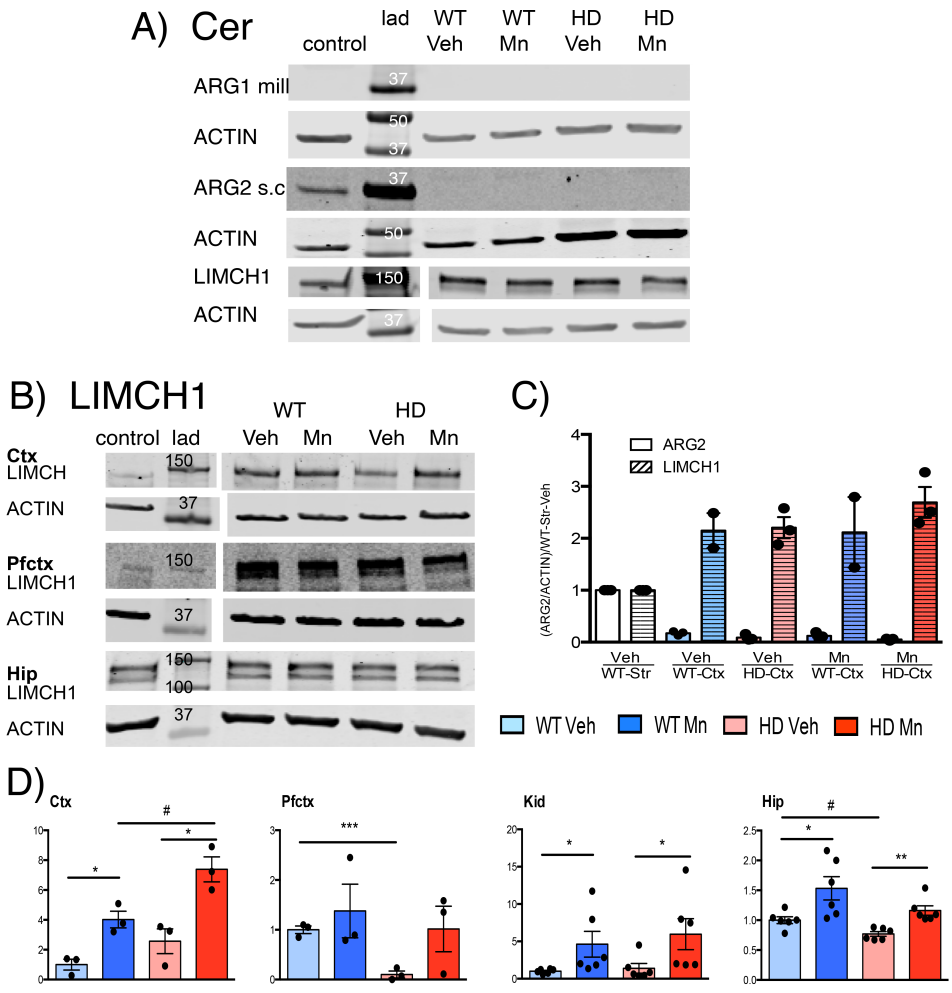

Figure 5-11. Neither ARG1 nor ARG2 protein detectable in cerebellum (Cer). LIMCH1 detectable in all brain regions tested but protein levels are unaffected by genotype or Mn exposure. (A) ARG1 (ab91279) and ARG2 (sc-20151) in cerebellum. LIMCH1 (Abcam ab96178 at 150kDa). Striatal tissue used as control. (B) LIMCH1 in cortex (Ctx), Pfctx, and hippocampus (Hip), 40mgs/lane of each tissue, striatal tissue used as control (Abcam ab96178). (C) Quantification of LIMCH1 vs. ARG2 in cortex, normalized to Str WT Veh, n=3. (D) Quantification of ARG2 protein (sc-20151), FVB kid (n=6, *p=.05), FVB pfctx (n=3, ***p=.001), FVB ctx (n=3 *p=.01, #p=.028), FVB hip (n=6, *p=.0253, **p=.0013, #p=.0076), representative blots shown in Figure. 5-9 C. Ctx and Pfctx protein levels very low relative to Str (see Figure. 5-9 B). Data are presented as means ±s.e.m *post-hoc* binary comparisons by t-test following a significant (p=<.05).

Though ARG2 protein levels were not reduced in the prodromal stage of this YAC128Q HD model, ARG2 protein was significantly reduced in another HD mouse model (the R6/2) at a more advanced disease stage **(Figure 5-12)** in both striatum and hippocampus. LIMCH1 protein was unchanged by genotype in these tissues.

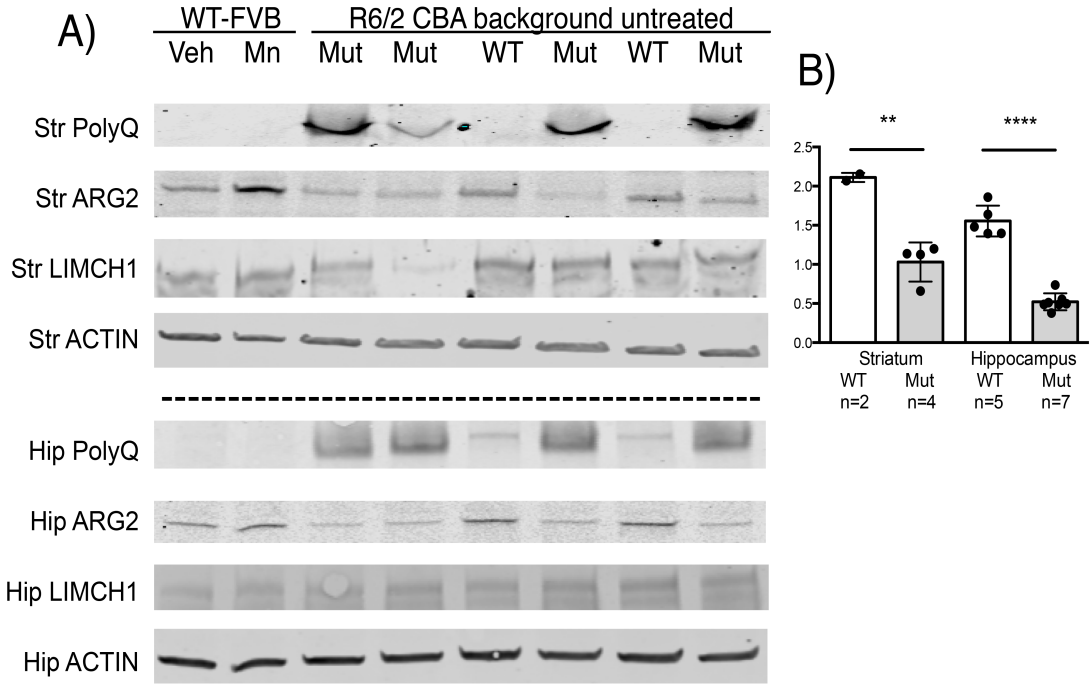

Figure 5-12. Model of HD at a symptomatic stage [the R6/2 at 12 weeks[31,32]] exhibits reduced ARG2 protein in striatum and hippocampus, while LIMCH1 protein is unchanged by genotype. (A) R6/2 striatum (str) and hippocampus (hip), same mice both regions, unexposed, 13 weeks, mixed gender, 40mgs, Poly-Q (MAB1574/IC2), ARG2 protein (sc-20151), LIMCH1 (ab96178). Representative blots. (b) Quantification of ARG2 in samples described in (a) normed to ACTIN and FVB-WT-Str-Veh on each blot. Data shown as ±sem, *post-hoc* binary comparisons by t-test following a significant (p=<.05), **p=<.01, ****p<.0001.

Arg2 mRNA expression did not increase with Mn exposure

We next explored whether the Mn-induced increase in ARG2 protein levels correlated with changes in mRNA by performing QRT-PCR on striatal extracts. There was no increase in

striatal *Arg2* mRNA expression after Mn exposure in the HD model, and striatal *Arg2* mRNA decreased following Mn exposure in WT **(Figure 5-13 A),** suggesting that the reduction in enzyme activity, as well as the increase in ARG2 protein after Mn exposure, were due to post-transcriptional mechanisms. Baseline *Limch1* was increased only in the HD model and expression levels were unaffected by Mn exposure **(Figure 5-13, B)**. While both *Arg2* and *Limch1* were detectable in striatum, neither *Arg1* nor *Agmat* were present, although both were expressed in liver, **(Figure 5-13, C-E)**.

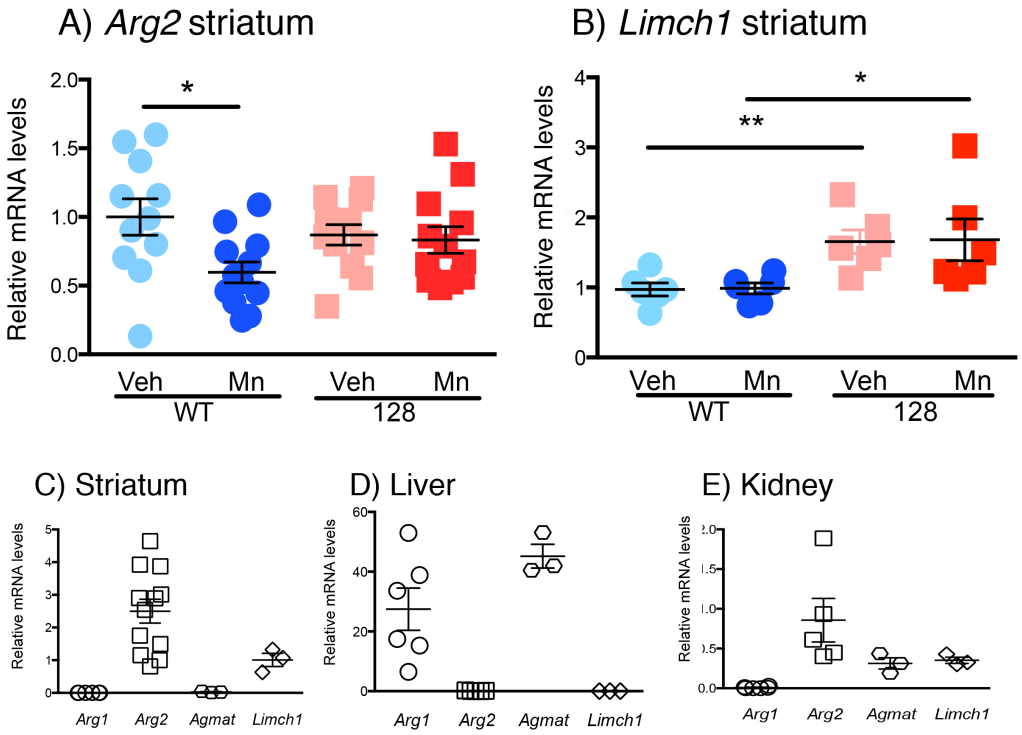

Figure 5-13. Striatal *Arg2* mRNA expression is reduced after Mn exposure in WT only, while *Limch1* is affected by genotype but not treatment, and *Arg1* and *Agmat* are undetectable. (A) Striatal *Arg2*, n=12. (B) Striatal *Limch1*, n=6. (C) Baseline striatal *Arg1* (n=6), *Arg2* (n=12), *Agmat* (n=3), *Limch1* (n=3). (D) Liver and, (E) Kidney baseline *Arg1* (n=6), *Arg2* (n=6), *Agmat* (n=3), *Limch1* (n=3). Data presented as ±sem, *p< .05, **p< .01, *post-hoc* binary comparisons by t-test following a significant (p=< .05) ANOVA.

Discussion

We report a prodromal HD striatal metabolic phenotype due to an apparent deficit in striatal Mn bioavailability, an essential cofactor for arginase enzymatic activity. Our data, for the first time, directly implicate Mn biology in HD pathogenesis. Though Mn exposure mitigated the metabolic alterations in the HD model, a robust homeostatic mechanism in the WT appears to tightly regulate the urea cycle in brain, as upregulation of arginase by ~3-fold caused a reduction of arginine without significant change in other metabolites **(Figure 5-4 and Figure 5-5)**. Given the near absence of ARG1 in striatum at this age in both genotypes, our findings strongly suggest that ARG2 is the isoform responsible for striatal arginase enzymatic activity deficits in this HD model at this early stage that precedes neuroinflammation [33].

The difference in arginase enzyme activity between WT and HD at baseline is most likely explained by insufficient bioavailable Mn, because supplementation of the extract with this co-factor *ex vivo* equalized activity between genotypes, suggesting a pool of dormant ARG2 in the mutant. In contrast, the increase in arginase activity after Mn-exposure *in vivo* is consistent with the increase of ARG2 protein; arginase is known to be stabilized *in vitro* by incorporation of Mn into each homomer.[34] Because the striatum exhibited more ARG2 than any other brain region, and because striatum normally accumulates Mn preferentially,[35] the region may be especially vulnerable to Mn deficiency,[36] though there is not a detectable difference in total striatal Mn levels between WT and YAC128Q at this stage.[37] The reduction in arginase enzyme activity in this HD model therefore suggests a specific cellular or subcellular deficit in Mn bioavailability for this enzyme.

The substantial technical hurdles to measuring Mn, or Mn-bound proteins, at sub-regional and sub-cellular resolution limits analysis of brain Mn bioavailability. Astrocytes have

very low *Arg2* expression,[38] but sequester more Mn than neurons,[39] which could cause total regional measures of Mn content to be increased with gliosis despite lower neuronal levels. ARG1 is primarily cytosolic, while ARG2 is primarily mitochondrial,[40] and Mn accumulates preferentially in the mitochondria,[41] so a change in the subcellular location of either Mn or ARG2 could change both enzyme activity and Mn accumulation. Changes in arginase activity may be exacerbated at symptomatic stages with further reductions in brain ARG2 protein levels in both striatum and hippocampus **(Figure 5-12)**. A recent publication by Langfelder, et al[42] included large data sets of gene expression and protein levels identified in genomics and proteomics performed on an allelic series of mice with varying numbers of CAG repeats. Examination of these primary data sets with searches on the genes and proteins relevant to our work supported our findings, revealing that striatal ARG2 protein was reduced in mouse knock-in models with reductions inversely correlated to increasing CAG length, while gene expression remained unchanged until a more advanced age[42] **(Figure 5-14, Table 5-1)**. In addition the stability of LIMCH1 protein in both early stage HD models **(Figure 5-11)** and late stage **(Figure 5-13, Figure 5-14, Table 5-1)** suggests that the changes to ARG2 are specific. Furthermore, *Arg2* is among the most abundant transcripts in D2-receptor containing MSNs, those most susceptible to HD neuropathology[22].

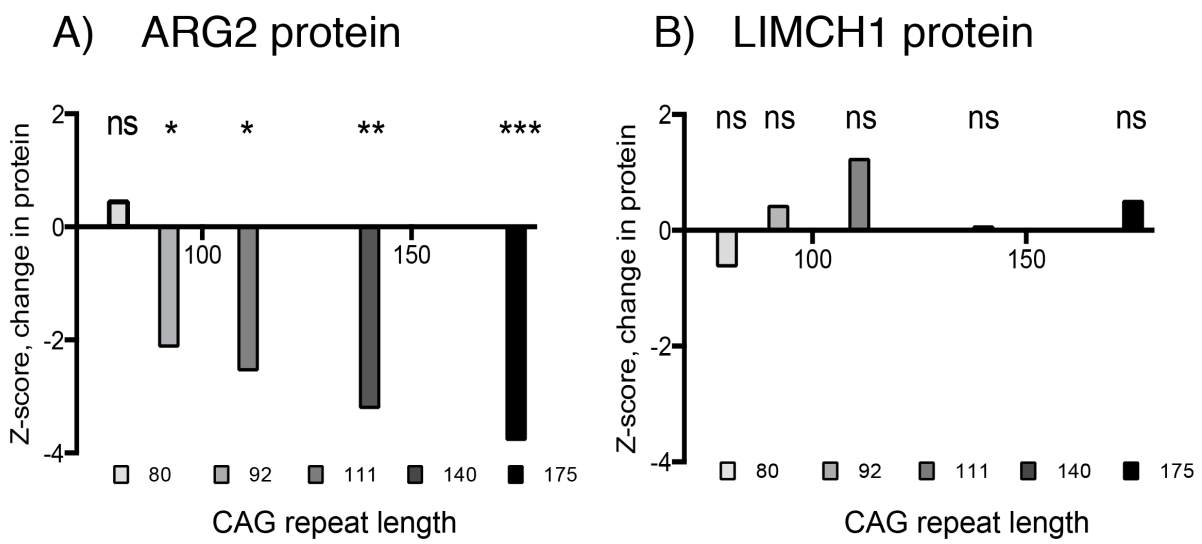

Figure 5-14. Analysis of proteomics data from Langfelder, et al[42] from later-stage HD models shows a decrease in ARG2 protein with increasing number of CAG repeats. (A) and **(B)** Z-score change in protein by CAG repeat length compared to 20 CAG repeats, using striatal tissue from 6 month old mice with CAG repeats inserted into exon 1 of a human/mouse *Htt.* **(A)** Striatal ARG2 and **(B)** Striatal LIMCH1. Table of results and significance for data shown in **Table 5-1**.

Table 5-1. Statistical description for ARG2 and LIMCH1 protein expression, striatum, 6 months of age, Langfelder, et al[42]

	ARG2			LIMCH1		
#CAGs	**Z-CAGs.v.20**	**p-value**	**FDR**	**Z-CAGs.v.20**	**p-value**	**FDR**
80	0.443	0.665	1	-0.611	0.551	1
92	-2.11	0.0442	0.66	0.414	0.685	0.978
111	-2.53	0.0166	0.27	1.22	0.237	0.765
140	-3.19	0.00307	0.0663	0.0559	0.956	0.991
175	-3.76	0.000612	0.0145	0.497	0.626	0.837
ContQ	-4.34	0.0000301	0.000805	0.672	0.504	0.741

Table of results and significance for data shown in Figure 5-14 (primary large dataset from Langfelder, et al.[42] reanalyzed for relevant proteins). ContQ indicates a differential comparison of Q as a continuous variable, revealing an effect of any and all CAG expansions on the tested protein. FDR refers to the calculated false discovery rate.

The process by which mutant HTT may cause alteration of Mn homeostasis is unknown. Systemic treatment with Mn could cause toxic levels of Mn in regions or cells less affected in HD, though delivery of bioavailable Mn to specific cells may be a future treatment strategy. It is noteworthy that several Mn-dependent enzymes are mechanistically tied to HD pathobiology (e.g. Mre11, Glutamine synthetase, SOD2), and in all cases, observed HD phenotypes are consistent with a loss of activity in the Mn-dependent enzyme.[39] The findings in the present study provide the first direct evidence that a deficiency in bioavailable Mn contributes to HD striatal pathology, manifested early as a urea cycle deficit **(Figure 5-3).**

References

1. Wiesinger H. Arginine metabolism and the synthesis of nitric oxide in the nervous system. *Prog Neurobiol* 2001; **64**(4): 365-91.
2. Gruber B, Klaczkow G, Jaworska M, et al. Huntington' disease--imbalance of amino acid levels in plasma of patients and mutation carriers. *Ann Agric Environ Med* 2013; **20**(4): 779-83.
3. Chiang MC, Chen HM, Lee YH, et al. Dysregulation of C/EBPalpha by mutant Huntingtin causes the urea cycle deficiency in Huntington's disease. *Hum Mol Genet* 2007; **16**(5): 483-98.
4. Chiang MC, Chen HM, Lai HL, et al. The A2A adenosine receptor rescues the urea cycle deficiency of Huntington's disease by enhancing the activity of the ubiquitin-proteasome system. *Hum Mol Genet* 2009; **18**(16): 2929-42.
5. Patassini S, Begley P, Reid SJ, et al. Identification of elevated urea as a severe, ubiquitous metabolic defect in the brain of patients with Huntington's disease. *Biochem Biophys Res Commun* 2015; **468**(1-2): 161-6.
6. Narayanan SP, Suwanpradid J, Saul A, et al. Arginase 2 deletion reduces neuro-glial injury and improves retinal function in a model of retinopathy of prematurity. *PLoS One* 2011; **6**(7): e22460.
7. Perez-Severiano F, Escalante B, Vergara P, Rios C, Segovia J. Age-dependent changes in nitric oxide synthase activity and protein expression in striata of mice transgenic for the Huntington's disease mutation. *Brain Res* 2002; **951**(1): 36-42.
8. Deckel AW, Volmer P, Weiner R, et al. Dietary arginine alters time of symptom onset in Huntington's disease transgenic mice. *Brain Res* 2000; **875**(1-2): 187-95.
9. Leopold NA, Podolsky S. Exaggerated growth hormone response to arginine infusion in Huntington's disease. *J Clin Endocrinol Metab* 1975; **41**(1): 160-3.
10. Patassini S, Begley P, Xu J, et al. Metabolite mapping reveals severe widespread perturbation of multiple metabolic processes in Huntington's disease human brain. *Biochim Biophys Acta* 2016; **1862**(9): 1650-62.
11. Hodges A, Strand AD, Aragaki AK, et al. Regional and cellular gene expression changes in human Huntington's disease brain. *Hum Mol Genet* 2006; **15**(6): 965-77.
12. Bernstein HG, Stich C, Jager K, et al. Agmatinase, an inactivator of the putative endogenous antidepressant agmatine, is strongly upregulated in hippocampal interneurons of subjects with mood disorders. *Neuropharmacology* 2012; **62**(1): 237-46.
13. Wang X, Ying W, Dunlap KA, et al. Arginine decarboxylase and agmatinase: an alternative pathway for de novo biosynthesis of polyamines for development of mammalian conceptuses. *Biol Reprod* 2014; **90**(4): 84.
14. Morris SM, Jr. Vertebrate agmatinases: what role do they play in agmatine catabolism? *Ann N Y Acad Sci* 2003; **1009**: 30-3.
15. Davis RH, Morris DR, Coffino P. Sequestered end products and enzyme regulation: the case of ornithine decarboxylase. *Microbiol Rev* 1992; **56**(2): 280-90.
16. Wolf C, Bruss M, Hanisch B, Gothert M, von Kugelgen I, Molderings GJ. Molecular basis for the antiproliferative effect of agmatine in tumor cells of colonic, hepatic, and neuronal origin. *Mol Pharmacol* 2007; **71**(1): 276-83.
17. Wu HY, Chen SF, Hsieh JY, et al. Structural basis of antizyme-mediated regulation of polyamine homeostasis. *Proc Natl Acad Sci U S A* 2015; **112**(36): 11229-34.

18. Perez-Leal O, Merali S. Regulation of polyamine metabolism by translational control. *Amino Acids* 2012; **42**(2-3): 611-7.
19. Kilpelainen P, Rybnikova E, Hietala O, Pelto-Huikko M. Expression of ODC and its regulatory protein antizyme in the adult rat brain. *J Neurosci Res* 2000; **62**(5): 675-85.
20. Caldwell RB, Toque HA, Narayanan SP, Caldwell RW. Arginase: an old enzyme with new tricks. *Trends Pharmacol Sci* 2015; **36**(6): 395-405.
21. Liu P, Fleete MS, Jing Y, et al. Altered arginine metabolism in Alzheimer's disease brains. *Neurobiol Aging* 2014; **35**(9): 1992-2003.
22. Doyle JP, Dougherty JD, Heiman M, et al. Application of a translational profiling approach for the comparative analysis of CNS cell types. *Cell* 2008; **135**(4): 749-62.
23. Stone EM, Glazer ES, Chantranupong L, et al. Replacing Mn(2+) with Co(2+) in human arginase i enhances cytotoxicity toward l-arginine auxotrophic cancer cell lines. *ACS Chem Biol* 2010; **5**(3): 333-42.
24. Quinones M, Cofre J, Benitez J, et al. Insight on the interaction of an agmatinase-like protein with Mn(2+) activator ions. *J Inorg Biochem* 2015; **145**: 65-9.
25. Cofre J, Montes P, Vallejos A, et al. Further insight into the inhibitory action of a LIM/double zinc-finger motif of an agmatinase-like protein. *J Inorg Biochem* 2014; **132**: 92-5.
26. Castro V, Fuentealba P, Henriquez A, et al. Evidence for an inhibitory LIM domain in a rat brain agmatinase-like protein. *Arch Biochem Biophys* 2011; **512**(1): 107-10.
27. Wynn TA, Barron L, Thompson RW, et al. Quantitative assessment of macrophage functions in repair and fibrosis. *Curr Protoc Immunol* 2011; **Chapter 14**: Unit14 22.
28. Garcia D, Ordenes P, Benitez J, et al. Cloning of two LIMCH1 isoforms: characterization of their distribution in rat brain and their agmatinase activity. *Histochem Cell Biol* 2016; **145**(3): 305-13.
29. Pandey D, Sikka G, Bergman Y, et al. Transcriptional regulation of endothelial arginase 2 by histone deacetylase 2. *Arterioscler Thromb Vasc Biol* 2014; **34**(7): 1556-66.
30. Pandey D, Bhunia A, Oh YJ, et al. OxLDL triggers retrograde translocation of arginase2 in aortic endothelial cells via ROCK and mitochondrial processing peptidase. *Circ Res* 2014; **115**(4): 450-9.
31. Mangiarini L, Sathasivam K, Seller M, et al. Exon 1 of the HD gene with an expanded CAG repeat is sufficient to cause a progressive neurological phenotype in transgenic mice. *Cell* 1996; **87**(3): 493-506.
32. Li JY, Popovic N, Brundin P. The use of the R6 transgenic mouse models of Huntington's disease in attempts to develop novel therapeutic strategies. *NeuroRx* 2005; **2**(3): 447-64.
33. Franciosi S, Ryu JK, Shim Y, et al. Age-dependent neurovascular abnormalities and altered microglial morphology in the YAC128 mouse model of Huntington disease. *Neurobiol Dis* 2012; **45**(1): 438-49.
34. Romero PA, Stone E, Lamb C, et al. SCHEMA-designed variants of human Arginase I and II reveal sequence elements important to stability and catalysis. *ACS Synth Biol* 2012; **1**(6): 221-8.
35. Dodd CA, Ward DL, Klein BG. Basal Ganglia accumulation and motor assessment following manganese chloride exposure in the C57BL/6 mouse. *Int J Toxicol* 2005; **24**(6): 389-97.

36. Ramos P, Santos A, Pinto NR, Mendes R, Magalhaes T, Almeida A. Anatomical region differences and age-related changes in copper, zinc, and manganese levels in the human brain. *Biol Trace Elem Res* 2014; **161**(2): 190-201.
37. Williams BB, Li D, Wegrzynowicz M, et al. Disease-toxicant screen reveals a neuroprotective interaction between Huntington's disease and manganese exposure. *J Neurochem* 2010; **112**(1): 227-37.
38. Cahoy JD, Emery B, Kaushal A, et al. A transcriptome database for astrocytes, neurons, and oligodendrocytes: a new resource for understanding brain development and function. *J Neurosci* 2008; **28**(1): 264-78.
39. Horning KJ, Caito SW, Tipps KG, Bowman AB, Aschner M. Manganese Is Essential for Neuronal Health. *Annu Rev Nutr* 2015; **35**: 71-108.
40. Chen F, Lucas R, Fulton D. The subcellular compartmentalization of arginine metabolizing enzymes and their role in endothelial dysfunction. *Front Immunol* 2013; **4**: 184.
41. Gunter TE, Gavin CE, Aschner M, Gunter KK. Speciation of manganese in cells and mitochondria: a search for the proximal cause of manganese neurotoxicity. *Neurotoxicology* 2006; **27**(5): 765-76.
42. Langfelder P, Cantle JP, Chatzopoulou D, et al. Integrated genomics and proteomics define huntingtin CAG length-dependent networks in mice. *Nat Neurosci* 2016; **19**(4): 623-33.

Chapter VI

Mn and HD: Conclusions and Future Directions

Note: A portion of this chapter has been derived from the following publication:

Bichell TJ, Halbesma T, Tipps KG, Bowman AB. Metal Biology Associated with Huntington's Disease. In: White A, Aschner M, Costa L, Bush A, eds. Biometals in Neurodegenerative Diseases: Mechanisms and Therapeutics. In Press: Elsevier; 2016.

Summary of findings

The novel findings described in this work add to the field of Huntington's disease research, the field of neurotoxicology, and the study of gene-environment interactions. The role of the HTT protein is vague but pervasive, perhaps involving an overarching function that would link the many crucial cellular pathways which are altered in HD, such as autophagy, vesicular transport, transcription regulation and metal homeostasis. The physical structure of the HTT protein has only recently been published,[1] and it makes clear that the polyglutamine expansion on the N terminal alters the entire three-dimensional structure. In humans, a relatively small increase in CAG repeats, changes the structure enough to cause debilitating functional deficits, Our work described in Chapter II, in which we lengthened the mouse polyQ sequence to an extreme of 225 repeats without substantially worsening an early-onset phenotype suggests that the mouse protein may have a slightly different conformation or function than the human protein, as longer sequences quickly become lethal in the human condition. These findings also suggest that the structurally-dependent function of HTT is changed by a lengthened polyglutamine sequence, but the toxicity of the mutant protein is not proportional to the size of the repeat.

Our separate work, on the Mn-dependent enzyme arginase, provides the first direct link between reduced metal accumulation and intracellular neuronal function. The neurotoxic effects of overexposure to heavy metals have been well-studied (See **Chapter I**), but there was

previously no evidence that a mutant gene could decrease metal accumulation in a region-specific manner which would lead to malfunction in a crucial biological pathway in live animals. Previous research in our lab showed that the HD mutation leads to a deficiency of Mn in cell culture models,[2,3] and our lab had also shown that Mn exposure altered neuronal biology[4,5] and structure,[6,7] but a direct link between Mn-deficiency *in vivo* and neuronal biology had not been demonstrated until now. Our exciting finding, that reductions in arginase activity is present in regions with reduced Mn accumulation, and that ARG2 directly increases with Mn exposre, suggests that the delivery of Mn to the striatum is a possible treatment strategy for HD,

Our work also contributes to the general fund of knowledge about the urea cycle in brain, a relatively unexplored pathway. We showed that ARG2 is the arginase present in non-gliotic mouse brain, though many previous researchers had thought that ARG1 was the neuronally active enzyme. We also showed that an acute Mn exposure increases ARG2 protein, without increasing ARG2 gene transcription, suggesting that the structural stability conferred by the metal co-factor could be the rate-limiting factor in the neuronal urea cycle. Further experiments to explore this possibility are described below.

In summary, our findings include: (1) generation of a novel mouse model of HD with characteristics reflecting human juvenile HD, (2) detection of altered urea pathway metabolites in HD striatum that are reversed with Mn exposure, (3) demonstration that ARG2, and not ARG1, is the arginase isozyme functioning in mouse brain, (4)) optimization of an enzymatic assay to measure arginase activity in mouse striatal tissue, (5) detection of a prodromal baseline reduction in a Mn-dependent enzyme activity in the striatum of an HD mouse model in two different strains that is reversible with Mn exposure, (6) demonstration of a Mn-dependent

increase in ARG2 protein, (7) detection of a decrease of both striatal and hippocampal ARG2 protein in the manifest disease stage of another HD mouse model.

The finding that arginase activity is reduced in prodromal HD model mouse striatum at baseline (**Chapter V**) confirms the over-arching hypothesis that Mn-dyshomeostasis in HD leads to pathological repercussions. Though mishandling of Mn had previously been identified in cell and mouse models, this is the first confirmation of downstream effects of this phenomenon. The explanation of this HD x Mn interaction effect, may fit into one of the following paradigms:

A) Striatal Mn dyshomeostasis is one minor result of major alterations caused by mutant HTT;

B) Stiatal Mn dyshomeostasis may be one of the major pathways altered by mutant HTT;

C) Striatal Mn dyshomeostasis is the major pathway impacted by mutant HTT, with all other pathologies resulting directly or indirectly from this alteration.

Our findings on arginase emphasize the importance of identifying which of these underlying hypothesis is in place in order to understand and treat HD. Our findings also help to explain the basic functioning of metal handling in the neuronal urea pathway, especially the unique characteristics of striatal MSNs. Future efforts suggested by this work will focus on the (1) mechanism by which mutant HD causes Mn dyshomeostasis, (2) the role of arginase in HD, and 3) the response of arginase to Mn concentration and pH.

Our findings on arginase in HD models leads directly to several lines of new inquiry which will help to uncover which of the three major hypotheses above is in force. Each of these potential future directions will be discussed below.

Future directions

Hypothesis I. If other Mn-dependent enzymes are also affected in HD, Mn-dyshomeostasis might be the central root of HD pathology

Working Hypothesis: Arginase is just one Mn-dependent enzyme affected by Mn-deficit in HD. Other enzymes which require Mn as a specific cofactor will also have reduced activity in HD at baseline.

If striatally restricted Mn deficit is the root cause of the regional pathology, it will be important to test whether other Mn-dependent enzymes are reduced in a regionally dependent manner as well. Current literature would suggest that striatal glutamine synthetase (GS), another Mn-dependent enzyme, is not affected.[8-10] The resilience of GS in conditions of Mn dyshomeostasis may be due to the fact that the enzyme can function with alternative co-factors, such as Mg.[11] Compensatory mechanisms which arise to allow biologically essential reactions to occur may also mask the Mn-related alterations in the activity of other enzymes. And, tight regulation of essential pathways may respond to metal influx, which would explain the fact that GS activity decreases over time with chronic Mn exposure.[10] One would expect Mn-dependent enzymes, such as MRE-11, which are strictly dependent on Mn as a co-factor, would be more strongly affected by Mn dyshomeostasis than the more promiscuous enzymes.

Our findings on arginase in HD models are novel because we demonstrate an abnormal phenotype which is directly related to striatal Mn dyshomeostasis. Furthermore, we pinpointed ARG2 as the isoform of arginase in the brain of this mouse model, and showed that arginase protein increased with exposure to its co-factor, unrelated to gene expression. Interestingly, one paper has shown the same Mn-induced protein increase phenomenon to occur with GS[8], but gene expression of GS following Mn exposure was not measured, so it is not clear if this GS increase is post-transcriptional.

Most importantly, the mechanism behind the Mn mishandling in HD striatal models is unexplained. Direct interference between mutant HTT and Mn transporters, especially if relegated to a receptor specific to the D2 containing MSNs, would clearly lead to a striatal Mn deficit. In the future, it will be important to identify the cell type or subregional localization of Mn pools under normal and Mn-deficit conditions to assist in pinpointing the mechanism behind the HD-related Mn dyshomeostasis, though the methodologies are lacking (**Chapter III**). Mn dyshomeostasis might be related to the interference of mutant HTT with inter- or intra- cellular Mn transporters blocking influx or storage, or increasing efflux, but a Mn-specific mechanism has not been shown. Our finding that arginase protein increases with Mn exposure may provide a surrogate Mn sensor in cell types or subcellular compartments where arginase is known to localize.

Arginase, itself, may serve as a repository of Mn, because the metal is tightly bound to the enzyme in a deep cleft,[12] a bind which is especially tight at a basic pH.[13] ARG2 resides in mitochondria[14] and the intra-organelle pH of mitochondria is very basic (**Figure 6-1**). As pH drops, Mn comes unbound from the enzyme,[15] and if the mitochondrial pH became unstable, this might allow the metal to efflux out of mitochondria.

Hypothesis II. If Mutant HTT causes abnormal intracellular pH, this would lead to metal mishandling, resulting in many altered pathways

Working Hypothesis A: HTT regulates ionic channels with regulate intracellular pH, and mutant HTT leads to disruption of this system which disrupts multiple enzymatic pathways

Working Hypothesis B: Mutant HTT causes dysregulation of pH which causes reduced Mn binding to ARG2

The involvement of the HTT protein in so many diverse biological functions suggests that the wild-type protein serves as an overarching regulator of an aspect of neuronal biology that leads to the myriad dysfunctional processes seen in the disease. Maintenance of the acid-base balance between cells and within organelles is one such possibility, and an imbalance could lead to the dysregulation of metals seen in HD. Acid-Alkaline gradients drive intracellular metal homeostasis in many ways, including regulating the direction of metal transport as well as the binding between metal cofactors and their associated enzymes. Each of the dysregulated metals described in **Chapter III** binds to enzymes that reside in specific organelles and function best within a very narrow pH range. Changes in pH can weaken or strengthen the intra- and intermolecular bonds with metal cofactors by changing the conformation of enzymes, thereby altering their enzymatic activity. For example, the ARG2 homotrimer binds tightly to six ions of Mn at a pH greater than 8,[15] which is the normal pH within mitochondria, where arginase2 is stored (**Figure 6-1**). As the pH drops, Mn disassociates from the ARG enzyme, reducing its activity and destabilizing the protein,[16] which could lead to downstream disturbances in both the urea cycle and nitric oxide signaling.

Each subcellular organelle maintains a specific pH, ranging from 4.7 in the lysosome to 8 in the mitochondria[17] (**Figure 6-1**).

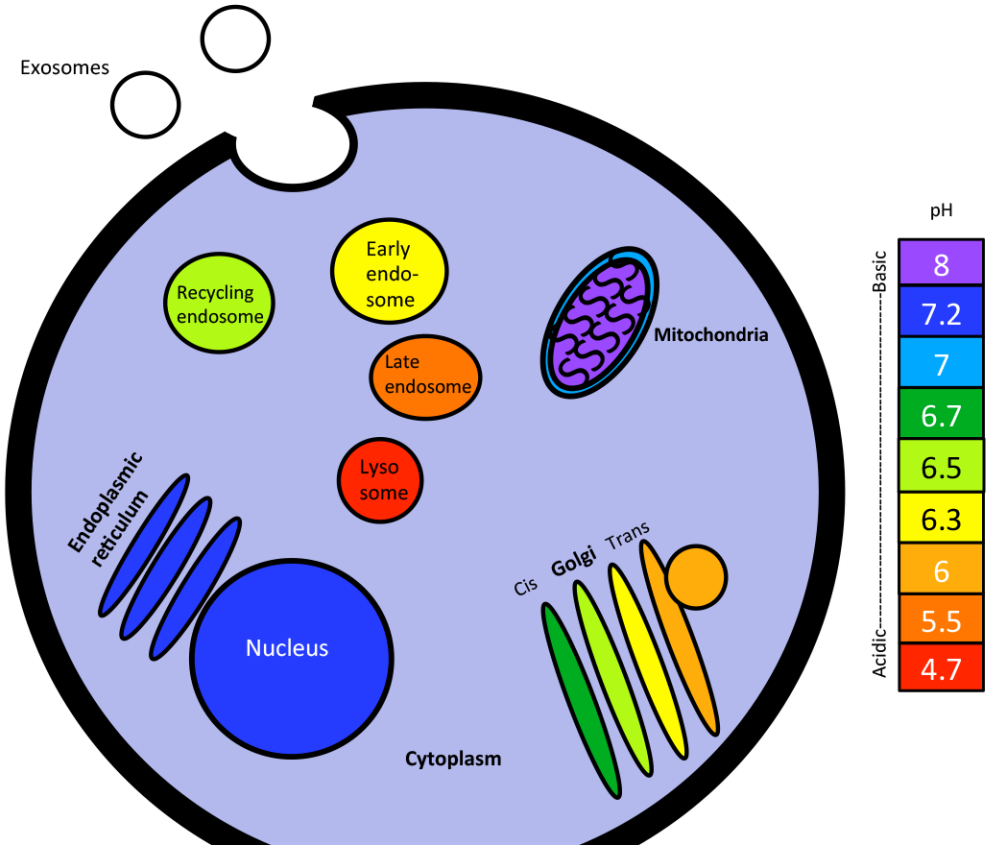

Figure 6-1. Each subcellular compartment and organelle maintains a specific pH, with mitochondrial matrix being the most alkaline while lysosome being most acidic. Adapted from Casey, et al[17].

Benzamil, an amiloride-derivative that blocks epithelial sodium channels (thereby stabilizing the cytosolic pH)[18] significantly reduces HTT aggregation in vitro and had therapeutic effect in live R6/2 model mice.[19] Several ion channels known to regulate pH are associated with the HTT protein. Chloride Channels (ClC channels) exchange protons for chloride on plasma membranes, which have only recently been described in brain. ClC channels have been recently linked to epilepsy[20] as well as to Myotonia Congenita, a rare skeletal muscle disease,[21,22] and they are found to be reduced in HD in skeletal muscle.[21] In a mouse model of HD, the CLC-1 channel has reduced chloride currents in skeletal muscles.[23]

Another possible HTT interactor that could control pH is the Acid Sensing Ion Channel (ASIC1a) is one of the subunits that forms the major acid-sensing calcium channels in neurons.[24] These ASIC channels sense extracellular H^+ ions, and maintain intercellular pH by the movement of Ca^{2+} across membranes. Blocking ASIC1a activity with RNA interference, prevents intracellular Ca overload and reduces aggregates and pathogenesis.[25]

In yeast, a pH regulator, the Golgi Ca receptor 1-dependent translation factor 1 protein (Gdt1) is a suppressor of mutant Htt toxicity,[26] suggesting that there may be a connection between intracellular pH and HD pathology, though direct links have not yet been found. The homolog for Gdt1 is Transmembrane Protein 165 (TMEM165), a novel protein involved in Golgi trafficking and pH homeostasis that has very recently been characterized.[27] Mutations in TMEM165 cause a congenital disorder of glycosylation. Experiments with the yeast ortholog demonstrate that it functions as a Ca^{2+}/H^+ antiporter, which regulates both Golgi calcium levels and pH. Mn treatment reverses the glycosylation disorder seen in the presence of high Ca concentrations in cells in which TMEM165 is knocked out. Interestingly, because lysosomal pH is altered in patients with TMEM165 mutation,[28] the counter ion for Mn^{2+} entry into the lysosome is said to be Ca^{2+} in yeast and H^+ in mammalian cells.[27]

It is possible that an abnormal ionic gradient importing Ca^{2+} into lysosomes could potentially drive Mn^{2+} export. The stability of a protein known as Golgi Phosphoprotein 4 (GPP130) is directly related to Mn concentration in Golgi,[27] i.e. GPP130 degrades in the presence of Mn, and is targeted for lysosomal degradation in cultured cells exposed to excess Mn^{2+},[29] though it has no such reaction when exposed to other transition metals.[30] In HeLA cells in which TMEM165 has been knocked down with shRNA, GPP130 is insensitive to Mn^{2+}

treatment. Together, these studies indicate that TMEM165, or another pH driver, may be the connection between Mn dyshomeostasis and HD pathology.

Yet another potential intracellular acid-base driver that may link metal homeostasis to HD is the Sodium Proton Exchanger 9 (NHE9) or Solute Carrier Family 9 (SLC9A9). NHE9 is a sodium-proton exchanger localized to recycling endosomes, that has recently been characterized as an autism susceptibility gene.[31] The function of NHE9 is to alkalinize luminal pH, which increases the uptake of transferrin as well as glutamate, and it also stabilizes the surface expression of the transferrin receptor.[31] It is found in both astrocytes and neurons. Interestingly, NHE9 interacts with HIP14 (known to be a metal transporter), as well as Vesicle Associated Membrane Protein-7 (VAMP7), two proteins which form complexes with HTT.[32] An alteration in the function of NHE9 by aberrant interaction with mutant HTT would help to explain both the Fe and Mn dyshomeostasis seen in HD.

In summary, mutations in HTT may cause alterations in the transporters and channels that control acid-base balance by regulating the movement of ions between organelles or cells. This pH dysregulation could have downstream effects on metal homeostasis that would lead to enzymatic failure and resultant HD pathology.

Hypothesis III. Mutant HTT causes inappropriate translocation of ARG2, resulting in reduction in Mn bioavailability

Working Hypothesis A: Mn exposure will cause a translocation of ARG2 from the mitochondria to the cytoplasm.

Working Hypothesis B: Mn deficit will influence ARG2 to remain in mitochondria

Working Hypothesis C: ARG2 is a Mn transporter, or storage compartment, affected by mutant HTT

Our findings in the HD models, that baseline striatal arginase activity is reduced and urea pathway metabolites are altered, both of which can be reversed with Mn exposure, demonstrate

that reduced Mn bioavailability is severe enough to cause biological harm. It is possible that ARG2 itself could serve as a crude sort of Mn transporter. Sastre, *et al*[33] used a radioactive CO trapping system to measure arginase and agmatinase activity in rat brain. They found that agmatinase activity was enriched in the synaptosomal-mitochondrial fraction about fourfold over that of the whole homogenate. In contrast, arginase activity was mostly enriched in cytoplasm and microsomes with lower activities in mitochondrial and synaptosomal fractions.

A study by Pandey, *et al*., showed that when aortic epithileal cells in culture are exposed to oxidized low-density lipoprotein (OxLDL), which causes oxidative stress, ARG2 moves from mitochondria into cytoplasm.[14] This intracellular translocation increases ARG2 enzymatic activity, which is surprising because the pH of the cytosol (pH7.2) is much lower than mitochondria and should reduce ARG activity, but the increase may relate more to the availability of arginine as a substrate. The translocation of ARG2 out of the mitochondria leads to reduced NO production (presumably due to reduced available arginine as a substrate for NO) and this increases the production of reactive oxygen species. The compartmentalization of arginine within cells has been shown not to play a role in NO production,[34] but those experiments were concentrated on ARG1 rather than ARG2 in fibroblasts, and as such, may not be relevant to neurons. The arginine paradox is described as the phenomenon where additional L-arginine is required for maximal NO release even when cytosolic concentration of L-arginine is well above saturation for NOS.[35] This is partially explained by the differing kinetics of the two enzymes; the affinity of NOS for arginine is much higher than that of arginase, but the V_{max} of arginase is much higher than that of NOS, meaning that the two pathways compete for free L-arginine. Interestingly, Elms, *et al*., found that arginase activity was much higher in cytosol than in mitochondria,[34] but Pandey, *et al* found that enzyme activity was completely inhibited when

the mitochondrial transport sequence on the arginase protein was mutated (the mitochondrial processing peptidase, or MPP), suggesting that arginiase must be processed in the mitochondria even to become active in the cytosol.[14] This translocation from mitochondria to cytoplasm may also allow for cellular efflux of Mn, as ARG2 could serve as a crude sort of Mn transporter. Pandey suggests that Heat Shock Protein 60 (Hsp60), a mitochondrial chaperone protein that has been shown to bind to ARG2, may regulate ARG2 folding, as it is also translocated from the mitochondria to the cytoplasm with exposure to OxLDL.[14] A connection with HD already exists, as overexpression of *HTT* causes Hsp60 to accumulate in mitochondria, and Hsp60 mitochondrial localization mitigates oxidative stress following rotenone exposure[36] and HTT has a domain which has been shown to control mitochondrial protein traffic.[37] If mutant HTT dysregulates the mitochondrial trafficking of arginase, this could lead to the altered arginase activity.

On the other hand, mutant HTT is known to cause oxidative stress. If oxidative stress causes mitochondria to eject ARG2, a translocation which decouples it from NO production and causes further damage from reactive oxygen species, then the HD-related Mn dyshomeostasis may be a result of HD mediated oxidative stress, and not the reverse. Pandey *et al*., noted that this type of reverse translocation-based dual targeting of proteins between mitochondria and cytosol in response to cellular stress represented a novel mechanism of cellular regulation that had not been previously been described in mammalian cells.[14]

To tease out the intracellular location of ARG2, experiments could be designed with cultured cells expressing mutant HTT and/or ARG2, exposed to Mn or vehicle and then fractionated. Subcellular fractions could then be measured for ARG2 protein by western blot, arginase enzymatic activity by the modified Wynn assay, and Mn content by ICPMS, or graphite

furnace. Animals cross-bred to bear both the YAC128 and a conditional ARG2 knockout (which could be activated at weaning to avoid any developmental compensation for lack of embryonic ARG2), would be expected to have an HD-like striatal phenotype in the ARG2 knockouts, and a worsened HD-like phenotype in the double-mutants. We are currently aging YAC128 animals to 10 months, which is just past the onset of HD symptoms in this animal, to measure ARG2 protein. We would expect to see a reduction in ARG2 protein in the HD model, as we found in the R6-2 model at 3 months (**Figure 5-12**), and in the proteomics data from Langfelder *et al*.[38] These animals, both the aged YAC128s and potential cross-bred ARG2-/- x YAC128, would be invaluable for study of gene and protein expression for other potential Mn transporters as well.

Hypothesis IV. Mutant HTT causes disregulation of urea transporters,which interferes with the neuronal urea cycle, causing arginase dysfunction and Mn mishandling

Working Hypothesis A: Excess urea is part of a feedback mechanism that causes reduced ARG2 activity

Working Hypothesis B: Excess urea is caused by the influence of mutant HTT on urea transporters, reducing their ability to efflux urea from neurons

Our finding, that there was increased ornithine in striatal samples, agrees with the findings of Patassini *et al*.[39], seeming to refute our discovery of reduced arginase activity in striatum. A reduction in arginase activity should result in a reduction in both ornithine and urea, but an elevation of urea was found in all brain regions studied, obtained from post-mortem HD patients. As the authors suggest, this excess urea could be due to local over-production, or to defective urea export, though this has not been measured in prodromal stage patients. The fact that a gene for a urea transporter (SLC14A1) is the most highly expressed gene in HD MSN's[40] indicates that alterations in the pathways for urea clearance may precede the elevation. It is conceivable that a build-up of urea would activate arginase regulatory feedback pathways in

brain, but this has not been studied. Blocking the urea transporter, and then measuring ARG2 protein and enzyme activity could help to confirm this mechanism.

Hypothesis V. Mutant HTT causes disregulation of arginase, which increases HTT aggregation

Working Hypothesis A: Enrichment of ARG2 leads to reduction in aggregates, possibly through increased polyamines

Working Hypothesis B: Mutant HTT is not able to reduce Mn accumulation in CA2 neurons, possibly because of unique compensatory transporters

Our conclusion, that ARG2 is the arginase isozyme in mouse brain was drawn from mRNA expression as well as protein findings in western blots and immunohistochemistry. Collaboration with the Alexander Osmand lab, Department of Biochemistry, University of Tennessee, Knoxville, TN began with immunohistochemistry studies of HTT aggregates in our BAC225 model and subsequently extended to an assay of aggregates and ARG2 in the Mn-exposed YAC128 mouse. These experiments uncovered an unexpected finding in our mouse brain slices: a strikingly visible enrichment of ARG2 in the CA2 region of hippocampus (**Figure 6-2 and Figure 6-3**). The CA2 area was first described as distinct from CA1 and CA3 in the 1940's by Lorente de Nó, but has been overlooked until recently.[41] CA2 neurons have been found to fire at high rates to encode location in stationary animals[42] and link to both CA1 and CA3 regions in a newly identified network. Recent characterizations of the region show that it is crucial for social memory and is uniquely altered in schizophrenia and in age-related dementia, and neurodenerative disorders including Lewy body dementia, PD, AD and transmissible spongiform encephalopathies.[42]

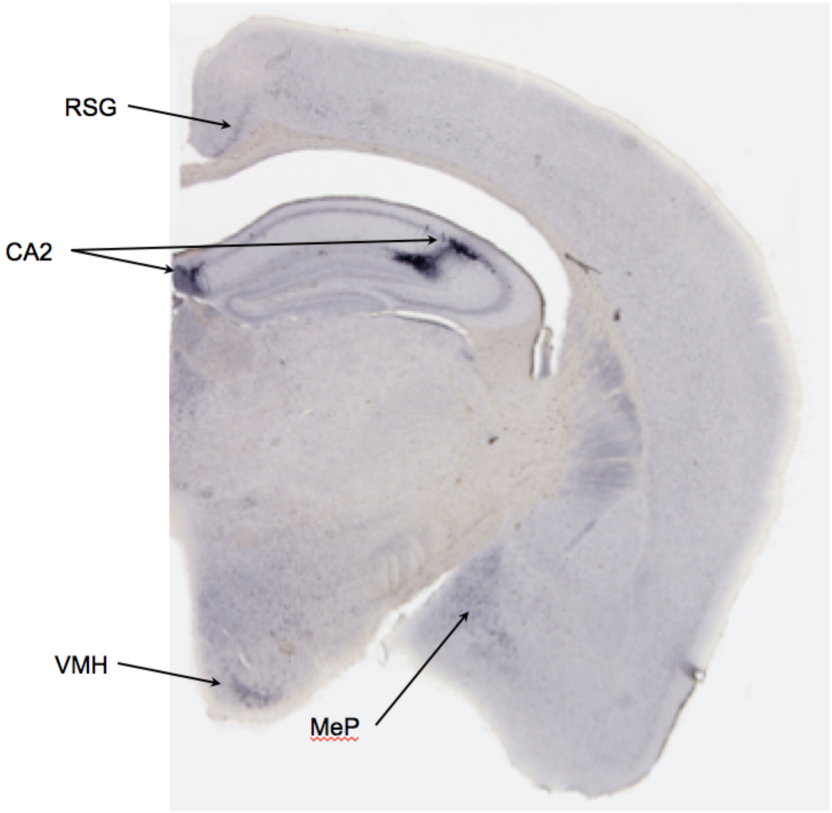

Figure 6-2. Low power image of ARG2 staining of YAC128-Mn showing dense staining of CA2 region of hippocampus and selective staining of cells in medial amygdala, ventromedial hypothalamus and retrosplenial cortex. All IHC images stained with sc-20151 as described in methods, Chapter IV.

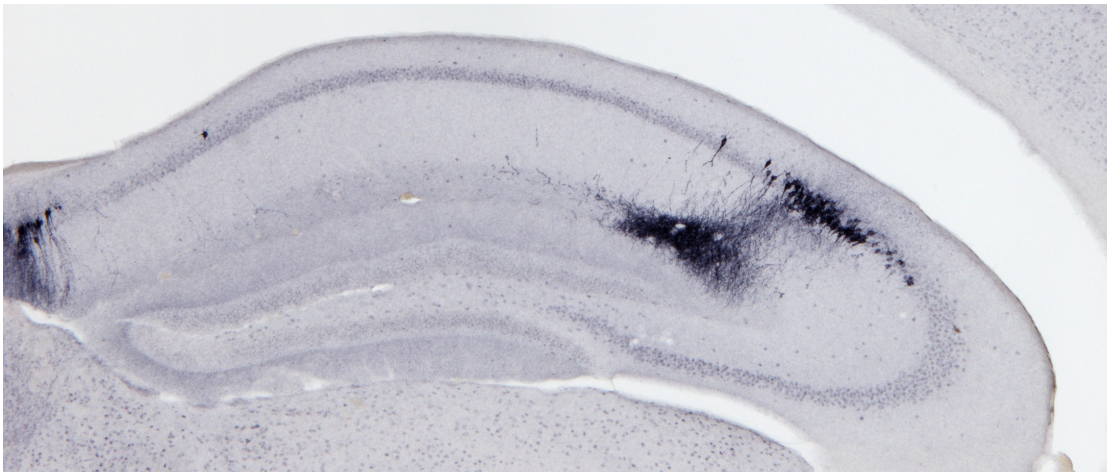

Figure 6-3. Intermediate power image of ARG2 staining of YAC128-Mn showing dense staining of CA2 neurons in hippocampus and of their processes extending into the lateral region of the molecular layer

There is a clear correlation between the number of Lewy bodies in cortex and degeneration of neurites in CA2,[43] which is especially interesting given the oppositional metal homeostasis between PD and HD. Expression of hippocampal arginase has not been linked to HD, nor to aggregate formation. Liu et al., plotted the regional localization of arginase, but those studies used a protein antibody which may be nonspecific (see discussion in **Chapter IV**), and quantitative analysis in that study merged CA2 and CA3 data together, as most researchers have done.[44]

Though the finding of ARG2 enrichment was unexpected, a connection with reduced aggregates in the region was even more interesting (**Figure 6-4**). This absence of HTT aggregates in the CA2 region was noted in four different HD mouse models, though aggregates are clearly stained in surrounding regions.

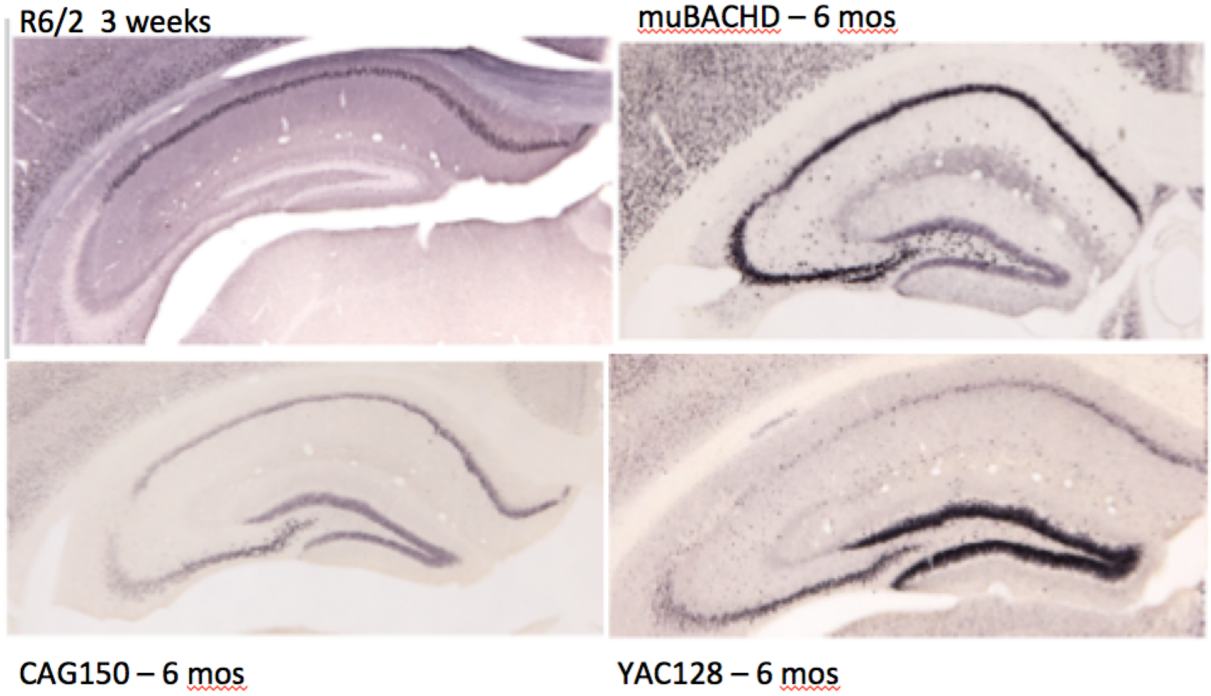

Figure 6-4. There is a remarkable lack of aggregates in the CA2 hippocampal region of HD mouse models.

Surprisingly, neurons in the CA2 region are resistant to long-term potentiation (LTP), which requires NO,[45] and presumably, an enrichment of ARG2 would result in reduced production of NO. CA2 has been shown to be both resistant to injury and synaptic plasticity,[41] which may partially be due to limited calcium levels and strong calcium buffering capacity in the region.[46] Interestingly, CA2 neurons are highly enriched for the IGF-1 receptor[47] and for IGF-binding protein[48], which may make the region especially sensitive to the beneficial effects of IGF-1.

Exposure to Mn appeared to increase the ARG2 staining in the CA2 region (**Figure 6-5**), as it did in the striatum (**Figure 5-10**), more so in HD than in WT in these pilot experiments, which remain to be quantified.

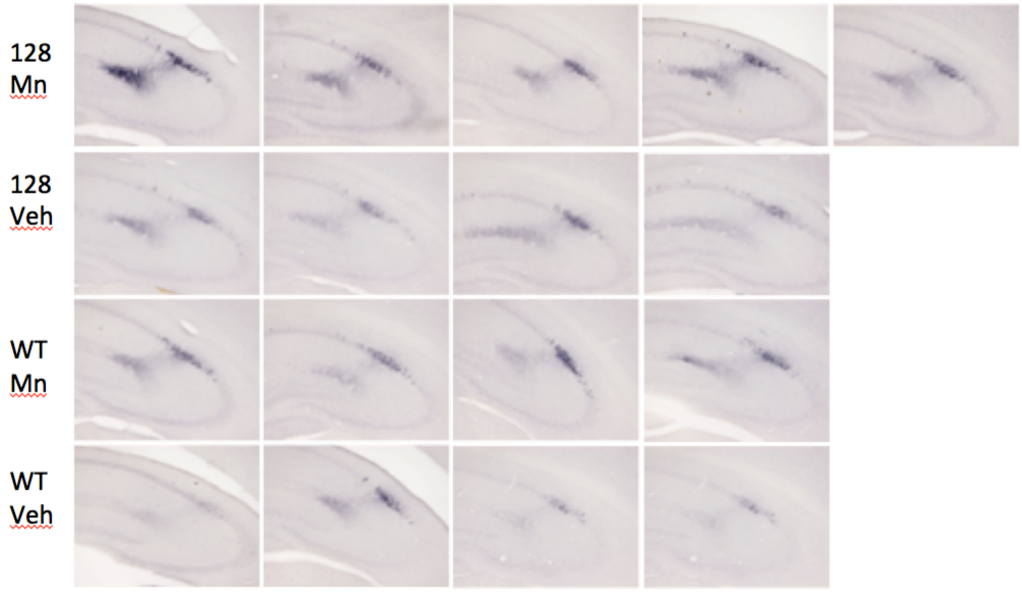

Figure 6-5. ARG2 is enriched in CA2 and increases with Mn exposure *in vivo*. CA2 cells and terminals in the hippocampus of Mn-treated YAC128 (top row), YAC128 (upper middle row), Mn-treated WT (lower middle row), and WT (lower row) mouse brains. Lower density of staining was due to the higher number of sections stained in the presence of limiting amounts of primary antibody. These images demonstrate a degree of variability within groups while showing the high induction of ARG2 staining in the terminal region of Mn-treated YAC128. ARG2 1:5,000.

Future work to explore the relationship between ARG2, Mn, mutant HTT and IGF-1 in hippocampal CA2 may prove to be very fruitful. The expression of certain receptors and transporters which are unique to CA2 may also provide clues to Mn homeostatic mechanisms. For example, TREK1 (also known as KCNK2) is much more abundant in CA2 than in surrounding hippocampal regions.[49] Interestingly, TREK1 is sensitively influenced by temperature and lipids as well as pH,[50] which could be an over-arching factor in HD neuropathology.

Hypothesis VI. If mutant HTT causes striatal-specific Mn-dyshomeostasis, then delivery of Mn to the region could correct HD neuropathology

Working hypothesis: Mn-dyshomeostasis in the striatum alone causes most of the neuropathology of HD

As mentioned in **Chapter I**, one metal-related medication, PBT2, has already moved through clinical trials for HD, without significant beneficial effect. The failure of PBT2 Cu chelators may have been due in part because these chelators also alter Mn levels, maybe even more than Cu levels, in the organ most vulnerable in HD. Moldovan *et al*., found that Cu chelation with cuprizone reduced Cu levels in blood and periphery, but not in brain, though it reduced Mn in striatum and cerebellum.[51] The balance of metals is exquisitely fine-tuned between brain regions, cell types and organelles, so metal-related therapeutic approach to HD may need to be designed for regional or even cell-type specific drug delivery.

Conclusions

In summary, our findings, especially those concerning ARG2, directly suggest further lines of inquiry to elucidate the role of metals and HTT in neuronal function. Divalent metal cations are involved in almost every aspect of HD on an anatomical and molecular level. Exactly how the excesss polyQ sequence on mutant HTT protein causes the derangements seen in metal homeostasis is not well understood. Our findings, together with the previous work from our lab showing reduced Mn bioavailability in HD striatal models, demonstrate that there is a strong Mn x HD interaction which may help to explain mechanisms of disease as well as point to possible treatments. Mn and other metal dysregulation can explain many, if not all, of the pathological effects seen in the presence of mutant HTT. The loss of function of wild-type HTT may contribute to some of the metal-related pathological effects, such as autophagosomal defects, at the same time that the toxic gain of function of mutant HTT may be contributing to the alterations in neuronal ionic channels or metal transporters. Recently, it has been shown that senescent fibroblasts in culture show increased Mn^{2+} uptake and utilization, suggesting that aging, even without disease, may require additional Mn, perhaps as a way to increase the activity of Mn-dependent enzymes to counteract aging-related increases in oxidative stress.[52]

By exploring the experimental directions described above; 1) the effect of Mn-dyshomeostasis on other enzymatic pathways, 2) the role of HTT in controlling intracellular pH, 3) the sub-cellular localization of Mn in non-excess conditions, 4) the subcellular translocation of ARG2 in differing Mn concentrations, 5) the role of urea transporters in arginase alterations, and 6) the connection between ARG2, Mn and HTT aggregates in hippocampus, it may be possible to elucidate whether Mn-dyshomeostasis is the root cause or the end result of HD pathology. There is, as yet, no evidence to show that metal-related treatments or exposures will ameliorate

any of the symptoms of HD, however, the gene-environment interaction between mutant HTT and Mn uncovered in our work may help to explain the functions of the wild-type protein, and point to additional therapeutic targets for HD.

References

1. Vijayvargia R, Epand R, Leitner A, et al. Huntingtin's spherical solenoid structure enables polyglutamine tract-dependent modulation of its structure and function. *Elife* 2016; **5**: e11184.
2. Williams BB, Kwakye GF, Wegrzynowicz M, et al. Altered manganese homeostasis and manganese toxicity in a Huntington's disease striatal cell model are not explained by defects in the iron transport system. *Toxicol Sci* 2010; **117**(1): 169-79.
3. Williams BB, Li D, Wegrzynowicz M, et al. Disease-toxicant screen reveals a neuroprotective interaction between Huntington's disease and manganese exposure. *J Neurochem* 2010; **112**(1): 227-37.
4. Stansfield KH, Bichell TJ, Bowman AB, Guilarte TR. BDNF and Huntingtin protein modifications by manganese: implications for striatal medium spiny neuron pathology in manganese neurotoxicity. *J Neurochem* 2014; **131**(5): 655-66.
5. Wegrzynowicz M, Holt HK, Friedman DB, Bowman AB. Changes in the striatal proteome of YAC128Q mice exhibit gene-environment interactions between mutant huntingtin and manganese. *J Proteome Res* 2012; **11**(2): 1118-32.
6. Madison JL, Wegrzynowicz M, Aschner M, Bowman AB. Disease-toxicant interactions in manganese exposed Huntington disease mice: early changes in striatal neuron morphology and dopamine metabolism. *PLoS One* 2012; **7**(2): e31024.
7. Madison JL, Wegrzynowicz M, Aschner M, Bowman AB. Gender and manganese exposure interactions on mouse striatal neuron morphology. *Neurotoxicology* 2011; **32**(6): 896-906.
8. Chen CJ, Liao SL. Oxidative stress involves in astrocytic alterations induced by manganese. *Exp Neurol* 2002; **175**(1): 216-25.
9. Weber S, Dorman DC, Lash LH, Erikson K, Vrana KE, Aschner M. Effects of manganese (Mn) on the developing rat brain: oxidative-stress related endpoints. *Neurotoxicology* 2002; **23**(2): 169-75.
10. Taylor MD, Erikson KM, Dobson AW, Fitsanakis VA, Dorman DC, Aschner M. Effects of inhaled manganese on biomarkers of oxidative stress in the rat brain. *Neurotoxicology* 2006; **27**(5): 788-97.
11. Monder C. Metal ion interactions and glutamine synthetase activity. *Biochemistry* 1965; **4**(12): 2677-86.
12. Di Costanzo L, Sabio G, Mora A, et al. Crystal structure of human arginase I at 1.29-A resolution and exploration of inhibition in the immune response. *Proc Natl Acad Sci U S A* 2005; **102**(37): 13058-63.
13. Stone EM, Glazer ES, Chantranupong L, et al. Replacing Mn(2+) with Co(2+) in human arginase i enhances cytotoxicity toward l-arginine auxotrophic cancer cell lines. *ACS Chem Biol* 2010; **5**(3): 333-42.
14. Pandey D, Bhunia A, Oh YJ, et al. OxLDL triggers retrograde translocation of arginase2 in aortic endothelial cells via ROCK and mitochondrial processing peptidase. *Circ Res* 2014; **115**(4): 450-9.
15. Kuhn NJ, Talbot J, Ward S. pH-sensitive control of arginase by Mn(II) ions at submicromolar concentrations. *Arch Biochem Biophys* 1991; **286**(1): 217-21.

16. Romero PA, Stone E, Lamb C, et al. SCHEMA-designed variants of human Arginase I and II reveal sequence elements important to stability and catalysis. *ACS Synth Biol* 2012; **1**(6): 221-8.
17. Casey JR, Grinstein S, Orlowski J. Sensors and regulators of intracellular pH. *Nat Rev Mol Cell Biol* 2010; **11**(1): 50-61.
18. Shono Y, Kamouchi M, Kitazono T, et al. Change in intracellular pH causes the toxic Ca2+ entry via NCX1 in neuron- and glia-derived cells. *Cell Mol Neurobiol* 2010; **30**(3): 453-60.
19. Wong HK, Bauer PO, Kurosawa M, et al. Blocking acid-sensing ion channel 1 alleviates Huntington's disease pathology via an ubiquitin-proteasome system-dependent mechanism. *Hum Mol Genet* 2008; **17**(20): 3223-35.
20. Chen TT, Klassen TL, Goldman AM, Marini C, Guerrini R, Noebels JL. Novel brain expression of ClC-1 chloride channels and enrichment of CLCN1 variants in epilepsy. *Neurology* 2013; **80**(12): 1078-85.
21. Imbrici P, Maggi L, Mangiatordi GF, et al. ClC-1 mutations in myotonia congenita patients: insights into molecular gating mechanisms and genotype-phenotype correlation. *J Physiol* 2015; **593**(18): 4181-99.
22. Liu XL, Huang XJ, Shen JY, et al. Myotonia congenita: novel mutations in CLCN1 gene. *Channels (Austin)* 2015; **9**(5): 292-8.
23. Waters CW, Varuzhanyan G, Talmadge RJ, Voss AA. Huntington disease skeletal muscle is hyperexcitable owing to chloride and potassium channel dysfunction. *Proc Natl Acad Sci U S A* 2013; **110**(22): 9160-5.
24. Chu XP, Close N, Saugstad JA, Xiong ZG. ASIC1a-specific modulation of acid-sensing ion channels in mouse cortical neurons by redox reagents. *J Neurosci* 2006; **26**(20): 5329-39.
25. Zhou RP, Wu XS, Wang ZS, Xie YY, Ge JF, Chen FH. Novel Insights into Acid-Sensing Ion Channels: Implications for Degenerative Diseases. *Aging Dis* 2016; **7**(4): 491-501.
26. Mason RP, Casu M, Butler N, et al. Glutathione peroxidase activity is neuroprotective in models of Huntington's disease. *Nat Genet* 2013; **45**(10): 1249-54.
27. Potelle S, Morelle W, Dulary E, et al. Glycosylation abnormalities in Gdt1p/TMEM165 deficient cells result from a defect in Golgi manganese homeostasis. *Hum Mol Genet* 2016; **25**(8): 1489-500.
28. Demaegd D, Foulquier F, Colinet AS, et al. Newly characterized Golgi-localized family of proteins is involved in calcium and pH homeostasis in yeast and human cells. *Proc Natl Acad Sci U S A* 2013; **110**(17): 6859-64.
29. Mukhopadhyay S, Bachert C, Smith DR, Linstedt AD. Manganese-induced trafficking and turnover of the cis-Golgi glycoprotein GPP130. *Mol Biol Cell* 2010; **21**(7): 1282-92.
30. Masuda M, Braun-Sommargren M, Crooks D, Smith DR. Golgi phosphoprotein 4 (GPP130) is a sensitive and selective cellular target of manganese exposure. *Synapse* 2013; **67**(5): 205-15.
31. Kondapalli KC, Hack A, Schushan M, Landau M, Ben-Tal N, Rao R. Functional evaluation of autism-associated mutations in NHE9. *Nat Commun* 2013; **4**: 2510.
32. Saudou F, Humbert S. The Biology of Huntingtin. *Neuron* 2016; **89**(5): 910-26.
33. Sastre M, Regunathan S, Galea E, Reis DJ. Agmatinase activity in rat brain: a metabolic pathway for the degradation of agmatine. *J Neurochem* 1996; **67**(4): 1761-5.

34. Elms S, Chen F, Wang Y, et al. Insights into the arginine paradox: evidence against the importance of subcellular location of arginase and eNOS. *Am J Physiol Heart Circ Physiol* 2013; **305**(5): H651-66.
35. Pandey D, Sikka G, Bergman Y, et al. Transcriptional regulation of endothelial arginase 2 by histone deacetylase 2. *Arterioscler Thromb Vasc Biol* 2014; **34**(7): 1556-66.
36. Sarangi U, Singh MK, Abhijnya KV, et al. Hsp60 chaperonin acts as barrier to pharmacologically induced oxidative stress mediated apoptosis in tumor cells with differential stress response. *Drug Target Insights* 2013; **7**: 35-51.
37. Orr AL, Li S, Wang CE, et al. N-terminal mutant huntingtin associates with mitochondria and impairs mitochondrial trafficking. *J Neurosci* 2008; **28**(11): 2783-92.
38. Langfelder P, Cantle JP, Chatzopoulou D, et al. Integrated genomics and proteomics define huntingtin CAG length-dependent networks in mice. *Nat Neurosci* 2016.
39. Patassini S, Begley P, Reid SJ, et al. Identification of elevated urea as a severe, ubiquitous metabolic defect in the brain of patients with Huntington's disease. *Biochem Biophys Res Commun* 2015; **468**(1-2): 161-6.
40. Hodges A, Strand AD, Aragaki AK, et al. Regional and cellular gene expression changes in human Huntington's disease brain. *Hum Mol Genet* 2006; **15**(6): 965-77.
41. Dudek SM, Alexander GM, Farris S. Rediscovering area CA2: unique properties and functions. *Nat Rev Neurosci* 2016; **17**(2): 89-102.
42. Chevaleyre V, Piskorowski RA. Hippocampal Area CA2: An Overlooked but Promising Therapeutic Target. *Trends Mol Med* 2016; **22**(8): 645-55.
43. Kim H, Gearing M, Mirra SS. Ubiquitin-positive CA2/3 neurites in hippocampus coexist with cortical Lewy bodies. *Neurology* 1995; **45**(9): 1768-70.
44. Liu P, Smith PF, Appleton I, Darlington CL, Bilkey DK. Hippocampal nitric oxide synthase and arginase and age-associated behavioral deficits. *Hippocampus* 2005; **15**(5): 642-55.
45. Pigott BM, Garthwaite J. Nitric Oxide Is Required for L-Type Ca(2+) Channel-Dependent Long-Term Potentiation in the Hippocampus. *Front Synaptic Neurosci* 2016; **8**: 17.
46. Simons SB, Escobedo Y, Yasuda R, Dudek SM. Regional differences in hippocampal calcium handling provide a cellular mechanism for limiting plasticity. *Proc Natl Acad Sci U S A* 2009; **106**(33): 14080-4.
47. Chung YH, Joo KM, Nam RH, Lee WB, Lee KH, Cha CI. Region-specific alterations in insulin-like growth factor-I receptor in the central nervous system of nNOS knockout mice. *Brain Res* 2004; **1021**(1): 132-9.
48. Beilharz EJ, Klempt ND, Klempt M, Sirimanne E, Dragunow M, Gluckman PD. Differential expression of insulin-like growth factor binding proteins (IGFBP) 4 and 5 mRNA in the rat brain after transient hypoxic-ischemic injury. *Brain Res Mol Brain Res* 1993; **18**(3): 209-15.
49. Talley EM, Solorzano G, Lei Q, Kim D, Bayliss DA. Cns distribution of members of the two-pore-domain (KCNK) potassium channel family. *J Neurosci* 2001; **21**(19): 7491-505.
50. Mathie A, Al-Moubarak E, Veale EL. Gating of two pore domain potassium channels. *J Physiol* 2010; **588**(Pt 17): 3149-56.
51. Moldovan N, Al-Ebraheem A, Lobo L, Park R, Farquharson MJ, Bock NA. Altered transition metal homeostasis in the cuprizone model of demyelination. *Neurotoxicology* 2015; **48**: 1-8.

52. Ghneim HK. The kinetics of the effect of manganese supplementation on SOD2 activity in senescent human fibroblasts. *Eur Rev Med Pharmacol Sci* 2016; **20**(9): 1866-80.

HDBuzz

Huntington's disease research news. In plain language. Written by scientists. For the global HD community.

Joint HDBuzz Prizewinner: Pennies for your neurons — copper's bad influence on Huntington's disease

There is copper in your brain! Check out how copper and the Huntington's disease protein are partners in crime.

By Terry Jo Bichell on January 30, 2014
Edited by Dr Jeff Carroll

Copper, the metal, may play a role in worsening the symptoms of Huntington's disease. Bing Zhou and his team looked for connections between HD and the amount of copper in neurons. They report that reducing copper in neurons or keeping it from binding to the HD protein improves symptoms.

This article was the joint winner of the 2013 HDBuzz Prize for Young Science Writers. Congratulations to Terry Jo Bichell of Vanderbilt University on her success.

Copper and HD

It is hard to imagine that a metal would have anything to do with Huntington's disease, but actually every cell in the brain needs metal to function. Tiny metal particles, called ions, carry electrical charges, and electricity is the currency of neurons. The brain needs metals like an economy needs money. And **copper**, among other metals like

This research was conducted in fruit flies. They're easy to manipulate genetically but can't

iron and manganese, is saved and spent differently in Huntington's disease brains.

tell us directly about human Huntington's disease

For one thing, copper collects in abnormally high amounts in HD brains, especially in the striatum, which is the part of the brain that is affected earliest in HD. Copper also increases **aggregates**, those globs of protein that show up in HD and Alzheimer's disease. In addition, fans of HDBuzz know about **PBT2**, a new drug in the early phase of clinical trials as a treatment for HD. PBT2 acts by keeping copper from sticking to the huntingtin protein, that is made by the mutant HD gene, and it reduces the toxic effects of aggregates. A new paper from the team of Bing Xhou, of Tsinghua University, China, reports on experiments that help explain these connections between copper and HD.

Copper is an essential nutrient, like other vitamins and minerals, and it is found in a variety of foods, from oysters to pumpkin seeds. It would be unhealthy to mess with copper in the human diet, so to study copper in HD, the researchers used genetically engineered fruit flies.

Why flies?

There are lots of great reasons to use fruit flies for research. Flies eat fly chow, so it is easy to change the recipe to add ingredients like copper. It is also faster to alter genes in a fly than in mice. Most importantly, fruit flies get symptoms similar to those of Huntington's disease when they have a mutation in the HD gene. Like people, flies with the HD mutation have more copper deposits in their heads, and they also develop aggregates in their brains.

The Zhou team used two different Huntington's disease model flies to compare the human and fly HD genes. One of them had its HD gene replaced with a mutant human HD gene. The other fly had the HD mutation inserted directly into the fly HD gene. Both of these flies developed

symptoms of ‘fly HD’, including shorter lifespan and movement difficulties. These symptoms changed when copper was kept in or out of their neurons.

Transporter proteins

How does copper get into and out of neurons? Neurons, like all cells, have proteins that serve as gatekeepers, called **transporters**. Transporters often act like doormen at a party, allowing partygoers with the right invitation to enter, while blocking the door to everyone else. Transporters can also kick out unwanted customers. To understand the effect of copper on HD, the researchers identified one transporter that brings copper into neurons and another that kicks copper out. Then they used genetic tools like keys to lock or unlock all the copper entrances and exits, one by one.

> “So it wasn’t the copper or HD mutation alone that caused symptoms – it was both of them working together!”

When Zhou’s team increased copper inside neurons by locking the exits or opening more entrances, HD symptoms got worse. When they decreased the entry transporter, or increased the exit transporter, the symptoms got better. In other words, boarding up the neuron’s entrances to copper so it can’t get in, or building extra exits so the copper quickly departs, improved the symptoms caused by the HD mutation.

How does copper cause problems?

Kicking copper out of the brain sounds like a good way to treat HD, but it is tricky, because cells need just the right amount of copper to be healthy. In fact, when the exit transporter was increased, it helped the HD flies with the human gene live longer, but it also caused them to have more abnormal movements. There’s no free lunch.

Perhaps the bad influence of copper on mutant HD has something to do with aggregates. If you put a bunch of HD protein fragments in a dish and add copper, they form more of the pesky globs. To investigate the influence of copper on aggregates in HD, the Zhou team used another fly with a glowing green protein attached to the HD protein. As these flies age, there are more glowing green spots visible under a microscope, meaning that more aggregates are forming. But, when the copper was ushered out of the neurons (by blocking entrances or increasing exits), fewer aggregates formed! And when copper was forced to stay inside neurons (by blocking the exits), aggregates increased.

Partners in crime?

So it seemed like the huntingtin protein might be the actual doorman, turning the doorknob on the copper entrances and exits. Nope. Nothing with HD is ever simple, and it turned out Zhou's team couldn't find any evidence that the HD protein directly controlled the copper transporters. They were never caught physically holding hands, so to speak. On the other hand, there could be a direct criminal relationship between copper and the HD protein. Previous research showed that copper binds to two spots on the first chunk of the HD protein. Suspiciously, that is the same part of the protein made by the HD mutation.

Perhaps the mutant HD protein needs a copper accomplice to do its dirty work. To investigate this idea, the authors created yet another fly, neutralizing the two copper binding sites near the HD mutation. It's as if they eliminated copper's two seats on a plane. Without a place to sit, copper can't catch a ride on the HD protein. Sure enough, with the copper binding sites blocked, the fly lived longer, even with the HD mutation! So, the point is that it wasn't the copper alone, nor the HD mutation alone that caused symptoms – it was the HD mutation *and* the copper working together!

To push this idea to the limit, the Zhou team blocked copper transporters in the fly with the neutralized copper binding sites. This time, when they pushed extra copper in or out of neurons, there was no change in HD symptoms and no increase in aggregates. In other words, copper needs to stick directly to the mutant HD protein to worsen symptoms.

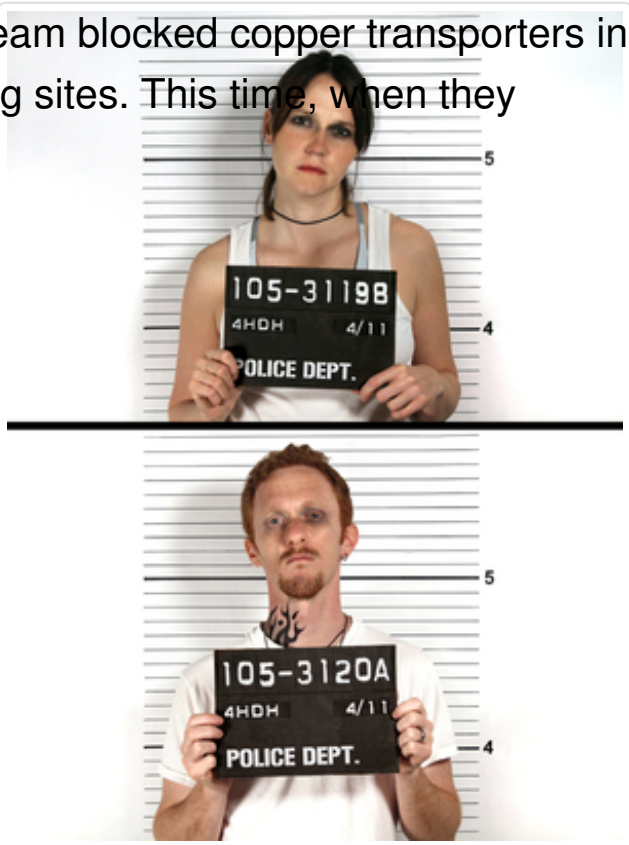

Copper and the mutant huntingtin protein may act as partners in crime, this research suggests.

What does this mean for patients?

Let's not forget that this is a study of flies, not people. This work can't tell us directly about Huntington's disease in humans. But it can give us clues.

In case you're wondering whether Zhou's report means that people with HD should avoid copper in their diets, remember that humans need copper to be healthy, so excluding copper from your diet is not the right thing to do.

What this study suggests is that copper has a bad influence on the HD mutation. These results help to explain why PBT2 might be a good medication to test in Huntington's disease. Maybe other drugs can be designed to block the copper entrances into neurons, or keep copper and mutant HD apart.

One key to HD might be made of copper!

The authors have no conflicts of interest to declare. For more information about our disclosure policy see our FAQ...

Glossary

huntingtin protein The protein produced by the HD gene.
aggregate Lumps of protein that form inside cells in Huntington's disease and some other degenerative diseases
neuron Brain cells that store and transmit information

HDBuzz

Huntington's disease research news. In plain language. Written by scientists. For the global HD community.

A starring role for astrocytes in Huntington's disease?

Brain cells called astrocytes might play a bigger role than previously thought in Huntington's disease

By Terry Jo Bichell on July 29, 2014
Edited by Dr Ed Wild

We know those famous cells called neurons are important in Huntington's disease. But the brain has other cell types with 'supporting actor' roles. New research has shown that brain cells called astrocytes may misbehave in HD, allowing the neurons to malfunction.

Not all brain cells are neurons

Neurons are famous. They are the stars of the brain show and get all the attention. Neurons are known for sending and receiving electrical signals to each other, and they get all the credit for forming memories and thoughts. However, like any movie star knows, the academy awards wouldn't be possible without a huge number of other players behind the curtains, working in the costume — makeup and scenery crews, for example.

The types of cells that play the supporting roles in the brain are called **glia**. Because glia don't do fancy electrical tricks, they are not front and center on stage, but they are the glue that keeps the whole brain working properly. In fact, the word 'glia' actually means glue. The most common kind of glia is **astrocytes**, which means 'star' cells. They're called that because they have a vaguely star-like shape. But, even though astrocytes are so important to the whole show behind the scenes, it still isn't clear exactly what they're doing to keep things running properly, especially in

Huntington’s disease.

Huntington’s disease and the striatum

Huntington’s disease particularly attacks neurons in an area of the brain called the striatum. That’s a part of the brain that’s important for movement. HD causes neurons in the striatum to gradually wither and then disappear. It isn’t clear yet how HD does harm to neurons in the striatum, or why HD picks on those neurons in particular, but there are a few signs of trouble ahead of time. For example, the striatal neurons with HD act differently than normal neurons. They’re more excitable, in an electrical sort of way. Downright jumpy, in fact.

Neurons are the ‘movie star’ cells of the brain… but let’s not forget the other brain cells like astrocytes, that have important jobs in the background.

And, striatal neurons with HD look a little different than expected — they have tiny blobs in them that can be seen under the microscope. The gene mutation that causes HD creates a protein that is stickier than the normal Huntingtin protein, so it clumps together into blobs, called **inclusions**, which given the striatal neurons a freckled appearance under a microscope. So these neurons act slightly different and look slightly different, even before they start to degenerate.

Studying microglia in HD

A new paper, produced by the teams of Drs. Sorfoniew and Khakh at University of California Los Angeles, describes experiments which try to tease out what HD does in astrocytes separately from their accompanying

neurons. They focused on the astrocytes in the striatum, because of its known importance in HD.

In a prequel, another group had shown that putting the HD mutation only in astrocytes, caused them to develop inclusions just like neurons do, even though glia are a completely different type of cell. Even more surprising, putting the HD mutation into astrocytes caused neighboring neurons without the HD mutation to degenerate! This suggested that astrocytes do something very important to keep nearby neurons alive, even healthy neurons. Somehow, the HD mutation interfered with the ability of astrocytes to keep neurons healthy.

In the new paper, Sorfoniew and Khakh used two different mouse models of HD to explore the astrocyte story. In both of these mouse models, they found that the HD mutations caused astrocytes to act up, electrically. The astrocytes got very excitable, in fact, but only in the striatum — not in other parts of the brain. This was important to the storyline, because it showed that astrocytes were affected by the HD mutation before they caused the neurons to die.

Astrocytes, sucking up potassium with Kir4.1

Excitability is good in movie stars, but not so good in the brain. Too much excitability can actually cause a form of neuronal burnout, which leads to neuronal death. One thing that makes neurons excitable is too much free-wheeling potassium. Extra potassium needs to be cleared out from between the neurons, like smoke in a crowded bar, or it will make the neurons too excitable.

Astrocytes to the rescue! Astrocytes have a special ‘channel’ protein, a bit like an exhaust fan, that sucks potassium out of the space between cells. This channel has the catchy stage-name of **Kir4.1**. Astrocytes with the HD mutation have **less** Kir4.1 than is expected. That means that they can’t remove extra potassium from between the cells. It is as if the neurons are partying in a smoky room, and the fan is broken, making the neurons

gradually sicker and sicker.

Topping up the Kir4.1

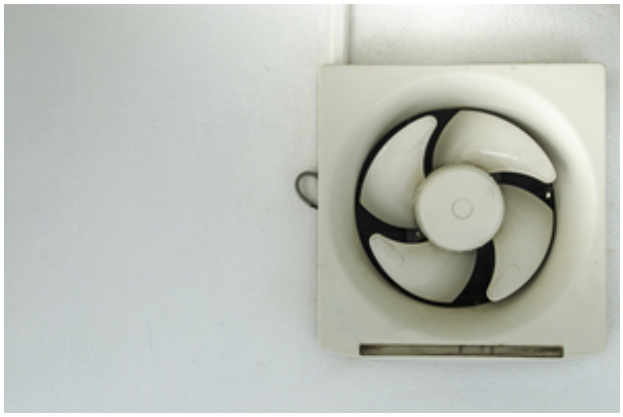

The astrocyte protein Kir4.1 functions like an extractor fan, removing excess potassium from around neurons and helping prevent them getting too excited.

The researchers wondered what would happen if they put more Kir4.1 into the astrocytes in the striatum. Would it remove the excess potassium and help the neurons stay healthy? They found a way to deliver Kir4.1 into the astrocytes of living mice. Not to their neurons, just to their astrocytes. Sure enough, the exhaust fan function was restored, and the extra potassium was removed, allowing the neurons in these mice to calm down and stop being so excitable.

These cellular changes were very promising, but what about the whole animal? It is important to find out if treating the astrocytes alone would actually help the HD mice to stay healthier and live longer. After delivering extra Kir4.1 to the astrocytes, the mice did not seem substantially healthier in tests of their movement and agility, but they did have a more normal walking pattern. So, treating astrocytes, the ‘supporting players’, somehow improved one of the movement symptoms.

Most importantly, the treated mice lived longer. Quite a bit longer. So, even though their movement symptoms did not substantially improve, treating the astrocytes helped the mice with HD live longer.

A starring role for astrocytes in HD?

This experiment was really interesting because it showed that astrocytes might have more of a starring role than previously thought. Maybe, treatments that are focused on neurons alone may be pointing the camera in the wrong direction.

There are a lot of loose ends to the story, so a sequel is expected. This study did not explain **how** the HD gene mutation caused problems in the astrocytes, or how it reduced Kir4.1. It also did not explain how the Kir4.1 treatment helped the mice live longer, despite not improving most of their movement symptoms. This study used mice with very extreme HD mutations that might not do the same things that human gene mutations do. But, what it did was to change the storyline and bring the supporting actors into the forefront. It moved astrocytes into a starring role. The next installment will be very interesting.

The authors have no conflicts of interest to declare. For more information about our disclosure policy see our FAQ...

Glossary

huntingtin protein The protein produced by the HD gene.

microglia the brain's immune cells

neuron Brain cells that store and transmit information

HDBuzz

Huntington's disease research news. In plain language. Written by scientists. For the global HD community.

Taking new targets to the bank: the DNA repair protein 'ATM' is overactive in Huntington's disease

HD causes the normally helpful protein "ATM" to get a little overzealous. Now we can look for drugs to settle it down

By Terry Jo Bichell on March 09, 2015

Edited by Dr Tamara Maiuri

A recent study by the Yang lab at UCLA points to a new idea for preventing damage to neurons in Huntington's disease. The strategy is to tone down an overly helpful protein called ATM. Inside neurons, ATM provides a crucial role in repairing the cell's infrastructure, somewhat like that of a bridge inspector, but the expanded HD protein may be causing ATM to misjudge DNA damage.

Nature's inspectors, repair team, and demolition crew

ATM actually has nothing to do with a bank machine. ATM is an abbreviation for 'Ataxia Telangiectasia Mutated' because it is a gene that can cause a movement disorder called Ataxia Telangiectasia, but it may also play a role in Huntington's disease.

The function of ATM in the cell is something like a building inspector. When bridges get old they often rust, and parts need to be replaced to keep roads safe. Most bridges are inspected at least once a year by intrepid engineers with climbing equipment who determine whether or not a bridge can be repaired, or will need to be condemned.

Inside our cells, DNA shows wear and tear with age too, developing cracks and even breaks in the structure. This DNA damage occurs as part of the normal aging process, but it is seen earlier than expected, or more often than expected, in Huntington's disease patients. DNA damage is also seen in HD cell and animal models.

Much like bridge inspectors, the job of the ATM protein is to detect structural cracks and breaks in DNA, and decide whether it should be repaired or condemned.

The job of the ATM protein is to detect this sort of DNA damage, and then hang around the damage site, calling in a team of specialized proteins to do the repairs. If the damage is too great, ATM activates a different set of proteins, a sort of demolition crew, which condemns and removes the cells harboring the damaged DNA. It is a tricky business—an overzealous inspector could actually condemn a structure prematurely, while an unobservant inspector might fail to detect and repair structural damage.

Making the right call

Actual bridge inspectors usually communicate with their teams via walkie-talkie. In cells, communication is done by fastening chemical tags known as phosphate groups to the right proteins. ATM calls in the repair team by 'phosphorylating' a protein called H2AX. H2AX then settles down at the site of the structural DNA break and gets the repair started. If the damage is too far-gone, ATM can phosphorylate a different protein, called p53, which brings in the demolition crew instead of the repair team. The demolition

crew shuts down the entire cell in a process called apoptosis, or programmed cell death. Needless to say, a lot of problems can arise if the demolition crew is called in by mistake.

The work done in the Yang lab shows that ATM signaling is increased in Huntington's disease, and this signaling may be going awry. When cells with the HD mutation were stressed, they showed more H2AX phosphorylation, and more cell death than expected. Excess H2AX phosphorylation was also found in brain tissue from HD patients, especially the portions of the brain that are known to be vulnerable in HD.

The question is whether extra ATM signaling in HD is a good thing, or a bad thing: in vulnerable brain regions, HD might cause more DNA damage, so ATM might be doing the right thing by signaling H2AX to make repairs. On the other hand, if overzealous ATM signaling is one of the detrimental effects caused by the expanded HD protein, then it could make a good target for a potential therapy.

> "At this point, we don't know how the HD protein causes abnormal ATM signaling. But reducing ATM may be a promising new way to treat HD, and perhaps to prevent damage caused by the HD mutation."

Less is more

ATM is essential to normal health—patients with mutations in both copies of their ATM gene have a serious disorder called Ataxia Telangiectasia. Yet having only one functional copy of the ATM gene, a half dosage, doesn't seem to cause any symptoms at all.

With this in mind, the Yang lab set out to study ATM signaling in several ways. They started by reducing the amount of ATM produced in HD cells grown in a dish, and found that blocking ATM signaling actually made the cells healthier. Somehow, ATM signaling may have been calling in the demolition team rather than the repair crew in the HD cells.

The research team then looked at fruit flies with the HD mutation, which have trouble with their coordination when climbing up test tubes. They generated HD flies with a half dose of ATM (only one copy of the fly ATM gene). These flies were much better climbers than the regular HD flies.

Finally, when the researchers bred 'half dosage ATM' mice with HD mice, they found the most convincing results of all—the HD mice appeared healthy! HD mice with reduced ATM moved better, showed fewer signs of depression, had fewer aggregates, and less brain atrophy than the HD mice with normal amounts of ATM. In other words, having half of the normal ATM prevented some of the problems caused by HD.

While bridge inspectors usually communicate with their teams via walkie-talkie, cells coordinate signals by fastening chemical tags known as phosphate groups to the right proteins.

Taking the ATM target to the bank

It is possible to reduce the activity of ATM with a small molecule drug, called an inhibitor. The researchers put ATM inhibitors on neurons grown in a dish and they found that it protected the cells from damage done by the HD protein. This opens the possibility for the development of an ATM inhibitor medication to treat HD.

At this point, we don't know *how* the HD protein causes abnormal ATM signaling. But two other studies have noticed the same thing, and this type of independent replication goes a long way to boost our confidence that we're on the right track. Together, the results of these studies suggest that reducing ATM may be a promising new way to treat HD, and perhaps to prevent damage caused by the HD mutation.

The authors have no conflicts of interest to declare. For more information

about our disclosure policy see our FAQ...

Glossary

aggregate Lumps of protein that form inside cells in Huntington's disease and some other degenerative diseases

apoptosis A type of cell death where the cell uses specialized signals to kill itself

neuron Brain cells that store and transmit information

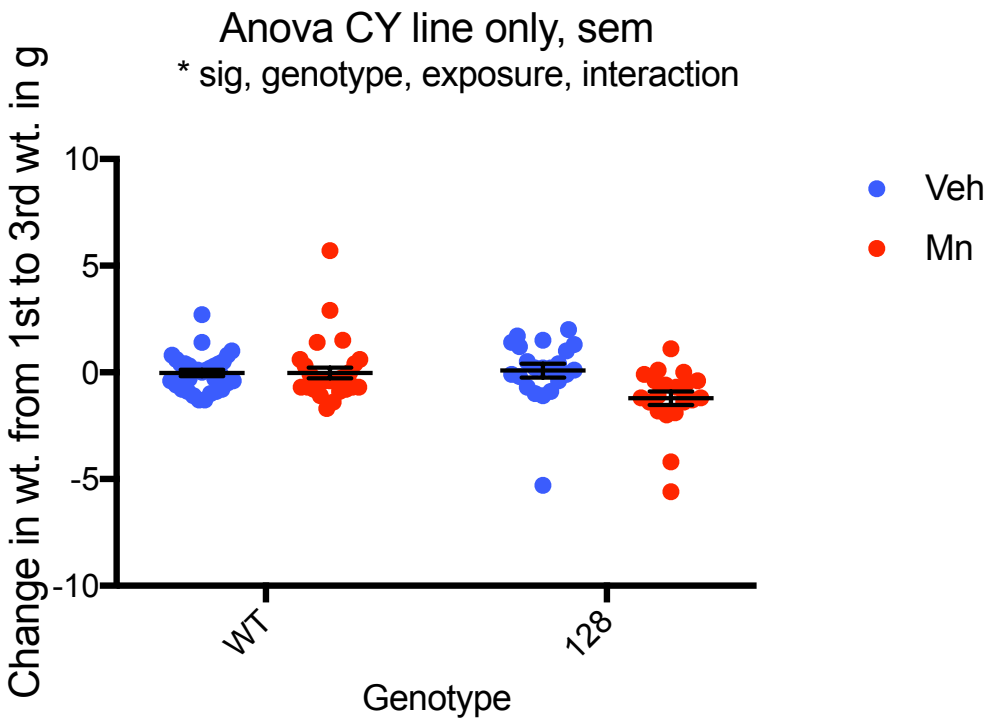
Anova CY line only, sem
* sig, genotype, exposure, interaction
Change in wt. from 1st to 3rd wt. in g
10
5
0
-5
-10
WT
128
Genotype
Veh
Mn

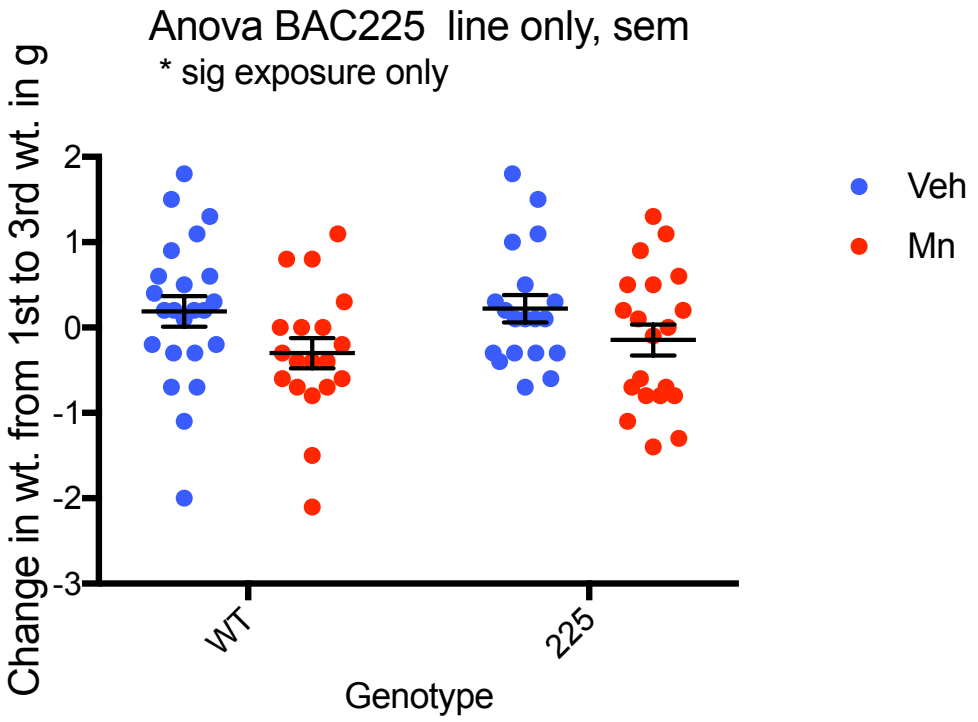
Anova BAC225 line only, sem
* sig exposure only
Change in wt. from 1st to 3rd wt. in g
2
1
0
-1
-2
-3
WT
225
Genotype
Veh
Mn

Anova change Allelic line only

*** sig for exposure only on ALL genotypes

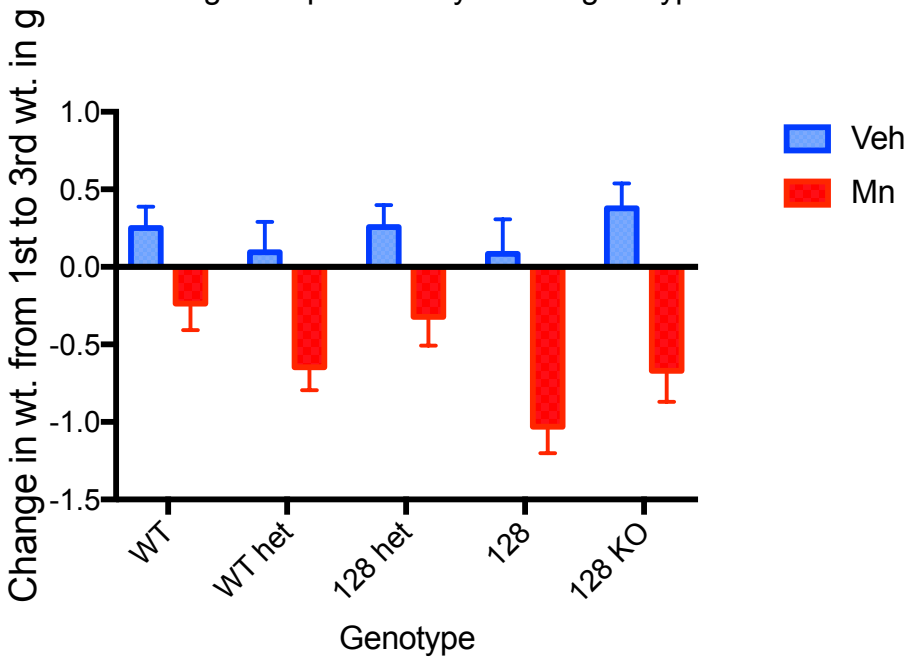

Anova raw Allelic line only

*** sig for genotype only on ALL genotypes

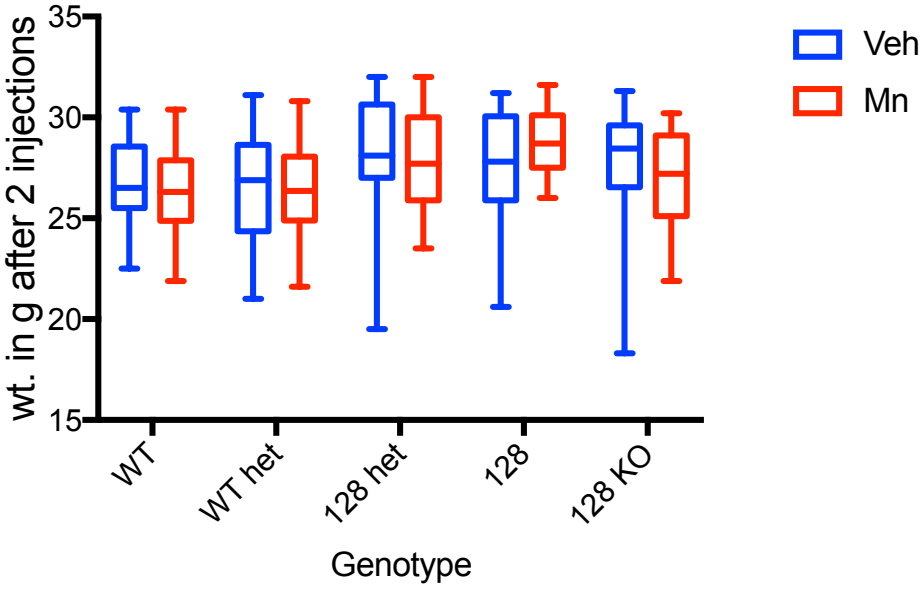

Anova Raw CY line only, sem

*p=<.01 sig interaction, **p=<.004 sig genotype, exposure

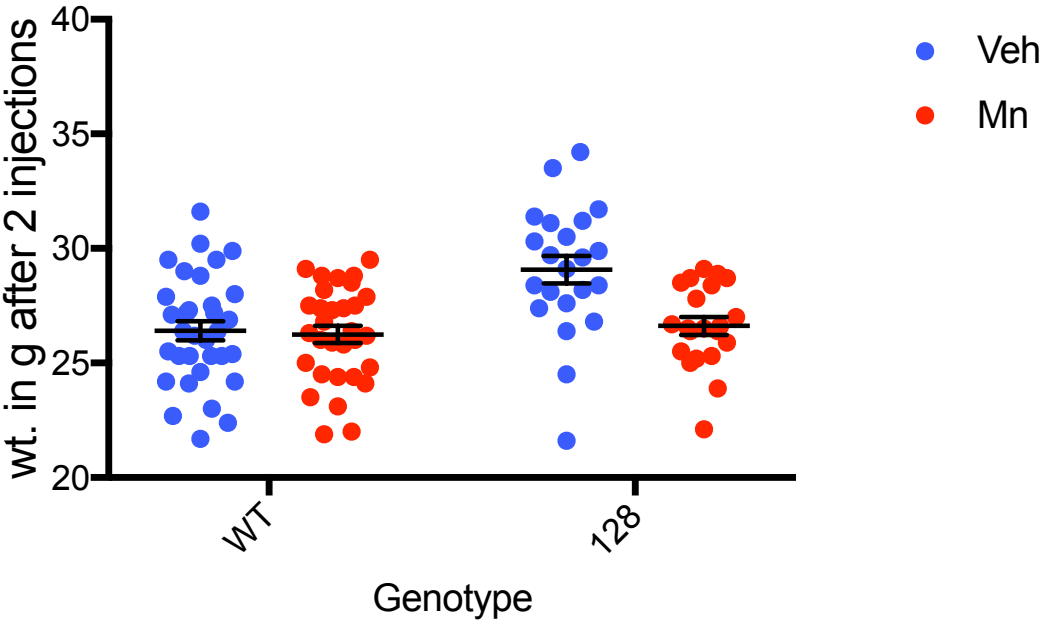

Anova Raw BAC225 line only, sem

not sig

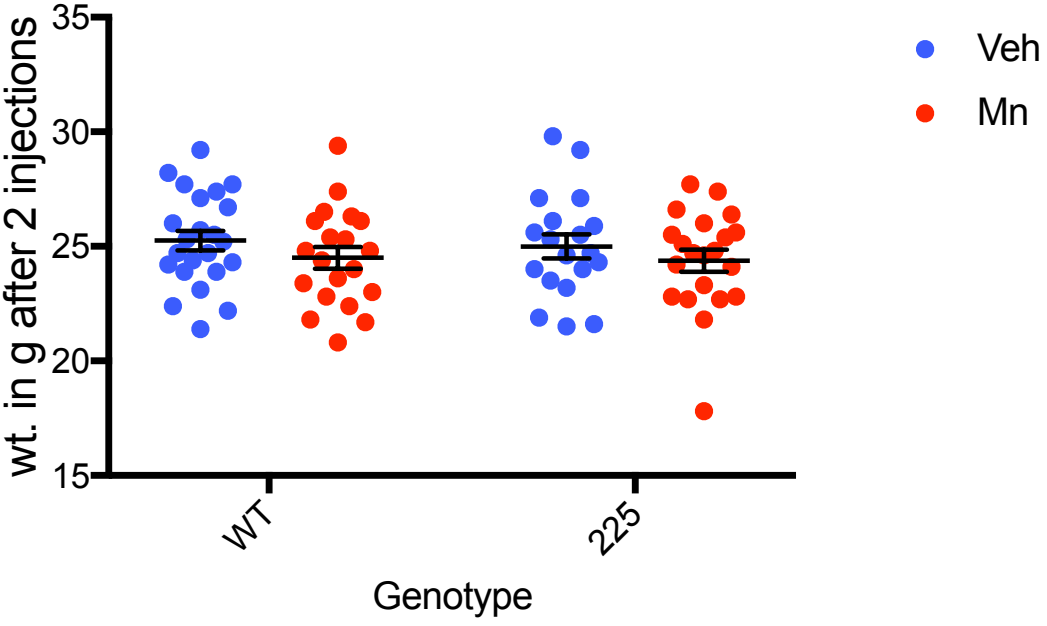

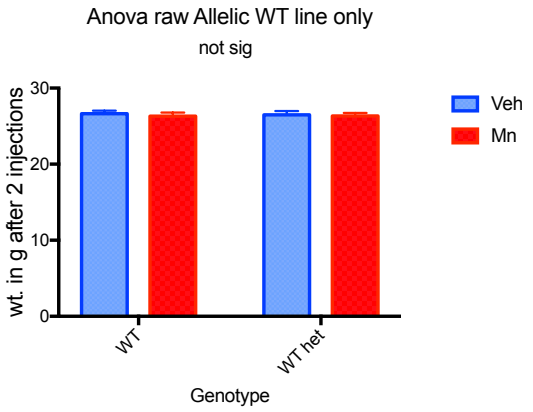
Anova raw Allelic WT line only
not sig
wt. in g after 2 injections
30
20
10
0
WT
WT het
Genotype
Veh
Mn

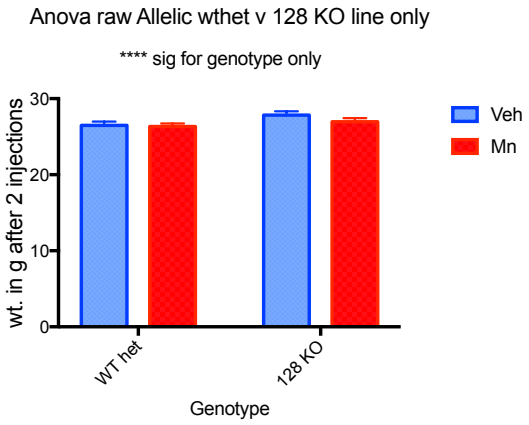
Anova raw Allelic wthet v 128 KO line only
**** sig for genotype only
wt. in g after 2 injections
30
20
10
0
WT het
128 KO
Genotype
Veh
Mn

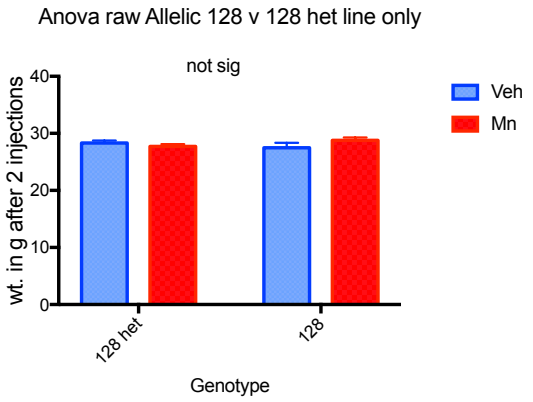
Anova raw Allelic 128 v 128 het line only
not sig
wt. in g after 2 injections
40
30
20
10
0
128 het
128
Genotype
Veh
Mn

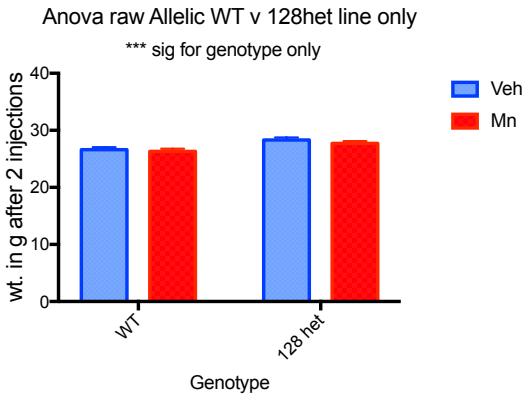
Anova raw Allelic WT v 128het line only
*** sig for genotype only
wt. in g after 2 injections
40
30
20
10
0
WT
128 het
Genotype
Veh
Mn

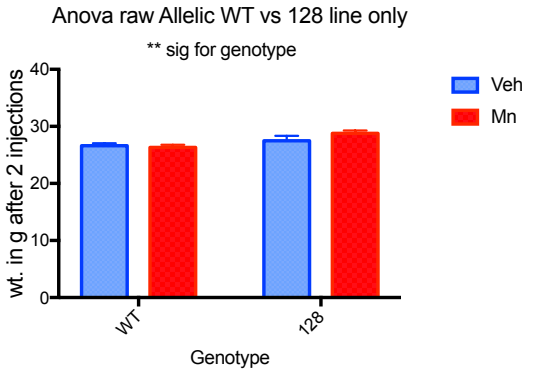
Anova raw Allelic WT vs 128 line only
** sig for genotype
wt. in g after 2 injections
40
30
20
10
0
WT
128
Genotype
Veh
Mn

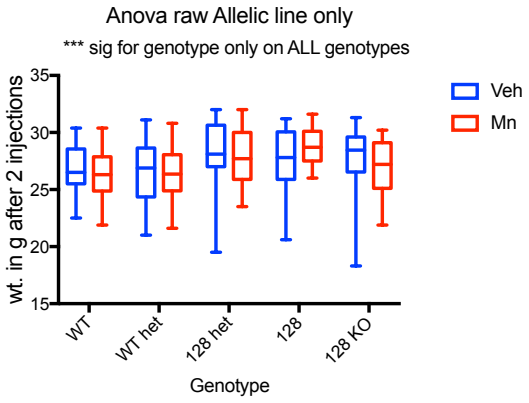
Anova raw Allelic line only
*** sig for genotype only on ALL genotypes
wt. in g after 2 injections
35
30
25
20
15
WT
WT het
128 het
128
128 KO
Genotype
Veh
Mn

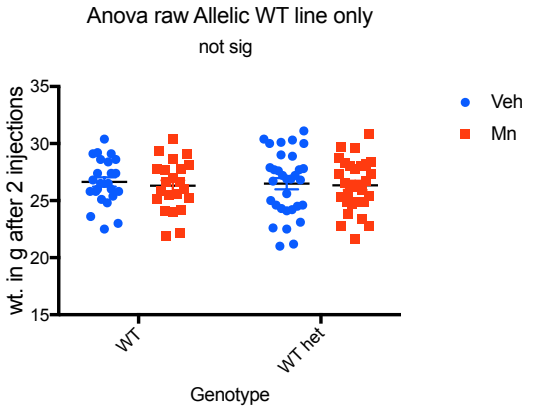
Anova raw Allelic WT line only
not sig
wt. in g after 2 injections
35
30
25
20
15
WT
WT het
Genotype
Veh
Mn

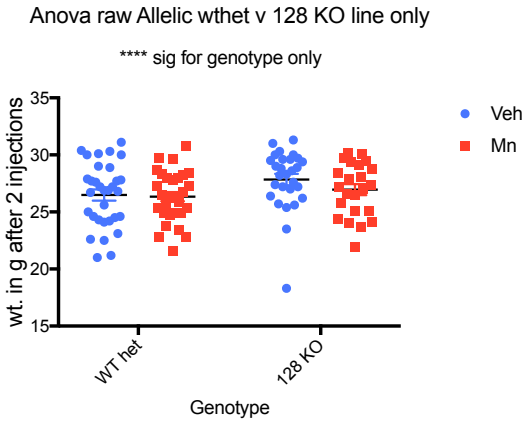
Anova raw Allelic wthet v 128 KO line only
**** sig for genotype only
wt. in g after 2 injections
35
30
25
20
15
WT het
128 KO
Genotype
Veh
Mn

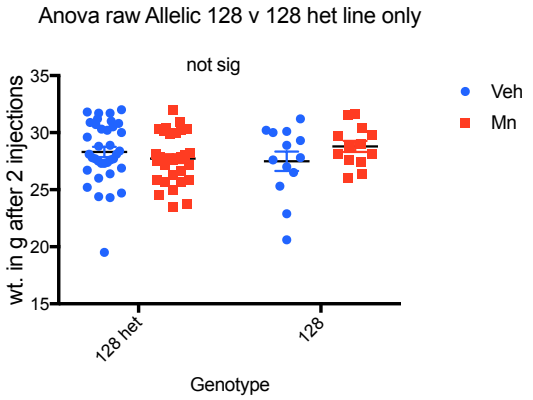
Anova raw Allelic 128 v 128 het line only
not sig
wt. in g after 2 injections
35
30
25
20
15
128 het
128
Genotype
Veh
Mn

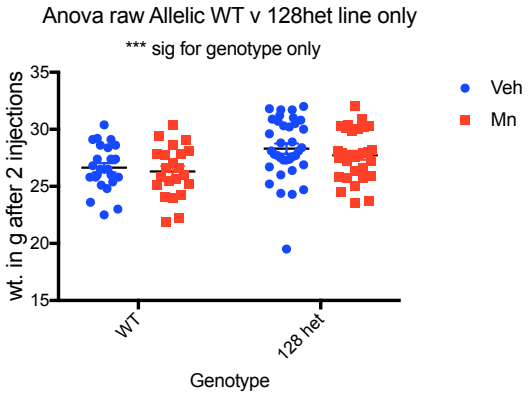
Anova raw Allelic WT v 128het line only
*** sig for genotype only
wt. in g after 2 injections
35
30
25
20
15
WT
128 het
Genotype
Veh
Mn

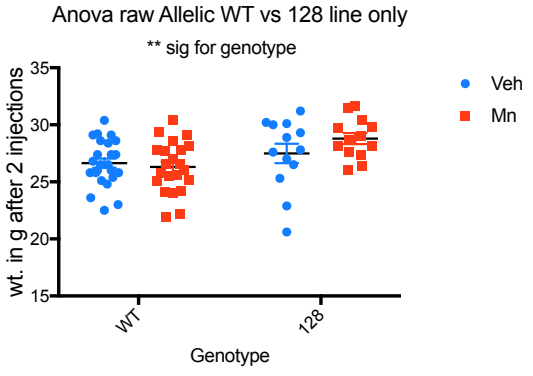
Anova raw Allelic WT vs 128 line only
** sig for genotype
wt. in g after 2 injections
35
30
25
20
15
WT
128
Genotype
Veh
Mn

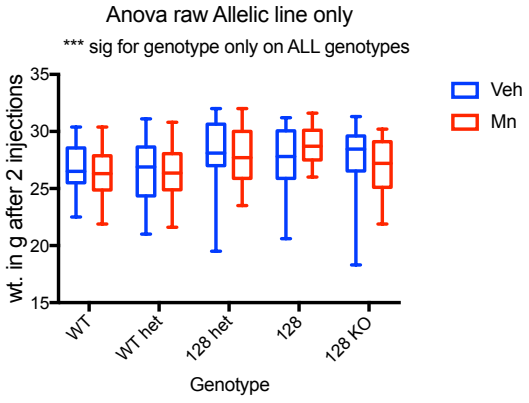
Anova raw Allelic line only
*** sig for genotype only on ALL genotypes
wt. in g after 2 injections
35
30
25
20
15
WT
WT het
128 het
128
128 KO
Genotype
Veh
Mn